University of Pavia
Department of Molecular Medicine

PhD course in Translational Medicine

XXXIII cycle

PhD thesis on

Asparaginase-based Antibody Drug Conjugates

Tutor:
Prof. Claudia Scotti

Candidate:
Dr. Greta Pessino

Academic year 2019-2020

Dedicated to my loved ones

Index

Abstract

L-Asparaginase (**ASNase,** EC 3.5.1.1) is a key component of the established combined chemotherapy used for the treatment of **pediatric acute lymphoblastic leukemia**, having significantly increased the percentage of complete remissions in patients since its introduction in 1970s The benefit of ASNase treatment is supported by extensive clinical data, while resistance to asparaginase is correlated with poor prognosis.
ASNase is an amidohydrolase which shows a prevalent asparaginolytic and a secondary glutaminolytic activity; its therapeutic benefit comes from the depletion of asparagine from the blood stream, on which leukemic cells depends, given their absent or compromised capability to express asparagine synthetase (EC 6.3.5.4) under stress conditions.
The ASNase molecules currently used in the clinics are derived from either *E. coli* (EcAII) or *E. chrysanthemi*, with the first line drug being PEG-Asparaginase (Oncaspar ®), a pegylated formulation of *E. coli* ASNase, which shows longer half-life compared to native *E. coli* and *E. chrysanthemi* molecules. However, most of the available ASNase products lack optimal pharmaceutical features, in particular because of ASNase high toxicity, due to its untargeted activity; high immunogenicity, due to its bacterial origin and large size; short blood serum half-life, and poor efficacy in specific sub-classes of patients (high risk).

The aim of this work was to address these limitations, in order to improve EcAII efficacy, and in particular its **high toxicity**, on one side, by *targeting* the drug onto leukemic cells, and its **high immunogenicity**, on the other side, by *miniaturizing* the drug. It is expected that tackling these two points should also help to increase the drug efficacy in the treatment of **high-risk patients**.

The adopted strategy consisted in the design of a radically new, **anti-CD19 Asparaginase-based Antibody Drug Conjugate (ADC)**, which was conceived by our research group after the successful engineering of a single domain antibody (sdAb) with asparagynolitic activity, obtained through the rational transfer of *E. coli* type II asparaginase catalytic residues onto a camelid sdAb backbone (**sdASNase**) (PATENT# E0115946). The addition of a targeting domain nanobody to the catalytic sdASNase lead to the new concept of **Targeted Catalytic Nanobodies** (**TCANs**).

In particular, the molecule designed in this work (**TCAN3**) was composed by a newly selected **anti-CD19 nanobody** (targeting domain) and by the **catalytic sdASNase nanobody** (catalytic domain). In order to produce such molecule, several steps were followed.
Firstly, the extracellular domain of **CD19** was expressed as a C-terminal fusion with the human Fc fragment. For the **selection of targeting nanobodies,** the Phage Display technique was set up in house, but, due to obstacles encountered in both recombinant CD19 purification and classical Phage Display selection, the Yeast Two Hybrid system was chosen as an alternative strategy for the screening of anti-CD19 intracellular nanobodies. The collaboration with the group of Prof. Cattaneo (SNS, Pisa) resulted in the successful isolation of a nanobody, whose binding to CD19 was confirmed through ELISA tests. The **TCAN3** was then assembled joining the selected anti-CD19 nanobody targeting domain to the available sdASNase nanobody through a linker. The TCAN3 was then expressed and purified, and its binding to CD19 was confirmed through ELISA tests. In the meantime, preliminary tests for **co-localization studies** of CD19 and lysosomes were set up in adherent and leukemic cell lines after a training at the laboratory of Prof. Marjia Jäättelä (DCSRC , Danish Cancer Society Research Center)
In conclusion, in this work, **TCAN3**, a promising targeted asparaginase-based molecule which could help in leukemia therapy, and especially in high-risk forms, was designed and expressed. TCANs, focusing for the first time on the specificity of the metabolic traits of a given tumor and coupling the correct catalytic activity to the appropriate target specificity, might potentially represent a novel general approach to tackle any type of cancer which shows sensitivity to a specific metabolite deprivation.

1. Introduction

1.1 Acute Lymphoblastic Leukemia (ALL)

1.1.1 Leukemia

Leukemia and lymphomas are cancers of blood producing cells, also referred to as hematological malignancies. They arise from aberrations in the regulatory pathways of hematopoiesis, a highly regulated maturation and differentiation process, which assures the renewal of blood cells over an individual's lifetime. Leukemia is characterized by an uninhibited proliferation of myeloid or lymphoid precursor cells in the bone marrow, while in lymphomas an abnormal lymphoid expansion is mainly observed in lymph nodes, but also in extranodal sites, such as tonsils and spleen.

Here, a short outline of leukemia classification will be given, focusing on the features of Acute Lymphoblastic Leukemia (ALL), as its therapy is the main object of this thesis.

1.1.2 Classification

The classification of myeloid and lymphoid neoplasms was published by the World Health Organization (WHO) in 2001 and updated in 2008 and 2016. This classification represents a worldwide consensus for the diagnosis of these tumors for clinicians, pathologists and basic scientists. [1,2] The WHO classification stratifies hematological malignancies principally in respect to *lineage*, which are myeloid, lymphoid, histiocytic/dendritic cell and mast cell.[3] Diseases are further classified within each lineage incorporating *morphology*, *immunophenotype*, *cytogenetics, genetic* and *clinical features,* with the aim of defining significant entities from a clinical point of view [2]. The classification of ***Myeloid*** diseases is summarized in **Table 1**. ***Lymphoid*** lymphomas and leukemias are classified together by the WHO, since in most lymphoid neoplasms both solid and circulating phases are concurrently observed, and they result to be different manifestations of the same neoplasm. [3] Their classification is summarized in **Table 2**.

Table 1. Myeloid Diseases Classification[2,4]

Class	Subclass	Distinctive Features
Chronic Myeloproliferative Diseases (CMPD)	Chronic myelogenous leukaemia (CML) Chronic neutrophilic leukaemia (CNL Chronic eosinophilic leukemia (CEL) Hypereosinophilic syndrome (HES) Chronic idiopathic myelofibrosis (CIMF)	*BCR/ABL,* Ph+
Myelodysplastic syndromes (MDS)	Refractory anemia (RA) Refractory anemia with ringed sideroblasts (RARS) Refractory cytopenia with multilineage dysplasia (RCMD) Refractory cytopenia with multilineage dysplasia and ringed sideroblasts (RCMD-RS) Refractory anemia with excess blasts-1 (RAEB-1) Refractory anemia with excess blasts-2 (RAEB-2) Myelodysplastic syndrome, Unclassified (MDS-U) MDS associated with isolated del(5q)	All: dysplastic maturation of several lineages, cytopenias
Myelodysplastic/ myeloproliferative diseases (MDS/MPD)	Chronic Myelomonocytic Leukemia (CMML). Atypical Chronic Myeloid Leukemia (aCML). MDS/MPD with ring sideroblasts and thrombocytosis. Juvenile Myelomonocytic Leukemia (JMML).	*BCR/ABL*, Ph+ SF3B1 mutation Ph-
Acute Myeloid Leukaemias (AML)	AML with recurrent cytogenetic abnormalities AML with myelodysplasia-related features Therapy related Myeloid Neoplasms (tMNs) AML not otherwise categorised (NOC).	tMNs: alkylating agent/radiation or topoisomerase II inhibitor–related

Table 2. Lymphoid Diseases Classification

B cell neoplasms	
Precursor B-cell neoplasms	B-cell Acute Lymphoblastic Leukaemia (B-ALL) B lymphoblastic Lymphoma (B-LBL)
Mature B cell neoplasms	Chronic lymphocytic leukaemia/small lymphocytic lymphoma B cell prolymphocytic leukaemia Lymphoplasmacytic lymphoma Splenic marginal zone lymphoma Hairy cell leukaemia Plasma cell myeloma Solitary plasmacytoma of bone Extraosseous plasmacytoma Extranodal marginal zone B-cell lymphoma of mucosa-associated lymphoid tissue (MALT lymphoma) Nodal marginal zone B cell lymphoma Follicular lymphoma
T cell neoplasms	
Precursor T cell neoplasms	T-cell Acute Lymphoblastic Leukaemia (T-ALL) T lymphoblastic Lymphoma (T-LBL)
Mature T cell and NK cell neoplasms	T cell prolymphocytic leukaemia T cell large granular lymphocytic leukaemia Aggressive NK cell leukaemia Adult T cell leukaemia/lymphoma Extranodal NK/T cell lymphoma, nasal type Enteropathy type T cell lymphoma Hepatosplenic T cell lymphoma Subcutaneous panniculitis-like T cell lymphoma Mycosis fungoide Sezary syndrome Primary cutaneous anaplastic large cell lymphoma Peripheral T cell lymphoma, unspecified Angioimmunoblastic T-cell lymphoma Anaplastic large cell lymphoma
Hodgkin Lymphoma	
	Nodular lymphocyte predominant Hodgkin lymphoma (NLPHL) Classical Hodgkin lymphoma (CHL)

1.1.3 Childhood Acute Lymphoblastic Leukemia (cALL)

Acute Lymphoblastic Leukemia (ALL) is a malignant neoplasm which arises from uncontrolled expansion of lymphoid progenitor cells, residing mainly in bone marrow and blood. ALL represents the most common cancer in children and adolescents, [5] and it can affect lymphoblast committed to both B-lineage and T-lineage.

1.1.3.1 Genetic Background in ALL

As all cancers, ALL could be described to a certain extent as a genetic disorder, since it arises from the accumulation in the cell genome of *somatic genetic alterations*. However, the timing and events which cause these multi-genomic alterations are not clearly understood, and most patients show no recognized inherited factors.[6] Nevertheless, recurrent genetic alterations have been identified in past decades, allowing to state that ALL comprises different entities, characterized by distinct configurations of *somatic genetic alterations* In particular, *chromosomal translocations* and *intrachromosomic rearrangements* are likely to be initial causative events in leukemogenesis. The main *somatic genetic alterations* found in childhood ALL which are briefly summarized in **Table 3**.[7]

Table 3. Genetic alterations in ALL

	Genetic Alteration	Features	Ref
Aneuploidy alterations	High hyperdiploidy (>50 chromosomes)	20-30% cALL cases, correlates with a favorable prognosis[8]	9
	Hypodiploidy (< 44 chromosomes)	1% cALL cases strong predictor of poor prognosis.[9]	10
Chromosomal Translocations* ***Class I***	cytokine receptor–like factor 2 (*CRLF2*) and erythropoietin receptor (*EPOR*) genes rearrangements under the regulation of the immunoglobulin heavy chain (IGH) and immunoglobulin light chain (IGK) enhancers	B-ALL [10,11]	11,12
	transcription factors *TLX1* and *TLX3* genes rearrangement in T-cell receptor (TCR) loci	T-ALL [12]	13
Class II	*ETV6-RUNX1*	20% cALL cases, strong favourable prognostic factor.[13]	14
	TCF3-PBX1	5% cALL cases, associated with pre-B-cell phenotype and higher risk of central nervous system (CNS) relapse.[14]	15
	KMT2A (MLL)	1% of ALL infant cases (< 1 year of age), associated with very poor prognosis.[15–17]	16-18
	BCR-ABL1 Philadelphia Chromosome (Ph +)	5% cALL cases, 25% adult ALL cases; associated with poor prognosis, selective tyrosine kinase inhibitors (TKIs) therapy.[18–21]	19-22
Other most common alterations	*PAX5*	31% cALL cases, poor prognostic factor [22]	24
	IKZF1	15% cALL cases, poor prognostic factor[22]	24
Genetic alterations of relapse	*CREBBP*	19% of B-ALL relapsed children, associated to steroid therapy resistance [23]	25
	NT5C2	associated with resistance to nucleoside analogue therapy [23]	25
	TP53		27[24]
Down Syndrome Patients	*CRLF2*	50% of Down Syndrome B-ALL patients[25]	29

* ***Class I***: a coding oncogene is placed in an actively-transcribed regulatory region; ***Class II***: fusion of distinct genes results in a new chimeric protein with oncogenic function.

1.1.3.2 Prognostic factors

Factors that can be used to predict the chance of recovering from a disease and the chance of its recurrence are called **prognostic factors**. Prognostic factors are essential for the stratification of ALL patients in different risk classes, a crucial process to allow the administration of a risk-based optimized therapy. ALL prognostic factors can be grouped into distinct categories, according to their nature.

The most important ***clinical factors*** are **age** and **white cell count** at the time of diagnosis, essential for the stratification of patients into the three risk groups, which are described in paragraph 1.1.4. Older age is consistently associated with poorer prognosis, with the exception of infants (< 1 year), in which a very high risk of relapse is observed.

Biological and genetic factors consist in recurrent genetic alterations (paragraph 1.1.3), which are closely associated with *favorable* (high hyperdiploidy, *ETV6-RUNX1*) or *poor prognosis* (hypodiploidy, *MLL* rearrangements, *BCR-ABL1*, Ph-like ALL, *PAX5*, *IKZF1*, *CRLF2*).
However, the most important prognostic factor in childhood ALL is probably represented by the ***early response to treatment***, which consists in the time required to eliminate the primary leukemic blast population since the initiation of the treatment. When this morphological remission is achieved within 1-2 week from the remission induction therapy administration (paragraph 1.1.4), the early response to treatment is predictive of a good prognosis.[26] Along with the early response to treatment, in the last years the levels of ***Minimal Residue Disease*** (MRD, defined as the *presence of resistant leukemic blasts after therapy at a level below the limit of conventional morphological detection)* has emerged as a strong independent predictive factor of relapse risk in patients (paragraph 1.1.5).[27] It is important to consider also ***prognostic factors at relapse***, which help predicting the outcome when a relapse occurs, basing on some important features regarding the relapsing event, which are:[28] *time to relapse*, the shorter the time needed for the relapse to occur, the poorer is the prognosis; *immunophenotype*, if the relapse shows a T-cell immunophenotype, it is associated with a poorer prognosis; *site of relapse*, bone marrow localization of the relapse is associated with poorer prognosis than extramedullary sites localization.

1.1.4 Childhood ALL Standard Therapy

ALL therapy is among the stronger and better consolidated in the history of cancer treatments. All the antileukemic drugs used nowadays were identified and developed before the 1970s, when only 30% of the children diagnosed with ALL survived. Since then, *multiagent combination chemotherapy*, *CNS-directed therapy* and *risk stratification* of patients allowed to increase the survival up to 90% of childhood ALL cases.[29]
The most important element is certainly represented by the stratification of patients into the *risk groups*, listed in **Table 4**, which allows to optimize the therapy by evaluating patients' risk of relapse, using known prognostic factors.[28]

Table 4. Risk Group Stratification

Standard risk	children between 1 and 10 years of age, with an initial white blood cell count lower than 50,000/cubic mm
High risk	children aged more than 10 years, with an initial white blood cell count higher than 50,000/cubic mm
Very high risk	children aged less than 1 year of age (infants)

ALL therapy consists of three phases: a *remission-induction* phase, an *intensification-consolidation* phase and a *maintenance-continuation* phase. For high risk patients, a CNS-directed treatment is performed in parallel early in the clinical course, in order to prevent a relapse of the disease in this site, which is associated with poor prognosis and frequently observed.[30]

1.1.4.1 Remission-Induction Therapy

The goal of ***remission-induction therapy***, the first phase of the treatment (taking around 4 weeks), is to eradicate more than 99% of the initial leukemic cell population, and to achieve the recovery of normal hemopoiesis along with healthy performance status.
For *standard risk* patients, this phase consists of the administration of three drugs: a *glucocorticoid* (dexamethasone, prednisone or prednisolone), *vincristine* and ***asparaginase***. The administration of dexamethasone rather than prednisone or prednisolone was assessed to be more effective, perhaps because of its longer half-life and deeper penetration into the CNS.[31] After this phase, MRD levels are measured, and an intensification of the treatment is implemented in those patients whose MRD levels are higher than 1%. With this adjustment, clinical remission is achieved in 96-99% of the patients.[30]

1.1.4.2 Intensification-Consolidation Therapy

The aim of ***intensification-consolidation therapy*** is to reduce the risk of relapse, by eradicating residual drug-resistant leukemic cells. Although the relevance of this phase is unquestionable, a consensus on the best regimens and time of treatment has not been established yet. However, the *administration of high-dose methotrexate plus mercaptopurine*, a *re-induction treatment* using the same agents that were administrated at the beginning, along with *frequent pulses of vincristine and corticosteroid plus high-dose* ***asparaginase*** for 20–30 weeks, are among the most regularly used strategies.[30,32,33]

1.1.4.3 Maintenance-Continuation Therapy

The aim of ***maintenance-continuation therapy*** is to continue preventing possible relapses. For this purpose, ALL patients undergo chemotherapy based on daily intake of mercaptopurine or thioguanine and weekly intake of methotrexate, sometimes with the addition of vincristine pulses, for 2-2.5 years.[6,28,34] An adherence to the therapy regimen lower than 90% is associated with a 4-time higher risk of relapse.[35]

1.1.4.4 Allogenic Haemopoietic Stem Cell Transplantation and CNS-directed treatment

Allogenic Haemopoietic Stem Cell transplantation (HCST) represents the most intensive and invasive treatment in ALL. It is often needed in patients with high risk and very high risk forms of ALL, in which, despite the standard treatment, relapses occur very often (15-20% of childhood ALL cases).[36] The prevention of *CNS leukemia* is crucial in order to obtain a positive outcome. Nowadays, low levels of cranial irradiation have been restricted to smaller subtypes of higher risk patients, and have been gradually compensated by *intensification of remission therapy* and *intrathecal chemotherapy*, which consists in the direct administration of the chemotherapy in the CSF.[6]

1.1.5 High Risk forms of Childhood ALL and Minimal Residue Disease (MRD)

It is well established that, despite the high rate of 5 years overall survival (OS) in cALL patients, which is assessed around 90%,[37,38] a significant worse outcome is observed in some subsets of patients.[30,39] So far, **risk stratification** represents the principal mean to predict the average outcome of a group of patients and to establish which interventions could modify the risk towards a favorable outcome.[40] Aiming to increase the chance of a favorable prognosis also for the 10% of the patients which fail to reach 5 years OS, a continuous optimization of the combination of factors which should be considered during risk stratification was pursued in recent clinical trials.[40]

1.1.5.1 High risk factors

It is clear that a worse outcome correlates with the recurrent relapse of the disease. Therefore, every factor which is associated with an increased risk of relapse has to be considered in the risk stratification.

Age at diagnosis is one of the ***clinical factors*** most predictive of the risk of relapse, with a consistently increased risk associated with older age. Infants represent an exception (< 1 year: high risk; < 3 months very high risk), where the presence of *MLL* rearrangements (75%) is associated with very poor prognosis. Another important predictive factor of the risk of relapse is CNS stage at time of diagnosis, with CNS3 status (presence of overt leukemia assessed in the CNS) being associated with a short event-free survival (EFS),[41,42] and CNS2 status (fewer than five leukocytes/µl with detectable blasts found in CSF) being also associated with poor prognosis.[34,44,46] Finally, Down Syndrome (DS) patients diagnosed with ALL have both higher risk of relapse and higher rate of treatment-related mortality (TRM).[25]

Some ***disease-related factors*** must also be considered. For patients diagnosed with T-ALL, prognostic factors result to be less clear. However, a specific subtype of T-ALL, called **Early T cell precursor (ETP) ALL** (10-15% of childhood T-ALL cases), is consistently associated with poor prognosis. [45] Patients with **high hypodiploidy** (<44 chromosomes), ***TP53/IKZF1*** genetic

alterations, intrachromosomal amplification of chromosome 21 (**iAMP21**) and **Philadelphia chromosome,** as well as **Ph+ like ALL,** have a higher risk of relapse. [39, 46–52]
Failure to obtain remission after 4-6 weeks of induction-remission therapy occurs in 2-3 % of childhood ALL patients, and it often correlates with unfavorable prognostic factors and high risk of relapse.[52] To date, the most important parameters considered for the evaluation of early response to treatment (***response factor***) are: ***prednisone response***, with *poor responders* (> 1000/µl blasts on day 8) correlating with poorer outcome; [53] ***BM Morphological assessment***, with an M1 marrow (< 5% blast) picture being a good response; [54] ***MRD measurement***, which proved to be the most important prognostic factor in recent years.

1.1.5.2 MRD monitoring in ALL: state of the art
Minimal Residue Disease (MRD) is defined as the *presence of resistant leukemic blasts after therapy administration at a level below the limit of conventional morphological detection*. It has been demonstrated that MRD levels represent the most important independent predictive factor of the risk of relapse by several randomized studies.[26,55–58]
However, the lack of standardized methods for its measurement, with strong sensitivity and reliability, represented an obstacle to its incorporation into treatment protocols. This issue was largely addressed during recent years, and current methods for MRD monitoring and their implications in risk-adapted therapy are summarized in **Table 5**. In early assessments (at the end of induction therapy), when a rapid turn-around time is required, *Flow cytometry* or *PCR-based methods* are more desirable, while at later stages (post-remission monitoring), a more sensitive method such as NGS should be preferred, as it may provide more sensitive identification of patients at higher risk of relapse.[27]

Table 5. MRD monitoring analysis techniques

Quantitative Real Time PCR (qPCR)	Immunoglobulin (IG) T-cell receptor (TCR) loci	standardized by Euro-MRD group; [59,60] theoretical sensitivity of 10^{-4} to 10^{-5} [27]
Multiparametric Flow Cytometry	detection of *leukemia-associated immunophenotypes (LAIPs)*	Standardized antibody panels, validated by the EuroFlows Consortium; [58] theoretical sensitivity of 10^{-4}
	"difference from normal" approach	more challenging standardization of the technique; [27] theoretical sensitivity of 10^{-4}
NGS	Immunoglobulin (IG) T-cell receptor (TCR) loci	high-level multiplexing capability, requires bioinformatic expertise

1.1.5.3 Treatment optimization for High risk ALL
The most significantly improved outcome in high risk patients was achieved with the intensification of conventional chemotherapy, associated, in a small percentage of patients, to HSCT at first remission.[40]
In high risk patients, **induction therapy** consists of the administration of four or more chemotherapy agents, including *vincristine*, an *anthracycline* (doxorubicin or daunorubicin), an ***asparaginase product*** and either prednisone or dexamethasone. As already mentioned, dexamethasone results to be more effective, but associated with higher risks of acute and long-term toxicities.[61] Intensification therapy is usually administered in high risk patients for 6-8 months after induction. Several intensification regimens have been tested in clinical trials, all including dexamethasone as corticosteroid, an ***intensive use of asparaginase formulations***,[62,63] along with an intensification of *consolidation treatment*.[64]

1.2 L-Asparaginase (ASNase)

L-asparaginase (**EC 3.5.1.1**) (ASNase) is an amidohydrolase. ASNase shows a *prevalent L-asparaginase activity*, catalyzing the hydrolysis of asparagine, and a *secondary L-glutaminase activity*, catalyzing the hydrolysis of glutamine.[65] Its therapeutic benefit comes from the depletion of asparagine from the blood stream, on which leukemic cells depend, given their absent or compromised capability to express asparagine synthetase (EC 6.3.5.4) under stress conditions.[66] Its mechanism of action is furtherly illustrated in paragraph 1.2.3.

1.2.1 Clinical Usage of L-Asparaginase

L-Asparaginase (**ASNase**) is a crucial component of the combination chemotherapy used for the treatment of cALL (childhood Acute Lymphoblastic Leukemia), having increased complete remission achievements in patients since its introduction in 1970s.[66] A unique standardized protocol for the administration of ASNase does not exist. In fact, the several preparations of ASNase on the market and the risk-based therapy concept, make the setting of a universal single protocol challenging. As a consequence, several protocols have been tested over the world by different groups. Historically, one of the most important protocol for the treatment of ALL is the classic Berlin-Frankfurt-Münster (BFM), introduced in 1970s.[67] The BFM is one of the most active and expert group in this field, and its protocols represent an important reference point worldwide. A table summarizing the most important groups involved in ALL treatment clinical research is reported below (**Table 6**).[68]

Table 6. Worldwide Groups and Institutions active in ALL clinical research [68]

Country	Group/Institution
United Kingdom	Medical Research Council (MRC)
USA	Children's Oncology Group (COG)
Germany	Berlin-Frankfurt- Münster (BFM) Group
Hong Kong	Hong Kong Pediatric Hematology and Oncology Study Group
Italy	Associazione Italiana di Ematologia e Oncologia (AIEOP)

Nevertheless, some general guidelines and considerations about ASNase usage in ALL therapy can be made. ASNase is always administrated during *remission-induction* therapy and *intensification-consolidation* therapy. In high risk and very high-risk patients, the usage of a very intensive ASNase regimen is recommended, along with its administration in *re-induction*, *post-induction* and *maintenance* therapy.[69,70] Several studies underlined that dosage intensity and overall duration of ASNase regimen have a stronger impact in favoring a positive outcome than the type of ASNase preparation used.[32,71,72]

1.2.1.1 ASNase types and formulations

Three types of ASNase are currently approved for the treatment of ALL: native Type II ASNase isolated from *E. coli* (EcAII), a pegylated form of *E. coli* Type II ASNase (PEG-ASNase), and a Type II ASNase isolated from *E. chrysanthemi*.

From a biochemical point of view, *E. coli* ASNase shows a marked asparaginolytic activity and a poor glutaminolytic one. *E. chrysantemi* ASNase, at comparable asparaginolytic activity, shows a higher glutaminolytic one, as indicated by its greater K_{cat} (**Table 7**).

Table 7. Biochemical properties of different ASNase [67,73]

	Asparagine		Glutamine	
Source organism	**Km (mM)**	**Kcat (mM)**	**Km (mM)**	**Kcat (mM)**
E. coli	0.015	24	3.5	0.33
E. chrysanthemi	0.058-0.080	397-440	1.7-6.7	65-72

Therapeutic asparagine depletion levels are achieved with an ASNase activity ≥ 0.1 IU/ml.[74–76] However, in order to correctly understand the relationship between asparagine depletion and ASNase dose and activity and to set up an optimal treatment regimen, several factors have to be considered. The most important are ***ASNase formulation***, ***route of administration***, ***interpatient variability*** and ***anti-ASNase antibody formation***.[73]

The pharmacokinetics properties vary remarkably between distinct ***ASNase formulations*** (**Table 8**).[77]

Table 8. Pharmacokinetic characteristics of the three ASNase formulations.[78–80]

	Native *E. coli* ASNase	PEG-asparaginase ASNase	*E. chrysanthemi* ASNase
Half-life (mean ± SD)	0.7 days	1.7 days	0.65 days
Asparagine depletion	14-23 days	26-34 days	7-15 days
ASNase activity peak	24-48 h	72-96 h	Within 24 h

E. coli native ASNase (commercially available as *Kidrolase*® or *Spectrila*®), has a median half-life of ∼17 h,[78] reaches the peak of asparaginase activity within 48 hrs and maintains an effective asparagine depletion for ∼ 18.5 days.
E. coli PEGylated ASNase (commercially available as *Oncaspar*® or *Calaspargase*®),[81] is the native *E. coli* ASNase chemically conjugated with polyethylene glycol (PEGylation). This formulation shows a median half-life of 1.7 days,[79] reaches the asparaginase peak of activity within 96 hrs and maintains an effective asparagine depletion for ∼ 30 days.
E. chrysanthemi ASNase (commercially available as *Erwinase*® or *Crisantaspase*®) has the shortest median half-life (IV 6 h; IM 16 h),[80] along with the shortest asparagine depletion time (∼ 11 days). It reaches the asparaginase activity peak within 24 h.
E. coli native and *PEGylated ASNase* are both considered first-line drugs, even if the longer half-life of PEG-ASNase makes it preferable. *E. chrysanthemi* ASNase is instead used as a second-line drug when hypersensitivity reactions to *E. coli* ASNase preparations occur in patients.[82]
ASNase formulations can be administrated both *intravenously (IV)* or *intramuscularly (IM)*. The first route is preferred in Europe, while the second in the US.[73] These two ***routes of administration*** have an important impact on pharmacokinetics parameters. For instance, IV administration allows to use high-continuous-dose schedules, but correlates with drugs shorter half-life. [77,83–85] Therefore, an increase of dose or frequency may be needed when ASNase is administered intravenously.[73]
A significant ***interpatient variability*** in ASNase levels was observed between patients under the same treatment regimen.[86–88] This underlines the importance of measuring serum ASNase activity during treatment, in order to monitor asparagine depletion.
Finally, ***anti-ASNase antibodies production*** in patients under treatment can cause hypersensitivity reactions and severely affect the drug efficacy, as better described in paragraph 1.2.2.

1.2.2 Side effects and limitations

Although ASNase is an essential component of ALL treatment, several limitations remain in its therapeutic use, especially for the associated side effects, mainly due to its systemic effect and immunogenicity, which are briefly discussed below.

Given its bacterial origin and large size, ASNase is a highly **immunogenic** protein, thus able to elicit an immune response in patients, leading to anti-ASNase antibody formation.[89] The occurrence of adverse immune reactions towards ASNase is referred to as hypersensitivity. Such reactions can be classified as *subclinical hypersensitivity* (***silent inactivation***) or *clinical hypersensitivity*.

Subclinical hypersensitivity or Silent Inactivation consists in the production of anti-ASNase antibodies, which results in reduced ASNase enzymatic activity. During remission-induction phase, silent inactivation can occur in up to 29% of patients,[90] with even higher rates at the time of relapse.[91,92] The major risk of this condition consists in the presence of levels of asparagine depletion lower than required, causing ineffective treatment. For this reason, the regular monitoring of ASNase activity is highly recommended by many reports.[86,87,93] The early identification and addressing of this condition are in fact associated to improved outcomes.[93]
Clinical Hypersensitivity reactions are graded from 1 to 4 according to their severity. Grade 1/2 correspond to infusion reactions correlated to IM and IV administration,[94,95] while grade 4 corresponds to anaphylactic shock.[70] The risk of anti-ASNase antibody formation increases with renewed prolonged exposure to ASNase after a break from the treatment, explaining the high occurrence of such episodes during consolidation and re-induction treatment.[96] Simultaneous administration of corticosteroids can reduce hypersensitivity symptoms; thus, they could be administered as a pre-medication.[90,94,97–100] However, this is not recommended, since it could hide silent inactivation, causing a delay in the identification of anti-ASNase antibody formation and leading to a prolonged reduction of ASNase activity in patients under treatment. For this reason, it is advisable to administer glucocorticoids, which are part of ALL multi-drug therapy, before ASNase doses.[70] The incidence of hypersensitivity is higher in patients treated with *E. coli* native ASNase than in patients treated with PEG-ASNase and *E. chrysanthemi* ASNase.[97] Patients in which hypersensitivity reactions are observed should immediately switch to a different ASNase formulation. Since a switch from *E. coli* native to *E. coli* PEG-ASNase is not possible, due to antibody cross-reactivity, an immediate switch to *E. chrysanthemi* ASNase is recommended.[90,91,97,99,100]
In the US, the FDA-approved dosage substitution is 25000 IU/ml three times a week for six doses, for each dose of *E. coli* ASNase previously planned.[82]

The incidence of acute **pancreatitis** (grade 3-4) in ALL cases lies between 5-10%.[101–106] The most probable role of ASNase in the pathogenesis of this condition consists in the systemic depletion of asparagine and the consequently reduction of protein synthesis.[103] Both *clinical features*, such as abdominal pain, nausea and vomiting, and *laboratory analysis*, such as elevated amylase and lipase, are considered for the diagnosis. In some patients, it can lead to multiple organ failure and be fatal.[70] Thus, ASNase treatment should be interrupted in case of severe pancreatitis,[101,107] and re-exposure to ASNase should be monitored very carefully, since pancreatitis recurrence occurs in 63% of patients.[104]

Lower levels of proteins involved in coagulation and fibrinolysis are a consequence of ASNase activity. ASNase treatment is therefore associated with an increased **risk of thrombosis** and bleeding.[108–112] The incidence of bleeding associated to ASNase treatment events is 5% in cALL, with **intracranial hemorrhage** incidence lower than 0.5%.[70]

The incidence of **neurological complication** is lower than 10% in ALL cases. The most common neurological conditions associated to ASNase treatment are visual abnormalities, seizures, lethargy and coma. The development of hyperammonemia due to ASNase asparaginolytic activity could also be associated to encephalopathy.[113–115]

ASNase treatment is commonly associated with **liver toxicity**, with dysfunctions and abnormalities in hepatic transaminases, bilirubin and alkaline phosphates.[116] Again, ASNase-induced protein synthesis reduction is believed to play an important role.[107] However, the simultaneous administration of ASNase and other drugs with known hepatotoxic effects (e.g. corticosteroids, alkaloids, anthracyclines, and antimetabolites) makes it difficult to establish the impact of ASNase alone on the liver.[96]

ASNase treatment is associated with a reduced insulin production, possibly due to a decreased expression of insulin receptors.[117,118] Since corticosteroids administration is associated with a more intense hepatic gluconeogenesis and insulin resistance, **hyperglycemia** is more frequently observed during ALL treatment phases which requires both ASNase and glucocorticoids.[117,119]

Alterations in lipids metabolism are also associated with ASNase treatment. Again, the known role of corticosteroids in the transient elevation of triglyceride levels[120] makes ASNase role unclear in combined therapies, where 67% of patients develop **hypertriglyceridemia**.[121] Hypertriglyceridemia is usually transient and asymptomatic, but patients in which triglyceride levels are particularly high should be closely monitored for symptoms of pancreatitis.[121,122]

In **Adult Young Patients** (AYA, 16-39 years of age), **higher ASNase-associated toxicity** is observed. Hence, AYA treatment protocols strictly limit ASNase usage.[123] However, recent evidence suggests that AYA patients who are included in pediatric protocols, which are based on intensive ASNase therapy, show a greater long-term survival, suggesting that also these patients could greatly benefit from ASNase treatment.[124–128]

1.2.3 Structure and Mechanism

1.2.3.1 L-Asparaginases reaction and types

L-Asparaginases are amidohydrolases (EC 3.5.1.1) which catalyze the simple hydrolysis of L-Asparagine (L-Asn) into ammonia and L-Aspartate (L-Asp). To a different extent, they also show a secondary L-Glutaminase (L-Gln) activity, resulting in the release of ammonia and formation of L-Glutamate (L-Glu) (**Fig. 1**).

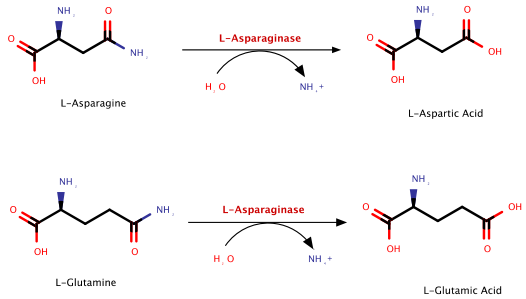

Fig. 1 ASNase Catalytic reactions.

Bacterial L-Asparaginases, especially those derived from *E. coli*, are the most studied and clinically relevant. They are divided into two distinct classes: Type I and Type II.
Type I L-ASNases are constitutively expressed by cells in the cytoplasm. They catalyze both asparagine (Asn) and Glutamine (Gln) hydrolysis, with higher catalytic efficiency displayed *vs* Asn, despite its low binding affinity (K_m *vs* Asn, mM). They lack antitumoral activity.[129]
Type II ASNases are periplasmic protein expressed only under oxygen or nutrients stress conditions. They show a high affinity for Asn (K_m *vs* Asn, µM) and a lower affinity for Gln. They show antitumoral activity, with the most studied and clinically relevant enzyme being ***E. coli* ASNases Type II (EcAII)**. From this point onward, the discussion will focus on the **EcAII** enzyme.

1.2.3.2 Catalytic mechanism

The catalytic mechanism of ASNases has been compared to the classic serine protease one, which relies on the presence of a "catalytic triad", consisting in a Serine (Ser)- Histidine (His)-Aspartate (Asp) configuration found within the enzyme active site. [130] The three residues are connected through hydrogen bonds, which drive a charge re-distribution, granting a functional configuration. The Ser represents the nucleophilic residue, which is activated by a hydrogen bond

with a nearby general base, here represented by the His residue. His itself is engaged in a hydrogen bond with an acidic residue, here represented by Asp (**Fig. 2**).
L-ASNases show two highly conserved uncommon catalytic triads. The first, composed by Thr-Lys-Asp, is mainly involved in the *catalysis of the reaction*, while the second one, composed by Thr-Tyr-Glu, is involved in *substrate binding* and *products release*. EcAII catalytic reaction occurs in two steps, both consisting in a nucleophilic attack (**Fig.3**).

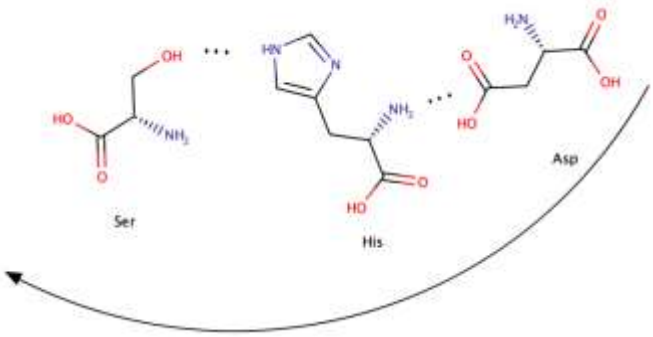

Fig. 2 Schematic representation of a standard catalytic triad. *Ser, the nucleophilic residue, is involved in a H-bond with His, a basic residue, which is in turn involved in a H-bond with Asp, an acidic residue.*

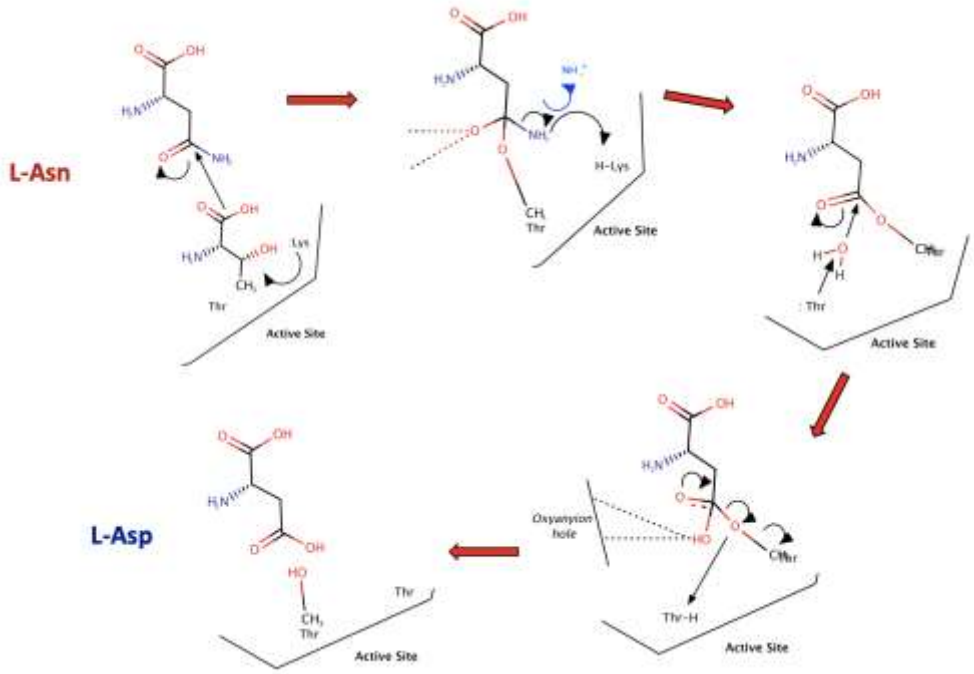

Fig. 3 Proposed mechanism for EcAII catalytic cycle*. Modified from Michalska 2006.*[129]

In the first step, the strong OH…B(Lys) hydrogen bond activates the enzyme's nucleophile, which is represented by the first Thr. The activated nucleophile attacks the C atom of the amide substrate, leading to the formation of an acyl-enzyme intermediate product *via* a tetrahedral transition state. The negative charge delocalized on the O atom of the amide group during the transition state is stabilized by hydrogen bonds formation with main chain NH groups, and it is called "oxyanion hole". In this first step an ammonium ion is released. The second step of the reaction consists in another nucleophilic attack driven by an activated nucleophilic molecule of water, which attacks the ester C atom, leading to the product formation (L-Asp) *via* another transition state, again characterized by the formation of an oxyanion hole.[129]

1.2.3.3 EcAII Structural aspects

Bacterial L-Asparaginases Type II are **homotetrameric proteins**, where each monomer is composed of 326 amino acids, has a mass of ~ 35,5 kDa, and consists of two α/β domains connected by a random coil of ~ 21 amino acids [PDB: 3ECA].[131] The **N-terminal domain** secondary structure shows an 8-stranded mixed β-sheet and 4 α-helices (**Fig. 4**).

Helices Nα1 and Nα4 are placed on the solvent-exposed side of the β-sheet, while Nα2 and Nα3 are located on the interface side. A directional change is observed between Nβ1 and Nβ3 strands: their C-ends fold into α-helices developing in opposite directions. This creates a cleft which serves as a pocket for the ligand binding. In the N-domain, a rare left-handed crossover between Nβ4 and Nβ5 is also found, which is characteristic of all bacterial L-ASNases.[132] Moreover, a disulphide bond unique to EcA molecules is found in the N-domain between Cys 77-Cys 105.[133] The **C-terminus domain** is smaller, and consists of a 4-stranded parallel β-sheet, plus 4 α-helices. Helices Cα1 and Cα2 are placed on the distal side from the interface, while Cα3 and Cα4 are placed on the interface.[131]

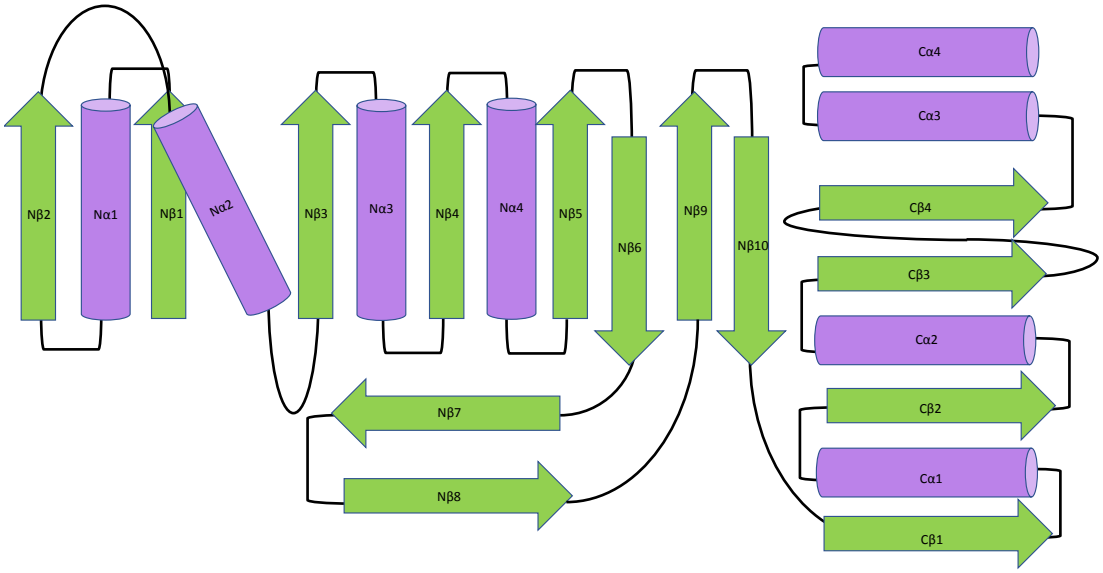

***Fig. 4 Topology representation of L-Asparaginase monomer**. Left: N-domain, Right: C-domain. α-helices are represented as purple cylinders, β-strands as green arrows, loops are colored in black. Modified from Swain 1993.*[131]

EcAII tetrameric structure, which shows a 222 symmetry, has been defined as a "*dimer of intimate dimers*".[129] In fact, each subunit interacts with nearby ones through *intimate contacts* and *distant contacts*. Massive intimate contacts are observed between subunits A/C and subunits B/D, which are therefore called **intimate dimers** (**Fig. 5**).

The formation of the enzyme active sites occurs at the interface of the intimate dimers. Two active sites for each intimate dimer are present, formed by residues mainly located at the N-termini and a single residue from the intimately bound subunit.[131] Four active sites are operative in a single tetrameric EcAII molecule, which represents the only enzyme active form.[131] The active site consists of flexible loop (14-27) and a rigid structure. Highly conserved residues are found in this region, and are involved in the catalytic mechanism. A pair of Thr residues, Thr12 and Thr89, are placed at opposite sides of the substrate scissile bond. Thr12 and Tyr25 are located on the flexible loop, while Thr89, Lys162, Asp90 and Glu283 are located in the rigid region.[134]

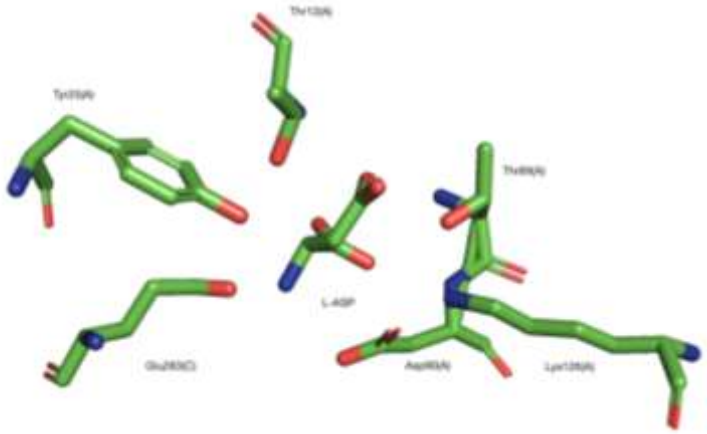

Figure 5 EcAII Catalytic Triads (PDB:3ECA). *Stick representation of the residues constituting the catalytic triads and of the L-ASP product (light purple).*

Their spatial organization and the relationship between Thr89, Lys162 and Asp90 was strongly associated to the classic Ser-His-Asp catalytic triad.[130,135] However, the engineering of a T89V mutant clearly defined that the primary nucleophile is represented by Thr12, and not by Thr89 [PDB: 4ECA].[136] An alternative triad, consisting in Thr12-Tyr25-Glu283 was later proposed.[137] However, the chemical properties of Tyr25 are not compatible with those of a general basis, while evidence of Tyr25 importance in providing a spatial orientation to Thr12 favorable for catalysis was reported.[134,138] Moreover, Glu283 resulted to be inessential for the catalysis to happen, discouraging a Thr12-Tyr25-Glu283 triad hypothesis.[139] Therefore, the actual accepted mechanism is the one proposed above, with Thr12-Lys162-Asp90 as a catalytic triad and Thr89-Tyr25-Glu283 residues involved in mediating crucial interactions within the active site, such as substrate binding and product release.[140]
The residues forming more interactions with the other possible substrate, L-glutamine, are instead Gln59, Thr89 and, to a smaller extend, Asp90 and Lys162.[65]
Since the active sites of the enzymes are deeply buried at the interfaces of intimate dimers and therefore not directly exposed to the solvent, the enzyme activity results to be stable in a wide range of pH (4.5-11.5), with a pH optimum value of 6.0.[141] The enzyme works at an optimum temperature of 37°C.

1.2.3.4 EcAII Kinetics
EcAII has a hyperbolic kinetics *vs* both Asn and Gln, and shows a strong preference for L-Asparaginase, which represents its primary substrate. Kinetic parameters of EcAII are summarized in **Table 9** .[67]

Table 9. Kinetic properties of EcAII

	Asn			**Gln**		
	Km (mM)	**Kcat** (s^{-1})	**Kcat/ Km**	**Km** (mM)	**Kcat** (s^{-1})	**Kcat/Km**
EcAII	0.015	24	1600	3.5	0.33	0.01

An enzyme **substrate binding affinity** is represented by the $\mathbf{K_m}$ parameter, which corresponds to the *substrate concentration at which the reaction rate is half maximal*. The **maximal catalysis rate ($\mathbf{V_{max}}$)** corresponds to the *rate of conversion obtained at saturating concentrations of substrate*. Therefore, the lower the Km, the higher the substrate affinity. EcAII K_m *vs* Asn (15 μM) is around 200-fold lower than the one *vs* Gln (3.5 mM).[67]
Another important kinetic parameter for enzymatic catalysis is the **turnover number ($\mathbf{K_{cat}}$)**, which corresponds to the *number of reactions catalyzed by each active site of the enzyme in a*

discrete time unit, typically seconds. Efficient enzymes have high K_{cat} values. EcAII kcat (s^{-1}) *vs* Asn is 24, while *vs* Gln is 0.33.
A last important parameter used in order to measure the **catalytic efficiency** of an enzyme is represented by the **K_{cat}/K_m ratio**; the higher it is, the more efficient the enzyme is.

1.2.3.5. Cancer cells metabolic addictions

It is well known that cell metabolism is significantly reprogrammed in cancerous cells. This can lead to the development of the so-called metabolic addictions, that several types of cancer present towards specific metabolic substrates, such as sugars, lipids and in particular amino acids (**Table 10**). Metabolic addictions are becoming more and more important for the development of targeted therapies, tackled especially through enzyme-based drugs, among which Asparaginase is the most solid example.[142]

Table 10. Cancer Amino acid addiction (modified from Maggi, Scotti 2019)[142]

Tumor Type	**Addiction substrate**	**Role**	**Enzymatic activity for therapy**
CNS tumors	Methionine	Biosynthesis of GSH and polyamines	L-methioninase
ALL Ovarian carcinomas Non-Hodgkin lymphoma	Asparagine	Protein synthesis Cell cycle progression	Asparaginase
Ovarian cancer ALL Hepatoma	Glutamine	Protein synthesis Amino nitrogen transporter	Glutaminase
Melanoma Hepatocellular carcinoma Small cell lung carcinoma Pancreatic carcinomas	Arginine	NO synthesis	L-Arginine deaminase
Breast cancer	Glycine	Purine synthesis	Glycine Deoxidase
Breast cancer	Serine	Glutamine synthesis	Serine deaminase
Prostate cancer Burkitt lymphoma	Proline	Glutamine synthesis	Proline dehydrogenase
Melanoma	Tyrosine	Melanin and hormones synthesis	Tyrosine transaminase
Prostate cancer	Phenylalanine	Melanin and hormones synthesis	Tyrosine transaminase

1.2.3.5.1 ASNase antitumoral mechanism: Asparagine depletion

The dependence of leukemia cells on asparagine extracellular supply is considered to be the cause of the L-ASNases antitumoral effect.[143]
The role of Asparagine in cells, including leukemic ones, it is not limited to its confirmed use in protein synthesis,[144–146] since recent evidence also showed an involvement of Asn in the coordination of nucleotide synthesis.[147]
Asparagine is not an essential amino acid. In fact, most human healthy cells are able to synthetize Asn *de novo* through Asparagine Synthetase (ASNS), an enzyme which catalyzes the conversion of aspartate and glutamine into asparagine and glutamate, in an ATP-dependent reaction (**Fig. 6**).[148]

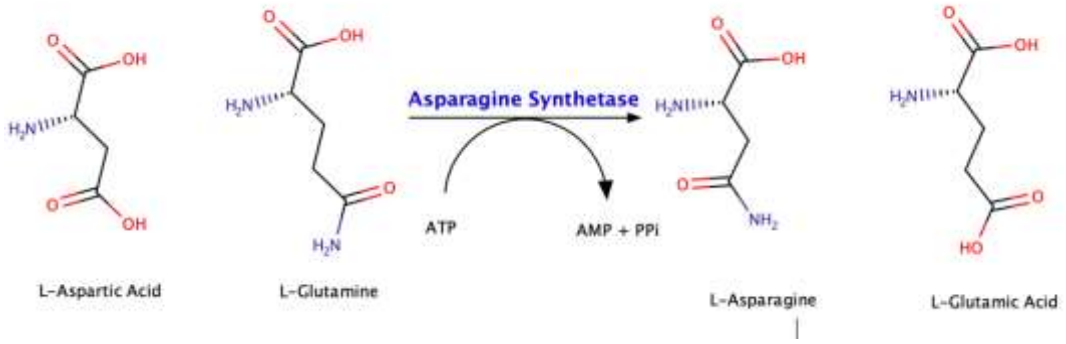

Fig. 6 Asparagine synthetase catalytic reaction.

However, the expression of the *ASNS* gene is strictly regulated, and only through its upregulation human heathy cells are able to compensate for Asn depletion in the blood. *ASNS* gene upregulation is mediated by the *integrated stress response* (*ISR*), or *amino acid response* (AAR).[149] This response is triggered by amino acid deprivation, which causes uncharged tRNAs to accumulate inside the cells, which causes the direct activation of GCN2 (general control nonrepressible 2). GNC2 is a kinase protein which represents a fundamental check-point in the regulation of global protein synthesis. In fact, its binding to uncharged tRNAs increases its kinase activity towards eIF2 (eukaryotic Initiation Factor 2 complex). The phosphorylation of the eIF2 mediated by GNC2 results in a general protein synthesis reduction *via* mTOR pathway and energy conservation required for cell survival, [150] and in the promotion of the translation of a subset of mRNAs, mainly encoding for self-defense proteins and apoptosis-mediating proteins. Among this sub-population of mRNAs, there is ATF4 (Activating Transcription Factor 4), which is responsible for the upregulation of *ASNS* gene expression.[150]

The reason for leukemia cells Asn dependence relies in their *reduced* or *complete loss of ASNS expression*, even though the precise molecular basis of this phenomenon has not been fully elucidated yet.[151] According to the general proposed scheme, ASNase catalytic activity depletes the Asn pool in blood, depriving leukemic blasts of their extracellular supply. Leukemic blasts inability to express ASNS in order to catalyze Asn *de novo* synthesis leads them to cell cycle arrest and apoptosis, as a consequence of amino acid starvation (**Fig. 7**).

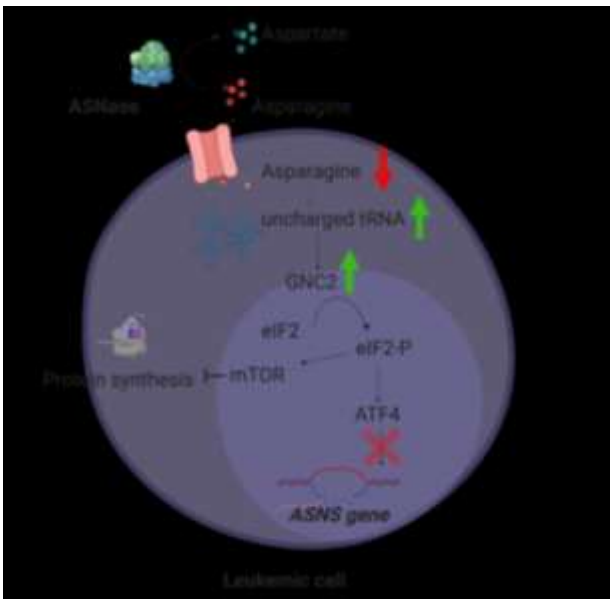

Fig. 7 Proposed mechanism for leukemic blasts dependence on Asn extracellular supply.

A lot of evidence supports the strong correlation between ASNS protein expression in cancerous cells response to L-asparaginase treatment.[152–155] Actually, leukemia cells can be stratified into *high ASNS* and *low ASNS*, with high ASNS blasts being the most resistant to ASNase therapy.[65] However, from a clinical point of view, such correlation has not been confirmed yet. In fact, a correlation between ASNS upregulation and early poor response in children was not found.[156,157]

1.2.3.5.2 ASNase antitumoral mechanism: Glutamine depletion

Glutamine represents the most abundant amino acid in the cytoplasm, with a tissue-dependent concentration that can reach 20 mM.[158] Moreover, Glutamine plasmatic concentration ranges from 600 to 900 μM, making Gln the most abundant amino acid also in the human blood,[158] with a concentration ten times higher than that of Asn.[159]

As previously reported, L-Asparaginases show a secondary catalytic activity towards Glutamine. For many years, Asparaginase activity was held responsible for the drug antitumoral effect, while Glutaminase activity was considered accountable for the severe side effects correlated to ASNase therapy.[160] However, controversial evidences were reported in the past years. The engineering of an EcAII lacking L-Glutaminase activity (Q59L mutant)[65] demonstrated that glutaminase activity is essential in order to have a cytotoxic activity against leukemic blast expressing high levels of ASNS. In fact, as showed in **Fig. 6**, glutamine is a substrate of ASNS in the asparagine synthesis reaction. High ASNS leukemic cells are able to restore their intracellular asparagine pool using glutamine, when a therapeutic glutaminase activity is absent. On the contrary, in negative ASNS cancer cells, asparaginase activity alone was sufficient to obtain a complete cytotoxicity. These findings therefore suggest that glutaminase activity benefits and risks should be evaluated according to protein levels of ASNS expressed by leukemic blasts.[65]

Another important consequence of the ASNase-induced glutamine reduction is the specific inhibition of the mTOR pathway, not observed when using ASNases lacking glutaminase activity.[67] mTOR pathway inhibition causes the suppression of protein synthesis, leading to cell cycle arrest and eventually cell death.[161] In particular, in AML cells a cytotoxic effect correlated with glutaminase activity levels from both *E. coli* and *E. chrysanthemi* L-asparaginases was observed. The cytotoxic effect was caused by a significant inhibition of mTORC1, which triggered a strong autophagic response and apoptosis.[162]

In conclusion, the predominant opinion still considers glutaminase activity as the main responsible for the toxic effects of ASNase,[160,163,164] but it is now assessed that glutaminase activity is needed in order to maintain a sustainable Asn depletion, especially in case of high ASNase cancerous cells.[90,165]

1.2.3.5.3 ASNase resistance mechanisms

Extensive clinical data support the benefit of ASNase treatment,[32,76,166] and it has been demonstrated that asparaginase resistance is correlated with a poor prognostic factor,[167–170] In recent years, a strong effort was made in addressing ASNase resistance mechanism.[171] Despite some progress, many open questions remain.

ASNS baseline expression and upregulation seem to play a major role. Different studies showed controversial correlations between ASNS baseline expression and ASNase resistance, both in leukemic cell lines and patients' samples.[153,154,172–177] A major contribution in the interpretation of these conflictual data was given by Su et al,[152] who, after estimating ASNase IC_{50} on different cell lines, tested the correspondence between mRNA expression by RTQ-PCR and ASNS protein levels using immunoblotting. They observed a much stronger correlation between IC_{50} and ASNase protein levels than between IC_{50} and mRNA levels, suggesting that protein quantification is more predictive of ASNase resistance than mRNA levels. [178]

ASNS upregulation upon Asn depletion induced by ASNase treatment could also be involved in ASNase resistance. This was observed in *in vitro* experiments on leukemia cell lines, such as MOLT4, where this effect was not fully reversible even after 6 weeks from ASNase removal from

the culture medium.[179,180] Also, in leukemia patients, a 7-time fold increase in ASNS protein expression levels was observed in the asparaginase-resistant group after ASNase treatment.[153] ***Alternative sources of Asn***, as well as of substrates and proteins involved in its synthesis, may play a relevant role in favoring ASNase resistance (**Fig. 8**).

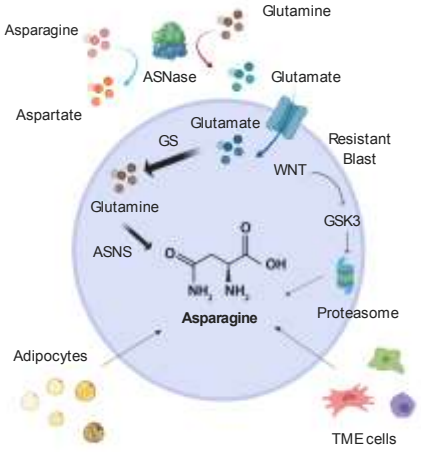

Fig. 8 Principal mechanisms of resistance to ASNase.

First of all, it has been demonstrated that resistant cells are able to produce more *glutamine*, the primary substrate for the synthesis of Asn catalyzed by ASNS, thanks to an increased activity of Glutamine Synthetase (GS). These cells also showed an enhanced uptake of extracellular glutamine via secondary active Na^+-dependent transporters.[179]
Proteasomal degradation pathways could also be a sufficient source of Asn for the compensation of circulating Asn depletion, as suggested by the fact that WNT-dependent inhibition of proteasomal degradation, through the inhibition of glycogen synthase kinase 3 (GSK3), induces the sensitization to asparaginase in resistant sub-types of acute leukaemia.[181]
Tumor Microenvironment (TME) cells are likely involved in the protection of ALL cells from ASNase activity. Bone marrow-derived mesenchymal cells express high levels of ASNS, increasing both their synthesis and secretion of asparagine.[182,183] ALL cells themselves can stimulate ASNS expression and Asn secretion in bone marrow stromal cells *via* the secretion of insulin-like growth factor (IGF)-binding protein 7 (IGFBP7), as demonstrated *in vitro*.[184]
Moreover, an upregulation in the GS gene expression was observed in *adipocytes*, with a consequent increase in glutamine synthesis and release.[182] This supports the correlation between increased ASNase resistance observed in obese children ALL cases.[185,186]

Finally, ***protein synthesis*** is fundamental in all living cells, and unresolved amino acid deprivation leads eventually to cell cycle arrest and cell death. For this reason, it is not surprising that in asparaginase resistant leukemic cells several ribosomal proteins are found to be overexpressed, suggesting an attempt to maintain a sustainable protein synthesis.[173] Moreover, several resistant B-lineage ALL cells showed recurrent upregulation in three among 70 tested genes involved in ***apoptosis regulation.***[187] These confirms that regulatory alterations in apoptosis patterns are likely involved in the development of resistance to ASNase. Among these genes, *BCL2L13* was particularly relevant, since it is already associated with unfavorable clinical outcome.[187]

1.2.4 L-Asparaginase biobetters

Despite being a cornerstone in the treatment of ALL, most of the current ASNase products lack optimal pharmaceutical characteristics, in particular due to their high toxicity, high immunogenicity and reduced blood serum half-life. A lot of effort has been made in the past decades in order to develop ASNase molecules which would overcome those issues. These molecules could be defined *biobetters*.

Biobetters are drugs developed from the original product through chemical or molecular modifications, intentionally designed in order to obtain functionality changes which may include increased half-life, reduced toxicity, reduced immunogenicity, and enhanced pharmacokinetics and/or pharmacodynamics.[66] They represent a new category of biological drugs emerged over the last few years which, due to their correlated reduced commercial risk, are gaining increasing attention from the market.[188,189]

1.2.4.1 ASNase protein engineering

Protein engineering, bioinformatic analysis, molecular dynamics, docking and site-directed mutagenesis are among the most sophisticated techniques used to develop ASNases molecule, mainly with ***reduced glutaminase activity***, ***reduced immunogenicity*** and ***increased in vivo stability***.[190,191]

As previously discussed, ***glutaminase activity*** role is controversial. Despite its confirmed importance in sustaining Asn depletion against ASNS positive leukemia cells,[65] most of the side effects of ASNase treatment can still be attributed to the systemic depletion of glutamine.[192]

L-glutamine is in fact an important amino acid for the metabolism of every organ, and plays a particularly essential role in the CNS, being an important precursor for neurotransmitter synthesis. L-glutamine depletion has been also addressed as one of the main causes of immune system failure, resulting in a reduced synthesis of IgG and IgM.[67]

Therefore, the development of a therapeutic ASNase molecule lacking glutaminase activity could still be desirable, and has been pursued through different approaches. The most important one has been site-directed mutagenesis of commercial ASNase involving amino acids residues surrounding the active site, without being directly involved in substrate interactions. An N248A mutant was developed, since N248A seems to be involved in the formation of hydrogen bonds which influence substrate binding. N248A showed a reduced glutaminase activity but also a strongly compromised asparaginase activity (about 12% of EcAII asparaginase activity).[139] Since L-Glutamine is larger than L-asparagine, another strategy was to develop a double N24A/Y250L mutant, which has a more compact and smaller active site volume and retained ~72% of asparaginase activity, lacking the glutaminase one.[165] However, none of those molecules were furtherly developed, since asparaginase activity was always affected to an excessive extent.

Immunogenicity is the main responsible for the development of hypersensitivity reactions. Hence, its reduction would greatly improve ASNase quality profile. Several studies were performed in order to identify the main epitopes accountable for EcAII immunogenicity, revealing the presence of several B-cell epitopes.[193–195] Site-directed mutagenesis towards some of these epitopes was attempted, with the most promising results obtained by Jianhua et al., (2006), who proposed a sequence change from 195RKH197 to 195AAA197, resulting in reduced enzyme antigenicity. Later Mahboobi et al. (2017) obtained a four mutations-EcAII mutant (L23G, K129L, S263C, and R291F) which presented lower toxicity, higher stability and increased half-life.

Finally, the ***low in vivo stability*** of ASNase preparations, resulting in their short plasmatic half-life, represents a weakness in the drug profile, since frequent administrations are required. This issue can be solved by increasing ASNase resistance to protease degradation, mainly mediated by Asparagine Endopeptidase (AEP) and Catepsin B (CTSB).[196]

Being the N24 residue the primary cleavage site for AEP, a N24G mutant was designed by Patel et al (2009), which resulted resistant to AEP cleavage, but with a significant drop in catalytic activity, as N24 is involved in the active site stabilization.[197] In our laboratory, structural studies lead to the production of an N24S mutant, which shows resistance to proteases derived from leukemia cells and which retains complete original enzymatic activity.[197] These improved biochemical characteristics provide a promising alternative. N24S pharmacokinetic and pharmacodynamic behavior are now under evaluation *in vivo*.

1.2.4.2 Optimization of ASNase formulation

An optimized drug delivery could play a significant role in the reduction of silent inactivation and ASNase proteolysis. ASNase immobilization, which consists in the enzyme confinement into nanostructured materials, could protect the drug from the action of proteases and increase its half-life. Two forms of enzyme immobilization have been investigated for the development of ASNase biobetters: covalent bonds and encapsulation. The best results were achieved through EcAII PEGylation, as proven by the fact that, since the approval of the first ASNase formulation (Elspar®) in the 1970s, the only ASNase biobetter approved for clinical use was PEGylated ASNase (Oncaspar) in 1994.[66]

Protein PEGylation consists of the conjugation *via* covalent bond of the therapeutic protein to polyethylene glycol (PEG), a polymer whose use in therapeutic protein formulation is approved by the FDA. This approach results into increased circulation half-life of the drug, *via* reduced rate of glomerular filtration, without affecting the biological activity.[198–200] PEGylation, in fact, increases the protein hydrophilicity reducing its aggregation, and shields the protein's immunogenic epitopes reducing silent inactivation; in case of anti-drug antibody formation, it protects ASNase from antibody recognition.

Oncaspar, was officially introduced as a first-line drug in the treatment of ALL after FDA approval,[201] showing a half-life 5 and 10 times longer, respectively, when compared to native *E. coli* and *E. chrysanthemi* enzymes.[97,202–204] *Oncaspar*® PEGylation process consists in random attachments of PEG to lysine/N-terminal groups, and results in a mixture of isomers subject to batch-to-batch variations, an important limitation from the reproducibility point of view.[205–207] Another limitation consists in the ability of endogenous esterases to hydrolyze the ester group present in the SS linker of the PEG derivative, which prevents further improvement of *in vivo* stability.[208]

Two new PEGylated ASNases are currently under development: PEG-crisantaspase from *E. chrysantemi* (*Asparec* ®), which is under Phase II and III clinical trials, and *Calaspargase Pegol*®, from *E. coli.* The latter differs from *Oncaspar*® in the SS linker used for the PEGylation, which has been replaced by a succinimidyl carbamate linker, in the attempt to overcome endogenous esterase sensitivity and obtain a more stable conjugation. *Calaspargase Pegol*® was recently approved by FDA.[81]

Nanoencapsulation is based on nanotechnology, a growing field which boasts several FDA-approved nanomedicines, such as antibody–drug conjugates, liposome-based delivery platforms, and albumin-bound nanoparticles. This kind of formulations allow the increase of the permeation and retention effect (PRE), thanks to extravasation from the circulation and accumulation at the tumor site.[209]

Despite several attempts to encapsulate ASNase into nanoparticles and liposomes, none of such formulations is currently in use in the clinical practice, due to the several challenges that they imply.[210] The main issues concern the nanosystems stability in the blood stream, as nanocarriers bind to blood components. Also, aspecific binding to the endothelium must be avoided, as well as uptake by the mononuclear phagocyte system.[211] More recently, an ASNase encapsulated in red blood cells (RBC) (GRASPA ®) was developed.[212] This system was in phase-III clinical trial,[213] but has been recently withdrawn from the experimentation in Europe, due to EMA perplexities about its benefit-risk balance, particularly related to insufficient evaluation of the pharmacokinetic and pharmacodynamic parameters.[214]

Novel approaches are being investigated for the generation of novel ASNase biobetters.

Tabandeh and Aminlari (2009)[215] conjugated ASNase with oxidized inulin, obtaining a better resistance to trypsin digestion and higher thermal stability, longer half-life, reusability after repeated freezing and wider optimum pH range when compared with native ASNase, while Zhang et al. (2005)[216] conjugated ASNase with silk fibroin, obtaining a reduced immunogenicity, along with acceptable residual activity (~ 80%), increased thermal and storage stability, resistance to

trypsin digestion and longer half-life (63 h) when compared to the native enzyme (33 h). However, both of these formulations have still to undergo clinical trials.
So far, the targeting approach through antibody drug conjugates has not been thoroughly explored for ASNase yet. This project aims exactly to explore the feasibility of such an approach in the development of ASNase biobetters.

1.3 Targeting Therapy in ALL

1.3.1 State of the art

Several targeted therapies have been developed during the past decades for the treatment of ALL. The most relevant targeted drugs can be grouped in ***immunotherapeutic***, including *monoclonal antibodies*, *antibody-drug-conjugates*, *Bispecific T-cell engaging*, *CAR-T*, and in ***pathway inhibitors***, such as *tyrosine-kinase inhibitors (TKIs*) and *Notch inhibitors* (**Table 11**).

Table 11. Targeting Therapy in ALL

Immunotherapeutic approaches					
	Mechanism	**Name**	**Target**	**Disease**	**State**
Monoclonal antibodies	antibody-dependent cytotoxicity (ADCC), complement-dependent cytotoxicity (CDC)	Rituximab *(I generation)*	CD20	pre-B ALL, and of adult patients with CD20+, Ph-negative B-ALL.[217]	FDA approved
		Ofatumumab *(II generation)*	CD20	CLL[238,]	FDA approved
		Obinutuzumab *(III generation)*	CD20	CLL.[218]	FDA approved
		Epratuzumab	CD22	relapsing ALL	Clinical Trials-Phase III
		Alemtuzumab	CD52	B and T-ALL and AML[219]	Clinical Trials-Phase I/II
Antibody Drug Conjugates (ADCs)	Targeting and cytotoxic activity	Denintuzumab	CD19/ monomethylauristatinF (MMAF)	lymphomas	Clinical Trials-Phase II
Bi-specific T-cell engaging (BiTEs)	recruiting of cytotoxic T cells and targeting on cancer cells	Blinatumomab	CD3 (Cytotoxic T cells) CD19 (B-cells)	relapsed Ph-positive and Ph-negative ALL[220]	FDA approved
CAR-T Cell Therapy	trigger of T cells cytotoxic activity towards targeted cancerous cells.[221,222]	Tisagenlecleucel	CD19	relapsed pre-B ALL	FDA approved
Pathway Inhibitors approaches					
	Mechanism	**Name**	**Target**	**Disease**	**State**
Tyrosine Kinase Inhibitors	Inhibition of chimeric tyrosine kinases (BCR-ABL1)	Iminatib (I generation)	Tyrosine Kinases	Ph+ ALL and Ph-like ALL	FDA approved
		Dasatinib and Nilotinib (II generation) [223,224]	Tyrosine Kinases	Ph+ ALL and Ph-like ALL	FDA approved

		Ponatinib (III generation)	Tyrosine Kinases	Ph+ ALL and Ph-like ALL	Clinical Trials-Phase I/II
		ABL001[262]	Tyrosine Kinases	Ph+ ALL and CML	Clinical Trials-Phase I
		Entospletinib	Spleen Tyrosine Kinase (SYK)		Clinical Trials-Phase I
Notch Inhibitors	Inhibition of NOTCH1 signalling[225]	LY3039478	Gamma secretase inhibitors	T-ALL	Clinical Trials-Phase I/II

1.3.2 Antibody Drug Conjugates (ADCs)

An important approach used to improve the results obtained in cancer immunotherapy consists in the conjugation of monoclonal antibodies to effector molecules that help accomplishing cell death upon target binding. The effector molecules are also called payloads, and include cytotoxic agents, immunotoxins of bacterial or plant origin, and radiopharmaceutical agents. These bioconjugates are called *Antibody Drug Conjugates* (ADCs).[226]

1.3.2.1 ADCs development, structure and function

An ideal ADC is composed of a monoclonal antibody (mAb) showing high affinity for a tumor-associated antigen, a linker stable in blood but easily cleavable once internalized, and an ultra-toxic payload, that efficiently induces target cell death after its release. Therefore, a proper combination of all these components is crucial for the design of a successful ADC.[227] ADCs approved for hematological malignancies therapies are reported in **Table 12**.

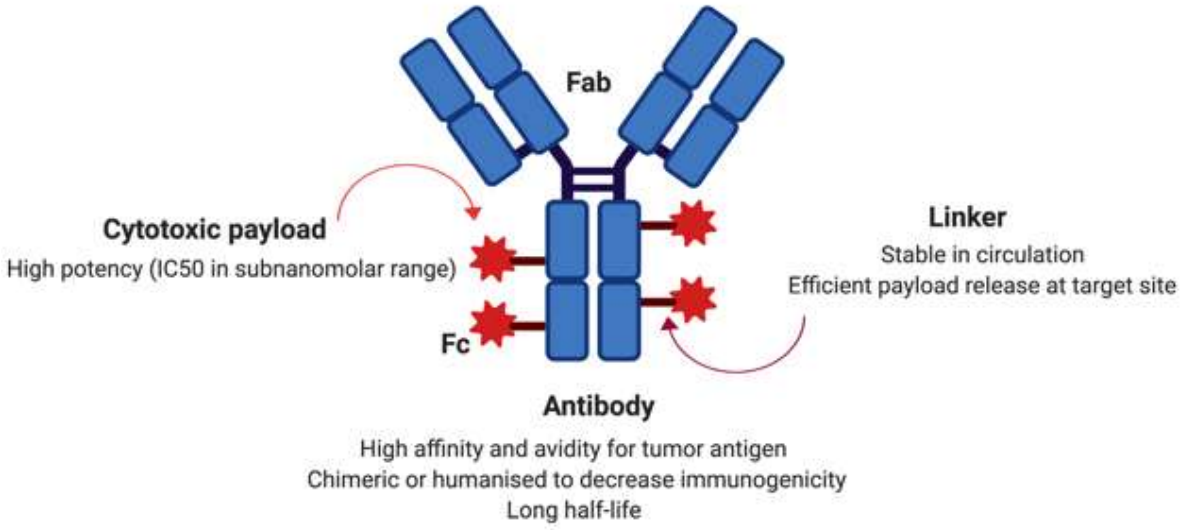

Fig. 9 Schematic representation and important features of an Antibody Drug Conjugate. *Modified from Chau 2019.*[227]

Table 12. Approved ADCs in hematological malignancies

Name	Target	Cytotoxic payload	Mechanism	Disease
Brentuximab vedotin (SGN-35)	CD30	monomethyl auristatin E (MMAE)	tubulin polymerization inhibition [228]	CD30-positive Hodgkin lymphoma, stage III or IV classical Hodgkin Lymphoma, systemic and relapsed anaplastic large-cell lymphoma, peripheral cell lymphoma.[227]
Inotuzumab ozogamicin	CD22	semisynthetic derivative of calicheamicin	double-strand breaks in DNA minor grooves[229]	Relapsed B-ALL (adults)
Gemtuzumab ozogamicin	CD33	calicheamicin	double-strand breaks in DNA minor grooves[229]	CD33 AML (adults) [230,231]
Polatuzumab vedotin-piiq	CD79b	monomethyl auristatin E (MMAE)	tubulin polymerization inhibition [228]	relapsed diffuse large B-cell lymphoma

A proper selection of the **target antigen** represents the major issue in the design of an effective ADC. An ideal target receptor should be expressed homogenously on the surface of cancerous target cells, while showing very low or absent levels of expression on healthy tissues.[232] The extracellular localization of the target receptor is also required, along with its ability to mediate drug-internalization *via* the *endocytic pathway* upon binding, allowing the payload to be released and to act intracellularly.[233]

For the **antibody component**, desirable features are *minimal immunogenicity* (humanized or human antibodies), *high target specificity and affinity*, and *long circulating half-life*.[227]

The last component of an ADC is represented by the **payload**, a **cytotoxic** drug that usually targets DNA or tubulin. DNA-targeted drugs are usually natural antibiotic products, which interact with DNA minor grooves, impairing its replication. Calicheamicins induce double-strand breaks, while duocarmycins and pyrrolobenzodiazepines (PDBs) cause DNA alkylation, by binding specifically to A-T-rich regions (duocarmycins) and guanine residues (PDBs).[232,234,235] Tubulin-targeted drugs are mainly represented by auristatins, which inhibit microtubule polymerization, causing cell-cycle arrest.[236] The payload potency is an important criterion for its selection, and is usually assessed by IC_{50} values in the subnanomolar range in cell culture.[226] The drug to antibody ratio (DAR), defined as the number of payloads molecules conjugated to the antibody, and the site of conjugation, also have a strong impact on ADC potency and toxicity.[227]

Linkers mediating the conjugation are crucial in determining ADCs stability, pharmacokinetic and pharmacodynamic properties, along with therapeutic window.[237–239]

Desirable characteristics for the linker are *stability in the blood stream*, in order to prevent premature cleavage of the ADC and consequent aspecific toxicity, and rapid cleavage once internalized, in order to release the payload.[240]

Linkers are therefore classified in *cleavable* or *non-cleavable*, on the basis of their payload release mechanism. **Cleavable linkers** include those whose payload is released accordingly to the physiological environment, such as: *acid-label linkers*, cleaved in low pH conditions; *protease-cleavable linkers*, sensitive to proteolysis; *disulphide linkers,* sensitive to high intracellular glutathione concentrations.[241] **Non-cleavable linkers** require lysosomal degradation in order to release the payload, and therefore an optimal ADC internalization and trafficking to lysosomes.[242]

1.3.2.1.1 Mechanism of action

The usual route of administration for ADCs consists in the *intravenous* injection. Once circulating, the ADC reaches and binds to its target receptor, triggering the internalization process. Early endosomes containing the ADC-receptor complex are formed. Here, the acidic environment

facilitates the binding of the antibody component to the FcRns primarily expressed in endosomes, and its later recycle to the cell surface.[233,243] Early endosomes mature into late endosomes and eventually fuse with lysosomes. *Cleavable* linkers can already be cleaved into early or late endosomes, *while non-cleavable linkers* require to complete the progression into lysosomal trafficking, in order to achieve complete proteolytic degradation. In lysosomes, a specific acidic environment, created by proton pumps localized on their membranes, facilitates proteolytic cleavage mediated by specific proteases (i.e. cathepsin B and plasmin). The released payload is then transported into the cytosol, where its cytotoxic activity induces apoptosis or cell death.[243]

4. Target Receptors in B-ALL

1.4.1 B cell differentiation and B-lineage restricted antigens expression profile

Hematopoiesis is a long-life process, which consists in the continuous differentiation of hematological cells of different lineages from a common multipotent progenitor. During the differentiation process, the hemopoietic stem cell progeny lose their potency, becoming progressively restricted to different lineages and cell types. For the ***lymphoid lineage***, the lymphoid precursor is restricted to differentiate into *T, B, NK (Natural Killer) lymphocytes* and *dendritic cells*.[244] B lymphocyte development occurs in the fetal liver and bone marrow of adult individuals,[245,246] and it is driven by differential regulation of specific genes.

The surface markers which characterize the early stages of B cell development are CD34, CD22, CD10 and CD19. In particular, as shown in **Fig. 10**, CD19 is the earliest expressed surface marker of B-lineage throughout the whole development, lost only on ultimately differentiated plasma cells.[247] ***CD34+ hemopoietic stem cells*** lack CD19, whose expression in combination with CD10 corresponds to commitment to the B-lineage. ***CD19+ CD10+*** progenitors are called ***proB***, and correspond to the stage in which the rearrangement of immunoglobulin V-D-J genes begins.

The next B-lineage surface markers expressed over B-cell development are ***CD22*** and ***CD20***, whose expression corresponds to ***early*** and ***late pre-B cell stage***, respectively. When the ability to express a functional Ig on their surface is acquired, the ***immature B-cell*** stage is reached, and *downregulation* of ***CD10*** expression occurs. Immature B-cells migrates to the periphery, where they reach maturation. The stage immediately preceding plasma cells differentiation is called ***B-germinal center***, and is characterized by a *reappearance* of ***CD10*** expression.[248] **CD19** is therefore the most steadily B-lineage restricted expressed antigen throughout the differentiation process, appearing at the earliest proB stage and being lost only upon plasma cells differentiation.[249]

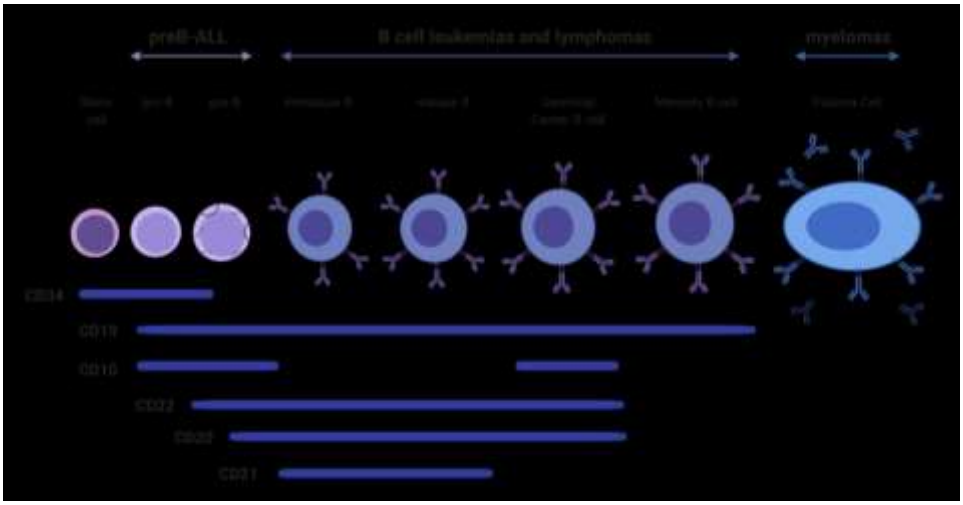

Fig. 10 Schematic representation of B-cell differentiation and marker expression. *Modified from Scheuermann 1994 and Schroeder 2010.*

1.4.2 CD19

CD19 is a transmembrane receptor expressed throughout the whole differentiation process of B-cells and on memory B cells, but not on differentiated plasma cells. It is a BCR co-receptor which forms a complex with CD21 and CD8, crucial in the quantitative and qualitative modulations of B cell responses.[250,251] CD19 deficiency does not impact pre-B cells in the bone marrow, but eventually results in primary antibody deficiency, characterized by poor antigen-specific response.[252] It represents a suitable target receptor for B-cell malignancies, with approved successful CD19-targeted therapies, such as BiTEs and CAR-Ts.

1.4.2.1 CD19 complex role in BCR signaling

From a biological point of view, CD19 is well known for being a co-receptor of the BCR signaling. CD19 is, in fact, a 95 kDa surface marker of B-cells, classified as a type I transmembrane protein belonging to the Ig superfamily.[253] It presents an extracellular (EC) N terminus, rich in N-glycosylation sites, a single transmembrane domain, and a cytoplasmic C terminus. The CD19EC domain, further analyzed in the next paragraph, forms a complex with CD21, CD81 and Leu-13, which plays a crucial role in the BCR signaling modulation. The cytoplasmic domain presents nine highly conserved tyrosine residues at the C terminus, whose phosphorylation allows SH2-recognition motifs to recruit several signaling molecules, mediating the regulation of different important pathways related to the BCR signalling.[254–258] The BCR is an antigen-binding transmembrane immunoglobulin, associated on the cytoplasmic side to an Igα-Igβ heterodimer, representing a tyrosine-based signal transduction module. The main pathways activated upon antigen binding regulates proliferation, differentiation and survival of B cells, with the most important being PI3K pathway, the MAPK pathway, and the PLCγ2/Ca2+ pathway.[259]

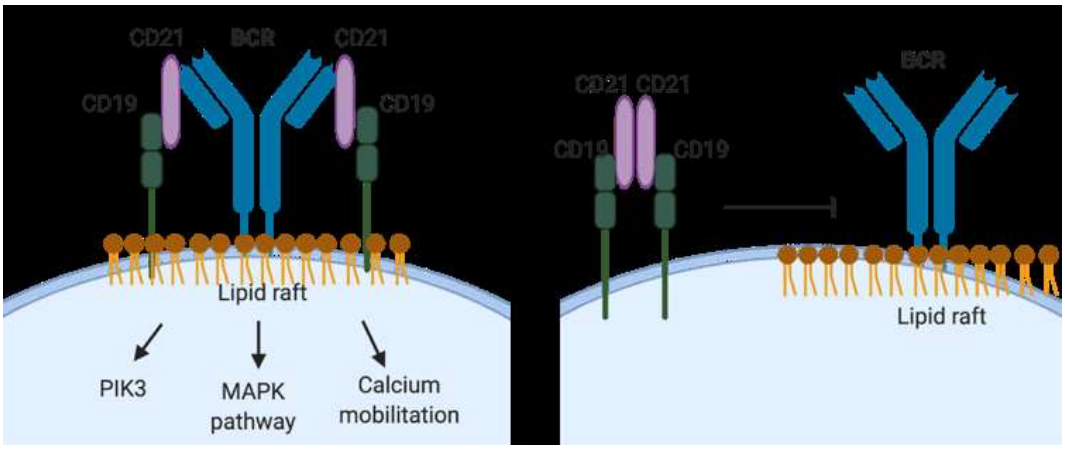

Fig. 11 CD19 dual role in BCR signaling. *Co-ligation of CD19 to the BCR complex into lipid rafts positive regulate BCR signaling, activating PKI3, increasing MAP kinase activity and inducing Calcium mobilization. When CD19 engagement occurs outside the lipid rafts and away from the BCR complex, it leads to BCR signaling suppression.*

Recent evidence highlights two main effects of CD19 on BCR signaling, depending on how it is engaged: co-ligation of CD19 with the BCR complex in lipid rafts leads to a synergic increase of MAP kinase activity, while CD19 engagement away from the BCR complex suppresses BCR signaling (**Fig. 11**).[251] Further studies are needed in order to fully understand detailed CD19 molecular signaling mechanisms.

1.4.2.2 CD19 Structure

CD19 is a 95 kDa transmembrane receptor. The amino acid sequence of its extracellular domain shows the presence of two tandem Ig-like domain, and the prediction of two consecutive c-type Ig-like domains was commonly accepted[255,260] However, the structure observed by Teplyakov et al. revealed a swapped arrangement of the two Ig-like domains, which represents a unique fold up to now.[261]

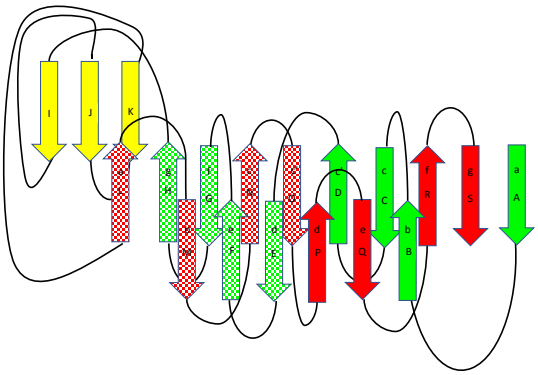

Fig. 12 CD19EC Topology diagram (PDB ID: 6AL5). *β-strands are labelled sequentially by capital letters from A to S. The β-strands forming the two Ig-folds are labelled with small letters according to the standard nomenclature,[262] and are striped and fully colored, respectively. Following the N termini-C termini direction, β-strands are colored in green, yellow and red. Modified from Teplyakov, 2019.*[261]

CD19 structure can be described as a β-sandwich, whose characteristic topology is represented by two Ig-folds related by a two-fold axis running across the β-sheets (**Fig. 12**). Each Ig-fold is composed of 8 β-strands, grouped in a first 3-stranded β-sheet (b, e and d) and in a second 5-stranded β-sheets (a, g, f, c and c'), according to the standard nomenclature introduced by Bork et al.[262] CD19 EC shows a hybrid type of Ig-fold, given the presence of a c' strand, typical for v-type Ig-fold, and the absence of a c'' fold, which is characteristic of c-type Ig-fold. Since between c' and d strands one Ig-fold is inserted into the other, CD19EC could also be described as a unique extended Ig-folds. Another key element of Ig-folds found in CD19EC is a disulphide bond between strands b and f, with a tryptophan residue facing the disulphide localized in strand c. [263]
More in details, in CD19EC the two Ig-like domains are formed by 6 and 10 β-strands respectively. The two Ig-folds have swapped four out of eight β-strands, so that each domain is composed of four strands (a, b, c, c') from one sequence pattern and four strands (d, e, f, g) from the other (**Fig. 13**).

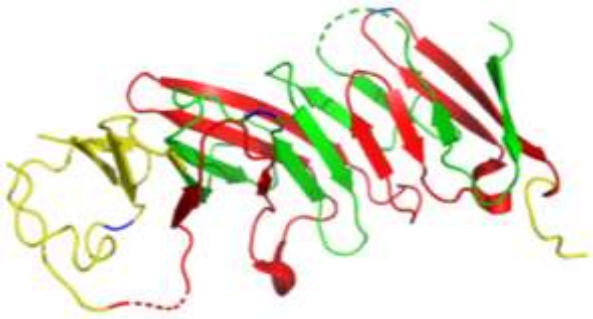

Fig.13 Ribbon presentation of CD19EC (PDB ID: 6AL5). *Colors refer to the topology diagram showed in Fig. 12. Modified from Teplyakov, 2019.*[261]

The N and C termini are both placed at one end of the β-sandwich, while on the opposite side a less regular region is found, where three β-strands of mixed topology (I, J, K) are placed between two partially disordered loops. The loops are held together by a disulphide bridge between

Cys134–Cys173. Two other disulphide bonds link strands B–R and G–M, Cys38–Cys261 and Cys97–Cys200, respectively. Five potential N-glycosylation sites are found on CD19EC: Asn138, Asn86; Asn125, Asn181 and Asn265.

1.4.2.3 CD19 targeting in hematological malignancies

As reported above, CD19 is steadily expressed throughout B-cell differentiation, appearing at the earliest proB stage and being lost only upon plasma cells differentiation.[249] Moreover, several studies confirm that CD19 expression is maintained during neoplastic transformation.[264–267] More specifically, CD19 is expressed on preB-ALL, B-ALL, HCL (hairy cell leukaemia), B-CLL, Burkitt's lymphoma and other non-Hodgkin's lymphomas malignant cells. On the contrary, CD19 expression is not observed in CML, AML or T-ALL.[264,265,268] The fact that CD19 expression is 1) restricted to the B-lineage; 2) absent from all other cell types; 3) rarely lost during neoplastic transformation, makes it a suitable tumor-associated antigen for targeted therapies. Certainly, CD19 targeted therapies would eliminate both neoplastic and healthy B-cells, but the presence of CD19- hemopoietic stem cells allows continuous healthy B-cell replenishment, during and after the treatment.[249] The most important CD19-targeted approved therapies, already described in previous paragraphs, include a new format of bispecific antibody (BiTE) called Blinatumomab, and CAR-T cell therapies, such as Tisagenlecleucel and Axicabtagene ciloleucel.

1.4.3 CD20

CD20 is a 33-37 kDa non-glycosylated B-lineage restricted antigen, which represents the target of Rituximab, the first effective anti-cancer monoclonal antibody to be developed, which paved the way for the cancer immunotherapy breakthrough.

1.4.3.1 CD20 biological role

Despite the therapeutic success of anti-CD20 mAbs in cancer immunotherapy, little is known about the biology of CD20.[269–271] CD20 belongs to a protein family called MS4A, which includes 21 proteins.[272,273] CD20 resides in particular membrane protrusions known as microvilli, in dimeric or tetrameric forms.[274] It localizes with CD40, MHC class II molecules and the BCR receptor,[275–277] suggesting a possible cooperation in BCR signaling. It is believed that CD20 may be involved in the calcium flux generated upon BCR activation.[278] This hypothesis is also supported by the fact that CD20 is a tetra-span phosphoprotein without intrinsic enzymatic activity, with cytoplasmic N and C termini, reminding the structure of other known calcium channel components.[279–281] A CD20 redistribution into lipid rafts is observed upon type I mAb binding.[282–284] Lipid rafts are glycosphingolipids, cholesterol and Src kinases-rich membrane domains, believed to be highly involved in signal transduction, further suggesting an important signaling role for CD20.[285] Historical data shows low or absent levels of CD20 modulation *in vitro*, but interestingly recent evidence reported CD20 modulation *in vivo* in CLL. In order to elucidate possible implications of CD20 modulation in targeted immunotherapy, further investigation is needed.[286–288] Up to now, no known ligand for CD20 has been identified. However, it is well established that its engagement with mAbs can result in an enhanced cell survival and proliferation, [289,290] as well as in cell growth inhibition and death.[291283,291–296]

1.4.3.2 CD20 structure

CD20 is a non-glycosylated membrane phosphoprotein which crosses the plasmatic membrane four times and presents two extracellular regions: a small (79-84) and a large loop (142-188). The large loop is the only one involved in mAb interactions, presenting two residues (Ala170 and Pro 172), which are crucial for the binding to occur.[285]

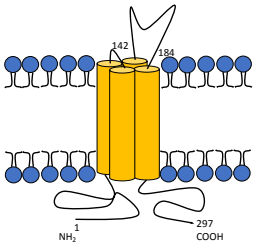

Fig. 14 CD20 molecule. *CD20 crosses the plasmatic membrane four times and presents two extracellular regions, a small one (79-84) and a larger loop (142-188). Modified from Craggs 2005.*[285]

1.4.3.3 CD20 targeting in hematological malignancies

Several reasons make CD20 an optimal target for hematological malignancies.

Firstly, in healthy cells, CD20 is expressed from the early pre-B cell stage and lost during plasma cells terminal differentiation, while being preserved on the majority of B cell malignancies.[281] Secondly, CD20 is highly expressed on most B-cells, at approximately 100 000-200 000 copies per cell.[285] Additionally, CD20 is not shed from the cell surface upon mAb binding and is reported not to internalize in most of the studies.[280,297] Finally, the development of CD20-negative cancerous cells is rarely observed after treatment, allowing an effective repeated usage of anti-CD20 mAbs.[285]

For all these reasons, CD20 mAb development has being pursued for many years, with the first anti-human CD20 mAb (B1) being characterized over 40 years ago.[298] Nowadays, a large panel of anti-CD20 mAbs have been developed, which can be classified in two functional groups, Type I and II.[296,299] mAbs from both groups are able to induce Antibody-dependent Cytotoxicity (ADCC). However, *type I mAbs*, including Rituximab and IF5, also induce complement-dependent cytoxicity (CDC) and CD20 re-localization into lipid rafts, while *type II mAbs*, including B1, induce more homotypic aggregation and apoptosis.[283,299]

The efficacy of the chimeric anti-CD20 mAb Rituximab in treating B cell disorders, such as cancer and more recently autoimmunity, has been remarkable, in particular when used in combination with chemotherapy.[270] Rituximab cytotoxic effect is mediated by three different mechanisms: complement-dependent cytotoxicity (CDC), antibody-dependent cellular cytotoxicity (ADCC), and apoptosis-induction.[300] Rituximab resistance leads to the development of next-generation anti-CD20 antibodies. Among them are Ofatumumab and Obinutuzumab, glycosylated enhanced versions of Rituximab, which are currently successfully used for the treatment of hematological malignancies.[301,302]

1.5 Therapeutic Antibodies

Natural immunoglobulins play a fundamental role in the immune system, by being among the most important effectors of adaptive immunity. Antibodies (Abs) are heterodimeric proteins, whose structure is characterized by a peculiar Y shape, composed by two Heavy chains (H) and two Light Chains (L). In each chain, two functionally distinct domains are present, which are the variable region (V) and constant region (C).[303]

The glycosylated constant domains of the heavy chains CH2 and CH3 form the Y-stem, and are referred to as Fc. The Fc is responsible for effector functions, such as CDC and cross-linking-mediated agonism, triggered by the interaction with Fc receptors. [304,305] The Fc also provides longer plasmatic half-life through its interaction with the FcRn.[306] Five main classes of heavy chain constant domains exist, and define the IgM, IgG, IgA, IgD and IgE isotypes. The heavy chain constant domains forming the Fc can be switched, an event known as *isotypic switch*, in order to allow different effector functions while retaining antigen specificity.[303]

The variable domains of heavy and light chains, VH and VL respectively, represent the binding domain, determining the specificity and affinity of the antibody.

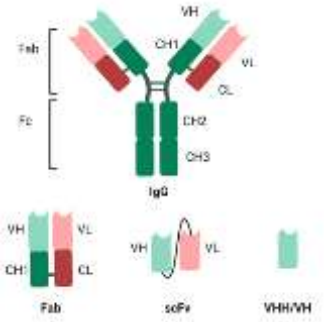

Fig. 15 Recombinant antibody fragments.

They are built through a complex series of genetic rearrangements, and are then subjected to somatic hypermutation after antigen exposure, to allow affinity maturation. Each variable domain is composed of 3 regions of high sequence variability, called complementarity-determining regions (CDRs), paired together and forming the classically defined antigen-binding site. The rest of each VH and VL is composed of 4 regions of relatively-constant sequence, referred to as framework sequences. In the VH and VL CDR regions, the amino acid residues which establish the direct contact with the antigen are called *paratope,* while the surface of the antigen in direct contact with the Ab is called *epitope*.[303,307]

1.5.1 State of the art

The turning point in the development of therapeutic antibodies was represented by the introduction of the "Hybridoma" technique, set up by Köhler and Milstein in 1975.[308] This technique allows the continuous production of a monoclonal antibody (mAb), obtained by the expansion of a single hybridoma clone. Thus, large quantities of the antibody of interest can be produced, allowing further therapeutic development. Since then, 79 therapeutic mAbs have been approved for clinical use,[309] with the first mAb ever to be put on the market being murine muromonab-CD3 (Ortho-clone OKT3), in 1986.[310] Muromonab-CD3 is an immunosuppressant used for the treatment of acute transplant rejection, and is no longer commercially available since 2001.[311]

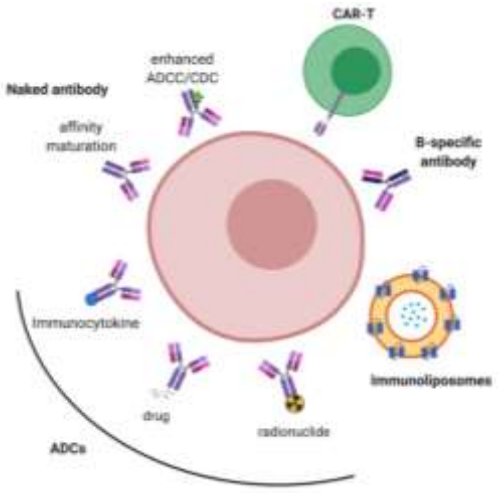

Fig. 16 Schematic overview of antibody-based therapeutics. *Naked antibodies, enhanced ADCC/ CDC; affinity maturation; ADCs, immunocytokine, radionuclides; immunoliposomes; bispecific antibodies; chimeric antigen receptor T cell (CAR-T) therapy.*[240,312–316]

Since then, the therapeutic antibody field has undergone a massive expansion, with applications in the treatment of cancer, autoimmune disease, as well as infectious disease.

Currently, therapeutic antibodies can be grouped into distinct categories, mainly according to their format and cytotoxic mechanism (**Fig. 16**).

1.5.2 Production of Therapeutic Antibodies

The hybridoma technology, which granted the Nobel Price to Köhler and Milstein in 1984, allowed the production of mAbs from the hybridomas, which are derived from the fusion of murine B cells and murine myeloma cells. Murine B cells carry the genetic information which allows the expression of an antigen-specific antibody, while murine myeloma give the ability to replicate indefinitely to the fusion cells.[308] Murine B cells are obtained *via* mice immunization against the antigen of interest, allowing potentially the generation of mAbs against almost any antigen of interest. However, from a clinical point of view, the administration of murine mAbs presents several limitations. In fact, in most patients a rapid human anti-mouse antibody (HAMA) is observed, generating allergic reactions and undesired tumor penetration. Moreover, murine Fc have a limited effector function, with the consequent induction of poorer ADCC.[307,311]

The features of an ideal mAb are indeed high antigen binding activity, high stability, and low immunogenicity.[317] Antibody immunogenicity is particularly problematic, since the reaction of the host immune system against the drug can induce both severe allergic reactions and the production of anti-drug antibodies (ADA), which can neutralize the therapeutic action, hampering the drug efficacy.[318,319]

For these reasons, researchers put a great effort in creating approaches which would allow to make murine antibodies more similar to human ones. The most relevant platforms currently available for the production of less immunogenic and more efficient therapeutic antibodies are (**Fig. 17**): the chimerisation and humanization of murine mAbs; the use of transgenic mice (**Table 13**); the use of human B-cells (**Table 14**) and the use if **display techniques**, and in particular of ***phage display***, on which this project focuses on.

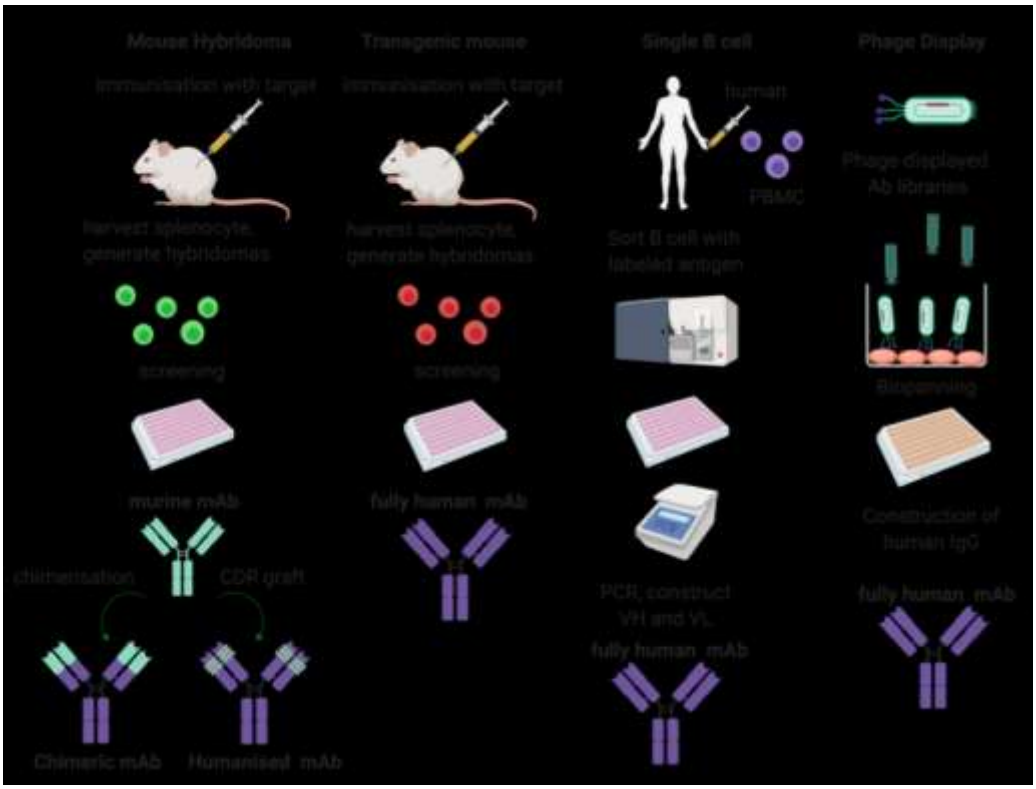

Fig. 17 Approaches for the development of therapeutic antibodies. *Traditional mouse hybridoma technique, which allows the production of murine mAbs, as well as chimeric (chimerisation) and humanized (CDR graft) mAbs. Transgenic mice, Single B cell and Phage Display, allows the production of fully human mAbs. Modified from Lu 2020.*[311]

Table 13. Transgenic mice currently available for the production of antibodies.[311]

Company	Product	Reference	hVH*	hVK**	Constant	Country	Antibody
Medarex	HuMAbMouse	1994 Longberg et al[320]	4	4	Human	US	Human
Abgenix	XenoMouse	1994 Green et al[321] 1997 Mendez et al[322]	17	17	Human	US	Human
Ligand	OmniRat	2013 Osborn et al[323]	22	12	Rat	US	Chimeric
Kymab	KyMouse	2014 Lee et al[324]	43	37	Mouse	UK	Chimeric
Regeneron	VelocImmune	2014 Murphy et al[325]	47	23	Mouse	US	Chimeric
Harbour Antibodies BV	H2L2 mouse	https://harbourantibodies.com	18	11	Mouse	US	Chimeric
Trianni	Trianni Mouse	https://trianni.com	44	39	Mouse	US	Chimeric

* number of human heavy chain variable region, ** number of human kappa chain variable region

Table 14. Single B cell technology-derived antibodies.[311]

mAb	Disease	Ref	State
Dengue neutralising	Dengue fever	326,327	pre-clinical
Anti-cytomegalovirus	Cytomegalovirus	328	pre-clinical
Anti-Zika Virus	Zika Virus	329	pre-clinical
Anti-CHF	Cancer	330	pre-clinical
mAb114	Ebola Virus	331	Phase I/II/III
3BNC117	HIV	332	Phase I/II
VRC01	HIV	332	Phase I/II
PGT121	HIV	332	Phase I/II
N6	HIV	332	Phase I
MHAA4549A	influenza A	333	Phase I/II

1.5.3 Phage Display

Several strategies have been developed throughout the years, in order to generate synthetic combinatorial libraries for the selection of human target-specific antibodies. Strategies that allow a cell-surface display of the antibodies are generally referred to as **antibody display methodologies**, and can be divided into *microbial display techniques* and *eukaryotic display techniques*, which are listed in **Table 15**.

Table 15. Antibody Display Techniques

	Name	Advantages
Microbial Display techiniques	*Phage Display*	high effectiveness, robustness and suitability for high throughput screening processes[334]
Eukariotic Display technique	*Yeasts Display*	usage of eukaryotic folding pathways[335–337]
	Ribosome Display	Cell-free system [307]

Phage display is a technology which is able to directly link a protein (*phenotype*) to its related gene (*genotype*) *via* a phage particle. This is achieved through the fusion of a gene encoding an antibody binding domain to a gene coding for a coating protein of the phage, resulting in the expression of a hybrid coat protein, which is incorporated into virions particles and displayed on their outer surface when released from the host cell.[338,339] A phage display library is therefore an heterogenous mix of phage clones, each carrying distinct foreign DNA inserts and consequently displaying distinct antibody binding fragments on their surface. Phage display currently

represents the most widely used *in vitro* technique for the selection of high affinity antigen-specific antibodies.[340] Since its introduction in 1985, which earned the Nobel price to its inventors George P. Smith and Sir Gregory P. Winter in 2017, different antibody formats have been used for the construction of phage antibody libraries. Firstly, whole fragments antigen binding antibodies (Fabs) were employed, followed by diabodies (bivalent scFv) and single chain variable fragment (scFv), until most recent times, when the nanobodies were introduced, such as heavy domain camelid and shark antibody fragments (VHHs) and single heavy-domain human antibody fragments (VHs).[341–344] Among the main advantages of this technology there are its high effectiveness, robustness and suitability for high throughput screening processes.[334]

1.5.3.1 Phages

Phages are viruses that specifically infect bacterial cells and are also referred to as bacteriophages. Different bacteriophage systems can be used for phage display, such as T4 and λ phages. However, the most widely used bacteriophage system is represented by the filamentous phages (Ff), and in particular M13 phage.[345] M13 is a Ff phage able to infect only *E. coli* strains expressing the F pilus, since the adsorption into the bacterial cells is mediated by a coating protein which binds to the F pilus.[346,347] M13 phage infection results into a chronic infection of its hosts cells, which continuously release newly assembled phage particles without encountering lysis. This kind of phages are typically referred to as chronic non-temperate.[348,349]

The M13 genome consists of a single-stranded DNA (ssDNA) of 6407 bp, encoding 5 out 11 proteins for the coating.[350] The most abundant protein found in the capsid structure is **pVIII**, which helically arranges to form a tube-shaped envelope around the phage genome, composed by ~ 2700 pVIII copies per virion. The other minor coating proteins, **pIII**, pVI, pVII and pIX, are represented on the coating surface in 5 copies per virion, with pIII and pVI copies at one tip, and pVII and pIX copies at the other tip.[339,349]

1.5.3.2 Phage and phagemid vectors, polyvalent and monovalent display

In the development of the phage display technique, foreign DNAs coding for antibody binding domains have been mainly fused to the exposed N-terminus of coat proteins pVIII and pIII. This genetic information can be inserted into two kind of vectors: **phage vectors** and **phagemid vectors**.

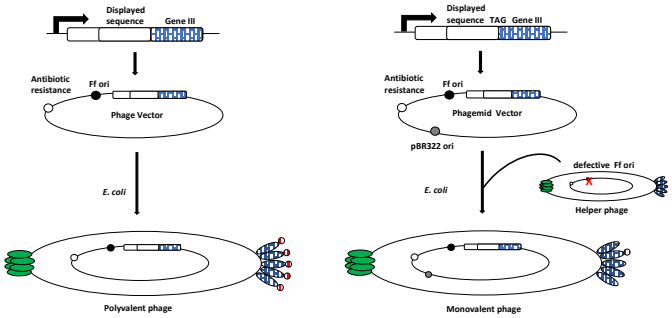

Fig. 18 Schematic representation of polyvalent and monovalent Phage Display. *Modified from Clackson 2004.*[351]

In the first case, foreign antibody genes are inserted directly into the genome of the M13 phage, which is referred to as a **phage-vector**, since the phage genome itself functions as a vector carrying the recombinant DNA insert. This implies that each copy of the coating protein chosen for the fusion design will be expressed on the virion surface in the fusion form, leading to what is called a **polyvalent display**. This can increase the number of low-affinity antibodies selected at the end of the process, given the increased avidity of the displaying particles (**Fig. 18**). [349,351]

In the second case, **phagemid vectors** carry the gene encoding the antibody-coat protein fusion, while the rest of the genetic information, needed to produce functional displaying phage particles, is provided by a **helper phage** (M13K07 being the most common). In this case, displaying phages

contain a single copy of the antibody-coat protein fusion, leading to a **monovalent display**, for which the pIII coat protein is generally chosen as fusion partner. [352] This type of display is preferred for the selection of high affinity antibodies. [351] (**Fig. 18**)

1.5.3.3 Selection by affinity

The screening of phage display libraries is an affinity-based process, consisting in repetitive selection rounds, called biopannings, which allow to enrich the population of the target-binding phages.[311]

The first round of panning is also referred to as "library packaging", since phage displaying particles are obtained from the infection by a helper phage, of *E. coli* cells carrying phagemids covering the whole antibody repertoire. At this point, the selection process starts, and it is divided in three main phases: **binding**, **washings** and **elution** (**Fig. 19**).

During the **binding** phase, the displaying particles are exposed to the target antigen, which needs to be immobilized on a solid surface. During this step, the phages displaying antibodies showing affinity for the target, bind to the immobilized antigen. Stringent **washings** are needed in order to remove unbound phages. The third step is represented by the **elution**, which is typically performed *via* trypsin digestion, in order to elute the binding phages and, at the same time, to decrease the background noise by making bald phages non-infective, which are not trypsine-resistant. [353] At this point, the eluted population, enriched in infective displaying phages, is amplified *via* the infection of fresh naïve *E. coli* cells. The panning process is repeated, usually from 3 to 5 times and then a polyclonal phage ELISA is used to confirm the selection of binders, subsequently analyzed through standard ELISA.[311,354] At this point, positive clones are selected and characterized individually.

This efficient and stringent process allows the selection of antibodies of interest in a relative short time, when compared to the traditional hybridoma method.[355,356]

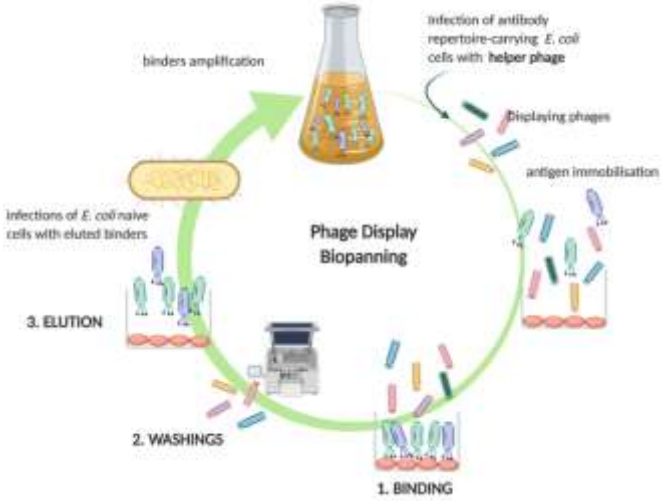

Fig. 19 Schematic representation Phage Display Biopannings. *After library packaging and displaying phages exposure to the antigen, the selection procedure starts. Binding, washings and elution phases are followed by infection of naïve E. coli cells in order to amplify the population of the eluted phages and perform subsequent rounds of biopannings.*

1.5.3.4 Antibody Repertoire

A phage display library can be defined, according to different sources and designs, as *naïve*,[357] *immune*,[358] *synthetic* and *semi-synthetic*.[359,360]

Phage display naïve and synthetic antibody libraries can be used for the selection of antibodies potentially against any target (***single pot library***), although such antibodies generally show a lower affinity than those isolated from an immunized library, where affinity maturation occurs *in vivo*.[357,361,362] On the contrary, the major limitation of an immunized library is that the preparation of a new library is required for every new antigen of interest. For non-immunized single pot

libraries, several *in vitro* affinity maturation strategies have been studied, in order to increase the affinity of the selected antibodies. [311]

Nowadays, most of the commercially available libraries are based on *highly diverse non-immunized antibody repertoires*. Actually, a very limited number of libraries allowed the selection of antibodies currently used in the clinics: 1) Cambridge Antibody Technology's (now MedImmune, a subsidiary of AstraZeneca) scFv-fragment library; 2) Dyax Corp's (now Shire) human Fab-fragment libraries; 3) XOMA's scFv and Fab libraries; 4) MorphoSys libraries of fully synthetic human combinatorial antibody scFv (HuCAL) and Fab (HuCALGold).[363]

Up to now, the only fully human antibodies approved for clinical use were produced either using phage display or transgenic mice.[364] There are nine antibodies derived from phage display libraries currently approved by the FDA and the most important are listed in **Table 16**.

Table 16. Phage Display Selected antibodies in the Clinic

Name	Format	Species	Target/Mechanism	Disease	Library/ Company	Year
Adalimumab (Humira®)	Fab	Human	TNFα suppression	inflammatory diseases (i.e. rumatoid arthritis)	Cambridge Antibody technology	2002[365]
Belimumab (Benlysta ®)	Fab	Human	BLYS (B-lymphocyte stimulator)	lupus erythematosus (SLE) [366]	Cambridge Antibody technology	2011
Necitumumab (Portrazza®)	Fab	Human	EGFR	squamous non-small cell lung carcinoma (NSCLC) [367]	Dyax	2015
Ramucirumab (Cyramza®)	Fab	Human	VEGFR2	gastric cancer, metastatic NSCLC and colorectal cancer [368–370]	Dyax	2014
Avelumab (Bavencio®)	Fab	Human	PDL1[371]	metastatic Merkel Cell Carcinoma (MCC)	Dyax	2017
Guselkmab (Tremfya®)	Fab	Human	IL-23	plaque psoriasis [372]	HuCAL	2017
Lanadelumab (Takhzyro®)	Fab	Human	plasma kallikrein inhibitor	acute attack of hereditary angioedema [373]	Dyax	2018

1.5.4 Antibodies Manufacture

As explained in the previous paragraphs, the process for the discovery and development of therapeutic antibodies is rather long and expensive, and consists in two main phases. In the first one, early candidates, referred to as *hits*, are detected, while the second phase is focused on the selection of advance candidates, referred to as *leads*.

Once the leads are identified, the expression system choice is one of the most crucial in the production process, which has to guarantee high yield at reasonable costs, as well as safety criteria. The most common expression systems are listed in **Table 17**.

Table 17. Expression systems in antibodies manufacture

Expression System	Antibody format	Advantages	Cell line/Strain
Mammalian cells	mAb	proper introduction post-translational modifications, disulphide bonds and proper secretion	CHO (Chinese Hamster Ovary) SP2/0 NS0 Hybridomas [374]

Bacteria	recombinant antibody fragments (Fab, scFv, sdAb)	lower costs and easy manipulation [374]	*E. coli*
Yeasts	recombinant antibody fragments (Fab, scFv, sdAb)	introduction of post-translational modification (slightly different than humans), disulphide bonds and proper secretion [374]	*P. Pastoris* *S. cerevisiae*
Plants	recombinant antibody fragments (Fab, scFv, sdAb)	mammal pathogens-free, introduction of post-translational modification (different than humans)	*Nicotiana tabacum*

1.5.5 Single Domain Antibodies (sdAb) or Nanobodies ®

The huge impact of therapeutic antibodies requires a constant improvement of their features, in order to overcome their main limitations, such as poor tissue and tumor penetration, low i*n vivo* efficacy, impractical administration, aggregation due to low solubility and high production costs.[375] During the years, novel recombinant formats of therapeutic antibodies have been developed, also referred to as next generation or antibodies biobetters.

Intact IgG antibodies most important features are their *bivalency*, which provides higher avidity and retention times, and the *effector functions* of their Fc domain, *via* the interaction with Fc receptors, such as CDC mediation and longer serum half- life.[376,377]

However, in a wide range of applications, the Fc mediated effects results to be undesirable. For example, in *in vivo* imaging, prolonged serum half-life results in poor contrast; furthermore, in some cases, an improper activation of cells expressing the Fc receptors can induce a massive cytokine release with severe consequences.[378] At the same time, the reduction of the antibodies dimensions was always another important aim in antibody production improvement.[379]

The dissection of the IgG lead to the production of several recombinant antibody fragments.

Monovalent fragments were engineered, such as Fabs, scFv, single variable VH and VL domains, as well as bivalent one, including Fab', diabodies and minibodies (**Fig. 20**).

Fab fragments are constituted by the VH and VL domains and CH1 and CL domain.

Single-chain Fvs (**scFvs**) are a widely used recombinant format, in which a flexible polypeptide linker joins VH and VL domains. Both Fabs and scFvs retain the binding affinity of the parental IgG and show improved tissue penetration.[378]

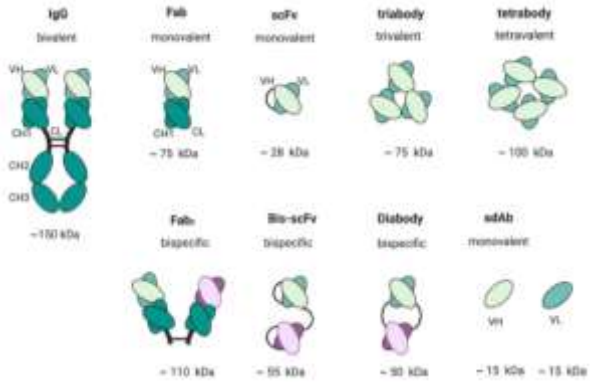

Fig. 20 Recombinant Antibody fragments. *From the left, schematic representations of IgG, Fab, Fab$_2$ bispecific, scFv, scFv bispecific and VHH. Modified from Holliger 2015.*[378]

A growing interest in single domain antibodies started with the identification of high-affinity single V-like domains in camelids (camels and llamas) and cartilaginous fish (wobbegong and nurse shark).[380–383]

In camelid serum, antibodies with an atypical structure were identified.[384,385] They were called Heavy Chain antibody (HCAbs), and they are characterized by the absence of the light chain as well as of the first constants domain, CH1.[386]

The concentration of HCAbs among all different immunoglobulins present in the serum greatly varies in different camelids: in llamas their representation spans between 25-45%, in

dromedaries it is greater than 50%, and in camels greater than 75%.[387,388] The antigen binding domain of the HCAbs is referred to as VHH, also commonly identified as single-domain antibody (sdAb) or nanobody (Nb).[389]
VHHs are characterized by the presence of four framework regions, which show an 80% homology with human VH domains, and three CDRs.[390] As in traditional antibodies, the CDRs resides in loops, usually linking two β-sheets of the immunoglobulin domain with a disulphide bond. A longer CDR3, derived from the absence of the light chain, is stabilized by a disulphide bond with CDR1 (camels), or CDR2 (llamas). This longer CDR3 confers a convex shape to the VHH, allowing it to reach unconventional epitopes in clefts and concave surface of the target, such as catalytic sites of enzymes.[391]
A similar class of antibodies, always referred to as HCAbs, was detected also in cartilagineous fish.[392] In sharks, the HCAb antigen binding site is called vNAR, and shares many characteristics with camelid VHH. However, its clinical applications are at an earlier stage of development, while VHH have already been successfully tested in early stage clinical trials.[393–398]

Fig. 21 Schematic representation of Nanobodies structure. *From the left, IgNAR, found in sharks, with the correspondent vNAR. On the left, camelid HCAb and the correspondent VHH, composed by 4 framework regions and three CDR domains. Characteristics are the presence of four hallmark amino acids in FR2 (green stars) and the particularly long CDR3. Modified from Holliger 2005 and Khodabakhsh 2018.*[378,386]

sdAb fragments represent the smallest available recombinant format of antibody, with a length of about 120 aa, a molecular mass of roughly 12-15 kDa, and a 4x2.5 nm size.
Among the most important **advantages** that nanobodies bring in the setting of an efficient **production process**, there are: 1) the fact that they can be easily expressed in bacteria and yeasts in a recombinant form;[399] 2) their conformational stability due to their simple monomeric structure;[400] 3) their capability of easily refolding in their native structure after heating;[401] 4) the retention of their biological activity also in the presence of high concentration of detergents and proteases;[402] 5) their resistance to high pressure and low pH;[400] 6) the possibility to be easily engineered into multivalent, multi-specific fragments and conjugated for drug delivery systems;[403–406] 7) the fact that the overall process for sdAb fragments production results to be easier to perform and less expensive, compared to the standard monoclonal antibody methods.[407]
Nanobodies have also been used for the construction of phage display libraries, mainly derived by immunized animals, from which B lymphocytes are isolated and VHH (or vNAR) genes are amplified, through PCR. The nanobody repertoire is then ligated into phage display vectors and an immune VHH library is created.[408,409]

The **advantages** that strongly encourage development of Nb for **clinical applications** are: 1) the maintenance of a target-affinity equivalent to the original HCAbs;[410] 2) little to no immunogenicity in humans, due to the high homology of the framework regions with human ones;[411] 3) their easily penetration into intracellular spaces and tissue due to their very small size;[412] 4) their ability to efficiently bind into cavities and clefts onto protein surface, reaching also unconventional epitopes;[413] 5) their ability to pass the blood brain barrier and therefore reach the tissues of the central nervous system;[414,415] 6) the possibility to be expressed in intracellular environments as "intrabodies", and therefore to target intracellular antigens;[416,417] 7) the possibility to be orally

administered and used for the therapy of gastrointestinal diseases provided by their high structural stability.[418]

Some disadvantages must be considered anyway in the use of Nb, such as the fact that: 1) chemical conjugation to other molecules could affect their binding properties more severely than for traditional antibodies; 2) their preference for conformational epitopes make them inefficient in the identification of denatured protein, and therefore in WB applications; 3) due to their small dimensions, they are quickly cleared from the blood through kidney glomerular filtration, requiring repeated high dosage regimens for cancer treatment and making their usage as imaging instruments difficult.[419]

Due to their unique characteristics and the reasons explained above, numerous Nanobodies have been selected and produced for diagnostic and research applications, as well as for clinical applications.[379]

The most interesting results were obtained in the therapy of neoplastic diseases.[420] With respect to *haematological malignancies*, some applications are emerging for the treatment of B lymphomas and Multiple Myeloma (MM).

An important target for **B-lymphoma** is the B cell-activating factor (BAFF), also called B lymphocyte stimulator (BLys), which is a cytokine belonging to the TNF ligand superfamily. Several interesting Nbs against this target have been selected and will be furtherly developed.[421–424]

For Multiple Myeloma, CD38 represents an important target, against which a group of Nb with high affinity has been recently isolated.[425] Another target for MM is represented by c-MET, the tyrosine kinase receptor of the hepatocyte growth factor (HGF). HGF concentration detected in the serum and BM samples of MM patients are significantly higher than in controls, and represents a poor prognostic factor. Nbs against c-MET were isolated and proved to cause a decrease in the phosphorylation levels of MAPK, Akt and c-MET.[426]

2. Aim of the thesis

L-Asparaginase (**ASNase,** EC 3.5.1.1) is a crucial component of the combined chemotherapy used for the treatment of pediatric acute lymphoblastic leukemia, having significantly increased complete remission achievements in patients since its introduction in 1970s.[66] ASNase is an amidohydrolase with prevalent asparaginolytic activity and lower glutaminolytic activity. Its therapeutic benefit comes from the depletion of asparagine from the blood stream, on which leukemic cells depends, given their absent or compromised capability to express asparagine synthetase (EC 6.3.5.4) under stress conditions.[66]
Extensive clinical data support the benefit of ASNase treatment,[32,76,166] and it has been demonstrated that asparaginase resistance is correlated with a poor prognosis.[167–170]
Despite being a cornerstone in the treatment of ALL, most of the current ASNase products lack optimal pharmaceutical characteristics, in particular because of:

- high toxicity, ascribable to its untargeted activity;
- high immunogenicity, ascribable to its bacterial origin and large size;
- reduced blood serum half-life;
- poor efficacy in specific sub-classes of patients.

ASNase molecules designed in order to overcome those issues are defined *biobetters*. They are developed from the original product through intentionally designed chemical or molecular modifications.[66] Protein engineering, bioinformatics analysis, molecular dynamics, docking and site-directed mutagenesis are among the most sophisticated techniques used to develop new ASNases molecules. [190,191] Novel approaches are also being investigated for the generation of novel ASNase biobetters. Since the high therapeutic success of PEG-Asparaginase (Oncaspar ®), conjugation with other chemicals has been furtherly attempted. [215, 216] However, a targeting approach in the formulation of an Antibody Drug Conjugate (ADC) has not been fully explored yet for ASNase. ADCs consists of monoclonal antibodies conjugated to effector molecules that help accomplishing cell death upon target binding. The effector molecules are also called payloads, and include cytotoxic agents, immunotoxins and radiopharmaceutical agents.

The objective of this project is to **explore the feasibility of an ADC-based targeted approach for the development of ASNase biobetters.**

More specifically, *the aim of this thesis was to generate a **targeted**, re-sized version of ASNase,* with a ***targeting moiety*** represented by a *nanobody* (antibody component) and a ***catalytic moiety*** represented by a *catalytic nanobody* with asparaginolytic activity (cytotoxic payload). Such a molecule should address some of the major limitations in the therapeutic use of ASNase, and in particular: 1) its high immunogenicity; 2) the severe side effects due to its systemic action; 3) its poor efficacy in specific sub-classes of patients.

The **first objective** of this project was the *production of the CD19 target antigen in recombinant form*, in order to select anti-CD19 nanobodies and perform functional tests. As a secondary goal, also the production of CD20 in recombinant form was pursued.
CD19 was selected as a first choice target receptor, since it is a transmembrane receptor expressed throughout the whole differentiation process of B cells and on memory B cells, but not on differentiated plasma cells. It is a BCR co-receptor crucial in the quantitative and qualitative modulation of B cell responses.[250,251] Moreover, CD19 is able to efficiently drive receptor-mediated endocytosis. For all these reasons, CD19 represents a promising target receptor for B-cell malignancies, with already approved CD19-targeted therapies, such as BiTEs and CAR-Ts.[251]
CD20 was selected as second line target receptor, since it does not drive receptor-mediated endocytosis. However, it is considered a major target in hematological malignancies, being the B-

lineage restricted antigen targeted by Rituximab, the first effective anti-cancer monoclonal antibody to be ever developed. These two proteins in recombinant form were necessary for the next step.

The **second objective** of this project was the *selection of anti-CD19 nanobodies through in vitro selection techniques*, in particular through Phage Display, followed by their production and characterization.
For the targeting antibody moiety, nanobodies were chosen. Nanobodies, or single domain antibodies (sdAbs), represent the smallest available recombinant format of an antibody (12-15 kDa) and present several advantages: they can be expressed in bacteria and yeasts in a recombinant form;[399] they show higher stability; [400] they can be be easily engineered into multivalent, multi-specific fragments and conjugated;[403–406] they show little to no immunogenicity in humans, due to the high homology of the framework regions with the human ones;[411] they are able to easily penetrate into intercellular spaces and tissue thanks to their very small size;[412] they are able to efficiently bind into cavities and clefts onto protein surfaces, reaching also unconventional epitopes[413] and, in principle, they are able to pass the blood brain barrier and therefore reach the tissues of the central nervous system.[414,415]
For the selection of the nanobodies, it was chosen to use the Phage Display technique, which is the most important, successful, and widely used *in vitro display* technique for the selection of high affinity antigen-specific antibodies.[340] Among the main advantages of this technology, there are its high effectiveness, robustness and suitability for high throughput screening processes.[334]

The **third objective** of this project was the *cloning, production and characterization of the targeted, re-sized modular version of ASNase*. Our research group has been working for many years on the engineering of ASNases. In particular, the re-sized ASNase representing the catalytic moiety was engineered and produced in our laboratoy (PATENT #E0115946). It consists in a camelid nanobody provided with ASNase catalytic activity, o by transferring its relevant catalytic residues onto the nanobody scaffold. This way, a catalytic domain (single domain Asparaginase, sdASNase), with ten times lower molecular weight compared to *E. coli* L-Asparaginase (EcAII), was obtained. The sdASNase was therefore used as a catalytic moiety in the design of new ADC proteins, based on the nanobodies selected throughout the second step described above.

3. Materials and Methods

3.1 Materials

3.1.1 DNA cloning

Platinum® *Pfx* polymerase (Invitrogen), dNTPs (mixed dATP, dTTP, dGTP, dCTP, Sigma-Aldrich), Platinum® *Pfx* polymerase amplification buffer (Invitrogen), 5 mM $MgSO_4$ (Invitrogen), Molecular Biology Grade water (Sigma-Aldrich), Techne TC-300 thermocycler, Restriction Enzymes and Buffers from New England BioLabs (NEB), Takara or Invitrogen, Alkaline Phosphatase kit (rSAP, Roche), DNA ligation Mighty Mix kit (Takara), In-Fusion HD Cloning Kits (Takara), CloneAmp HiFi PCR Premix (Takara), *E. coli* Stellar Competent Cells® (Takara), SOC medium (Takara, powders of analytical grade, pET45b(+) (Novagen), 6x Loading Dye (ThermoFisher), (GeneRuler™, Fermentas), (Biostep Darkhood DH-30/30), Argus X1 software (Biostep®), QIAquick Gel Extraction Kit (QIAGEN), POLARstar Omega Plate reader Spectrophotometer (BMG Labtech), DNA sequencing by GENEWIZ® (Bahnhofstraße 86, Leipzig, Germany, GenElute Plasmid MiniPrep Kit (Sigma Aldrich).

3.1.2 Expression of Recombinant proteins

E. coli BL21(DE3), Origami(DE3)-ch5 (Novagen), HEK293T (ATCC), BugBuster® Protein Extraction Reagent (Novagen), HG-DMEM (Euroclone), EX-CELL™ 610-HSF Hybrydoma Serum-free Medium (Sigma Aldrich), Soniprep 150 Aibra (Omni Sonic Ruptor 400, Omni International), analytical grade chemicals, Chaperone Plasmid Set (Takara).

3.1.3 Protein purification and downstream processing

FPLC system (ÄKTA pure, GE Healthcare), His-trap FF Nickel columns (GE Healthcare), Bio-Scale™ Mini Profinity™ IMAC Cartridges (BIORAD), Mab_select columns (GE Healthcare), micro-BCA kit (Pierce), Superdex 75 10/300 GL resin (GE Healthcare), Amicon® Ultra-15, Amicon® Ultra-4 or Microcon® concentrators (Millipore), HiPrep 26/10 Desalting column (GE Healthcare).

3.1.4 Protein analysis

NNN′N′-tetramethylethylenediamine (TEMED, Applichem), 30% acrylamide:bis-acrylamide solution (37.5:1) (SERVA), Precision Plus Dual Color Protein™ Standard (Biorad), SilverQuest™ Silver Staining kit (Invitrogen), 3M filter paper (Millipore), PVDF, 0.2 μm cut-off, Millipore, Enhanced Chemiluminescence ECL Kit (Pierce), Clarity Western ECL Substrate (BIORAD), Ponceau solution (Sigma-Aldrich), autoradiographic films (Santa Cruz Biotechnology), Carestream X-Omat Ex II, Developer and Replenisher, DAB, SigmaFast™ tablets (Sigma-Aldrich), POLARstar Omega (BMG Labtech), Azure c600 (Applied Biosystems), glutamic acid dehydrogenase (GADH) (SERVA), analytical grade chemicals, HRP-conjugated anti-His pAb (Sigma-Aldrich), HRP-conjugated anti hIgG (Dako), Biotin-conjugated anti-myc (910E) (Merck Millipore), Extravidin-HRP (Sigma Aldrich), HRP-conjugated anti-mouse (Sigma Aldrich), anti-His (mAb, Sigma Aldrich).

3.1.5 Antibody specificity and affinity measurements

96-well Nunc Maxisorb ELISA plates, HRP-conjugated anti-His pAb (Sigma-Aldrich), HRP-conjugated anti hIgG (Dako), Biotin-conjugated a-myc (910E) (Merck Millipore), Extravidin-HRP (Sigma Aldrich), HRP-conjugated anti-mouse (Sigma Aldrich), anti-His (mAb, Sigma Aldrich).

3.1.6 Phage display

Analytical grade chemicals, Christ dAb library (SourceBioscience), KM13 helper phage (Source Bioscience), T-phage resistant *E. coli*. TG1 (SourceBioscience), *E. coli*. HB2151 (SourceBioscience),

EZ- Link ™ Sulfo-NHS-LC Biotinilation Kit (Thermofisher), μMACS Streptavidin kit (Miltenyi Biotec), 96-well Nunc Maxisorb ELISA plates, Biotin-conjugated anti-myc (910E) (Merck Millipore), Extravidin-HRP in 2% BSA (Sigma Aldrich), anti-KM13 antibody (Progen), HRP-conjugated a-mouse antibody (Sigma Aldrich).

3.1.7 Yeast two hybrid

Analytical grade chemicals, Chemidoc XRS (Biorad), GoTaq polymerase (Promega), Restriction enzymes from New England Bioscience, Wizard® *Plus* SV Minipreps DNA Purification System (Promega).

3.1.8 Mammalian cells and culture media

HEK293T (ATCC), HeLa (ATCC), HG-DMEM (Euroclone), Raji; RS4;11, HL60; MOLT, RPMI 1640 (Euroclone), cell culture grae chemicals, MTT, 3-(4,5-dimethylthiazol-2-yl)-2,5-diphenyltetrazolium bromide (Sigma Aldrich).

3.1.9 Immunofluorescence

Hoechst 33258 (Sigma Aldrich), anti-CD19 (HD37) (Merck Millipore), anti-LAMP2 (H4B4) (Invitrogen), anti-LAMP2 (H4B4) AlexaFluor 647 (Invitrogen), anti-mouse AlexaFluor488 (Invitrogen), anti-mouse DyLight 594 (Invitrogen). STED Leica TCS SP8 WLL STEDONE Flexible Supply Unit WLL Confocal. Microscope. Nanolive Cell 3D Explorer Microscope.

3.2 Methods

3.2.1 DNA cloning

The expression “DNA cloning” or “molecular cloning” refers to the molecular biology techniques which are used to generate recombinant DNA molecules, typically encoding a protein of interest, in order to amplify or express it in a host organism for experimental purposes. The origin of the gene can be natural, when the target sequence is extracted from the natural source, or artificial, when the DNA sequence is modified or completely designed in the laboratory. The DNA sequence can be amplified from ideally one molecule to an indefinite number, identical to the original one (*cloning*), either through a cell-free technique, PCR (Polymerase Chain Reaction), or through molecular vectors amplification into a cellular host. Molecular vectors are DNA-based molecules carrying the foreign DNA of interest (recombinant vectors), which can be of various origin, such as bacterial, viral or artificial. The most commonly used for molecular biology applications are of bacterial origin, and are called plasmid vectors. Plasmids are double-stranded circular DNA molecules, naturally found in bacterial cytoplasm, capable of autonomous replication with respect to chromosomal bacterial DNA. Plasmid vectors are natural plasmids optimized through DNA engineering to better fit for the intended use.

The main functional features of vectors used to amplify the target DNA, called *cloning vectors*, are the **origin of replication**, the **multiple cloning site (MCS)** and the **selection markers**. The *origin of replication* allows autonomous DNA replication, often insensitive to inhibiting stimuli. The *MCS* consists of a region enriched in restriction enzyme recognition sites present only once in the plasmid sequence, which allow the insertion of the DNA of interest through cut-and-paste strategies. Several *selective makers* can be used to select and screen the host cells which are actually carrying the plasmid of interest: some of them confer survival advantage under given conditions (*positive selection*, e.g. antibiotic resistance genes), others can negatively affect survival capability (*negative selection*) or allow the development of distinctive features (e.g. blue-white selection). Plasmid vectors used for the expression of proteins of interest are called *expression vectors*, and show a promoter sequence upstream the MCS region, which allows inducible target protein overexpression in the cellular host.

Bacterial cells are the most used host for DNA engineering techniques. In particular, *E. coli* strains represent a well-characterized organism with fast-replicative cycle and economic maintenance costs. Besides, several *E. coli* strains are commercially available, allowing the choice of the most suitable for different applications.
The general purposes of molecular cloning are: 1) definition and analysis of the amplified DNA sequence; 2) target protein expression in a host organism, often of a species distinct from the isolation source one; 3) generation of DNA libraries.
In conventional cloning methods, several cloning steps are needed in order to transfer the DNA of interest, referred to as *insert*, into a recipient *vector*.
Firstly, the DNA of interest is amplified through PCR using properly designed primers, in order to obtain a PCR product flanked by the restriction sites chosen during the cloning strategy design. Then, the PCR product often needs to be inserted into a *cloning plasmid*, which allows to introduce the PCR product into the vector through a ligation-independent strategy (TOPO, TOPO-TA, Blunt). This way, it is possible to amplify large quantities of insert in order to digest it with the desired restriction enzymes. The same restriction enzymes are used to digest the "final" recipient vector, which is then dephosphorylated. At this point, the insert and vectors carrying complementary sticky ends are ligated through DNA ligase.
Since this represents a time-consuming procedure, alternative cloning methods have been developed during the years, in order to speed up the whole process.

3.2.1.1 Golden Gate Cloning
The Golden Gate cloning (**Fig. 3.1**) constitutes an innovative strategy which allows a seamless and efficient assembly of up to nine DNA fragments in a single cloning step. [427]

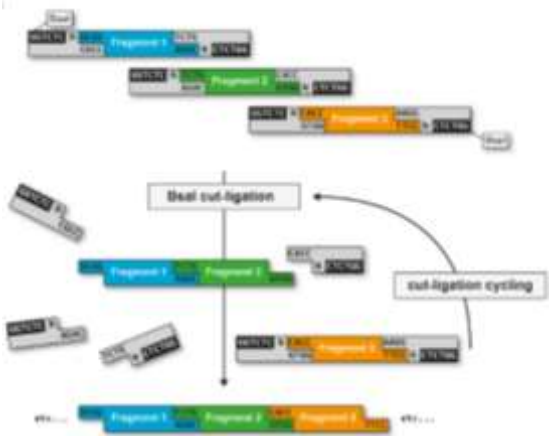

Figure 3.1 Example of Golden Gate cloning. *Figure adapted from Binder A et al 2014.*[428] *Golden Gate Cloning requires a type IIS recognition site. In this case a Bsa I restriction site (GGTCTC) was added to both ends of the DNA insert. Following the restriction digestion, these sites are left behind, with each insert bearing the proper-designed 4-base overhangs able to direct the assembly.*

Golden Gate cloning exploits type IIS restriction enzymes, such as *Bsa* I, capability to cleave DNA at a predictable position outside of the recognition site, resulting in 5' or 3' DNA sticky overhangs of whichever 4 nucleotides. For these reasons, a proper design of the cleavage sites allows to perform the restriction digestion and ligation reaction in one step, alternating the optimal temperature for the digestion (37 °C) and ligation (16 °C) to occur. The ligation product will not be sensitive to *Bsa* I restriction digestion, since it will not contain *Bsa* I restriction sites anymore.

<u>Primer Design</u>
Proper Primer Design is essential in order to guarantee DNA amplification specificity. In addition, through primer design, desired modifications, such as point mutations, insertions and deletions, can be introduced into the original sequence, by including them in the primer sequence. The most

important example is represented by the insertion of the desired restriction sites at the 5'- and 3'-terminus of the insert sequence, which are necessary in order to allow subcloning into vectors, but also recombinant Tag sequences, such as His-Tag, can be inserted through primer design.
In general, some basic features to consider in order to design good quality primers are (Primer design tips and toll, ThermoFisher): a length between 20-24 nt; a melting temperature (Tm) of forward and reverse primers between 65-75 °C, with no more than 5 °C of difference between each other; GC content between 40-60 %, with the 3'- end of the primer enriched in CG in order to promote a strong and specific binding; 3 to 6 extra nucleotides at the 5'-end of the primer if a restriction site is inserted, in order to allow efficient digestion. It is also necessary to avoid the design of regions prone to form secondary structures, regions with more than 4 repeated bases and dinucleotide repeats, since intra- and inter-primer homology could lead to self-dimers or primer-dimers instead of annealing to the desired DNA sequences.
The annealing temperature (Ta) for a forward/reverse primer pair is generally calculated to be 3-5°C lower than the lowest estimated Tm. However, the optimal temperature for PCR often needs to be empirically determined.

In this thesis, primer pairs for the Gloden Gate cloning of two human-CD19 based constructs were designed and used for the cloning into phFc expression vector (**Table 3.1**). CD19 sequence was imported by OriGene. Designed primers were ordered and purchased from Sigma Life Science. The Custom Oligos design tool (Sigma Aldrich) was used to check and evaluate manually designed primer sequences. *Bsa* I restriction sites were introduced in each primer sequence, while a 6xHis Tag was introduced only in the forward primer used for the cloning of the CD19_Fc construct.

Table 3.1 PCR primers for Golden Gate cloning into phFc

Construct	Vector	Forward	Reverse
CD19EC	phFc	#335 ATAAATGGTCTCACTCAGC GAAGCTGGGTGCCCCGG	#336 AGCAATGGTCTCTTTCCT GGCCGAGCAGTGATCTCC AGG
CD19_Fc	phFc	#358 AATGGTCTCACTCACATCA TCATCATCATCATGCGAAG CTGGGTGC	#365 AGCAATGGTCTCTCTTCT GGCCGAGCAGTGATCTCC AGG
CD19_Fc_wo_His	phFc	#335 ATAAATGGTCTCACTCAGC GAAGCTGGGTGCCCCGG	#365 AGCAATGGTCTCTCTTCT GGCCGAGCAGTGATCTCC AGG

All primers are reported in a 5' to 3' direction.

PCR
PCR has been developed in 1983 by Kary Mullis, and has revolutionized biology, biotechnology and molecular medicine. Its main purpose is to allow the specific amplification of a target DNA, starting theoretically from one template molecule and obtaining millions of copies in a cell-free reaction. A PCR reaction relies on thermal cycling: three steps with different temperatures (T) are sequentially repeated many times (cycles). The first step consists in the *denaturation step*, carried out at high T (94-98 °C) that forces the double strand DNA template molecule to open into single strand structures, as a consequence of the disruption of hydrogen bonds between complementary bases. The second step consists of the annealing step, in which T is decreased (50-68 °C), in order to allow the pairing of short DNA oligonucleotides, i.e. specific primers, to complementary regions of the template strands, which are still denatured. In this step, T should be carefully modulated, as a too high T does not allow the primer annealing, while a too low T could result in unspecific primer pairing, and thus off-target amplification: normally, a good starting point is to set T of annealing 3-5 °C below the primer melting T (Tm), which is defined as the T at which 50% of the

primer molecules form a stable double helix and the other 50% is in single strand form. The third and last step of PCR consists in the 5' to 3' elongation of the complementary strand starting from the annealed primers, carried out by a thermophile DNA polymerase that catalyzes the addition of triphosphate nucleotides (dNTPs). The parameters of the elongation step must be set according to the specific features of the thermo-resistant polymerase used in the reaction. Several types of thermostable DNA polymerase suitable for PCR are known nowadays. They derive from different thermophilic organisms, such as *Thermus acquaticus* (e.g. Taq polymerase) and *Pyrococcus furiosus* (e.g. Pfu polymerase), or from artificially modified proteins (e.g. Pfx polymerase), and each one is characterized by different specifications (proofreading activity, fidelity, processivity, target size, etc.). The number of PCR cycles can be modulated, typically ranging from 20 to 40, according to the amount and quality of material required, considering that the number of molecules doubles from one cycle to the next (exponential growth), but also that the frequency of mutation and insertions increases along with the number of cycles.

PCR Experimental Settings

Platinum® *Pfx* polymerase (Invitrogen), a recombinant enzyme derived from the *Thermococcus* species strain KOD, was used in all preparative PCR reactions, because of its high fidelity (3'-5' proofreading activity) and processivity. The PCR reaction mixture required plasmid DNA template, dNTPs (mixed dATP, dTTP, dGTP, dCTP, Sigma-Aldrich), Platinum® *Pfx* polymerase amplification buffer (Invitrogen), 5 mM $MgSO_4$ (Invitrogen) and suitable forward/reverse primers and was prepared in Molecular Biology Grade water (Sigma-Aldrich), as described in **Table 3.2.**

Table 3.2 PCR reaction mixture.

DNA template (10-100 ng)	1-5 µl
10x Platinum® *Pfx* polymerase buffer	5 µl
50 mM $MgSO_4$	1 µl
10 mM dNTPs	1.5 µl
10 µM sense primer	1.5 µl
10 µM antisense primer	1.5 µl
Platinum® *Pfx* polymerase (1 unit)	0.4 µl
Molecular Biology Grade water	to 50 µl

Cycle timings and temperatures in PCR programs were based on primer pairs estimated Tm (influencing Ta) and on template bp length (influencing the time of the elongation step). A representative three-step PCR program is illustrated in **Table 3.3**. A Techne TC-300 thermocycler was used.

Table 3.3 Three-step PCR cycling.

Step	Temperature	Time	Cycles
Pfx polymerase heat activation	94 °C	2 min	1
Denaturing	94 °C	15 s	30
Annealing	55-65 °C	30 s	
Elongation	68 °C	30 s - 1 min	
Final extension	68 °C	3 min	1

Pfx polymerase is provided in an inactive form, bound to an antibody; thus, heat activation provides enzyme activity restoring. Denaturing, Annealing and Elongation steps are sequentially repeated, respectively, in every cycle.

Restriction Enzyme and DNA Digestions

The preparation of DNA for traditional cloning methods, also referred to as "cut-and-paste", typically includes DNA digestion by restriction enzymes to generate compatible ends that can be ligated together by a DNA ligase.

Restriction enzymes are a class of endonucleases (REase, restriction endonucleases) that recognize specific sequences, called restriction sites, generally 4-6 nt long, which can coincide or be near to the site of cleavage. Restriction enzymes were originally isolated from bacteria, in which they constitute a natural defensive system against foreign DNA molecules (e.g. of viral origin).

There are four main classes of restriction enzymes, each class being characterized by similar subunit composition and structure, cleavage position, sequence specificity and cofactor requirements: type I, type II, type III and type IV.

Type I REase cut DNA randomly, far from their recognition sites, and are therefore a not useful tool for molecular cloning.

Type II REase cut DNA at defined positions, adjacent or inside their recognition sites, producing restriction fragments of predictable length. Type IIS (e.g. *Bsa* I) and type IIG, are two specific subgroups of type II enzymes and cleave outside of their recognition sequences, which are asymmetric. As already mentioned, Type IIS are used in particular applications, such as Golden Gate Cloning.

Type III REase cut outside of their recognition sites, but require two similar sequences with opposite orientations along the same DNA molecule. Therefore, completely digested DNA fragments are rarely achieved with type III enzymes.

Type IV REase, instead, recognize modified (methylated) DNA.

Restriction endonucleases can generate both blunt and sticky ends upon cleavage, depending on the generation of nucleotides overhang (sticky ends) or not (blunt end) at the extremities of the restriction fragment.

Generally, sticky ends are preferred in order to clone a DNA fragment (insert) into a vector, since a directional cloning is facilitated by the usage of two different REase. The choice of the pair of restriction endonucleases to be used is mainly determined by the specific features of the vector MCS and the absence of such recognition sites within the insert sequence. Upon digestion using the selected REase of both insert and vector, their complementary ends can be ligated using a DNA ligase. Afterwards, the same REase can be used as post-cloning confirmatory tools.

Experimental settings for restriction Digestions

The digestion mixture must be set up according to the features of the REases selected for the cloning. Each restriction endonuclease, in fact, has specific working features, such as working T, and inactivation T. Buffers for optimal activity can vary according to the company from which the REases are purchased. In this thesis, restriction endonucleases and 10x digestion buffers containing bovine serum albumin (BSA) to optimize REase activity were from New England BioLabs (NEB) or Takara. Whether necessary, Molecular Biology Grade water (Sigma-Aldrich) was added to restriction digestion mixture. The temperature of reactions was set according to each REase optimal working T, using a Techne TC-300 thermocycler. DNA digestion was performed for a time ranging from 2 h (analytic purposes) to 8 h (preparative purposes), then REase inactivation was achieved by raising the temperature to 65-80 °C for 20 min.

To verify the presence of the insert of interest in recombinant plasmid vectors, an analytic restriction enzyme digestion can be set up (**Table 3.4**) using either the cloning sites or two plasmid recognition sites flanking the insert (REase 1 and REase 2).

Table 3.4 Analytic restriction digestion mixture

Plasmid DNA from Miniprep (2 µg)	10-15 µl
10x digestion buffer	2 µl

REase 1 (5-10 units)	1 µl
REase 2 (5-10 units)	1 µl
Molecular Biology Grade water	to 20 µl

Preparative enzymatic digestions were normally performed as described in **Table 3.5**, in order to subclone inserts from a donor vector to a recipient vector and to provide recipient vector with the suitable sticky ends. To maximize the final yield of purified insert/recipient vector, higher amounts of starting DNA were used here.

Table 3.5 Preparative restriction digestion mixture

DNA from Miniprep/Midiprep (up to 1 µg)	10-40 µl
10x digestion buffer	5 µl
REase 1 (5-10 units)	1 µl
REase 2 (5-10 units)	1 µl
Molecular Biology Grade water	to 50 µl

Digestion mixtures were analyzed through agarose gel electrophoresis and, when needed, the separated insert/recipient vector bands were purified from agarose gel and quantified as described in following sections.

Vector Dephosphorylation

To avoid spontaneous re-circularization of a digested vector, a dephosphorylation reaction (**Table 3.6**) was performed on the digested recipient plasmid, upon purification from agarose gel. This procedure removes the phosphoric group at the 5'-end of the linearized vector, preventing the reconstitution of DNA phosphodiester bond in the absence of the insert (which carries 5' phosphoric groups). The reaction was performed using the Alkaline Phosphatase kit (rSAP, Roche) and incubated at 37 °C for 16 h. The phosphatase was then inactivated by heat incubating the mixture at 65 °C for 20 min.

Table 3.6 Dephosphorylation reaction

DNA agarose gel extraction	27 µl
10x Dephosphorylation buffer	3.1 µl
Shrimp Alkaline Phosphatase	1 µl

Vector-Insert Ligation

Ligation reactions were carried out in order to introduce a digested and purified insert into a dephosphorylated recipient vector, normally being an expression plasmid. Ligation was achieved through a DNA ligase-driven enzymatic reaction using the DNA ligation Mighty Mix kit (Takara).
In particular, for the Golden Gate Cloning a mass ratio of 1:1 between insert and vector was required, with 75 ng being the desired amount of DNA.
The ready-to-use reaction mixture provided in the Takara kit as a 2x concentrated solution was then added in a 1:1 volume ratio (**Table 3.7**). Molecular Biology Grade water (Sigma-Aldrich) was used whether necessary. The stages and numbers of cycles required to perform the Golden Gate cloning are reported in **Table 3.8**.

Table 3.7 *Bsa I* Ligation reaction

Vector	75 ng
Insert	75 ng
Bsa I	1 µl
2x Mighty Mix	5 µl
Mol Biology Grade water	to 10 µl

Table 3.8 Golden Gate Cloning stages

Temperature	Time	N° of cycles
37 °C	20 sec	1
37 °C	3 min	26
16 °C	4 min	
50 °C	5 min	1
80 °C	5 min	1
16 °C	∞	Final Hold

The whole volumes were then transformed into competent *E. coli* MACH-1 cells, as described in the following paragraphs. Then, the transformed colonies grown were counted and the percentage of ligation efficiency was calculated as follows:

$$Transformation\ efficiency = \frac{Colonies\ on\ ligation\ plate\ (+)}{Colonies\ on\ negative\ control\ plate\ (-)} x\ 100$$

For efficiency values higher than 25%, picking four colonies out of the positive plate was considered enough to get at least one positive (recombinant) clone.

3.2.1.2 InFusion Cloning

In-Fusion HD Cloning Kits (Takara) are designed for fast, directional cloning of one or more fragments of DNA into any vector. The main feature of In-Fusion cloning technology consists in the use of the In-Fusion Enzyme© (Takara), which fuses DNA fragments (e.g., PCR-generated inserts and linearized vectors) efficiently and precisely, by recognizing 15-bp overlaps at their ends. These 15-bp overlaps can be engineered by designing primers for amplification of the desired sequences. In-Fusion cloning allows to clone multiple DNA fragments simultaneously into any vector in a single reaction, without the need of restriction digestion, which is used only to linearize the vector, and not for ligation reactions. Moreover, final constructs are seamless with no extra or unwanted base pairs (**Fig. 3.2**).

Primer Design

Primer design and quality are critical for the success of the In-Fusion reaction. In order to join two or more fragments (e.g. vector and insert) using In-Fusion technology, they must share 15 bases of homology at each end. Therefore, In-Fusion PCR primers must be designed in order to generate PCR products containing ends that are homologous to those of the vector.

The following considerations must be considered when designing In-Fusion PCR primers:

1. the 5' end of the primer must contain 15 bases that are homologous to 15 bases at one end of the DNA fragment to which it will be joined (i.e., the vector or another insert). The 3' end of the primer must contain a sequence that is specific to the target gene.
2. The 3' portion of each primer:
   - should be gene-specific;
   - should be between 18–25 bases in length, and have a GC-content between 40–60%
   - should have a melting temperature (T_m) between 58–65 °C, with a T_m difference between the forward and reverse primers ≤4 °C. Moreover, the T_m should be calculated based upon the 3' (gene-specific) end of the primer, and not on the entire primer;
   - should not contain identical runs of nucleotides. The last five nucleotides at the 3' end of each primer should contain no more than two guanines (G) or cytosines (C).
3. Avoid complementarity within each primer to prevent hairpin structures, and between primer pairs to avoid primer dimers.

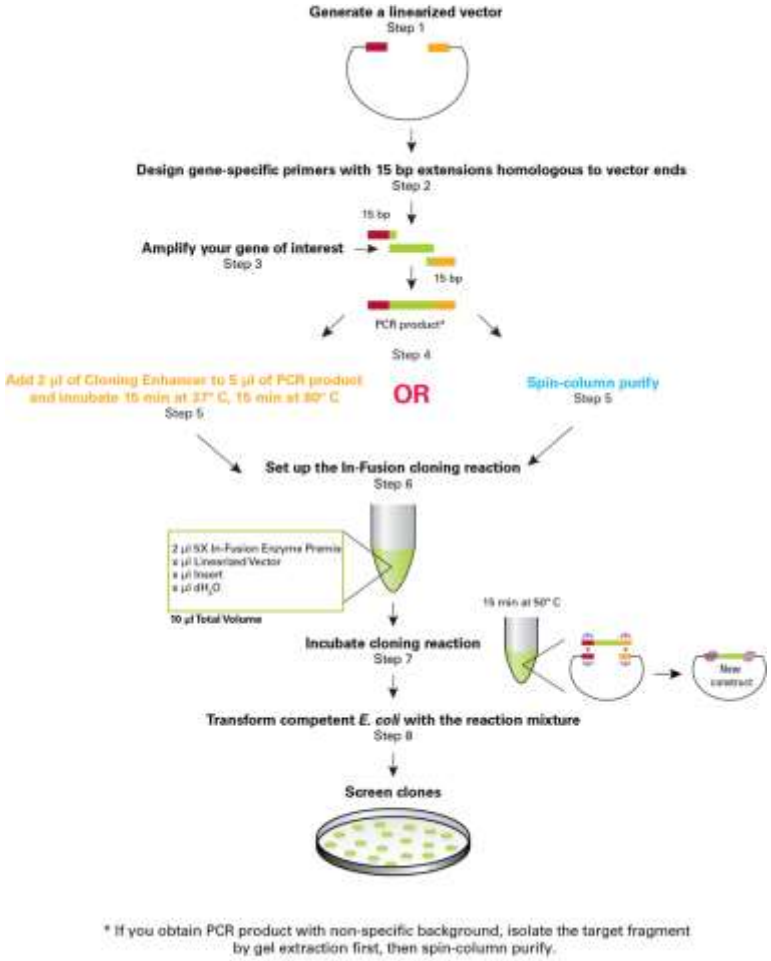

Fig. 3.2 In-Fusion Cloning protocol scheme.[429]

An online tool (InFusion Primer Design Tool, Takara) was used in order to design primers for the cloning of pET45b(+)_CD20_141_188, pET45b(+)_CD20_141_184 and pMICBD1_CD19, reported in **Table 3.9.**

Table 3.9 PCR primers for InFusion cloning into expression vectors

Construct	Vector	Forward	Reverse
CD20_141_188	pET45b(+)	#394 AGGAGATATACCATGCATCACCACCACCATCACATTAAAATTTCCCATTTT	#395 CTTTACCAGACTCGAGTTATTAAGATTGTATGCTGTAACAGTATTGG
CD20_141_184	phFc	#394 AGGAGATATACCATGCATCACCACCACCATCACATTAAAATTTCCCATTTT	#396 CTTTACCAGACTCGAGTTATTAGTAACAGTATTGGGTAGATGGGGAG
CD19EC	pMICBD1	#382 CGACTGGCTGGAATTCGAGGAACCTCTAGTGGTGAAGG	#383 GCAGGTCGACGGATCCTTATTAAGCGTAATCTGGAACATCGTATGGGTATGGCCGAGCAGTGATCTCC

All primers are reported in a 5' to 3' direction and for *Nco I* and *Not I* cloning sites.

PCR settings

CloneAmp HiFi PCR Premix (Cat. No. 639298, Takara) consists in a convenient 2X master mix that provides efficient DNA amplification, using CloneAmp HiFi Polymerase (Takara).
The recommended PCR cycles for amplification are reported in **Table 3.10**.

Table 3.10 Three-step PCR cycling

Step	Temperature	Time	Cycles
Clone AmpHiFi pol heat activation	94°C	2 min	1
Denaturation	98°C	10 s	35
Annealing	55-65°C	15 s	
Elongation	72°C	30 s - 1 min/kb	
Final extension	72°C	5 min	1

Denaturation, Annealing and Elongation steps are sequentially repeated, respectively, in every cycle.

InFusion reaction

In general, for optimal cloning results using InFusion reaction, a vector to insert molar ratio of 1:2 is recommended, but for the cloning of small DNA fragments (between 150 bp and 350 bp), the suggested vector to insert molar ratio is between 1:3 and 1:5. The optimal vector to insert molar ratio for pET45b(+)_CD20_141_188, pET45b(+)_CD20_141_184 and pMICBD1_CD19 was calculated using the online tool InFusion molar ratio calculator (Takara).

The InFusion reaction mixture was set up as described in **Table 3.11**, and the reaction was performed for 15 min at 50 °C. The reaction product was then transformed into *E. coli* Stellar Competent Cells (® Takara) as described below.

Table 3.11 InFusion reaction mix

Vector	x µl
Insert	x µl
5x InFusion HD Enzyme Premix	2 µl
Mol Biology Grade water	to 10 µl

3.2.1.3 Gene Synthesis

Chemical gene synthesis represents an alternative option to isolation of the target gene from the genome or transcriptome. In particular, this method is preferred when working with an exceptionally long target gene or when extensive modifications need to be introduced into the original gene. Synthetic VHH21A_8xHis and TCAN3 were obtained by Twist Bioscience (CA, USA).

3.2.1.4 Bacterial cells for DNA cloning

Bacterial cells constitute an efficient and cost-effective system to amplify plasmid DNA of interest *in vivo*. In this thesis, *Escherichia coli* (*E. coli*) bacteria were used as cellular hosts for recombinant DNA cloning purposes.
In particular, *E. coli* MACH-1 (W Δ*recA1398 endA1 fhuA* Φ80Δ(*lac*)M15 *Δ(*lac*)X74* hsdR*(*$r_K^-m_K^+$*)* were used, since they represent a particularly indicated strain for high-copy plasmid DNA replication in a short period of time. In fact, doubling time is approximately 50 min, which allows a rapid colony growth in solid medium (~ 8 h at 37 °C). Moreover, in MACH-1 cells *endA1* (endonuclease A1) and *hsdR* (endonuclease R) are deleted, protecting from unspecific and un-methylated DNA degradation, respectively.

Bacterial Competent Cells preparation

Bacterial cells which are able to mediate foreign DNA uptake are referred to as *competent*. Non-naturally competent cells, such as *E. coli*, can be artificially treated through chemical or electroporation methods in order to become competent.

For this thesis, *E. coli* MACH-1, BL21(DE3), BL21(DE3)Δ*ansA*/*ansB*, Origami (DE3)-Tig factor and HB2125 strains were prepared as competent through chemical methods and used for subsequent transformation. Chemical procedures generally involve cells exposure to divalent cations (e.g. Ca^{2+}), which act as a bridge between DNA phosphate groups and negatively-charged macromolecules of the bacteria cell wall.[430]

E. coli chemically competent cells were prepared by streaking the glycerol stock onto a TSA (Tryptone Soya Agar: 15 g/l casein enzymic hydrolysate, 5 g/l papaic digest of soyabean meal, 5 g/l NaCl, 0.7 g/l lecitin, 5 g/l Polysorbate 80, 15 g/l agar) plate, which was incubated at 37 °C o.n. (overnight). From this plate, one single colony was picked and inoculated into 5 ml of 2xTY (16 g/l tryptone, 10 g/l yeast extract, 5 g/l NaCl) liquid medium and incubated at 37°C, 250 rpm overnight. The following day, 1 ml of overnight culture was diluted into 100 ml of fresh 2xTY broth in a 500 ml flask and incubated at 37°C, 250 rpm, until cells reached log phase of growth (i.e. when OD550nm=0.48). Cells were then collected by centrifugation (4000 x g for 5 min at 4°C), resuspended in TfbI buffer (30 mM potassium acetate, 100 mM rubidium chloride, 10 mM calcium chloride, 50 mM manganese chloride, 15% glycerol, pH 5.8) and iced for 15 min. Cells were pelleted again by centrifugation as above, resuspended in TbfII buffer (10 mM MOPS, 10 mM rubidium chloride, 75 mM calcium chloride, 15% glycerol, pH 6.5) and iced for 15 min. Freshly prepared competent cells were either used immediately or flash-frozen in liquid nitrogen and stored at -80°C.

Bacterial Cells Transformation *via* Heat Shock

Bacteria can acquire foreign genetic material through different biological processes, divided into conjugation, viral transfection and transformation. Particularly, bacterial transformation consists in the intracellular uptake of exogenous DNA from extracellular environment by competent bacteria cells.

For this thesis, chemically competent *E. coli* MACH-1, BL21(DE3), Origami (DE3)-ch5 and HB2125 strains cells were transformed with the recombinant plasmid DNA of interest using the heat-shock method. This strategy is based on short-transient increased permeability of the microorganism cell wall, given by the abrupt temperature shift, which allows the foreign DNA to enter the cell. The plasmid DNA in the cell remains separated from the genome and can be independently replicated. According to the protocol, 5-100 ng (in a volume comprised between 1 and 10 µl) of DNA were pipetted into a snap-top tube and 50 µl of either freshly-prepared or thawed *E. coli* competent cells were placed above the DNA without mixing. The mixture was incubated on ice for 20 min, then heat-shocked using a water bath at 42°C for 45 s and then re-incubated on ice for 5 min. Cell recovery was performed by adding 150 µl of 2xTY non-selective medium and incubating the culture at 37°C at 250 rpm for 1 h. This recovery step allows the production of the factor involved in antibiotic resistance in successfully transformed cells. Under sterile conditions, recovered cells were plated onto TSA selective plates and incubated at 37°C o.n.

Stellar Competent cells transformation

E. coli Stellar Competent Cells (® Takara) are optimized for In-Fusion cloning, in order to be less sensitive to InFusion enzyme potential cytotoxicity. During the procedure, 2.5 µl of the In-Fusion reaction mixture were put at the bottom of a Snaptop tube and added with 50 µl of freshly thawed Stellar Competent Cells. The mixture was incubated on ice for 25 min, and then a heat shock at 42°C in water bath was performed for 45 s. The tube was re-incubated on ice for 5 min, and then 450 µl of pre-warmed at 37 °C SOC medium (Takara) was added. Cells were incubated at 37°C for

1 h, centrifuged at 1600 rpm for 5 min, resuspended in 150 µl of SOC medium and plated on TSA selective plates, which were then incubated at 37 °C o.n.
For pET45b(+)_CD20_141_188, pET45b(+)_CD20_141_184, the InFusion reaction mix had to be diluted 1:5 into TE Buffer (10 mM Tris-HCl, 1 mM EDTA pH 8), as suggested in the Troubleshooting, in order to obtain a successful cloning.

Selective Bacterial Media
Artificial plasmids generally contain one or more genes that assure resistance to specific antibiotics through their encoded proteins (e.g. β-lactamases). This functional feature allows to positively select cell clones that contain the plasmid of interest when the specific antibiotic is comprised in the bacteria medium (selective medium). Antibiotics can be included both in solid media (containing agar-agar solidifying agent) and liquid media, after autoclave sterilization and cooling of the medium. Antibiotic-containing solid media allow selection of discrete colonies deriving from a single cell that express the desired antibiotic resistance, while antibiotic-containing liquid media guarantee growth of a previously selected resistant clone, contrasting potential contamination.
Selective media were prepared by adding one or multiple antibiotics to the normal components required for bacterial growth at the following final concentrations:

- 100 µg/ml ampicillin or carbenicillin
- 50 µg/ml kanamycin
- 15 µg/ml tetracycline
- 20 µg/ml chloramphenicol

Differential Bacterial Media
In order to differentiate bacterial clones that contain recombinant plasmid from those that carry non-recombinant plasmid, culture media highlighting specific phenotypic features may be used. The blue/white screening is a common strategy for recombinant colonies selection, based on the use of a recipient vector containing the LacZ reporter gene, expressing β-galoctosidase. In fact, the active form of β-galoctosidase is able to metabolize lactose analogues, such as the 5-bromo-4-chloro-3-indolyl-β-D-galactopyranoside (X-gal) substrate, which can be included in the bacterial medium, producing an insoluble blue compound (5,5'-dibromo-4,4'-dichloro-indigo), which precipitates *in situ* and becomes visible in the bacterial colonies. The LacZ cassette is generally introduced within the plasmid sequence in a site where it is inactivated upon insertion of the gene of interest (recombinant plasmid). The presence of blue-colored colonies is therefore indicative of intact β-galoctosidase activity, while non-blue (white) colonies are presumably those in which β-galoctosidase activity was impaired by gene insertion, i.e. those carrying recombinant plasmid. Solid media were used for blue/white screening of transformed MACH-1 cells with phFc vector, by adding 20 µg/ml of X-gal to TSA plates. After plating bacteria, the blue color was visible, together with colonies growth, after o.n. incubation at 37°C.

3.2.1.5 Expression plasmids
phFc
phFc is an in-house engineered vector, modified from the pMYTH vector, which allows to express C-terminal recombinant fusion proteins with the human Fc fragment. This vector allows the cloning of the insert *via* Golden Gate Cloning procedure and a white/blue screening. phFc is designed for expression into mammalian cells hosts, and carries the SV40 origin of replication, allowing an increased amplification and an extended temporal expression of the protein of interest in cells expressing SV40-T antigen (Simian Vacuolating Virus 40 Ag), such as HEK293T mammalian cells.

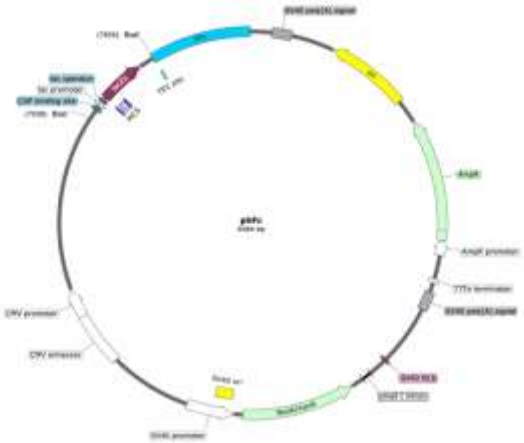

Fig. 3.3 phFc vector Map *(created with SnapGene Viewer)*

pET45b(+)

pET45b(+) (Novagen) is part of the pET™ plasmid series from Novagen and represents an effective vector system specifically designed for the expression of recombinant proteins in *E. coli*. In this system, the expression of the target protein is under the control of the T7 bacteriophage promoter. Upon induction, a significant portion of cell resources are redirected to target gene expression, to the point that the desired product can represent >50% of total protein within the cell in a few hours of induction.

The rich multiple cloning site of pET45b(+) was used to insert VHH21A_8xHis, hCD20_141_184, hCD20_141_188 and TCAN3, using *Nco* I at 5' and *Not* I at 3' as cloning sites. In all of them, the *Nco* I restriction site (CCATGG), containing one ATG start codon, imposed the reading frame (**Fig 3.4**).

Figure 3.4. pET45b(+) vector Map *(created with SnapGene Viewer)*

pMIC-BD1

pMIC-BD1 is a vector used for the selection of antibodies against a target antigen *via* Intracellular Antibody Capture Technology, a Yeast Two Hybrid-based technique modified from Cattaneo et al. (see paragraph 3.2.7).[431]

pMIC-BD1 was designed as a bait vector by Cattaneo et al., allowing to clone target fusion proteins in-frame with the *E. coli* lexA DNA binding domain. Some important features of this vector are bacterial chloramphenicol resistance, TRP1 gene (which allows yeast containing this plasmid to grow in minimal medium lacking tryptophan) and the 2μ origin of replication. *E. coli* lexA protein expression is under the control of the yeast alcohol dehydrogenase I (ADH1) promoter.

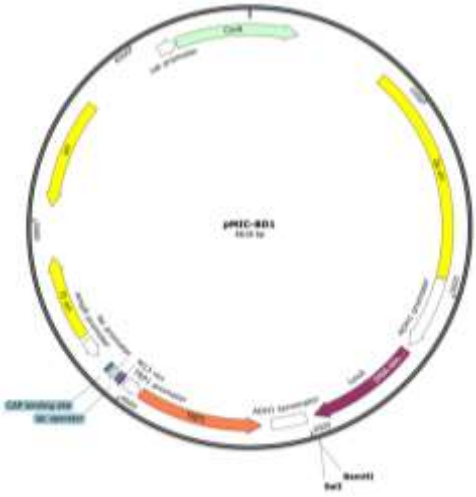

Figure 3.5 pMICBD1 vector Map *(created with SnapGene Viewer)*

3.2.1.6 Agarose Gel Electrophoresis

Agarose gel electrophoresis represents an analytical technique that is used to separate molecules according to their mobility, determined by molecular charge/mass ratio, under the action of an electric field. In this thesis, agarose gel electrophoresis was used to separate different DNA molecules according to their size, for both analytical and preparative purposes. In fact, nucleic acids display constant charge/mass values, thanks to the presence of one negatively-charged phosphate group in each nucleotide: therefore, on agarose gel electrophoresis, a nucleic acid migrates and separates depending on its length only.
Agarose is a non-ramified polymer of repeated disaccharide units, which forms a semi-solid gel upon dissolution in a suitable buffer, followed by boiling and cooling procedures. Agarose concentration can be modulated in order to obtain gels with variable matrix porosity, according to the desired resolution power. Concentration commonly varies from 0.7% (w/v) to 3% (w/v) agarose, adapted to separate large (up to 25 kb) and very small (down to 100 bp) DNA molecules, respectively. During the preparation of the gel, marker compounds such as Ethidium Bromide (EtBr) are added into the matrix, in order to allow efficient visualization of separated DNA molecules in the agarose gel. In particular, EtBr interposes between nucleic acid bases and, once exited by UV radiation, it becomes fluorescent, intensifying the signal almost 20-fold upon binding to nucleic acid, reporting the presence of DNA.
In this work, 0.32-0.48 g to 0.8-1.2 g of agarose powder (Agarose low EEO, Agarose Standard; Applichem), were dissolved in 40 ml/60 ml of 1x TBE buffer (89 mM Tris Base, 89 mM Boric Acid, 2 mM EDTA, pH 8.0), to obtain 0.8% to 2% agarose gels. The solution was microwaved until agarose dissolution, then cooled to about 50°C. EtBr (2.5 µl-3.75 µl of a 10 mg/ml water solution) was added before pouring the resulting solution into a suitable horizontal electrophoresis tank, equipped of a comb to create wells, and cooled down until gel solidification. The gel was covered with 1x TBE buffer and samples, previously mixed with 3x loading buffer (30% Glycerol, 3 mM EDTA, 0.25% Bromophenol Blue, pH 8.0) or 6x Loading Dye (ThermoFisher) were applied to the wells. The loading buffer allows to visualize the samples in the wells and to control the progression of migration. As molecular weight standards, 1 kb and/or 100 bp DNA ladders (GeneRuler™, Fermentas) were used. The electrophoretic run was carried out at 100 V until the blue dye reached the bottom of the gel and the visualization of fluorescently-labeled RNA and DNA was achieved through a transilluminator (Biostep Darkhood DH-30/30) and dedicated Argus X1 software (Biostep®).

3.2.1.7 DNA extraction from Agarose Gel electrophoresis

Agarose gel electrophoresis may be used as a preparative technique. The separated band of interest can be recovered from agarose gel and brought into solution using dedicated reagents: in this thesis, the QIAquick Gel Extraction Kit (QIAGEN) was used, in order to obtain pure PCR products and discrete DNA restriction fragments (related to insert or vector) after REase digestion.

For the procedure, the protocol of the QIAGEN kit was followed. Briefly, after verifying the correct size of the DNA fragment of interest according to agarose gel electrophoresis, the corresponding band was excised from the gel, using a fine scalpel, and then recovered into a clean tube and weighed. In order to allow agarose gel solubilization, three (for 1% agarose gels) or six (for 2% agarose gels) volumes of QG buffer (5.5 M Guanidine Thiocyanate, 20 mM Tris-HCl, pH 6.6) were added to each volume of gel, considering the 100 µl buffer-100 mg gel equivalence. To facilitate dissolution, the tube was incubated at 37°C for about 10 min, and then vortexed. The procedure was repeated until the dissolution was complete. Then, one volume of isopropanol was added to the tube. The final mixture was transferred to a QIAquick Spin Column, whose resin selectively binds DNA molecules, centrifuged at 13000 rpm for 1 min (or at 2000 rpm for particularly long fragment e.g. linearized vectors), and the flow-through solution was then discarded. 500 µl of QG buffer were applied to the column and centrifuged at 13000 rpm for 1 min to remove agarose residues. 750 µl of PE buffer (20 mM NaCl, 2 mM Tris-HCl, pH 7.5, 80% ethanol) were added as a wash and centrifuged as above. The flow-through was discarded and centrifugation was repeated to remove every residue of PE buffer. The column was then placed into a clean Eppendorf tube and the DNA bound to the column resin was eluted by incubation with 30 µl of EB buffer (10 mM Tris-HCl, pH 8.5) for 1-7 minutes and then by centrifugation at 1300 rpm for 1 min. Extracted DNA was quantified using the NanoDrop system of the POLARstar Omega Plate reader Spectrophotometer (BMG Labtech).

3.2.1.8 DNA sequencing and Sequence analysis

After a molecular cloning procedure, in order to verify that the DNA sequence obtained is actually the desired one and correctly encodes the product of interest, a DNA sequence analysis is typically performed. In this thesis, Sanger DNA sequencing service was performed by GENEWIZ® (Bahnhofstraße 86, Leipzig, Germany) at least once for all the generated recombinant constructs. DNA sequence analysis of constructs was performed using SnapGene Viewer and CLC Sequence Viewer software and bioinformatics tools, such as SIM Alignment ExPASy Tool.

3.2.1.9 Glycerol Stocks

For long-term time storage, 1.5 ml of cell culture were preserved at -80°C in 20% sterile glycerol.

3.2.1.10 Plasmid Preparation

Plasmid preparation is a common method used to extract and obtain pure recombinant plasmid DNA from a liquid bacterial culture. For this purpose, several commercial kits are available, known as, in order of DNA yield, Minipreps, Midipreps, Maxipreps, Megapreps, and Gigapreps. They allow to obtain the desired construct in a simple and rapid way, by exploiting the same basic principles. Generally, alkaline lysis of bacterial cells represents the first step, using a buffer containing a detergent (sodium dodecyl sulfate, SDS), that disrupts the phospholipid bilayer of membranes, and a strong base (sodium hydroxide) that denatures structural membrane proteins. Then, cell debris, proteins and chromosomal DNA are precipitated and removed by centrifugation. Plasmid DNA, which remains in solution, is then applied to a suitable chromatographic resin for further purification. In order to extract plasmid DNA from positive recombinant clones, two types of kits were used, according to the required yield: GenElute Plasmid MiniPrep Kit (SIGMA ALDRICH, plasmid DNA yield: up to 15 µg) and the QIAGEN plasmid Midi prep kit (QIAGEN, average plasmid DNA yield: 100-350 µg). Both SIGMA ALDRICH and QIAGEN resins for plasmid purification are organic polymers based on anion-exchange and bound DNA can be eluted under appropriate low-

salt and pH conditions. Extracted plasmid DNA was quantified using the NanoDrop system POLARstar Omega Plate reader Spectrophotometer (BMG Labtech).

GenElute Plasmid Mini Prep Kit (Sigma Aldrich)
On day 1, one single clone picked from a selective TSA plate was inoculated into 10 ml of selective 2xTY broth o.n. The next morning, 2 ml of culture were harvested by centrifugation (6000 rpm, 10 min) and resuspended into 200 µl of Resuspension Buffer (Resuspension buffer: 50 mM Tris-HCl pH 8.0, 10 mM EDTA, 100 µg/ml RNaseA). To lyse cells, 200 µl of Lysis Solution (200 mM NaOH, 1% SDS), were added and mixed by gentle tube inversion for 4-6 times. Then, 350 µl of Neutralization Buffer (4.2 M Glu-HCl, 0.9 M Potassium Acetate, pH 4.8) were added and mixed by gentle tube inversion for 4-6 times. Precipitated material was removed by centrifugation (14000 rpm, 10 min). The supernatant was then added onto a GenElute MiniPrep Binding Column, previously equilibrated with 500 µl of the Column Preparation Solution, and the DNA was allowed to enter the resin by centrifugation at 14000 rpm for 10 min. The DNA binding-resin was washed two times, the first time with 500 µl of an Optional Wash Solution and one with 750 µl of Wash solution (70% Ethanol), and centrifuged a third time without addition of liquid, in order to remove ethanol traces. The Binding Column was then placed into a new 1.5 ml tube and the DNA was eluted by adding 100 µl of EB Buffer and by centrifugation at 1400 rpm, 1 min.

QIAprep Midi Prep Kit
On day 1, one single clone picked from a selective TSA plate was inoculated into 0.5 ml of selective 2xTY broth. This starter culture was incubated at 37°C, 250 rpm for 8 h, then diluted into 100 ml of fresh selective 2xTY medium and grown at 37°C, 250 rpm overnight. Bacterial cells were harvested by centrifugation (6000 x g at 4 °C for 15 min) and resuspended into 10 ml of P1 buffer (Resuspension buffer: 50 mM Tris-HCl pH 8.0, 10 mM EDTA, 100 µg/ml RNaseA). To lyse cells, 10 ml of P2 buffer (Lysis buffer: 200 mM NaOH, 1% SDS) were added by mixing thoroughly and incubating at room temperature for 5 min. Then, 10 ml of chilled P3 buffer (Neutralization buffer: 3.0 M potassium acetate, pH 5.5) were added and the resulting precipitate-containing solution was incubated on ice for 20 min. Precipitated material was removed by centrifugation (20000 x g at 4 °C for 30 min), which was eventually repeated until the supernatant containing plasmid DNA was clear. After that, the supernatant was applied to the QIAGEN-tips column, previously equilibrated with 4 ml QBT buffer (Equilibration buffer: 750 mM NaCl, 50 mM MOPS, pH 7.0, 15% isopropanol (v/v), 0,15% Triton X-100 (v/v)), and allowed to enter the resin by gravity flow. The DNA-binding resin was washed two times with 10 ml of QC buffer (Washing buffer: 1.0 M NaCl, 50 mM MOPS, pH 7.0, 15% isopropanol(v/v)) and the DNA was eluted with 5 ml Buffer QF (Elution buffer: 1.25 M NaCl, 50 mM TrisCl, pH 8.5, 15% isopropanol (v/v)) in a clean tube. The eluted DNA was precipitated by adding 0.8 volumes (3.5 ml) isopropanol and centrifuging at 15000 x g for 45 min at 4°C. The DNA pellet was washed with 2 ml of 70% ethanol and precipitated again by centrifugation at 15000 x g for 10 min at 4°C. The pellet was left to dry completely o.n. and resuspended with 100-200 µl of EB buffer.

Individual Mini and Midi plasmid preparations were subsequently analyzed by restriction enzyme digestion, using REases recognition sites flanking the insertion site within the vector, to verify the presence of the insert. In order to control the DNA sequence and integrity of the insert GENEWIZ® (Hope End, Takeley, Essex, UK) sequencing service was used, as described above.

3.2.2 Expression of recombinant Proteins

Several methods for protein expression are available nowadays. Such biotechnological approaches allow to produce high levels (over-expression) of the desired protein in reduced times and with remarkable batch-to-batch reproducibility, thanks to the possibility to easily standardize many steps of the entire production process.[432] The most suitable conditions for production of a given protein must be chosen among a wide spectrum of possibilities, with regard to expression

host strains and vectors. These features make recombinant expression the favorite strategy for obtaining the protein of interest both at the research laboratory and at the industrial level.
In this thesis, CD19, CD20, VHH21A and TCAN3 recombinant proteins were expressed using both prokaryotic and eukaryotic host systems and using different expressing vectors.

3.2.2.1 Hosts for expression
The choice of a host organism for the expression of proteins in recombinant form is pivotal to define the outline of the whole expression and part of the purification process, such as reagents and technical equipment. A wide variety of cellular hosts has been used and optimized for protein production. Among prokaryotes, *E. coli* bacteria are indeed the preferred organisms, while among eukaryotes, the most commonly used cell systems comprise yeasts, insect and mammalian cells. The use of each of them show strengths and weaknesses, thus the selection of a specific host should be evaluated according to intrinsic features of the gene product to be expressed (e.g. codon usage, protein MW, post-translational modifications).
In this thesis, bacteria (*Escherichia coli*), yeasts (*Saccharomyces cerevisiae*) and mammalian cells (*Homo sapiens*) were tested for expression of recombinant proteins.

Bacterial Hosts
E. coli is extensively used also as an expression host for production of recombinant proteins, since it presents several advantages. Firstly, its fast growth rates: when exposed to optimal conditions (nutrients, temperature, oxygen, etc.), *E. coli* cells doubling time is about 20 min. However, it should be noted that a quick cell growth does not necessarily correspond to efficient protein expression and, on the other hand, over-production of a recombinant protein may interfere with the physiologic metabolism of the microorganism, having a negative impact on its fitness. Secondly, *E. coli* liquid cultures can reach very high density, increasing the efficiency of production process. Moreover, *E. coli* physiology is very well known and growth parameters can be easily modulated according to needs. Thirdly, rich culture media suitable for *E. coli* contain canonical and inexpensive components. Fourthly, exogenous recombinant DNA can be easily and efficiently transformed into pre-treated competent *E. coli* cells and expression vectors have been designed for usage in this simple organism.
In this thesis, three *E. coli* strains were used for protein expression: BL21(DE3), Origami(DE3)-Tig factor (Novagen) were evaluated for the expression of human CD20 protein and VHH21A nanobody cloned in pET45b(+), while BL21(DE3)Δ*ansA/ansB* were used for TCAN3 protein expression.
BL21(DE3) strain is a standard and efficient system for over-expressing proteins. It lacks *lon* and *ompT* endogenous proteases, which mediates intracellular protein degradation.
BL21(DE3)Δ*ansA/ansB* are BL21(DE3) cells custom-engineered by Dr. Douglas Scott Merrell (University of the Uniformed Services University of the Health Sciences, Bethesda, MD, USA) to lack the *ansA* and *ansB* genes, encoding the *E. coli* endogenous type I and type II L-Asparaginases, respectively. These deletions enhance the overexpression of proteins with asparaginolytic activity, such as recombinant EcAII and TCAN3.
Origami (DE3) strain may be particularly useful for the production of disulfide bond-containing active proteins. These cells are characterized by a less reducing cytoplasmic environment, thanks to inactivation mutations introduced in the thioredoxin reductase (*trxB*) and glutathione reductase (*gor*) genes, greatly enhancing disulfide bond formation. The used Origami strain was also added with a vector expressing Tig factor protein, in order to favor a correct protein folding. For the selection of Origami (DE3)-Tig factor, 4 antibiotics were used: ampicillin (100 μg/ml), kanamycin (50 μg/ml), tetracycline (12.5 μg/ml) and chloramphenicol (20 μg/ml).
All the used *E. coli* strains are characterized by the "DE3" feature. This refers to the fact that, in such systems, the expression of the recombinant protein is regulated by the lactose-inducible T7 RNA polymerase derived from λ prophage, through a double-control system. A T7 RNA

polymerase promoter site is usually present upstream the target gene in the expression vectors used in bacteria. The synthesis of T7 RNA polymerase is regulated by the lac operon of the host cell genome. In bacteria, the lac operon controls the expression of three genes (β-galactosidase, lactose permease, and galactosidase O-acetyltransferase) involved in uptake and processing of lactose substrate. In the engineered DE3 *E. coli* strains, an extra gene encoding for the T7 RNA polymerase from λ prophage (T7lac operon) is included downstream the operator. A repressor constitutively binds to the operator sequence, inactivating the operon. Repression is removed in presence of lactose, when the amount of glucose as carbon source is deficient and causes cAMP accumulation that activates the CRP (cAMP Receptor Protein) recognition site in the operator, facilitating RNA polymerase binding to the promoter. Furthermore, lactose binds and inhibits the operator repressor activity. In such conditions, the expression of genes within the lac operon is activated.
In order to induce recombinant protein synthesis, the T7lac operon can be activated by adding to the culture medium a synthetic molecule similar to α-lactose, namely isopropyl β-D-1-thiogalactopyranoside (IPTG). The IPTG induction efficacy is related to its concentration, providing a way to modulate protein expression, together with other growth parameters, such as cell density, time and temperature of induction.

Mammalian Hosts
Mammalian cells are often considered the best hosts for production of high-quality recombinant proteins of mammalian origin, in terms of correct protein folding, post-translational modifications and molecular assembly, and consequently proper biological activity. However, the currently available technologies that allow to set up and maintain mammalian expression systems are relatively expensive and require dedicated laboratory equipment.
In order to produce recombinant CD19EC constructs, a mammalian cell system, represented by human embryonic kidney cells (HEK293T) was used. The choice of this human cell host was dictated by the complex nature of the CD19 protein: an expression system as similar to the natural source is more likely to produce appropriate folding and post-translational processing of the protein itself.

3.2.2.2 Small scale Recombinant Proteins expression
Expression tests were performed in small scale for each host and recombinant protein of interest, in order to determine the best conditions of recombinant protein expression in a host organism, by changing some basic parameters of cell growth (e.g. temperature, time of induction, type and concentration of inducing agent) and evaluating the protein yields.

Small scale Expressions in *E. coli* (CD20, VHH21A and TCAN3)
Typically, on day -1, one colony for each recombinant pET45b(+) *E. coli* strain of interest, among BL21(DE3) and BL21(DE3)Δ*ansA/ansB*, was inoculated in 10 ml of selective 2xTY medium (pre-culture) and incubated at 37°C, 250 rpm overnight. The day after, 1 ml of each overnight culture was added to 50 ml selective 2xTY and incubated at 37°C, 250 rpm, till OD_{600nm} reached 0.6-0.8. Each culture was then split into two flasks
For BL21(DE3) transformed with CD20 constructs, one of the flasks was induced by adding 1 mM IPTG, while the second was grown without induction. Cultures were shaken at 25 °C, 250 rpm, for 5 h. 1 ml of each culture were sampled at different time points (0 h, 3h, 5 h,), and centrifuged at 14000 rpm, at 4°C, for 10 min.
For Origami(DE3)-Tig factor strain, transformed with CD20 constructs, one of the flasks was induced by adding 0.4 mM IPTG, while the second was grown without induction. Cultures were shaken at 18 °C, 250 rpm, for 24 h. 1 ml of each culture were sampled at different time points (0 h, 24 h), and centrifuged at 14000 rpm, at 4°C, for 10 min.

For BL21(DE3) transformed with TCAN3 construct, one of the flasks was induced by adding 0.4 mM IPTG, while the second was grown without induction. Cultures were shaken at 17 °C, 250 rpm, for 24 h. 1 ml of each culture were sampled at different time points (0 h, 5 h, 24 h), and centrifuged at 14000 rpm, at 4°C, for 10 min.
As expression of recombinant protein was expected to be intracellular, according to pET45b(+) features, supernatants were discarded and cell pellets were stored at -20 °C.

Before analysis, the frozen samples were thawed on ice. Cell pellets were then resuspended in 200 µl BugBuster® Protein Extraction Reagent (Novagen). 1 mg/ml lyophilized lysozyme (Applichem) was added in order to increase cell lysis efficiency. Resuspended pellets were rolled for 20 min at room-temperature. This represents a non-mechanical lysis strategy, which results into efficient release of soluble proteins. In fact, BugBuster® contains non-ionic and zwitterionic detergents that induce cell wall perforation and determine protein release without significant denaturation. Samples were subsequently centrifuged at 8000 x g, at 4 °C, for 10 min. The obtained supernatants contained the cellular soluble fraction and were separated from the pellets, which instead represented the cellular insoluble fraction and were resuspended into 100 µl of Denaturing Buffer (100 µM NaH2PO4, 10 mM Tris-HCl, 8 M Urea, pH 8).
All fractions were immediately analyzed by SDS-PAGE and Western blotting and stored at -20 °C.

Small scale Expressions optimization with chaperones in *E. coli* (VHH21A and TCAN3)

Issues encountered in protein expression in *E. coli* are often due to improper folding of the recombinant protein. Molecular chaperones are involved in protein folding, and their co-expression with target recombinant proteins is reported to increase their recovery from the soluble fraction. In this work, three plasmids from Takara Bio's Chaperone Plasmid Set, encoding for different molecular chaperones, were used for small scale expression optimization tests. Such plasmids were co-transfected in cells expressing the target recombinant proteins, which were selected according to the antibiotic resistance reported in **Table 3.12**. The induction of chaperones was then performed as described in **Table 3.12**, while paying attention to follow the induction procedure of the target recombinant protein, which was performed as described in previous paragraphs.

Table 12. Molecular Chaperons

Plasmid	Chaperon	Promoter	Inducer	Resistant Marker	References
pG-KJE8	*dna*K-*dna*J-*grp* E *gro*ES-*gro*EL	*ara*B *Pzt*-1	L-Arabinose Tetracycline	Chloramphenicol	[433-434]
pG-Tf2	*gro*ES-*gro*EL-tig	*Pzt*-1	Tetracycline	Chloramphenicol	[434]
pTf16	tig	*ara*B	L-Arabinose	Chloramphenicol	[434]

L-Arabinose: 2 % v/v
Tetracycline: 12.5 µg/ml
Chloramphenicol: 20 µg/ml

Fig. 3.6 Molecular Chaperons Vectors

A)

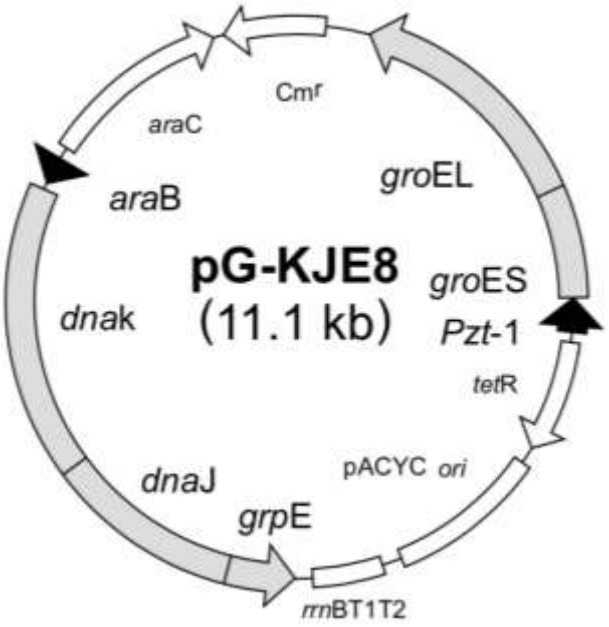

B)

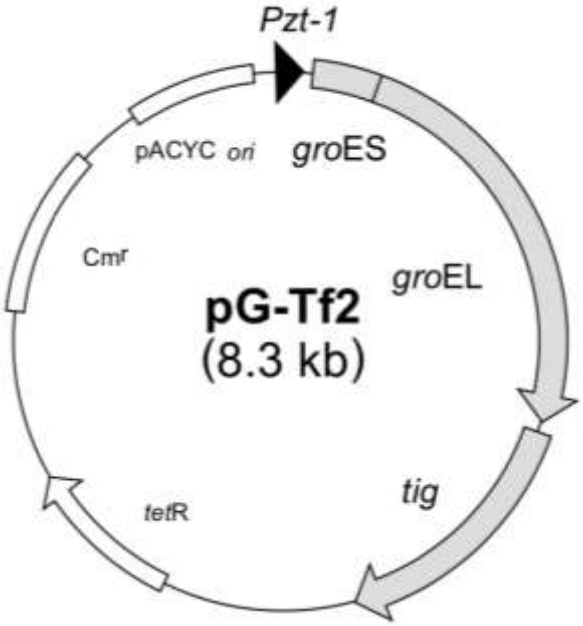

C)

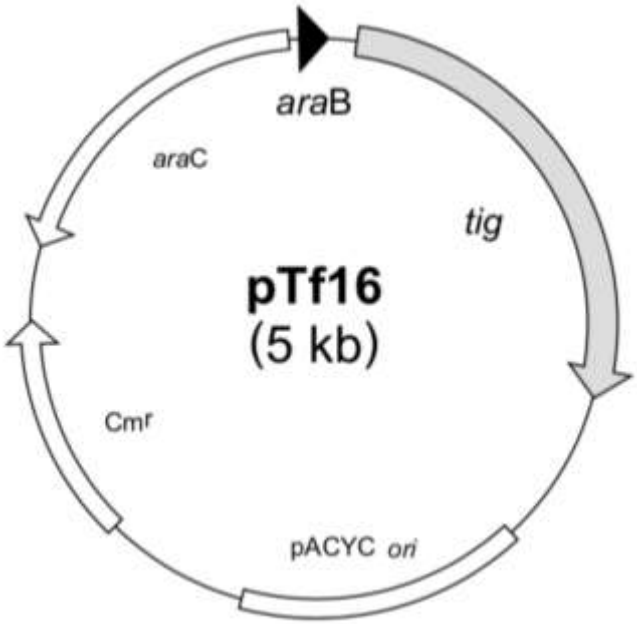

A) *pG-KJE8 vector map.* ***B)*** *pG-Tf2 vector map.* ***C)*** *pTf16 vector map (Takara Chaperon Plasmid set Cat. # 3340*

Small scale Expressions in HEK293T (CD19)

The term *transfection* refers to the uptake of exogenous DNA by an animal cell. In a *transient* transfection, in contrast to a *stable* transfection, the foreign DNA, typically a plasmid, is not integrated within the host cell genome. During mitosis, the transfected DNA is normally diluted by distribution to the cell progeny or degraded. As a consequence, when transfecting cells with a recombinant expression plasmid, expression of the target gene product is transient and typically results in maximum expression levels during the 48-96 h following DNA transfection.

In order to facilitate exogenous DNA to enter inside the cells, different approaches can be used: chemical, non-chemical, particle-based and viral vectors (transduction).

In this thesis, transient transfections using polyethylenimine (PEI) as transfecting agent were performed. PEI is a stable cationic polymer, composed of repeated units of amine group and two carbons aliphatic space. It acts by condensing DNA molecules into positively-charged particles that bind to anionic cell surfaces, stimulating endocytosis and the release of DNA into the cytoplasm.[435] Moreover, it is not significantly toxic for cells at the typical concentrations used for transfection.

For the small scale transfection, when HEK293T culture reached 90% of confluence, cells were detached and counted on a Bürker chamber. 2 ml of 4 x 10^5 HEK293T cells/ml suspensions were seeded in each well of 6-well plates and incubated at 37°C, 5% CO_2 in a humidified incubator. After 24 h, the cells were transfected by using 2 µg of recombinant plasmid DNA per well. The transfection mixture was composed by the DNA, PEI, and DMEM without fetal bovine serum (FBS) up to 100 µl. Different DNA:PEI mass ratio were tested in order to find the optimal conditions for protein expression (1:2; 1:3; 1:4; 1:5). These mixtures were incubated at room-temperature for 20 min, and then vortexed for 15 seconds, before adding 200 µl of transfection mixture to each well, in which exhausted medium was previously replaced with 1.8 ml of fresh DMEM (FBS 5%, L-Gln 1% and P/S 1%). Plates were incubated at 37°C, 5% of CO_2, in a humidified incubator.

In some cases, during optimization, three hours after transfection 4 mM valproic acid was added to some test wells. Through its histone deacetylase inhibitor (HDAi) action, valproate can inhibit removal of acetyl groups from histone Lys residues, preventing the formation of a condensed and transcriptionally silenced chromatin. In the presence of valproate, DNA hyperacetylation state is favored, allowing an increased gene expression.[436] After 24 h, DMEM FBS 5% medium was replaced with 2 ml of EX-CELL™ 610-HSF Hybrydoma Serum-free Medium (Sigma Aldrich). In order to monitor protein expression, 200 µl of supernatant were sampled from each well every 24 h for up to 10 days after transfection. Supernatants samples were centrifuged at 1200 x g for 5 min, in order to remove traces of cell contamination, and then added with 3x Reducing Loading Buffer (10% glycerol, 50 mM Tris-HCl, pH 6.8, 100 mM DTT, 0.1 bromophenol blue). Samples were then boiled at 99°C for 5 min and left at 4 °C until analysis through electrophoresis.

3.2.2.3 Large Scale Recombinant Protein Expression

Once basic cell growth conditions for optimal recombinant protein expression in the chosen host organism are determined through small-scale experiments, larger volumes of culture can be prepared in order to produce high amounts of the same protein, by reproducing the best conditions found from the small-scale test. However, as these two approaches are intrinsically different, it is not assured that the same positive results will be observed in a large scale experiment, which often requires further optimization. To have a better control on the influence of different growth conditions on protein expression, it is good practice to change only one parameter per batch of production and compare protein yields.

Cell Lysis and Cell Extract Clarification from *E. coli* soluble fraction

To recover cytoplasmic recombinant proteins from the soluble fraction, the culture media was removed by centrifugation (6000 x g, 4°C, 10 min) and cells were resuspended in resuspension buffer with a ratio 1000:50 (culture:buffer, ml:ml). Cell Lysis by sonication is a technique which exploits mechanical vibration transmitted by the liquid phase to disrupt cell wall by shear stress, which results in the release of intracellular proteins upon cell cavitation. Sonication was performed on ice, at variable power (from 40%-80%) according to experimental needs, using Soniprep 150 Aibra (Omni Sonic Ruptor 400, Omni International) sonicator. Serial cycles of sonication were performed, generally consisting of 1 min of sonication and 1 min of rest. After sonication, the cell extract was clarified by centrifugation in order to remove cell debris. According to our protocol, a first gross clarification was carried out centrifuging the cell extract at 10000 x g, 4 °C, 15 min. The supernatant was then centrifuged again at 18000 x g, 4 °C, 45 min and filtered 0.22 µm.

Large Scale Expression in *E. coli* (Insoluble Fraction)

Over-expression of exogenous proteins often relates to a highly stressful condition for the *E. coli* hosts, whose cellular machinery is almost completely dedicated to production of recombinant protein, that starts accumulating inside the cell. Under these conditions, bacterial cells develop cytoplasmic or periplasmic insoluble proteins aggregates, known as *inclusion bodies* (IBs), which are almost exclusively constituted by over-expressed protein and can grow as big as the host cell itself, constituting a rich source of recombinant protein.

Depending on bacterial growth condition and individual protein features, a protein can be stocked in inclusion bodies either in its native or, more likely, in an unfolded state. Therefore, downstream processing from IBs constitutes a major bottleneck in protein purification, as refolding of proteins from IBs to obtain biologically active protein is often a complicated and time-consuming procedure, since refolding conditions need to be optimized and adapted for every different protein of interest.

Different strategies have been developed to facilitate extraction of properly folded protein from IBs. In the classical inclusion bodies procedure (cIBs), overexpressed recombinant proteins are incorporated into the inclusion bodies in an unfolded state. On the contrary, it was observed that a modulation of bacterial growth conditions influenced the accumulation of recombinant protein in its native form: in this case, the so-called non-classical inclusion bodies can be obtained (ncIBs).[437]

In this thesis, large-scale protein production in insoluble fraction was performed using pET45b(+) hCD20_141_184, pET45b(+)_hCD20_141_188, and pET45b(+)_VHH21A_8xHis *E. coli* BL21(DE3) clones. pET45b(+)_TCAN3 was instead expressed in *E. coli* BL21(DE3)Δ*ansAansB.*

On day -2, the recombinant pET45b(+) *E. coli* BL21(DE3) clone of interest was streaked on a selective TSA plate and incubated at 37 °C overnight. From that plate, one colony was inoculated into 10 ml of selective 2xTY medium and shaken at 37 °C, 250 rpm o.n. The next morning, this starter culture was diluted into 500 ml of the same selective 2xTY medium and incubated at 37 °C, 250 rpm, until OD_{600}=0.5-0.8. For classical IBs formation, induction was performed by adding 1 mM IPTG and incubating at 37 °C, 250 rpm for 5 h. For non-classical IBs production, induction was triggered by the addition of 0.4 mM IPTG and incubating the cultures at 18 °C, 250 rpm, for 24 h. Cells were harvested by centrifugation (8000 x g, 4 °C, 30 min) and stored at -80 °C until processing.

Protein extraction from cIBs

E. coli BL21(DE3) classical inclusion bodies were processed following a two-step protocol modified from Mahlawat P et al 2012.[438] The first step consisted in a denaturation step, in which protein release from IBs and solubilization was promoted through high concentrations of a chaotropic agent (i.e. urea). Second, the protein was refolded by dilution of the chaotropic agent into a suitable buffer.

E. coli BL21(DE3) cell pellet was thawed on ice and resuspended into 50 ml /l of culture of Lysis Buffer A (100 mM Tris-HCl, 10 mM EDTA, pH 8.3). Resuspended cells were sonicated on ice, at 40% power by 6 to 12 serial cycles of 1 min each, followed by 1 min of rest. Lysed cells were centrifuged at 14000 x g, at 4°C, for 20 min and the pellet, representing the insoluble fraction, was washed once with 50 ml of Washing Buffer A (100 mM Tris-HCl, 10 mM EDTA, 1 M NaCl, pH 8) and twice with 50 ml of Washing Buffer B (100 mM Tris-HCl, 10 mM EDTA, 1% (v/v) Triton X-100, pH 8.3). The pellet was finally resuspended into 50 ml Denaturing Buffer (100 mM NaH_2PO_4, 10 mM Tris HCl, 8 M urea, pH 8.0) and stirred overnight at room-temperature to allow protein solubilization into 50 ml of Denaturing Buffer (100 µM NaH_2PO_4, 10 mM Tris-HCl, 8 M Urea, pH 8). The next day, the remaining insoluble material was removed by centrifugation (18000 x g, 25 °C, 20 min) and His-tagged protein in the supernatant was purified using a 1 ml His-trap FF Nickel column (GE Healthcare), pre-equilibrated with Denaturing Buffer, through an FPLC system (ÄKTA

pure, GE Healthcare). The elution of the His-tagged protein was performed using 100% Denaturing Buffer added with 300 mM Imidazole (IMD). Reduced glutathione (60 mM final concentration) was added to eluted protein fractions, which were then stirred at room-temperature for 1 h. The sample was then diluted 1:80 in Refolding Buffer (50 mM Tris-HCl, 5% glycerol, 0.5 mM oxidized glutathione, pH 8), and stirred at 4 °C for 24 h. Refolded His-tagged protein was purified using a 5 ml HisTrap HP Nickel column (GE Healthcare), pre-equilibrated with Refolding Buffer (without oxidized glutathione), through the same FPLC system as above. The elution of the refolded protein was performed using 100% Refolding Buffer added with 500 mM IMD.

Protein extraction from ncIBs

In order to extract recombinant protein from *E. coli* cells non-classical inclusion bodies, a different protocol was used.

The key-player of this method is represented by arginine, which possesses advantageous properties in protein stabilization and inhibition of protein aggregation: the side chain of this amino acid, in fact, carries a guanidine group that interacts with aromatic residues, preventing the formation of protein complexes by interactions of their hydrophobic cores.[439]

To achieve protein solubilization by arginine, BL21(DE3) cell pellet was thawed on ice and resuspended in 50 ml (50 ml/l of culture) of Resuspension Buffer (50 mM Tris-HCl, 500 mM NaCl, pH 8.5). The cell suspension was aliquoted in 15 ml tubes and subjected to three cycles of freeze and thaw (alternating -80 °C and room-temperature), in order to disrupt cell walls. Then, the whole volume was pooled, and sonication was performed at 50% power, on ice, for 8 serial cycles of 1 min + 1 min of rest each. The Insoluble fraction containing ncIBs was precipitated by centrifugation (13000 x g, 4 °C, 20 min), washed once into 20 ml of Resupension Buffer, and then resuspended into 20 ml Extraction Buffer (2 M L-arginine, 500 mM NaCl, 50 mM Tris-HCl, pH 8.5) by homogenization using a glass potter. Mixed reduced and oxidized glutathione (5 mM and 0.5 mM final concentration, respectively) were added, and incubated for 3-4 days, stirring, at 4 °C to allow protein solubilization. Then, the remaining insoluble fraction was discarded by double centrifugation (18000 x g, 4 °C, 15 min) and the supernatant was diluted 1:100 into Resuspension Buffer. The whole volume was loaded onto a 5 ml HisTrap HP Nickel column (ÄKTA pure, GE Healthcare), pre-equilibrated in Resuspension Buffer, using the same FPLC system as above, in order to purify the His-tagged recombinant protein.

Mid Scale Expression in HEK293T

When HEK293T culture reached 90% of confluence, cells were detached and counted on a Bürker chamber. 15 ml of HD-DMEM FBS 10% containing 6 x 10^6 HEK293T per flask were seeded in 2 flasks (75 cm^2) and incubated at 37 °C, 5% CO_2 for 24 h. Cells were then transfected using 15 µg of recombinant phFc_CD19_Fc, 60 µg of PEI and 1.5 ml of HG-DMEM without FBS (DNA: PEI ratio 1:4). The transfection mixture was vortexed for 20'' and incubated at RT for 15 min. Exhausted HG-DMEM 5% in the roller bottle was replaced with 15 ml fresh DMEM (5% FBS, 1% L-Gln 1% and 1% P/S 1%). The transfection mixture was added and the flasks were incubated at 37 °C, 5% CO_2 for 24 h. After 24 h, HG-DMEM FBS 5% medium was replaced with 15 ml of EX-CELL™ 610-HSF Hybrydoma Serum-free Medium (SIGMA ALDRICH). Cells were inspected every day, adding fresh medium when needed, up to ~ 150 ml.

Large Scale Expression in HEK293T

When HEK293T flask culture reached 90% of confluence, cells were detached and counted on a Bürker chamber. 200 ml of HD-DMEM FBS 10% containing 15 x 10^6 HEK293T were seeded in a roller bottle, which was equilibrated in the static incubator at 37 °C 5% CO_2 for 6 h and then moved to the rolling incubator at 37 °C, 5% CO_2 for 4 days. Cells were then transfected using 480 µg of recombinant phFc_CD19_Fc, 1920 µg of PEI and 50 ml of HG-DMEM without FBS (DNA: PEI ratio 1:4). The transfection mixture was vortexed for 20 s and incubated at RT for 15 min. Exhausted

HG-DMEM 5% in the roller bottle was replaced with 200 ml fresh DMEM (5% FBS, 1% L-Gln 1% and 1% P/S 1%). The transfection mixture was added and the roller bottle was incubated in the roller incubator. After 24 h, HG-DMEM FBS 5% medium was replaced with 200 ml of EX-CELL™ 610-HSF Hybrydoma Serum-free Medium (SIGMA ALDRICH). Cells were inspected every day, changing medium when needed, up to ~ 500 ml (total volume).

3.2.3 Protein Purification and Downstream Processing

3.2.3.1 Chromatography

Chromatography consists of a series of analytical and preparative techniques aimed at separating the components (analytes) of a mixture, allowing to obtain distinct homogeneous species from raw preparations. Analytes separation is the result of their differential partitioning, due to their physical-chemical characteristics, between a stationary phase of a given chromatographic system, usually composed of porous solid particles, and a mobile phase, a fluid that dissolves and vehicles the analytes through the stationary phase.

The most informative outcomes of a chromatographic analysis are retention time and peak height/area, used to conduct qualitative and quantitative studies, respectively. In liquid chromatography (LC), the mobile phase is a liquid solvent or a mixture of liquid solvents. Fast protein liquid chromatography (FPLC) systems are especially adapted for preparative scale applications of protein purification. They exploit a system of pumps that pushes the liquid phase through the stationary phase, typically a resin embedded in a column. The FPLC can be used for analytical (both qualitative and semi-quantitative) preparations as well. The principal advantages of this system are good resolution, rapidity of analysis, accurate monitoring of run parameters (e.g. flow-rate, system pressure, conductivity and absorbance) and semi-automation.

The chromatographic equipment used in the experiments reported in this thesis is an FPLC system (ÄKTA pure, GE Healthcare), controlled by Unicorn 6.3 software, which also allowed data evaluation. The absorbance of the UV detector was set at 280 nm, which corresponds to the wavelength at which proteins show a sub-maximum of absorbance. Generally, fractions of purified protein were collected in different tubes, then pooled, concentrated and stored at 4 °C, while 20 µl/fraction were analyzed on gel electrophoresis. In this thesis, two different types of chromatography were used: affinity chromatography and size exclusion chromatography, which differ on the basis of their separation mechanisms and type of stationary phase.

Affinity Chromatography (AC)

The principle of Affinity chromatography (AC) is based on a reversible, non-covalent and selective interaction between the analyte and a specific ligand, which is immobilized onto the stationary phase. The raw sample containing the protein of interest is applied to the resin under specific conditions (buffer, pH, ionic strength, temperature), optimized in order to facilitate specific binding to the ligand. After washing away unbound contaminants, the bound protein is recovered in solution by changing buffer conditions in order to favor desorption from the ligand.

Several well-established methods are described for affinity purification, based, for example, on antibody-antigen specific binding (resins coupled with either the antibody or the antigen) or other kinds of molecular affinity.

Affinity Chromatography for His-tagged proteins

The first step to purify recombinant proteins tagged with a histidine tag (i.e. CD19EC, CD19EC_Fc_His, CD20_141_188, CD20_141_184, VHH21A, TCAN3) produced in large-scale was performed by immobilized metal-ion affinity chromatography (IMAC) on nickel-sepharose (HisTrap) matrix.

The technique is based on the affinity of the protein of interest for nickel, which is immobilized onto the chromatographic sepharose resin. Such affinity is mediated by the protein His-tag: 6-10 His residues at the N- or C-terminus are able to interact with nickel ions through non-covalent

binding. In principle, proteins without His-tag are not able to bind to the matrix and are eluted during the loading phase. Proteins bound to the resin are eluted using imidazole (ImOH), which competes with the tagged protein for the binding to nickel. Usually, the same loading buffer added with high imidazole concentration is used to create an imidazole gradient in order to elute the target protein.
Either 1 ml HisTrap FF, 5 ml HisTrap HP (GE Healthcare) or Bio-Scale™ Mini Profinity™ IMAC Cartridges (BIORAD) columns were used, depending on the desired binding capacity, using the same chromatographic method. The standard method used for IMAC was divided into the following consecutive steps:
- column equilibration with binding buffer, i.e. a buffer with suitable characteristics to allow protein interactions with the matrix and containing 10 mM ImOH to contrast unspecific binding;
- sample loading, usually, at a flow-rate equal to 1/3 column volume (CV);
- column washing, in which unbound contaminants are removed from the matrix with binding buffer (5-10 CVs);
- sample elution, in which proteins are eluted from the matrix typically establishing a step gradient of the elution buffer, generally identical to the binding buffer, but with 300-500 mM ImOH.
Elution fractions were collected and analyzed by SDS-PAGE and Western blotting and total protein quantified through micro-BCA kit.
Using IMAC strategy, some contaminants can unspecifically bind to the resin. Therefore, a second step of purification may be required, depending on the target degree of purity, according to the following application. The second round of purification, where needed, in the present thesis, involved size exclusion chromatography.

Affinity Chromatography for Fc fusion proteins
Protein A Sepharose is a stationary phase in which an inert matrix, such as agarose, usually cross-linked to form beads (Sepahrose), is coupled with protein A derived from *Staphylococcus aureus* cell wall, which is characterized by a high affinity for the Fc portion of antibodies from many species. Protein A contains four binding sites, but only two Fc domains can be bound at any one time, because of steric hindrance. This system allows efficient separation of the antibodies and Fc fusion proteins from complex mixtures. The detachment of the Fc from protein A occurs upon application of appropriate conditions that promote desorption (such as a pH decrease).
Purification of CD19_Fc recombinant constructs from HEK293T supernatant was achieved by loading the supernatant dialyzed versus binding buffer (0.1 mM sodium phosphate, pH 7.8) on a 1 mL r-protein A Sepharose column (Mab_select GE Healthcare) pre-equilibrated with binding buffer at 1 ml/min flow-rate. After washing the column with 5-10 CVs of binding buffer to remove unbound contaminants, isocratic elution was performed using elution buffer at pH 3.0 (0.1 M sodium citrate). 1 ml fractions were collected, supplied with 100 µl of 1 M Tris pH 8.0 to immediately neutralize the pH and analyzed by SDS-PAGE, while total protein content was quantified through micro-BCA kit (Pierce).

<u>Size Exclusion Chromatography (SEC)</u>
Size exclusion chromatography (SEC) or gel filtration allows the separation of raw components in a mixture basing on their molecular size. In SEC, the porous gel matrix must have a carefully controlled range of sizes in order to ensure high efficiency and reproducibility. Moreover, the stationary phase should be chemically stable and inert. These gels may be generated by cross-linking of polymers, such as agarose, to create three-dimensional networks of packed gel beads. Small analytes, because of their size, can diffuse into pores of the gel beads and be retained there. For this reason, small analytes are delayed in their passage through the resin compared with the larger molecules that are forced to move continuously through the column. This results in an early elution of large particles and in a late elution of small particles, allowing their separation.
Superdex 75 10/300 GL resin (GE Healthcare) were used to perform both analytical and preparative protein separation. This pre-packed column made of cross-linked agarose and

dextran allows high-resolution separation of proteins that have a size comprised within the molecular weight range of 3000-70000 Da. Thus, VHH21A purified from IMAC was analyzed and further purified using this kind of column. Typically, the sample to be applied on Superdex 75 10/300 GL was previously concentrated down to 250-500 µl. SEC runs were performed at 0.5 ml/min flow-rate, with isocratic elution and using 1x PBS as the only mobile phase. Fractions were collected with 2 ml volumes and analyzed through SDS-PAGE and Western blotting. Total protein was quantified by micro-BCA kit. and Superose™ HR 10/30 (Amersham Biosciences) was instead used for the purifiacion of TCAN3.

3.2.3.2 Protein Concentration and Dialysis

In order either to increase protein concentration or to exchange protein dilution buffer, centrifugations (4500 rpm, 4°C, 15-20 min) were performed using Amicon® Ultra-15, Amicon® Ultra-4 or Microcon® concentrators (Millipore), with suitable cut-off size, in order to hold the protein of interest inside the concentrator and to remove undesired buffer and other contaminants (30 kDa for CD19EC recombinant forms, 3 kDa for VHH21A, 10 kDa for TCAN3). For concentration, the protein solution, normally deriving from chromatographic pooled fractions, was simply put in a suitable concentrator and centrifuged until the desired final volume was reached. Buffer exchange, instead, was achieved through different centrifugation cycles using the same concentrator, adding several volumes of the desired buffer on the top of the concentrator, or using a Desalting HiPrep 26/10 column (GE Healthcare), pre-equilibrated in the desired exchange buffer.

3.2.4 Protein Analysis

3.2.4.1 Polyacrylamide Gel Electrophoresis

SDS PAGE

Polyacrylamide gel electrophoresis (PAGE) is an analytical technique which allows protein separation in a semi-solid matrix under an electric field, according to their charge and size. Sodium dodecyl sulfate (SDS) is an anionic surfactant which is commonly used in protein PAGE, thus referred to as SDS-PAGE. SDS-PAGE is generally performed in "reducing conditions", where SDS is coupled with protein sample boiling and the usage of denaturing sample loading buffer, in order to disrupt protein three-dimensional structures and folding. Since SDS binds to peptide chains in a stoichiometric ratio (~1.4 g SDS/g protein), it provides the same negative charge to mass ratio to each protein, eliminating the interference that protein net charge would introduce in electrophoretic migration. The electrophoretic run proceeds from the negative pole (cathode) to the positive one (anode), and, for the reasons explained above, protein mobility in SDS-PAGE depends on molecular weight only. Acrylamide acts as a molecular sieve, forming long single-chain polymers cross-linked by bisacrylamide; thus, its concentration can be modified in order to optimize resolution of protein separation, according to experimental needs.

In the method used in this thesis, in order to obtain acrylamide polymerization in a gel-form, a 37.5:1 ratio acrylamide:bisacrylamide (w/w) was mixed and a polymerizing agent, i.e. ammonium persulfate (APS), source of free radicals, was added to the mixture. A catalyzing agent, i.e. NNN′N′-tetramethylethylenediamine (TEMED), which acts by stabilizing free radicals, is needed to accelerate the polymerization reaction rate. A suitable buffer was used to control pH and facilitate protein separation thanks to the balance of charges determined by its composition. A discontinuous gel system, as described by Laemmli,[440] was applied: two gels with different pore size and pH were cast one on the top of the other: a 4% acrylamide:bis-acrylamide (37.5:1) stacking gel at pH 6.8, and a running gel at pH 8.8 with the desired (usually, 7-20%) concentration of acrylamide:bis-acrylamide. The stacking gel contains the wells for sample loading obtained by a comb mold. Composition of running and stacking gel, respectively, is reported in **Table 3.13.**

When polymerized, the cast gel was sub-merged in a running buffer (25 mM Tris-HCl, 192 mM glycine, 0.1% SDS). Samples to be loaded onto the gel were mixed with a 3x loading buffer

containing: 10% glycerol, 50 mM Tris-HCl, 10% bromophenol blue, pH 6.8. Samples were then boiled at 99°C for 5 min. Precision Plus Dual Color Protein™ Standard (Biorad) was used as a MW reference. Electrophoresis progress was followed by visualization of the bromophenol blue dye front. Run was performed at 60 V along the stacking gel and at 120 V along the running gel. The gels were either stained or used for Western Blot analysis.

Table 3.13 Gel composition for SDS-PAGE

STACKING GEL	
Stock solutions	**Final concentration**
30% acrylamide:bis-acrylamide (37.5:1)	5% (v/v)
0.5 M Tris-HCl, pH 6.8	0.125 M
1000x TEMED	1x
15% APS (w/v)	0.05% (v/v)
MilliQ water	to volume
RUNNING GEL	
Stock solutions	**Final concentration**
30% acrylamide:bis-acrylamide (37.5:1)	10-20% (v/v)
0.5 M Tris-HCl, pH 6.8	0.375 M
1000x TEMED	1x
15% APS (w/v)	0.05% (v/v)
MilliQ water	to volume

Tricine – SDS PAGE

Tricine–SDS-PAGE is used to separate proteins in the mass range 1–100 kDa as an alternative to Glycine SDS PAGE, also Known as Laemmli SDS PAGE (described above). Tricine–SDS-PAGE is preferred for the resolution of proteins smaller than 30 kDa, which can be achieved at lower concentrations of acrylamide than in other electrophoretic systems. The different separation characteristics of Tricine–SDS-PAGE and Laemmli– SDS-PAGE are directly related to the strongly differing pK values of the functional groups of glycine and tricine, that define the electrophoretic mobilities of such trailing ions relative to the electrophoretic mobilities of proteins. Gels with 16% polyacrylamide and including 6 M Urea further increase the resolution of small proteins.[441]

In this thesis, this technique was used for the electrophoretic analysis of CD20 recombinant proteins. Gel recipes are reported in **Table 3.14**. When polymerized, the gel was sub-merged in running buffer (0,1 M Tris, 0,1 M Tricine, 0.1% SDS). For the loading, samples were mixed with a 4x loading dye (30% glycerol, 0.05 % w/v Coomassie Blue G250, 150 mM Tris-HCl, 6% v/v ß-mercaptethanol, 12 % SDS, pH 7). Samples were then boiled at 99°C for 5 min. Precision Plus Dual Color Protein™ Standard (Biorad) was used as a MW reference. Run was performed at 30 V along the stacking gel and at 80 mA along the running gel. The gels were either stained or used for Western Blot analysis.

Table 3.14. Gel composition for Tricine SDS-PAGE

STACKING GEL	
Stock solutions	**Final concentration**
30% acrylamide:bis-acrylamide (37.5:1)	4% (v/v)
3 M Tris, 1 M HCl, 0.3% SDS, pH 8.45 (3X)	1 X
1000x TEMED	1x
15% APS (w/v)	0.05% (v/v)

MilliQ water	to volume

RUNNING GEL	
Stock solutions	**Final concentration**
30% acrylamide:bis-acrylamide (37.5:1)	16% (v/v)
3 M Tris, 1 M HCl, 0.3% SDS, pH 8.45 (3X)	1 M
UREA	6 M
1000x TEMED	1x
15% APS (w/v)	0.05% (v/v)
MilliQ water	to volume

3.2.4.2 Polyacrylamide Gel Staining

Coomassie Staining

Gels obtained from SDS-PAGE were exposed to staining using Coomassie Brilliant Blue G-250 (Sigma-Aldrich), in order to visualize protein bands. Coomassie dyes are colored triphenylmethane-derived compounds which bind to proteins through van der Waals' and ionic interactions. Coomassie Brilliant Blue G-250 is a particularly sensitive form of this class of dyes, being able to determine up to 0.5 μg of protein per square centimeter of gel matrix. SDS-PAGE gels were rinsed in water and then stirred in an aqueous solution of 0.1% (w/v) Coomassie Brilliant Blue G-250, 40% methanol (v/v) and 20% acetic acid (v/v) for at least 15 min, at room-temperature. Destaining was achieved by stirring gels in 10% (v/v) acetic acid, 40% (v/v) methanol in aqueous solution with several changes of solution.

Silver Staining

When a higher sensitivity was needed, protein staining with silver ions (up to 30-fold more sensitive than colloidal Coomassie G-250) was performed using the SilverQuest™ Silver Staining kit (Invitrogen), following manufacturer's instructions. Silver staining relies on chemical reduction of silver ions, which bind proteins, to dark-colored metallic silver.

The SDS-PAGE gel to be stained was placed in a Fixative solution (10% (v/v) acetic acid, 40% (v/v) methanol in water), microwaved at 700 W for 30 s and gently agitated for 5 min at room-temperature. The gel was then washed with 30% (v/v) ethanol in water, microwaved and incubated 5 min as above. The gel was put in Sensitizing solution (30% (v/v) ethanol, 10% (v/v) Sensitizer), microwaved and incubated 2 min as above. Two washing steps were performed using deionized water and microwaving and were followed by incubation of the gel in 1 ml of Stainer solution in water for 5 min after microwaving. Deionized water was used to remove excess of silver solution and then the gel was submerged in a Developing solution (10% (v/v) Developer in water, 1 drop of Developer Enhancer) and incubated at room-temperature for 5 min, with gentle agitation. Once the desired intensity band was achieved, 10 ml of Stopper solution were added and mixed for 10 min. The gel was finally rinsed with water.

3.2.4.3 Western Blot

Protein immunoblot analysis represents an analytical immunochemical technique which exploits the use of specific antibodies in order to identify the presence of a given protein in a mixed sample. In Western blot, proteins which have been separated by SDS-PAGE are then transferred from the gel to a suitable membrane using an electric field. Proteins transfer onto the membrane is needed in order to make the proteins accessible for the antibody-mediated detection (*blotting*). For Western blotting, a semi-dry blotting system was set up: the electrophoretic gel, stacked on the top of the membrane, was packed between four layers of 3M filter paper (Millipore) soaked into transfer buffer (25 mM Tris-HCl, 0.2 M glycine, 20% v/v methanol). An electric field with constant amperage (64 mA) was applied in a semi-dry blotting device (Sigma-Aldrich) for 1 h, to allow proteins migration from within the gel to the membrane. The blotting membrane was a

polyvinylidene fluoride (PVDF, 0.2 µm cut-off, Millipore) membrane, previously activated in 100% methanol.
Once the transfer was completed, the first step of the immunoblotting procedure was represented by the Blocking, which prevents unspecific protein binding to the membrane during the following steps. The membrane was usually blocked through an incubation into a 1% (w/v) bovine serum albumine (BSA) or 5% (w/v) milk solution, dissolved in 1x PBS supplied with 0.1% (v/v) Tween-20 (PBST), at room-temperature for 1 h 30 min. After the blocking, the membrane was eventually stored at 4 °C o.n.
After three washes of 10 min each into PBST, the membrane was incubated with the primary antibody, stirring either at RT for 1 h or at 4 °C o.n. After three washes of 10 min each into PBST, the membrane was incubated with a proper secondary antibody, if needed, and then washed again in PBST for three times. For both primary and secondary antibodies, the antibody dilution and incubation conditions were set accordingly to the antibody datasheet and then empirically optimized. A schematic representation of all the antibodies used for western blotting purposes in this thesis is reported in **Table 3.15.**
Signal detection was achieved using a specific antibody directed against the target protein and probed with a reporter enzyme. The anti-target antibody can be directly conjugated with the reporter enzyme (direct primary antibody) or can be recognized by another antibody (secondary antibody) conjugated to the reporter enzyme. The reporter system used was horseradish peroxidase (HRP). The substrate for chemiluminescent reaction was a solution containing luminol and modified phenols (Enhanced Chemiluminescence, ECL, Pierce ECL kit; Clarity Western ECL Substrate, BIORAD): in an alkaline environment, luminol is oxidized by HRP to an excited state, causing light emission. In particular, in our case, the membrane was incubated at room-temperature with ECL solution for 5 min and exposed in a darkroom to autoradiographic films (Santa Cruz Biotechnology), which are covered by an emulsion containing silver crystals that are activated to ionic form by light.
The signal was developed incubating the exposed film sequentially in developing (to reduce silver ions to precipitating metallic silver), washing (mild acidic pH) and fixing (to wash the silver crystal emulsion away) solutions (Carestream X-Omat Ex II; Developer and Replenisher), respectively. Protein signal was visible as a dark spot on the film and sensitivity limit of this assay was 1-10 ng of protein. Alternatively, a bioimaging system, Azure c600 (Applied Biosystems) was used in order to acquire images from the membrane, after an incubation with the ECL solution of 1 min.
Otherwise, 3,3'-diaminobenzidine (DAB, SigmaFast™ tablets, Sigma-Aldrich) was used as HRP substrate and incubated with the blotted membrane, generating a dark-brown precipitating product upon enzymatic activity. If required, prior or after immunoblotting the membrane was stained with Ponceau solution (Sigma-Aldrich), a protein unspecific dye, in order to check if the transfer procedure occurred correctly.

Table 3.15 Antibodies for immunoblotting

Primary antibody	Secondary antibody
Detection of His Tag (CD19_Fc_6xHis, CD20_144_194, CD20_144_188, VHH21A, TCAN3)	
1:7000 HRP-conjugated anti-His pAb (Sigma-Aldrich) in 5% BSA	/
1:15000 HRP-conjugated anti-His pAb (sigma Aldrich) in 5% BSA	/
Detection of human Fc (CD19_Fc)	
1: 1000 HRP-conjugated anti hIgG (Dako) in 3% BSA	/

Detection of c-myc tag (Phage Display clones)	
1:2000 Biotin-conjugated α-myc (910E) in 3%BSA (Merck Millipore)	1:15000 Extravidin-HRP in 2% BSA (Sigma Aldrich)

Protein Quantification

MicroBCA Assay (Pierce)

In order to quantify total protein concentration of a purified protein sample, the colorimetric bicinchoninic acid (BCA) method was employed. This biochemical method allows the detection of up to 5 µg/ml proteins in solution, exploiting the Cu^{2+} reduction to Cu^{1+} operated by proteins known as biuret reaction. The reaction occurs in the presence of sodium tartrate, which creates the alkaline environment needed for copper to bind to peptide bonds. The chelated copper ions react with the bicinchoninic acid, producing a characteristic purple color. The protein concentration is determined measuring the solution absorbance at 562 nm. In this thesis, the micro-BCA assay kit (Pierce) was employed.

The test was performed in 96-well plates and a standard curve was obtained with serial 1:2 dilutions starting from 2 mg/ml BSA solution in PBS using a final volume of 20 µl. The sample containing the protein at unknown concentration was processed as the standard. For colorimetric detection, a mixture of solutions Reagent A (sodium carbonate, sodium bicarbonate, bicinchoninic acid and sodium tartrate in 0.1 M NaOH), and Reagent B (Micro BSA reagent B: 4.0% cupric sulphate) was prepared in a 50:1 ratio. Aliquots of 200 µl of the resulting solution were added to each well of both BSA standard and sample dilutions and the plate was then incubated at 37°C for 30 min. Absorbance was measured at 562 nm using a POLARstar Omega (BMG Labtech) microplate reader, using PBS as blank. Absorbance data obtained were elaborated in a standard curve by using the least squares method, from which concentration of the sample was derived.

3.2.4.4 Enzymatic Activity Assay

L-asparaginase and L-glutaminase activity assays

In order to determine the L-asparaginase and L-glutaminase activities, a spectrophotometric method using the coupled reaction catalyzed by glutamic acid dehydrogenase (GADH) was employed. L-asparagine and L-glutamine deamination reactions are shown in **Figure 3.7**.

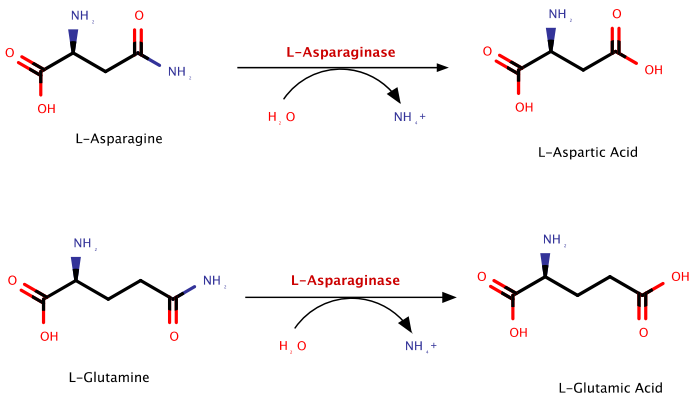

Fig. 3.7 L-Asparaginase reaction in presence of L-Asparagine and L-Glutamine. *In both cases, the reaction releases ammonium and the acidic form of the two substrates.*

A spectrophotometric assay of enzymatic activity is a reliable and precise method to determine enzyme activity. The method is based on the capability of the substrate or product of an enzymatic reaction to absorb the light at a precise wavelength. If the substrate or product of the enzymatic reaction of interest has no specific wavelength absorbance, as in this case, a coupled reaction can be exploited. A coupled reaction uses a product of the first reaction as a substrate, and produces a product with specific absorbance. It is important to stress that, to determine the first enzyme

activity, an excess of the second enzyme is needed, in order to avoid a rate-liming effect of the coupled reaction. The reactions stoichiometry must be considered as well.
The spectrophotometric continuous GADH-coupled assay employed to assess L-Asparaginase or L-glutaminase activities allows the determination of the ammonia released from L-asparagine (L-ASN) or L-glutamine (L-GLN) following NADH oxidation at 340 nm.[442] NADH is a cofactor for the reaction catalyzed by the GADH to form L-glutamate starting from α-ketoglutarate and ammonia, and it is often used in coupled reactions to determine enzymes activity using a spectrophotometric method. The method exploits the different absorption at 340 nm of the nicotinamide adenine dinucleotide in its reduced (NADH) or oxidized (NAD^+) form. NADH is capable of absorbing at 340 nm, instead its oxidized form has no absorbance at the same wavelength.
The standard reaction mixture used to measure ammonia release contained: 50 mM 4-(2-Hydroxyethyl)piperazine-1-ethanesulfonic acid (HEPES) buffer pH 7.5, 1 mM α-ketoglutarate (α-KG), 0.24 mM NADH, 20 U glutamic acid dehydrogenase and 10 mM L-ASN or 10 mM L-GLN, in a final volume of 0.5 ml. The reaction was started by adding enzyme solution (5-300 µg) and NADH consumption was monitored at 340 nm with a single-ray spectrophotometer.
The kinetic parameters V_{max} and K_m were determined by Lineweaver-Burk plot using the Enzyme Kinetic Module 1.1 for Sigma Plot (SPSS Inc.).
k_{cat} or turn-over number, is the number of catalytic events per second. K_m is the substrate concentration at which the reaction speed is half-maximal. k_{cat}/K_m is an index of catalytic efficiency at sub-saturating substrate concentration.
One Unit of L-Asparaginase is defined as the amount of enzyme needed to convert 1 µmole of substrate into the product in the above-described conditions.

3.2.4.6 Modeller
Modeller is a program which allows the computation of 3D models of protein structures. Comparative protein structure modeling uses the sequence of a given protein (target) and predicts its 3D structure basing primarily on its alignment to one or more proteins of known structure (templates). The prediction process relies on fold assignment, target-template alignment, model building, and model evaluation.[443] The structural model of VHH21A molecule was obtained using Modeller, after a sequence homology research performed using the PDB Data Bank. Three camelid VHH templates resulted to have the highest sequence homology and were used in the following steps (PDB ID: 6WAR, chain B; 6HHU, chain G; 60B0, chain C). The final model was computed using 6HHU chain G as a template.

3.2.5 Antibody Specificity and Affinity Measurements

3.2.5.1 ELISA
Enzyme-linked immunosorbent assay (ELISA) is an analytical technique, which exploits the antibody-antigen binding affinity, used to study molecular interactions and to quantify substances of different nature (e.g. peptides, proteins, antibodies, hormones). Applications of this technique are extremely heterogeneous, spanning from detection of serum antibodies or markers in the clinics to various assays in the research field.
The main principles of this technique are the immobilization of a molecule onto a multi-well polystyrene plate by physical absorption and an antibody-based detection. Different ELISA approaches exist: 1) direct settings, in which the antigen to be detected is coated onto the plate and a specific tagged primary antibody serves as a detector; 2) indirect settings, in which the primary antibody is not labeled and a secondary tagged antibody specific for the primary one is used for detection; 3) sandwich ELISA format, in which a coated capture antibody binds to the antigen, which is then detected either through direct or indirect strategy. The sandwich ELISA setting can be modified to create a competitive assay, where labeled purified antigen is used and competes with unlabeled antigens from the sample for binding with the coated antibody. While a direct detection is quicker and avoids unspecificity issues coming from secondary antibody

possible cross-reactivity, an indirect approach may be preferred because of its higher sensitivity and flexibility. In this thesis, both indirect and sandwich ELISA were applied to verify affinity of VHH21A and TCAN3 to CD19 (**Table 3.16**) as well as in the Phage Display, as further described below.

Table 3.16 ELISA settings

Indirect ELISA

	Antigen	**Antibody**	**Primary Ab**	**Secondary Ab**
Sample	C19_Fc	VHH21A	1:2000 anti-His (mAb, Sigma) in 2% BSA	1:4000 HRP-conjugated anti-mouse (Sigma) in 2% BSA
Positive Control	CD19_Fc	/	/	1: 1000 HRP-conjugated anti-hIgG (Dako) in 3% BSA
Negative Control	BSA 2%	VHH21A	1:2000 anti-His (mAb, Sigma) in 2% BSA	1:4000 HRP-conjugated anti-mouse (Sigma) in 2% BSA

Sandwich ELISA

	Capture Ab	**Antigen/ I Ab**	**Primary Ab**	**Secondary Ab**
Sample	VHH21A	CD19_Fc	1: 1000 HRP-conjugated anti hIgG (Dako) in 3% BSA	/
Positive Control	VHH21A	/	1:2000 anti-His (mAb, Sigma) in 2% BSA	1:4000 HRP-conjugated anti-mouse (Sigma) in 2% BSA
Negative Control	BSA 2%	CD19_Fc	1: 1000 HRP-conjugated anti hIgG (Dako) in 3% BSA	/

VHH21 is in purified form, while CD19_Fc is crude HEK293T supernatant.

The method included several steps, in order to set up consecutive "layers" of reagents:
1. Coating: 100 µl/well of samples (1-10 µg/ml of protein) were incubated in a 96-well plate (Maxi-Sorp Nunc), overnight, at 4 °C, in a humid box.
2. Blocking: 200 µl/well of 2% BSA (Sigma) or 5% milk powder in PBS were added; the plate was then incubated at room temperature o.n. Wells were then washed three times with 200 µl/well PBS.
3. Bridging (in sandwich ELISA only): 100 µl/well of sample were added and incubated at room-temperature for 1 h. Wells were then washed three times with 200 µl/well PBST.
4. First layer: 100 µl/well of primary antibody (in 1% BSA in PBS) were incubated at room-temperature for 1 h. Wells were then washed three times with 200 µl/well PBS.
5. Second layer: 100 µl/well of secondary antibody in (1% BSA in PBS) were incubated at room-temperature for 1 h. Wells were then washed three times with 200 µl/well PBS.
6. Chromogenic reaction: 100 µl/well of TMB Substrate Solution (0.2 M dibasic sodium phosphate, 0.1 M citric acid, 0.1 mg/mL 3,3',5,5'-tetramethylbenzidine, pH 5, Sigma-Aldrich) with 1 µl/10 ml of 30% hydrogen peroxide were added. Optimal degree of blue intensity usually occurred within 10-20 min.
7. Stop reaction: 25 µl/well of stop solution (2 M sulfuric acid) were added.
Absorbance was read at 450 nm POLARstar Omega Plate reader Spectrophotometer (BMG Labtech).

3.2.6 Phage Display

As largely discussed in the Introduction, phage display technology is a powerful method for the selection of monoclonal antibodies against a given antigen, which is based on the genetic engineering of coat proteins of filamentous bacteriophages of *E. coli*, such as M13. The most common format for the display of antibody fragments on phages consists in the antibody fragment fusion to the terminal phage geneIII protein. Such fusion can be achieved either by direct engineering of the phage genome (*phage format*) or by using a geneIII-expressing plasmid in combination with a helper phage system (*phagemid format*). In the phage format, all geneIII molecules are expressed as antibody fusions and 3–5 copies are displayed on the tip of the bacteriophage (*multivalent display*). On the contrary, in phagemid systems the majority of copies of pIII coat protein are derived from the helper phage genome and only a small proportion originates from the phagemid (less than one copy per phage on average), leading to a *monovalent display*. For this reason, the phage format results in the selection of binders with low to medium affinities due to tight binding to multivalent antigen, while the phagemid format is required for the selection of antibodies with higher affinities.[444]

The expression levels of full-length antibodies are generally poor in bacteria, while antibody fragments can be expressed at medium to high levels in the periplasm of *E. coli.*[445] This allowed the selection of Fab (VH-CH, VL-CL) and in particular of scFv (VH-VL) fragments by phage display.[338,357,446] Single domains have been observed in camels and sharks.[447,448] In 1989 Ward and Winter reported the selection of an even smaller antibody fragment based on a single VH domain.[449] Despite its small size (14 kDa), this domain antibody was capable of binding the model antigen hen-egg-lysozyme with high affinity and specificity. Although heavy and light chains are usually paired in the human immune system, VH and VL can in some circumstances exist in isolation, for instance as Bence-Jones proteins in multiple myeloma.[450] The small size and single domain nature of human domain antibodies allows them to be readily expressed in bacteria and yeast,[451] making them particularly suitable for engineering approaches.[452] Their compact size is also expected to improve tissue penetration in therapeutic applications and the recognition of cryptic epitopes in enzyme active sites and membrane proteins.

3.2.6.1 Christ dAb library (SourceBioscience)

The domain antibody repertoire of Christ dAb library of SourceBioscience is based on a single human VH framework (V3-23/D47), heavy chain germ-line segment, with synthetic diversity introduced by PCR mutagenesis into CDR1, CDR2 and CDR3. The repertoire was designed to contain short CDR3 of the heavy chains, while maintaining good antigen binding properties. The majority of clones bind to protein A. The repertoire is constructed in pR2 (MYC VSV tag), in a monovalent phagemid format. Diversified side chains in CDR1, CDR2 and CDR 3 are: H27-33, H35, H50, H52-H54, H94, H95-H100(a-k), H101, H102. The library size is 3×10^9 clones. The repertoire was engineered to withstand heat-induced aggregation on phage and has been shown to contain binders to model antigens that re-fold without major loss of antigen-binding activity upon cooling.[451]

3.2.6.2 Selection procedure

An overview of the phage display selection process can be seen in **Fig. 3.8.** As a first step, the frozen glycerol stock of the repertoire phagemid contained in *E. coli* TG1 bacteria is thawed and phage is produced in liquid culture after infection with KM13 helper phage. Phages are then purified by precipitation with polyethylenglycol (PEG).

After phage production, 5×10^{12} phages are incubated with antigen, thereby oversampling the antibody repertoires in excess of 1000-fold. According to the protocol, non-specific adsorption to plastic can be used for the antigen immobilization, as well as chemical coupling through biotinylation. After incubation with antigen and stringent washes, phages are eluted by incubation with trypsin protease, which elutes phage by cutting the c-myc tag between antibody fragment

and the phage geneIII protein. Trypsin cleavage also removes background infectivity originating from geneIII protein of the trypsin-sensitive KM13 helper phage, while geneIII protein originating from the repertoire phagemid is trypsin-resistant. The eluted phage is then used to infect TG1 bacteria and titres are determined by plating dilution series. For subsequent rounds of selections, colonies from the first round are scraped from agar plates and phages are produced in liquidculture, PEG purified and selected by binding to antigen.

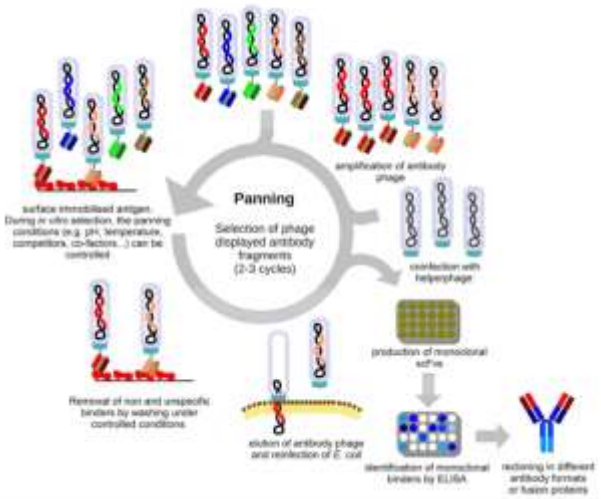

Fig. 3.8 Selection Procedure overview. *From Shirrmann et al* [453]

After three rounds of selection, individual clones are isolated, grown overnight and soluble fragments are produced in a 96-well format. Finally, antigen-specific clones are identified by ELISA using a biotinylated anti-myc monoclonal in combination with streptavidin-HRP and a colorimetric assay system. Alternatively, antigen specific clones can be identified on phage by ELISA using an anti-phage conjugate.

Growth of phage antibody repertoire (Library Packaging)

An aliquot of frozen antibody library, contained in phagemid format into *E. coli* TG1 (K12 D(*lac-proAB*) *supE thi hsdD5*/F' *traD36 proA*+B *lacIq lacZDM15*) cells, was thawed on ice and diluted into 500 ml 2xTY medium supplemented with 4% glucose and 100 µg/ml ampicillin. The presence of 4% glucose allowed the effective suppression of antibody expression during bacterial growth. The culture was grown at 37 °C, 250 rpm in a 2 liters glass flask up to OD_{600}=0.5 (approximately 1.5-2 hours).

In order to pack the library into displaying phages, $1x10^{12}$ KM13 helper phages were added to 250 ml of culture and incubated in a water bath at 37 °C for 30-60 minutes for the infection to occur. The culture was centrifuged at 3200xg for 10 minutes, and cells were resuspended into 500 ml of 2xTY medium supplemented with 0.1% glucose, 100 µg/ml ampicillin and 50 µg/ml kanamycin, selective for cells carrying the phagemid (Amp) and infected by the phages (Kan). Infected cells were grown for 16-20 h at 25 °C, 250 rpm in a 2 L glass flask.

Purification of the displaying phages repertoire by PEG precipitation

The culture was centrifuged at 3200xg, and the cell pellet was discarded. The displaying phages repertoire was precipitated by adding 100 ml of polyethylenglycol (PEG) solution (20% PEG 6000, 2.5 M NaCl) to 400 ml of supernatant, incubating on ice for one hour, and then centrifuging at 3200xg at 4 °C for 30 min. The supernatant was discarded and pellets were resuspended in 5 ml of PBS buffer. 1 ml of PEG solution (20% PEG 6000, 2.5 M NaCl) was added, phages were incubated on ice for 10 minutes, and then centrifuged at 3200xg at 4 °C for 30 min. Pellet was resuspended into 1 ml of PBS and centrifuged at 3200xg at 4 °C for 5 minutes. The supernatant was filtered through a 0.45 mM filter.

Phage titers was measured by absorption at 260 nm, using the following formula provided in the protocol: phage / ml = OD_{260} * 100 * 22.14 * 10^{10}. The phage preparation was diluted 100-fold into PBS prior to the measurement. Displaying phages can be stored at 4 °C for up to two weeks, with the addition of 1% EDTA and 0.1 mg/ml BSA to reduce proteolysis. Longer storage will lead to increasing proteolysis of the displayed antibody fragments. Displaying phages should not be frozen at this stage, as this may denature the displayed antibody fragments. Approximately 10^{13} phages should be obtained from 400 ml of supernatant.

First round of selection: binding and elution of phage

This is a critical step in the selection procedure, representing the enrichment of antigen-specific phage by binding to immobilized antigen. The first round of selection is the most important one as any bias or loss of diversity will be amplified in subsequent rounds. The antigen was immobilized initially by plastic absorption, and then by chemical coupling via biotinylation during optimization. Each immobilization strategy was followed by different washings and elution protocols.

Plastic absorption

A 96-well MaxiSorb plate was coated with 0.1 mg/ml of protein in PBS at 4 °C overnight. The next day, the plate was washed 3x with PBS buffer and blocked with MPBS buffer (5% w/v milk powder in PBS) over night at 4 °C. The next day, the plate was washed 3x with PBS buffer.

5x 10^{12} phages in 10 ml of MPBS were added to the plate (100 µlx well), which was incubated with gentle agitation for one hour, for the binding to occur. The plate was then washed 10x with 20 ml PBST buffer and 2x with 200 ml PBS buffer (200 µl x well), carefully removing all the liquid between washes by hitting the plates on tissue paper. After washes, 10 ml of trypsin solution (10 mg/ml trypsin in TBSC Buffer, 10 mM Tris pH 7.4, 137 mM NaCl, 1 mM $CaCl_2$ pH 7.4) were added (100 µl x well) and incubated at room temperature with gentle agitation for one hour, in order to elute binder phages.

Antigen biotinylation

During protocol optimization, antigen was biotinylated using EZ-Link ™ Sulfo-NHS-LC Biotinilation Kit (Thermofisher). *N*-Hydroxysuccinimide (NHS) ester-activated biotins are the most popular type of biotinylation reagent. NHS esters react efficiently with primary amino groups (-NH2) in pH 7-9 buffers to form stable amide bonds. Because proteins generally contain multiple lysine (K) residues in addition to the N-terminus of each polypeptide, they have multiple primary amines available as targets for labeling with NHS-activated reagents. EZ-Link Sulfo-NHS-LC-Biotin is water soluble, enabling reactions to be performed in the absence of organic solvents such as DMSO or DMF.

A 10-fold molar excess of biotin was used in order to obtain 2-3 groups of biotin per antigen molecule, as indicated on the Phage Display protocol provided by Miltenyi Biotec for the usage of µMACS Streptavidin Kit during the binding, washing and elution phases.

Millimoles of Sulfo-NHS-LC-Biotin to add to the reaction for a 10-fold molar excess were calculated using the following formulas reported in the protocol:

$$ml\ protein\ x \frac{mg\ protein}{ml\ protein} x \frac{mmol\ protein}{mg\ protein} x \frac{10\ mmol\ biotin}{mmol\ protein} = mmol\ biotin$$

$$mmol\ biotin\ x\ \frac{557\ mg}{mmol\ Biotin}\ x\ \frac{400\ \mu l}{2.2\ mg} = \mu l\ of\ biotin\ solution$$

557 = molecular weight of Sulfo-NHS-LC-Biotin

400 = µl of water in which 2.2mg of Sulfo-NHS-LC-Biotin is dissolved to make a 10 mM solution

The calculated amount of biotin solution was added to the protein antigen solution (EcAII 1.9 mg/ml) and the reaction was incubated 1 hr at RT.
A Thermo Scientific Zeba Spin Desalting Column was prepared by breaking off the bottom plug, placing the column into a new 15 ml collection tube, and centrifuging the column at 1000× *g* for 2 min in a fixed rotor centrifuge. The storage buffer was discarded, the column was marked on the side where the compacted resin was slanted upward and returned into the same collection tube. The column was equilibrated by adding 2.5 ml of BupH™ Phosphate Buffered Saline (Thermofisher) and centrifuging at 1000 × *g* for 2 min for 3 times. The column was placed into a new 15 ml collection tube and the protein sample was applied directly onto the center of the resin bed. Sample was allowed to absorb into the resin, and then centrifuged at 1000 × *g* for 2 min. The collected flow-through solution was the purified protein sample.

In order to measure biotin incorporation, the HABA Assay (Thermofisher) was used. In this assay, a solution containing the biotinylated protein is added to a mixture of HABA and avidin. Because of its higher affinity for avidin, biotin displaces HABA from its interaction with avidin and the absorbance at 500 nm decreases proportionately. An unknown amount of biotin present in a solution is estimated in a single well by measuring the absorbance of the HABA-avidin solution before and after addition of the biotin-containing sample. The change in absorbance relates to the amount of biotin in the sample. The HABA/Avidin solution was prepared by adding 10 mg of avidin and 600 µL of 10 mM HABA to 19.4 ml of PBS. In order to perform the assay, 180 µl of HABA/Avidin Solution into a 96-w microplate. The absorbance of the solution in the well was measured in the well at 500 nm and the value was recorded as A500 HABA/Avidin. Then, 20µl of biotinylated sample were added to the well containing the HABA/Avidin Solution. The plate was mixed using an orbital shaker, and the absorbance at 500 nm of the solution in the well was measured. The value should remain fairly constant for at least 15 seconds, in order to be recorded as A500 HABA/Avidin/Biotin Sample value. Thermofisher HABA calculator tool was used in order to evaluate moles of biotin per moles of protein.

For binding, washings and elution phases, the protocol provided by Miltenyi Biotec was followed, with some integration based on the work of Niccheri et al.[454]
For the removal of unspecific phages, 10 µl of Tris-H Buffer (100 mM Tris/HCl pH 7.5) were combined in a tube with 100 µl of µMACS Streptavidin MicroBeads and $5x10^{12}$ displaying phages, paying attention not to dilute the µMACS Streptavidin MicroBeads more than 1:10. The mixture was incubated at RT for 5 min. A µ Column was placed in the magnetic field of the µMACS Separator and prepared the by applying 100 µl of Equilibration Buffer for protein applications (supplied with the kit) on top of the column. Two washes with 200 µl of Tris-L Buffer (10 mM Tris/HCl pH 7.5) were performed. The phage-MicroBeads mix was applied onto the µ Column and let run through. Phages that unspecifically bound to µMACS Streptavidin MicroBeads were retained on the column. The flow-through was collected in a clean tube. 50 µl of Tris-L Buffer were added to the column, and the flow-through was collected in the same tube, while the column was discarded.
For the *binding* of the biotinylated target to the phages, the collected phages (= the collected flow-through from the µ Column) were mixed with 50 pmol of the biotinylated target molecule (calculated with Promega calculator) and the mixture was incubated at RT for 15 minutes.
For the magnetic labeling of the target-phage complex, 100 µl of µMACS Streptavidin MicroBeads were added to the target-phage solution, mixed and incubated at RT for 10 minutes.
For the magnetic separation, a second µ Column was placed in the magnetic field of the µMACS Separator and prepared by applying 100 µl of Equilibration Buffer for protein applications (supplied with the kit) on top of the column. The column was then washed twice with 200 µl of Tris-L Buffer. The mixture containing magnetically labeled target-phage-MicroBead complexes was added on top of the second µ Column and let it pass through. The magnetically labeled

complexes were retained on the column, which was washed two times with 200 µl of TBST (50 mM Tris pH 7.5, 150 mM NaCl, 0.1 % (v/v) Tween-20 to remove unbound phages.
Bound Phages were eluted by adding 20 µl of the Elution Buffer N (0.2 M Glycine-HCl pH 2.2, 1 mg/ml BSA) on top of the column, and incubated for 5 min at RT. Then, 80 µl of Elution Buffer N were added and drops from elution were collected into a clean tube containing 900 µl of PBS 1X pH 7.4. Then, 1 mg of Trypsin was added, and the mixture was incubated at RT for 30 min, in order to remove background infectivity.

First round of selection: infection of TG1 bacteria with eluted phage
TG1 bacteria were streaked from glycerol stock on a M9 minimal medium plate and incubated at 37 °C for 36 h. A single colony was inoculated into 5 ml of 2xTY and grown at 37 °C, 250 rpm overnight. The next morning, the culture was diluted 100-fold into 2xTY medium and grown at 37 °C, 250 rpm until OD_{600}=0.5. Eluted phage from the previous step were added to 30 ml of TG1 cells in exponential growth and incubated at 37 °C for one hour in a water bath, for the infection to occur. Infected cells were collected by centrifugation at 3200xg for 5 minutes, and resuspended in 1 ml of 2xTY medium. 166 µl of cells were plated onto 6 TSA plates supplemented with ampicillin 100 µg/ml, 4% glucose and incubated at 37 °C overnight, for the selection of infected cells onto solid medium. From the resuspended cells, 10-fold dilution series from 10^{-1} to 10^{-6} were prepared and plated on TSA plates supplemented with 100 µg/ml ampicillin, 4% glucose in order to monitor phage titer, using the following formula:

$$Colony\ forming\ units/ml = \frac{Number\ of\ colonies\ (cfu)\ x\ dilution\ factor}{volume\ plated\ (L)}$$

With an input of $5x10^{12}$ phages, it is expected to obtain approximately 10^5-10^7 bacterial colonies after the first and second round of selection. After three to four rounds of selections, titers should rise to 10^7-10^9. Such an increase frequently indicates the selection of binders.

Subsequent rounds of selection
Single colonies of infected TG1 were scraped from agar plates using 5 ml of 2xTY medium per plate and a glass spreader. Cells were mixed thoroughly by vortexing, and diluted into 500 ml of 2xTY medium supplemented with 4% glucose and 100 µg/ml ampicillin to an OD_{600} of 0.1, and grown to OD_{600}=0.5 at 37 °C, 250 rpm. At this point, another round of biopanning was restarted following the protocol reported above.

Screening of clones by ELISA in *E. coli* TG1 cells
After three rounds of panning, individual colonies from the dilution series were tested for antigen binding by ELISA. Colonies were picked using sterile pipette tips and placed into a 96-well round-bottom plate containing 200 µl of 2xTY medium supplemented with ampicillin 100 µg/ml and 4% glucose. Anti-ubiquitin positive control single colonies, previously streaked on TSA plates supplemented with ampicillin 100 µg/ml and 4% glucose and grown overnight at 37 °C, were also picked and placed into two wells of the same 96 well plate. Clones were grown in plate at 37 °C at 250 rpm in a plastic box overnight.
The next day, a fresh 96-well round-bottom plate containing 200 µl of 2xTY medium supplemented with 100 µg/ml ampicillin and 4% glucose was inoculated with 5 µl of the overnight culture. Glycerol stocks of the original 96-well overnight cultures were prepared by adding glycerol to the plate (20% final concentration) and storing it in a -80 °C freezer. The freshly inoculated plate was shaken at 37°C, 250 rpm for 3 h.
Cells were centrifuged at 3200xg in a plate centrifuge for 10 min. Supernatants were discarded by quickly inverting the plate, and pellets were resuspended in 200 µl of 2xTY medium supplemented with 100 µg/ml ampicillin and 1 mM IPTG, in order to induce the expression of antibody fragment.

Cells were grown overnight at 25 °C, 250 rpm for 16-24 h. During protocol optimization, when cells were grown into a 96-w plate, shaking was increased up to 800 rpm in a proper plate shaker. The next day, the plate was centrifuged at 3200xg for 10 min and the supernatant was transferred to a new 96-well plate and stored at 4 °C.
In some cases, the same procedure was performed in larger volumes, starting from a 10 ml inoculum and adjusting other volumes accordingly.

Antibodies in the supernatant were tested by ELISA, coating a 96-well Nunc Maxisorb plate with 100 µl of antigen solution 0.1 mg/ml per well ampicillin o.n. In addition, two wells were coated with 0.1 mg/ml ubiquitin, for positive control clones, and two wells were coated with BSA 0.1 mg/ml as negative control. The next day, wells were washed with 2x PBST and blocked with 200 µl per well of MPBS buffer (5% w/v milk powder in PBS). The next morning, wells were washed with 2x PBST. Using a separate 96-well round-bottom plate, 25 µl of supernatants were diluted in 75 µl of PBS supplemented with 3% (w/v) BSA with a multi-channel pipette. Diluted supernatants (100 µl) were transferred to the ELISA plate and incubated at room temperature with gentle agitation for one 1 h. Wells were washed with 5x PBST and then incubated with 100 µl/well of 1:2000 anti-myc monoclonal 9E10 in PBS supplemented with 3% (w/v) BSA at room temperature with gentle agitation for 1 hour. Wells were washed 3x with PBST, 1x with PBS, then incubated with 1:1000 Extravidin-HRP conjugate in PBS supplemented with 3% (w/v) BSA at room temperature with gentle agitation for 1 h. Wells were washed 3x with PBST, 1x with PBS, then incubated with 100 µl of room temperature TMB solution per well for ~15-30 min. The reaction was stopped adding 25 µl ml of 2 M sulphuric acid and plates were read at 450- 650 nm in a UV-Vis plate reader (Omega PolarStar, BMG LABTECH).

Screening of clones by ELISA in *E. coli* HB2151 cells
For promising clones, antibody fragments were also produced in *E. coli* HB2151 cells (K12 *ara D(lac-proAB) thi/F' proA+B lacIq lacZDM15*). This strain does not suppress the TGA amber stop codon located between the terminal myc-tag and the phage pIII protein (TG1: glutamate). However, even in TG1, amber suppression is of limited efficiency and the vast majority of antibody fragments are produced without the fusion to phage pIII. Some selected antibody fragments from this library may contain additional amber stops in a CDR region. This can be determined by sequencing plasmid preparations with primer 5'- CCCTCATAGTTAGCGTAACGA- 3'. These clones will have low-level expression in TG1, and no expression in HB2151. For high-level expression the additional amber stop codon should be mutated into glutamate. This also is essential if the antibody fragment gene is cloned into other expression plasmids for expression in *E. coli* strains such as BL21. The procedure was performed in *E. coli* HB2151 cells exactly as described above for *E. coli* TG1 cells.

Screening of clones by monoclonal phage ELISA
This step is not mandatory, but it is strongly recommended, since it can usually detect even a small percentage of positives in the selected population which are not detectable in ELISA. The reason for this frequent phenomenon is unknown, but may be due to lower solubility in the absence of the phage fusion proteins.

Single colonies were grown in 96-well plate as described for the ELISA procedure. After 3 h, 50 µl of 2xTY medium supplemented with $4x10^8$ KM13 helper phages were added to each well, from a solution of 5 ml 2xTY medium added with add $4x10^{10}$ KM13 phages. The plate was incubated at 37 °C without shaking for one hour, for the infection to occur. The plate was centrifuged at 3200xg for 10 min. Supernatant was discarded by quickly inverting the plate. Pellets were resuspended in 200 µl of 2xTY medium supplemented with 100 µg/ml ampicillin, 50 µg/ml kanamycin and 0.1% glucose by gentle agitation. Cultures were grown overnight at 25 °C, 250 rpm for 16-24 h.

During protocol optimization, when cells were grown into a 96-w plate, shaking was increased up to 800 rpm in a proper plate shaker.
The next day, the plate was centrifuged at 3200xg for 10 min and the supernatant was transferred to a new 96-w plate and store at 4 °C. In some cases, the same procedure was performed in larger volumes, starting from a 10 ml inoculum and adjusting other volumes accordingly. A 96-w plate was coated with antigen and blocked as described above. Using a separate 96-w round-bottom plate, 25 µl of phage supernatant were diluted in 75 µl of MPBS with a multi-channel pipette. Diluted phages (100 µl) were transferred to ELISA plate and incubated at room temperature with gentle agitation for 1 h. Wells were washed with 5x PBST and incubated with 100 µl/well of 1:20 anti M13_HRP conjugated antibody in 5% w/v MPBS buffer at room temperature with gentle agitation for 1 hour. Wells were washed with 3x PBST, 1x PBS, then added with 100 µl of room temperature TMB solution for ~15-30 min. The reaction was stopped by adding 25 µl ml of 2 M sulphuric acid and plates were read at 450- 650 nm in a UV-Vis plate reader (Omega PolarStar, BMG LABTECH).

Table 3.17 ELISA settings for Phage Display

ELISA			
	Antigen	**Primary Ab**	**Secondary Ab**
Sample	0.1 mg/ml EcAII	1:2000 Biotin-conjugated anti-myc (910E) in 3% BSA (Merck Millipore)	1:1000 Extravidin-HRP in 2% BSA (Sigma)
Positive Control	0.1 mg/ml ubiquitin		
Phage ELISA			
	Antigen	**Primary Ab**	**Secondary Ab**
Sample and Positive Control	0.1 mg/ml EcAII 0.1 mg/ml ubiquitin	1:6000 anti-KM13 in 5% MPBS (Progen)	1: 2000 HRP-conjugated anti-mouse2% BSA (Sigma)
Sample and Positive Control	0.1 mg/ml EcAII 0.1 mg/ml ubiquitin	1:20 anti-M13 HRP conjugated antibody in 5% MPBS (Progen)	/

Preparation of helper phage stock
TG1 bacteria were streaked from glycerol stock onto a M9 minimal medium plate and incubated at 37 °C for 36 h. An o.n. culture of 5 ml 2xTY medium from a single colony was grown at 37 °C, 250 rpm. The o.n. inoculum was diluted 100-fold into 5 ml of 2xTY medium and grown at 37 °C, 250 rpm until OD_{600}=0.5.
A dilution series of KM13 helper phage in PBS (10^1/ml to 10^5/ml) was prepared. 10 µl of each dilution of KM13 helper phage were added to 200 µl of TG1 culture each and incubated in water bath at 37 °C for 30 min. 3 ml of melted H-top agar were added to each tube, gently mixed with culture and poured onto pre-warmed TSA plates. Top agar was completely melted in microwave and cooled to 42 °C in a water bath before use. Plates were allowed to solidify at room temperature and were incubated o.n. at 37 °C. An o.n. culture of TG1 cells in 5 ml 2xTY medium from a single colony was grown at 37 °C, 250 rpm. The next morning, the culture was diluted 100-fold into 5 ml of 2xTY medium and grown at 37 °C, 250 rpm until OD600=0.5. Then a small plaque from the plates was picked with a sterile toothpick and placed into 5 ml TG1 culture at OD_{600}=0.5 and grown at 37 °C, 250 rpm for two hours.
The culture was then diluted 100-fold into 500 ml of 2xTY medium, and incubated for 2 h at 250 rpm at 37 °C. Kanamycin was added to a concentration of 50 µg/ml and the culture was grown at 250 rpm at 30 °C o.n. in order to select infected cells.

The supernatant was cleared by centrifugation and filtration and phages were isolated, purified and quantified through PEG purification as described above. Phage were frozen in liquid nitrogen with 20% glycerol and stored at -80°C. Trypsin cleavage could be tested by incubating 10^{10} phages in 1 ml of trypsin solution at room temperature for 30 min and preparing two dilution series, from 10^{10} to 10^{2} phages in PBS, one using trypsin treated phages and one using non treated phages (NT). 10 µl of each phage dilution were used to infect 200 µl of TG1 bacteria in exponential growth (OD_{600}=0.5). Each infection was plated on TSA plates supplemented with kanamycin 50 µg/ml and grown at 37 °C o.n. The number of colonies obtained from trypsin-treated phages should be at least 10^{6}-fold lower than for non-treated phages.

Library amplification

Stocks of the repertoire were produced by plating half of the original glycerol stock on eight large square (30 cmx30 cm, Nunc, Thermofisher) TSA plates supplemented with 4% glucose and 100 µg/ml ampicillin. After growing overnight at 37 °C, colonies were scraped off plates with a glass spreader in 20 ml of 2xTY medium per plate. Cells were carefully mixed by vortexing and frozen in 1 ml aliquots from an OD600=20 cell culture in liquid nitrogen (20% glycerol), and were stored -80 °C. Such aliquots could not be used for further library amplification, but just for library packaging during selection.

3.2.7 Yeast Two-Hybrid

The Yeast Two-Hybrid (Y2H) technique allows detection of interacting proteins in living yeast cells. In particular, the interaction between two proteins, called bait (protein of interest) and prey (interaction partner), respectively activates reporter genes that enable growth on specific media or the development of a colorimetric reaction. This technique was developed in 1989, by Fields and Song, who studied the modular structure of *Saccharomyces cerevisiae* Gal4 transcriptional activator,[455] which is composed of two different functional domains: a N-terminal DNA binding domain (DBD) and a C-terminal (transcriptional) activation domain (AD). Both domains resulted to individually maintain their function when the other domain was missing. The basic idea of Y2H is therefore to fuse the two proteins of interest, X and Y, to DBD and AD of Gal4, respectively, such that interaction between X and Y reconstitutes a functional transcription factor that can then drive reporter gene expression. From a methodological point of view, any Y2H screen implies the transformation of yeast cells with bait and prey cDNAs cloned into different vectors under the control of yeast promoters. Once expressed in the cytosol, bait and prey must be able to enter the nucleus to activate transcription of reporter genes. Suitable reporter genes are the *lacZ* gene, which generates a colorimetric reaction, and auxotrophic markers (e.g. LEU2, HIS3, ADE2, URA3, LYS2) that allow growth on minimal media. Actually, more than one reporter gene is assayed in parallel to increase the stringency of Y2H screens.[456,457]

3.2.7.1 IACT technology

The Intracellular Antibody Capture Technology (IACT), represents a specific application of the Y2H technique, optimized in order to select *in vivo* interacting antibody–antigen pairs.[458] For the screening of antibody-antigen interactions, the *Saccharomyces cerevisiae* L40 strain is used, which contains lexA operator-responsive reporters (Genotype: *Mata his3Δ200 trp1-901 leu 2-3, 112 ade2 LYS2::(lexAop)$_4$-HIS3 URA3:: ::(lexAop)$_8$-lacZ GAL4*). The reporter genes are *HIS3* and *lacZ*, which are driven, respectively, by minimal HIS3 and GAL1 promoters, fused to multimerized lexA binding sites. The expression of HIS3 provides a growth selection in case of positive interactions, while the expression of lacZ, which encodes the ß-galactosidase enzyme, provides a colorimetric assay, resulting in blue colonies in the presence of X-gal (5-Bromo-4-Chloro-3-Indolyl β-D-Galactopyranoside). In order to allow the selection of positive transformants, the L40 strain is deficient for TRP and LEU (auxotrophic phenotype) and therefore cannot grow on minimal

medium lacking tryptophane and leucine, unless functional *TRP1* and *LEU2* gene are introduced. Moreover, this strain carries the *ade2* mutation, which causes the accumulation of a red pigment in colonies on medium containing limiting amounts of adenine.

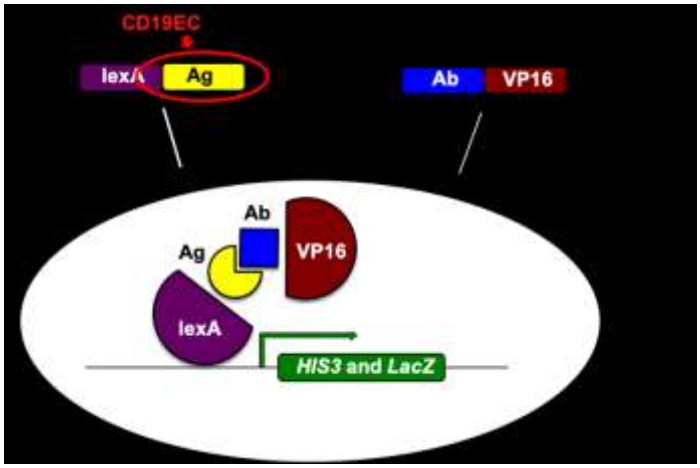

Fig. 3.9 IACT technology schematic view. *The llama nanobody library is screened in yeast transformed with the antigen bait (CD19). Only those VHH which are able to bind to CD19 in vivo will activate the expression of the reporter genes, HIS3 and LacZ.*

In this technology, *E. coli* repressor protein LexA is used as DNA binding domain and expressed in fusion format with the ***bait*** (**antigen of interest**), while Herpes simplex virus VP16 activation domain (AD) is fused in frame with the ***preys*** (**antibody library**) to be screened for binders. Reconstitution of the transcription factor is assayed using two reporter genes (*HIS3* and *lacZ*) chromosomally integrated into L40 strain, as described above. In this work, the target protein (CD19 antigen) fused in-frame to lexA DBD and llama-derived nanobodies library (naïve, 10^6) fused to VP16 AD were co-expressed in the *Saccharomyces cerevisiae* L40 reporter strain.[459]
As a vector for the cloning of lexA-CD9 bait, pMIC-BD1 vector was kindly provided by the Prof. Cattaneo's research group (Scuola Normale Superiore di Pisa, Pisa, Italy). This vector contains a bacterial chloramphenicol resistance gene, the *TRP1* gene, which allows yeast containing this plasmid to grow in minimal medium lacking tryptophan, and the 2µ origin of replication. This plasmid also contains the entire region of the *E. coli* lexA protein, whose expression is regulated by the yeast alcohol dehydrogenase I (ADH1) promoter.
The pLinker220 vector was the recipient vector for the antibody library. pLinker220 is a derivative of VP16* vector, [458,460] which contains two nuclear localization signals (NLS), the SV40 Large T antigen and the in-frame fusion of the VP16 acidic activation domain, whose expression is regulated again by yeast ADH1 promoter. The vector contains the *LEU2* gene as nutritional selection marker, the 2µ origin of replication, a bacterial origin of replication *ColE1*, and the ß-lactamase gene for prokaryotic selection.[431]

L40 yeast was transformed with the CD19-lexA bait construct following a small scale LiAc transformation protocol, and then L40 yeast cells containing the bait plasmid (lexA-CD19) were tested for CD19-lexA expression and the transactivation level. L40 CD19 bait was then transformed with the nanobody-VP16 fusion library following a maxi-scale LiAc transformation protocol, as described in Visintin et al 2001.[458]

<u>Grow the Culture Media and Selective Media</u>
Yeast strains which employ auxotrophic mutations as markers, such as *S. cerevisiae* L40, are usually grown on nutrient-rich media at 30 °C, in order to minimize the selection of revertants.

YPD represents the complete medium for the growth of yeasts, meaning that it cannot be used for the selection of auxotrophs. Adenine hemisulfate can be added, obtaining YPAD, and glucose could be removed, obtaining YPA (**Table 3.18**), according to experimental settings. YNB (Yeast Nitrogen Base), a synthetic medium, was used for the preparation of autotrophs selective media, as reported in **Table 3.20**, which were complemented with an amino acidic mixture and a salt mixture, reported in **Table 3.19**.

S. cerevisiae L40 is an autotroph strain for W, H and L amino acids. *TRP1* gene (W) is present in pMICBD1 vector, meaning that only cells successfully transformed with the bait construct (CD19), are able to grow on -W selective media. *LEU2* gene (L) is present in pLINKER220 vector, meaning that only cells successfully transformed with the prey constructs (llama nanobody library), are able to grow on -L selective media. *HIS3* is a reporter gene, meaning that only cells in which an antibody-antigen (bait-prey) interaction occurs, are able to grow on -H selective media (**Table 3.19**). However, it is possible for a bait construct to transactivate, meaning that its transformation alone into *S. cerevisiae* L40 could lead to an unspecific activation of reporter genes. In addition to a preliminary test, which allows to evaluate the growth level on -H plates and ß-galactosidase activity in the presence of the bait alone, 3AT, a competitive inhibitor of *HIS3* gene product, can be added into the selective media. In fact, in the presence of 3AT, cells will be able to grow only if the level of the *HIS3* gene product is sufficient to sustain the inhibitory effect of 3AT, that is to produce enough histidine to allow cell survival, which depends on the strength of the bait-prey interaction. Increasing concentrations of 3AT can therefore be used to increase the stringency of the selection.

Table 3.18 Nutrient-rich media for Yeast Culture

YPD		**YPAD**		**YPA**	
Yeast extract	10 g/L	Yeast extract	10 g/L	Yeast extract	10 g/L
Bacto peptone	20 g/L	Bacto peptone	20 g/L	Bacto peptone	20 g/L
D-glucose	20 g/L	D-glucose	20 g/L	D-glucose	/
Adenine hemisulfate	/	Adenine hemisulfate	0,1 g/L	Adenine hemisulfate	0,1 g/L
Add H_2O to 90% of the desired final volume. Adjust pH to 5,8, autoclave 121 °C for 15 min then cool to 50-60 °C.					

Table 3.19 Complementing solutions for selective media

AA mix		**Salts**	
NaOH	60 g/L	NaOH	36 g/L
Adenine hemisulfate	10 g/L	Succininc Acid	66,7 g/L
L-Arginine-HCl	10 g/L	Ammonium Sulphate	33,3 g/L
L-Cysteine	10 g/L	D- Glucose	146,7 g/L
L-Threonine	10 g/L		
L-Aspartic Acid	5 g/L		
L-Isoleucine	5 g/L		
L-Methionine	5 g/L		
L-Phenilalanine	5 g/L		
L-Proline	5 g/L		
L-Serine	5 g/L		
L-Tyrosine	5 g/L		

Table 3.20 Selective media for auxotrophic *S. cerevisiae* L40 auxotrophic strain

	Selective for	**YNB (12 g/L) w/o AA and $(NH_4)_2SO_4$****	**Salts**	**AA mix**	**W***	**H***	**L***	**H_2O**
- W	Bait positive transformants	800	150	10	/	10	10	20

- L	Preys positive transformants	800	150	10	10	10	/	20
- WL	Selective for positive bait + preys transformants	800	150	10	/	10	/	30
- WHL* **	Selective for positive interactors	800	150	10	/	/	/	40

volumes expressed in ml
* H (5 g/L), L (10 g/L), W (10 g/L)
** If solid plates are needed, YNB is prepared adding 20 g/L of bacto agar
*** When needed, 3AT was added using a 2 M stock

Small Scale LiAc Transformation

In order to obtain a positive and a negative control for bait-prey interaction to use during the screening procedure, the CD19 bait, consisting in *S. cerevisiae* L40 previously transformed with the CD19 bait construct, was transformed with an anti-lexA prey as a positive control of interaction and an unrelated bait as a negative control of interaction, as follows.
Few colonies of L40 CD19 bait were inoculated in 6 ml of selective – W medium and incubated at 30 °C, 225 rpm o.n. The next morning, the o.n. pre-inoculum was diluted into YPD to an OD_{600} = 0.3, and incubated at 30 °C, 225 up to OD_{600} = 0.6. The culture was then centrifuged at 3000 rpm (1000xg) at room temperature (RT = 24-25 °C) for 5 min and the pellet was washed with 15 ml of sterile H_2O. After a centrifugation at 3000 rpm for 5 min, the pellet was resuspended into 300 µl of 1xTE/1xLiAc solution (10 mM TE, 0,1 M LiAc). For each transformation, 100 µl of resuspended pellet were transferred into a tube containing 0.1 µg of the corresponding prey DNA and 0.1 mg of denatured salmon testis carrier DNA (**Table 3.21**). 600 µl of PEG/TE/LiAc solution (PEG 4000 40%, TE 10 mM, LiAc 0.1 M) were added into each tube. Cells were vortexed and incubated at 30 °C, 225 rpm for 30 min. After the addition of 70 µl of sterile DMSO, tubes were gently mixed by inversion and heat shocked at 42 °C in a water bath for 15 min. Cells were then incubated on ice for 2 min, pelleted by centrifugation at 14000 rpm for 30 s, and resuspended into 100 µl of sterile 1xTE. Cells from each transformation were then plated onto -WL plates, in order to monitor the transformation efficacy, and -WHL plates, in order to monitor the development of bait-prey interaction (**Fig. 3.9**)

Table 21. Transformation mixtures

	Interaction positive control	**Interaction negative control**	**Transformation positive control**
prey	anti-lexA	unrelated	/
prey DNA	0.1 µg	0.1 µg	/
Salmon testis carrier DNA	0.1 mg	0.1 mg	0.1 mg

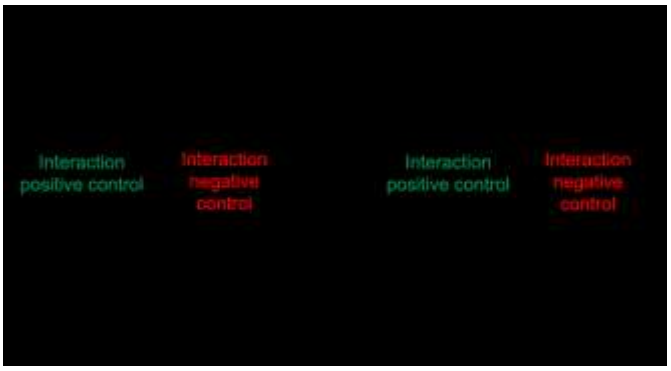

Fig. 3.10 Small scale transfection plating scheme

Screening

The screening procedure consists in a Maxi-Scale LiAc transformation of the CD19 bait with the Llama VHH library (naïve, 10^6).

On the first day, some colonies of L40 CD19EC bait were inoculated into 50 ml of -W selective medium, and incubated at 30 °C at 225 rpm o.n., in order to obtain the culture in a mid-log phase in the next day. On the second day, in the morning, the OD_{600} of the pre-inoculum was measured (1.61) and the T of incubation was lowered to 25 °C. In the late afternoon, the inoculum was diluted to an OD_{600}=0.2 into 150 ml of -W selective media, and incubated at 30 °C, 225 rpm o.n. On the next morning, the inoculum was diluted to OD_{600}=0.3 into 1 L of YPAD and incubated at 30 °C, 225 rpm) for 3 h. When the OD_{600} was between 0.6-0.7, cells were centrifuged at 3000 rpm (1500xg) at 24 °C for 5 min. The pellet was washed and centrifuged several times for a total amount of 500 ml of 1xTE.

After the washings, the pellet was resuspended into 20 ml of 1xLiAc/1xTE, and then added to a flask containing 140 ml of 40% PEG/1xLiAc/1xTE. At this point, 250 µg of library DNA and 10 mg of salmon testis DNA were added. Cells were then incubated at 30 °C, 160 rpm for 30 min. 17,6 ml of sterile DMSO were added, cells were mixed and then heat shocked at 42 °C in water bath for 15 min, swirling gently in order to mix every 2 min. Cells were rapidly cooled at RT by adding 400 ml of pre-warmed YPA and centrifuged at 4500 rpm at 24 °C for 5 min. The pellet was washed and centrifuged several times in a total amount of 1 L of YPAD. After the washings, the pellet was resuspended into 1 L of YPAD and incubated at 30 °C, 225 rpm for 1 h. Then, 1 ml of cells was centrifuged and resuspended into 1 ml of -WL medium in order to prepare serial dilution for the evaluation of transformation efficiency (10^{-4}, 10^{-5},10^{-6}, 10^{-7}, 10^{-8}). The culture was split and processed as follows.

200 ml were centrifuged at 4000 rpm, 24 °C for 5 min, and washed in several step in a total amount of 300 ml of -WL. The pellet was then resuspended into 10 ml of -WL, inoculated into 200 ml of -WL (OD_{600}= 0.2), and incubated at 30 °C, 225 rpm o.n., in order to allow also to the slower clones, referred to as "doublings", to grow.

The other 800 ml of culture were immediately processed, pelleted by centrifugation at 4000 rpm, 24 °C for 5 min, and washed in several steps in a total amount of 350 ml of – WHL. The washed pellet was resuspended into 6 ml of -WHL, and plated onto 15 -WHL + 1 mM 3AT plates (400 µl per plate). Plates were incubated at 30 °C for 72-96 hrs.

The next morning, doublings were processed in the same way and plated on 6 -WHL + 1 mM 3AT plates (400 µl per plate).

Picking

After 72-96 hrs from the screening, single colonies growing on pre-doublings and doubling -WHL + 1 mM 3AT plates were picked and streaked onto -WL plates, following the scheme of a 36-box ordered grid (**Fig 3.11**)

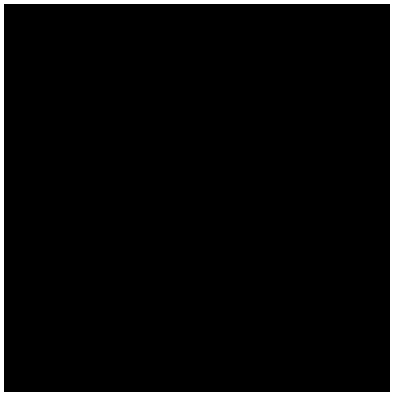

Fig. 3.11 Picking grid scheme

ß-gal Assay

A number of different techniques have been developed to assess ß-gal enzymatic activity in yeast. The available technical options allow variance of elements impacting all levels of the assay process. These include, first, growth conditions for yeast containing lacZ reporters. Growth can be on solid support (agar plates) or in liquid culture (either in tubes or microplates). Second, exposure to ß-gal substrates can occur while yeasts are actively growing, or subsequent to cell lysis. Third, in techniques where yeasts are lysed prior to assay, cell lysis can be achieved by multiple means, including freeze–thaw cycles, detergent extraction or solvent extraction. In the case of solid support assays, the assay can be done directly on growth plates, versus on lifted filters of a variety of compositions.[461]

In this thesis, two ß-gal assays were performed, one liquid-based, and the other solid-based (filter assay).

In the liquid-based assay, cells from each clone were lysed in a 96-well plate (**Fig. 3.11**), via incubation with 50 µl of containing 166,5 U/ml Lyticase in 20 mM Tris-HCl pH 7.5, at 37 °C, 150 rpm for 2 h. Then, 50 µl of Z Buffer (60 mM Na_2HPO_4, 40 mM NaH_2PO_4, 10 mM KCl 1 mM $MgSO_4$, pH 7) supplemented with X-gal 0.3 mg/ml and β-mercaptoethanol 0.3 % v/v, were added to each well, and the plate was incubated at 37 °C, 150 rpm for 1 h, and then moved to a static incubator at 37 °C o.n. The next morning, the development of blue was visually evaluated.

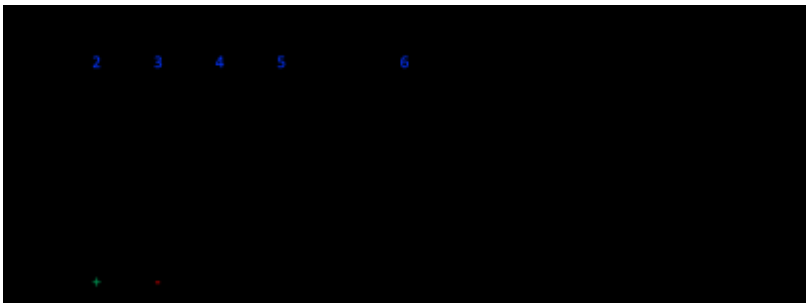

Fig. 3.12 Liquid ß-gal assay 96 well plate scheme

For the filter assay, ß-gal activity is standardly described as high or low based on colonies being white, light blue, or dark blue. Yeast colonies were patched onto a nitrocellulose filter circle, by pressing the filter directly onto the plate. The filter was lifted and placed colony side-up on an aluminum boat, subsequently positioned in order to float onto liquid nitrogen. After ~20 seconds of floating, the boat was submerged into liquid nitrogen for 5 sec. The filter was then allowed to warm up at RT and placed upon a Whatman which had been pre-wet with 5 ml of Z Buffer (60 mM Na_2HPO_4, 40 mM NaH_2PO_4, 10 mM KCl 1 mM $MgSO_4$, pH 7) added with 0.3 mg/ml X-gal and 0.3 % v/v β-mercaptoethanol. The filters where then incubated at 37 °C for ~5 h, and then left to dry o.n.

Colony PCR

Clones which developed a blue color into the ß-gal assay were analyzed through colony PCR, in order to confirm the presence of the prey DNA. Cells were lysed by incubation into 10 µl of 166,5 U/ml Lyticase in 20 mM Tris-HCl pH 7.5 for 45 min at 37 °C, followed by Lyticase inactivation at 95 °C for 5 min. A PCR master mix was prepared as described in **Table 3.21**. 10 µl of master mix were added to each tube and PCR cycles were performed as described in **Table 3.22**.

PCR were then analyzed through agarose gel electrophoresis, on a 1.3% agarose gel. Bands were visualized incorporating EtBr (10 mg/ml stock, DIL 1:16000) during gel preparation. Images were acquired using Chemidoc XRS (Biorad).

Table 3.22 Colony PCR reaction Master Mix		
Green Buffer 5x		320 µl
10 mM dNTPs		32 µl
10 µM Forward primer		80 µl
10 µM Reverse primer		80 µl
GoTaq polymerase		268 µl
Molecular Biology Grade water		20 µl
	V TOT	800 µl

Table 3.23 Colony PCR cycling

Step	Temperature	Time	Cycles
GoTaq pol heat activation	95 °C	5 min	1
Denaturing	95 °C	30 sec	
Annealing	50 °C	30 sec	29
Elongation	72 °C	1 min	
Final extension	72 °C	5 min	1

PCR DNA Fingerprint

Each individual prey-nanobody sequence should have its own fingerprint. For this reason, the amplification product of the colony PCR) from each clone was digested with *Nla* IV and *Alu* I restriction enzymes (**Table 3.24**) and analyzed through gel electrophoresis on 10% polyacrylamide gels. Bands were visualized incubating the gel for 10 min in an aqueous solution containing EtBr. Images were acquired using Chemidoc XRS (Biorad).

Table 3.24 *Nla* IV and *Alu* I double digestion master mix	
Green Buffer 5x	160 µl
10x CutSmart	160 µl
*Nla*IV	20 µl
*Alu*I	20 µl
Molecular Biology Grade water	960 µl

12 µl were added in tubes containing 8 µl of PCR product

Plasmid DNA extraction from Yeast

Clones which showed distinct DNA fingerprints were inoculated in 3 ml of selective -L media and incubated at 30 °C, 225 rpm o.n. The next morning cells were pelleted by centrifugation at 13000 rpm for 2 min and lysed via incubation into 250 µl of Lyticase Buffer (1.2 M Sorbitol, 10 mM Trs pH 8, 10 mM CaCl2, 10 % v/v β-mercaptoethanol, 95 U/ml Lyticase) at 37 °C for 1 h. Plasmid DNA was then extracted following the protocol of Wizard® *Plus* SV Minipreps DNA Purification System (Promega) and quantified via nanodrop.

Bacterial Transformation through electroporation

Plasmid DNA extracted from yeast cells was transformed into *E. coli* DH5α using electroporation. For each transformation, ~ 100 ng of DNA were added to 50 µl of competent *E. coli* DH5α cells, transferred into an electroporation cuvette, and shocked at ~2000 V for ~5 ms. Electroporated cells were added with 970 µl of SOC medium, transferred into a snaptop tube and incubated for at

37 °C, 250 rpm for 1 h in order to recover. 50 µl of cells were then plated onto LB-Amp (100 µg/ml) plates and incubated at 37 °C o.n.

Plasmid DNA extraction from bacterial cells

Transformed *E. coli* DH5α single colonies were inoculated in 3 ml of LB added with 100 µg/ml Amp, at 37 °C, 250 rpm o.n. The next morning plasmid DNA was extracted following. the protocol of Wizard® *Plus* SV Minipreps DNA Purification System (Promega) and quantified via nanodrop. DNA was sent for sequencing to Eurofins.

Secondary Screening (Small Scale Transfection and growth on selective media)

In order to confirm the antigen-nanobody (bait-prey) interaction of the selected candidates, and to exclude their affinity for lexA (CD19 fusion partner), their purified plasmid DNA was re-transformed in parallel into *S. cerevisiae* L40 CD19 bait and into an *S. cerevisiae* L40 unrelated bait, along with an internal interaction negative control, an interaction positive control and a transformation negative control. The small scale transformations were performed following the protocol reported above. Transformants were plated onto -WL and -WHL plates as reported in **Fig. 3.13**. Growth onto selective -WHL plates was expected to occur only when the candidates were transformed into L4 CD19 bait. When a growth on such plates is observed also for the transformed unrelated L40 bait, the possibility of a bait-prey interaction with lexA should be considered.

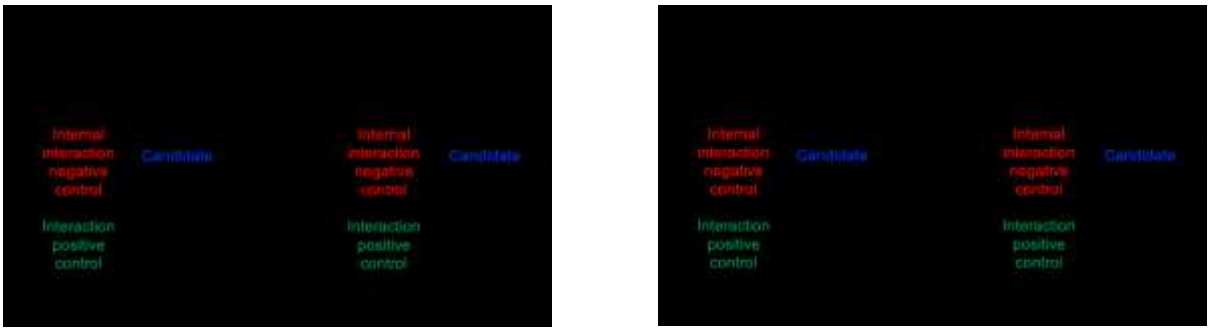

Fig. 3.13 Secondary screening plating scheme

3.2.8 Mammalian cells

Tissue culture or cell culture refers to *in vitro* techniques used to grow tissues or cells derived from living tissues or organs *ex vivo*, which means in an artificial controlled and favorable environment. A cell line is defined as a cell population derived from a single clone, which shares an identical or similar genome. Cell lines can be distinguished into *primary* or *immortalized*. Primary cell lines are derived from a donor organism and have a finite life span, which means that once reached the confluence stage in flask, they can be sub-cultured for a limited number of passages prior to become senescent, loose their own morphological/functional features and die. Immortalized cell lines are well established cell populations that can permanently replicate, maintaining their peculiar features. They are generally isolated from *in vivo* tumors, but they can also be derived from primary cell lines engineered to become immortal. Immortalized cell lines are commonly used as *in vitro* model systems for several kinds of studies.

An aseptic work area is needed when working with cell cultures, in order to prevent any possible contact between cells and contaminating microorganisms. Such area is generally represented by a cell culture hood, in which the laminar flow is filtered by High Efficiency Particulate Air (HEPA) filter units and the use of sterile equipment is required. In general, to favor proliferation outside the original living organism, cells are cultured in specific media, which consist in saline solutions that reproduce the physiological environment and contain all the needed nutrients. Essential nutrients supply is typically provided by addition of fetal bovine serum (FBS) to media and L-glutamine, which is required by most of the cultured cells, especially those derived from tumors. Some cell lines could require specific compounds for survival and proliferation that must be

provided separately (e.g. cytokines, growth factors). Media can also be supplied with antibiotics in order to prevent contamination by prokaryotic organisms. Cells are usually cultured in a humidified incubator at 37°C in presence of 5% CO2, which is needed to allow the carbonate buffer system of cell media to work.

3.2.8.1 Cell Lines and Media

HEK293T

HEK293T cells are an epithelial, adherent and highly transfectable variant of HEK293 cells. HEK293 cells are human embryonic kidney cells immortalized through the incorporation of ~4.5 kb adenovirus 5DNA genome. HEK93T cells express in addition the SV40 T-antigen (Simian Vacuolating Virus 40 Ag), which allows a greater replication of vectors carrying the SV40 origin of replication. They are cultured in HG-DMEM medium added with 10 % FBS, 1% PenStrep, 15 L-Glutamine, with a recommended subcultivation ratio between 1:4-1:8.

HeLa

HeLa cells are an epithelial, adherent, human tumoral cell line derived from a cervix adenocarcinoma patient, Henrietta Lack. These cells are highly transfectable and can be used to screen for *E. coli* strains with invasive potential. Four typical HeLa marker chromosomes have been reported in the literature, as well as cytogenetic instability. They are cultured in HG-DMEM medium added with 10 % FBS, 1% PenStrep, 15 L-Glutamine, with a recommended subcultivation ratio between 1:2-1:6.

Human Acute Lymphoblastic Leukemia (ALL) cells employed for the experiments described in this thesis were obtained from ATCC. Raji, RS4;11, HL60, MOLT-4 were grown in RPMI 1640 complete media (10% FBS, 2 mM L-glutamine, 100 IU/ml penicillin and 100 µg/ml streptomycin). Cells were monitored and passaged when needed.

Raji

Raji cells are a human, suspension lymphoblastic cell line derived from an 11 years old patient with Burkitt Lymphoma. They are suitable for transfection and are $CD19^+$ and $CD20^+$. There is 6% polyploidy and occasional disparity in the size of the homologs of the number 1 chromosome and the number 4 chromosome. They are cultured into RPMI medium added with 10 % FBS, 1% PenStrep, 15 L-Glutamine, maintaining cell density at $4x10^5$ viable cells/ml.

RS4;11

RS4;11 cells are a human, suspension lymphoblastic cell line derived from a 32 years old patient with Acute Lymphoblastic Leukemia. The cells have a characteristic chromosomal abnormality, t(4;11)(q21;q23), and are $CD19^+$ and $CD20^-$.

They are cultured into RPMI medium added with 10 % FBS, 1% PenStrep, 15 L-Glutamine, maintaining cell density between 1 X 10^5 and 1 X 10^6 viable cells/ml.

HL60

HL60 cells are a human, suspension pro-myeloblastic cell line derived from a 36 years old patient with Acute Promyelocytic Leukemia. HL-60 cells spontaneously differentiate and differentiation can be stimulated by butyrate, hypoxanthine, phorbol myristic acid (PMA, TPA), dimethylsulfoxide (DMSO, 1% to 1.5%), actinomycin D, and retinoic acid. The cells exhibit phagocytic activity and responsiveness to chemotactic stimuli. The line is positive for *myc* oncogene expression. The cells are $CD19^-$ and $CD20^-$.

They are cultured into RPMI medium added with 10 % FBS, 1% PenStrep, 15 L-Glutamine, maintaining cell density between 1 X 10^5 and 1 X 10^6 viable cells/ml.

MOLT4

MOLT4 cells are a human, suspension T-lymphoblastic cell line derived from a 19 years old patient with Acute Lymphoblastic Leukemia. This is a human cell line with the hypertetraploid chromosome number. The cells are $CD19^-$ and $CD20^-$. They are cultured into RPMI medium added

with 10% FBS, 1% PenStrep, 15 L-Glutamine, maintaining cell density between $4x10^5$ and $2x10^6$ viable cells/ml.

Dose-response assay

Determination of the *in vitro* cytotoxic effect of the drugs can be assayed by dose-response experiments. The assay consists in evaluating the cytotoxic effect of different concentrations of the drug to be tested. Two important parameters can be derived from dose-response experiments: the drug cytotoxic kinetic, meaning the time needed for the drug to exert a cytotoxic effect; and the IC_{50} parameter, a value that indicates the amount of drug needed to obtain 50% of cell growth inhibition.

Full dose-response experiments were performed on HEK293T and HeLa cells using EcAII, in order to determine their sensitivity to EcAII activity and use them as adherent control in CD19 internalization experiments. EcAII proteins pure to homogeneity and dialyzed in cell-culture tested Phosphate Buffered Saline (PBS), pH 7.4, were 0.22 µm filtered under a laminar flow-hood in order to obtain sterile solutions. In all cases, the enzyme concentration was established as U/ml of ASNase activity. Cells were plated in a 96-well plate at 5 x 10^5 in 100 µl complete media and treated with 6 different concentrations of protein. In all cases, cells were treated with a final volume of 50 µl PBS solution. As a control, cells were treated with 50 µl PBS-only. After 72 h incubation, cell viability using MTT assay, as described below.

***In vitro* cell viability assays**

Cytotoxicity of compounds or drugs can be evaluated by *in vitro* tests using cell lines as a model system. The system is highly simplified with regard to the physiological one; nevertheless, the data can provide valid information on the effects of cytotoxic agents.

Metabolic activity of live cells can be measured to determine cytotoxicity of a treated sample *versus* a not-treated control. A common method measures the mitochondrial reducing activity by using a tetrazolium salt (MTT, 3-(4,5-dimethylthiazol-2-yl)-2,5-diphenyltetrazolium bromide). NADPH-dependent oxidoreductase enzymes can reduce tetrazolium salt to its insoluble form, formazan. The latter compound can be solubilized and measured by a colorimetric assay.

Both apoptosis and necrosis cause changes at a plasmatic membrane level, resulting in improved membrane permeability. Living-cell exclusion dye, such as propidium iodide and trypan, can be exploited to obtain an indication of the number of live cells (negative to the dye) and dead cells (positive to the dye) both in the treated and un-treated samples.

3.2.9 Immunofluorescence

Immunofluorescence (IF) is a fundamental technique in molecular biology, which combines the use of antibodies with fluorescence imaging techniques in order to visualize target proteins and other biomolecules within fixed cell or tissue samples. Through this process, the localization, relative expression, and even activation states of target proteins can be observed. Proteins of interest can be detected through *direct detection,* which relies on the use of primary antibodies covalently conjugated to fluorophores, or *indirect detection,* a two-step method which relies on the use of unlabeled primary antibody followed by fluorophore-conjugated secondary antibody. Both methods allow the combination of multiple fluorophores, which makes IF ideal for the investigation of protein co-localization, changes in subcellular localization, identification of different cell subsets, and several other analyses. IF imaging depends on light emission from a fluorophore, which is a fluorescent chemical compound that can absorb light at a specific wavelength, resulting in light emission at a longer or lower energy wavelength, which is conjugated to the antibody.[462] The visualization of multiple antigens on the same biological samples is possible thanks to the fact that distinct fluorophores have different excitation and emission wavelengths. IF images can be captured on a confocal microscope to determine the

cellular localization of the protein of interest. Confocal microscopy enhances optical resolution by filtering out the light emitted from the out-of-focus planes.[463]

An IF protocol consists in a multistep procedure. Initially, the sample is attached to a solid support such as a slide to facilitate visualization by a microscope. The sample is then fixed to stop the biochemical cellular reactions, in order to preserve cells and tissues. The samples could then be permeabilized to facilitate antibody binding to intracellular antigens. The sample is incubated with primary antibody and multiple washes are then performed in order to remove the excess unbound antibody. If the primary antibody is already bound to a fluorophore (*direct*), the sample can be mounted for imaging, otherwise, the sample is incubated with a fluorophore-conjugated secondary antibody which recognize the primary antibody (indirect IF). After several washes to remove the excess unbound antibody, the sample is then mounted for imaging.[464]
For this thesis, the Abcam protocol for immunofluorescence reported below was followed and optimized for the study of CD19 internalization through receptor-mediated endocytosis (lysosomes).

Cells were grown on coverslips (22 cm x22 cm) into 6-w plates. Cells were fixed using 2.5 % PFA in PBS at RT for 15 min. After 3 washings of 5 min each in ice-cold PBS, cells were permeabilized by adding 1 ml of PBS supplemented with 0.1% (v/v) Triton and incubating them at RT for 30 min. After 3 washings of 5 min in ice-cold PBS, cells were incubated in pre-chilled 50% v/v methanol diluted in PBS and incubated for 15 min at RT. After 3 washings of 5 min each in ice-cold PBS, cells were blocked at RT in 2% BSA for 2 h. When a direct method was used, a single incubation with properly diluted antibody in 1% BSA was performed at RT for 1 h. When an indirect approach was used, after the incubation with the primary antibody, 3 washings of 5 min in ice-cold PBS were performed, and then cells were incubated with properly diluted antibody in 1% BSA at RT for 1 h. After 3 washings of 5 min in ice-cold PBS, counterstaining was performed using Hoechst 33258 properly diluted in PBS and incubated at RT for 15 min. After 3 washings of 5 min in ice-cold PBS, coverslips were mounted on slides pre-washed in 100% methanol, using MOVIOL as mounting agent.

Adherent Cells HEK293T IF
HEK293T cells were chosen as adherent positive control in order to set up the staining and the internalization experiment. In order to express CD19, HEK293T were transfected in small scale with CD19fl (Full length) imported by OriGene. For the internalization studies, HEK293T cells were grown and transfected onto coverslips for 48 h. Then cells were incubated with anti-CD19 (HD37) antibody (Merck-Millipore, Invitrogen, 1:100) for 10, 30, and 90 min,[465–467] and stained following the protocol reported above.

Suspensions cells IF
In order to study CD19 internalization, leukemic cells such as RAJI, RAJI CD19$^-$ and RS4;11 were used. Suspension cells are more difficult to treat for IF, so the following optimizations were performed.
Coverslips coated with **poly-lysine** were placed at the bottom of a tube, in which 1 ml of 30% saccharose was added. 500 000 cells resuspended into 200 µl of PBS were then added onto the top of the saccharose solution and centrifuged for 5 min at 1300 rpm. The coverslips with adhered cells was then placed into a 24-w plate and stained as described above.
In alternative, the staining was performed in liquid and the cells were attached on the poly-lysine coverslips before the mounting steps. As another option, cells were stained in liquid and mounted using Low-Melting Temperature Agarose.

Table 3.25 IF antibodies

Antigen	Primary Antibody	Secondary Ab
CD19	1:100 anti-CD19(HD37) (Merck Millipore)	1:100 anti-mouse AlexaFluor488 (Invitrogen)
LAMP2 (lysosomes)	1:100 anti-LAMP2 (H4B4) (Invitrogen)	1:100 anti-mouse DyLight 594 (Invitrogen)
	1:100 anti-LAMP2 (H4B4) AlexaFluor 647 (Invitrogen)	/

3.2.10 Nanolive Cell 3D explorer

Nanolive Cell 3D Explorer is a time-lapse microscope which allows label-free *in vivo* imaging at organelles level. The patented technology (US 8,937,722 & EU WO 2011/121523) is based on the combination of *holography* and *rotational scanning*. *Holography* allows the observation cells in their native environment in a label-free, non-invasive, manipulation-free, and interference-free way, while *rotational scanning* allows 3D reconstructions, noise robustness, and high-resolution imaging.[468]

In the experiment, RAJI cells were observed in time-lapse for 20 min without stimuli. Then, anti-CD19(HD37) (Merck Millipore, 1:100) was added, and cells were observed for 90 min, in order to monitor a potential increase in endocytosis upon CD19 antigen binding.

4. Results

4.1 Part I: Production of recombinant antigens

CD19 and CD20 extracellular domains were cloned and expressed in recombinant form in different expression systems (HEK293T mammalian cells and *E. coli* cells, respectively). Here, the main results obtained for the expression and purification of these proteins will be illustrated.

4.1.1 Recombinant CD19 expression and purification

The plasmid carrying the CD19 DNA sequence was imported from OriGene (SC127938). Our group had previously cloned two CD19 extracellular domain constructs starting from this template (CD19EC; NCBI Database: NM_001770.5), and a third one was cloned in this work (Table 4.1). All the three constructs were cloned into the phFc expression vector (paragraph 3.2.1.5). All of them comprised exons from 1 to 4, corresponding to the extracellular domain of the protein. Two of them were engineered as a C-terminal fusion form with the human Fc fragment (hFc), in order to increase their stability and solubility. A Histidine Tag (6xHis residues) was added only in two out of the three constructs, in order to test different purification strategies (Table 4.1).

Table 4.1 CD19EC recombinant constructs

Construct	Name	hFc fusion	His Tag	Vector	Small-scale tests	Mid-Scale tests	Large-scale tests
1	CD19EC_His	×	✓	phFc	✓	×	/
2	CD19EC_hFc_His	✓	✓	phFc	✓	✓	/
3	CD19EC_hFc	✓	×	phFc	✓	✓	✓

In order to clone the CD19EC_hFc construct (3, Table 4.1), the insert was amplified through PCR using *Pfx* polymerase. The PCR product was purified through gel extraction and cloned into the phFc vector in *E. coli* MACH-I cells using the Golden Gate cloning procedure (paragraph 3.2.1.1). The three constructs were all tested for expression into HEK293T *via* transient transfection, as described in paragraph 3.2.2.2. The DNA was prepared for transfections following MINI or MIDI prep procedures according to the needed amount (paragraph 3.2.1.10). The three constructs were tested for expression in small scale experiments (paragraph 3.2.2.2) giving positive results. In mid-scale expression tests (paragraph 3.2.2.3), only constructs 2 and 3 were successfully produced (Fig 4.1, 4.2).

For CD19EC_hFc_His (construct 2, Fig. 4.2), the purification of HEK293T supernatant (120 ml) was performed *via* a single step affinity chromatography using a Nickel column (HisTrapFF, 1 ml, GE Healthcare) and a two-step elution (50% and 100%) with 500 mM Imidazole (ImOH) in PBS (Fig. 4.1, A). Positive fractions were pooled and stored as follows: in 500 mM ImOH 2 mM Sodium Azide at + 4°C; added with 20% glycerol and stored at -80 °C. Samplings were performed at days 3, 8 and 15 and analyzed through WB and verified the absence of protein degradation (Fig. 4.1, B). A sandwich ELISA confirmed the functional protein stability after 1 month of storage at -80 °C (Fig. 4.1, C).

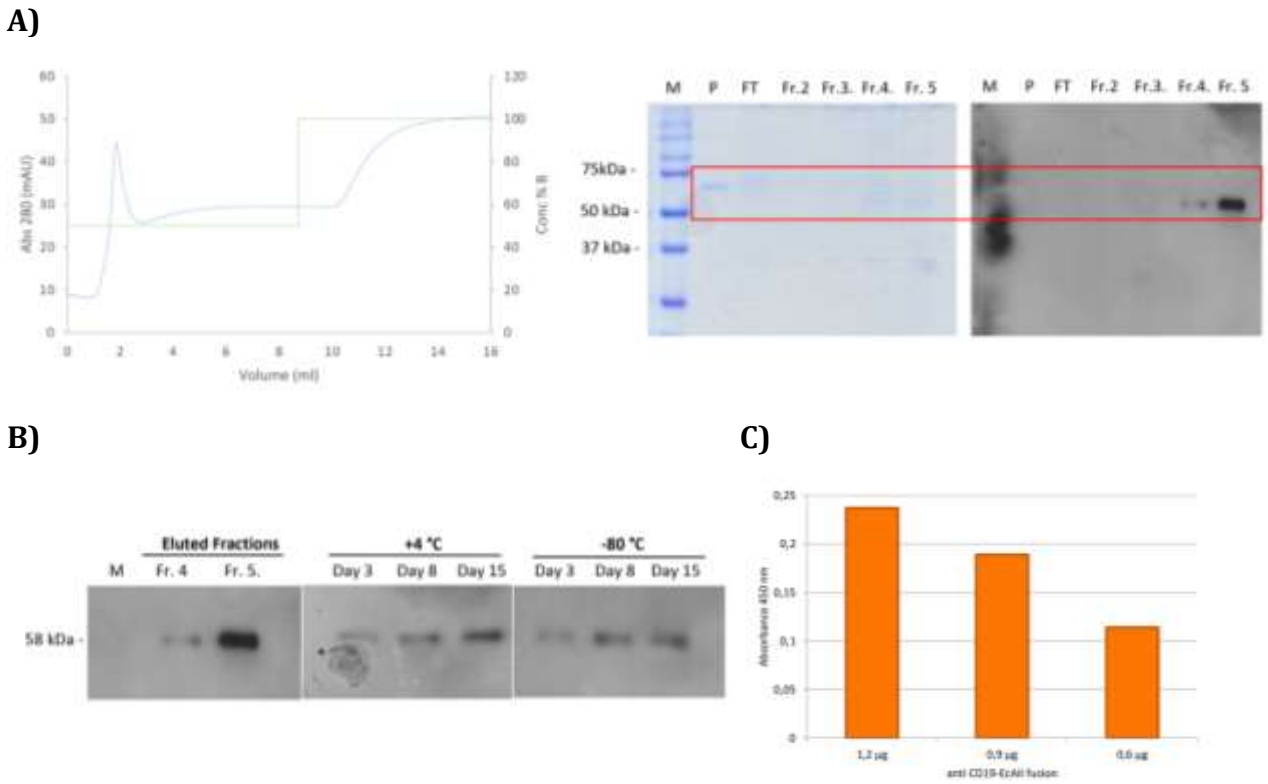

***Figure 4.1 CD19EC_hFc_His expression panel**. **A)** CD19_hFc_His mid-scale purification. HisTrapFF 1 ml column (GE Healthcare), 2 step elution in 500 mM ImOH PBS. Chromatogram, Coomassie and WB (anti-His antibody). **B)** CD19_hFc_His Stability Test. Pooled fractions were: stored in 500 mM ImoH 2 mM Sodium Azide at + 4°C; added with 20% glycerol and stored at -80 °C. Samples: day 3, 8, 15, WB (anti-His antibody). **C)** Sandwich ELISA. Coating: anti-CD19_EcAII; Binding: CD19_Fc_His (stored at – 80 °C for 1 month); detection: ant-hIgG-HRP.*

For CD19EC_hFc (construct 3, Fig. 4.2)), HEK293T supernatants from day 3, 6, 9 and 12 were analyzed *via* ELISA in order to confirm CD19_hFc expression and binding capability (Fig. 4.2, B). The purification was then performed through single step affinity chromatography using a protein A column (Mab select, 1 ml, GE Healthcare, Binding Buffer 0.1 M Sodium Phosphate pH 7.8) and an isocratic elution using 0.1 M Sodium Citrate pH 3. Eluted fractions were immediately neutralized by adding 0,1 M Tris-HCl pH 8. Fractions positive in WB analysis were pooled and concentrated 10x (yield: 100 µg/L) (Fig. 4.2, C). Pooled fractions were stored at +4° C in neutralized 0.1 M Sodium Citrate for 2 weeks. Samplings were performed at day 5, 10, 15 and analyzed through WB in order to verify the absence of protein degradation (Fig. 4.2, D).
CD19EC_hFc (construct 3) was selected as more promising, basing both on obtained yields (construct 2 was not quantifiable while construct 3 gave 100 µg/L) and subsequent purification strategy. In fact, CD19EC_hFc lacked the His Tag present instead on the recombinant TEV protein, which could be therefore used in order to remove the hFc fragment if needed, followed by a further IMAC purification step.
A further small-scale optimization experiment using 4 mM VPA (Valproic Acid), a small molecule which inhibits histone deacetylase activity, was performed, to test if such condition could favor a raise in yield. 4 mM VPA was added after three hours from the transfection procedure. The results confirmed DNA:PEI ratio 1:4 without VPA as the best expression condition (Fig. 4.2, E).
CD19EC_hFc large scale expression tests were then performed in roller bottles as described in paragraph 3.2.2.3. The purification of HEK293T supernatant (500 ml) was performed as described for the mid-scale transfection. Eluted fractions were immediately neutralized by adding 0,1 M Tris-HCl pH 8 (Fig. 4.2, F). Fractions positive in WB analysis were pooled, dialyzed into Tris-HCl pH 7.5 and then concentrated 20X, however obtaining a yield lower than in mid-scale expression tests (12 µg/L).

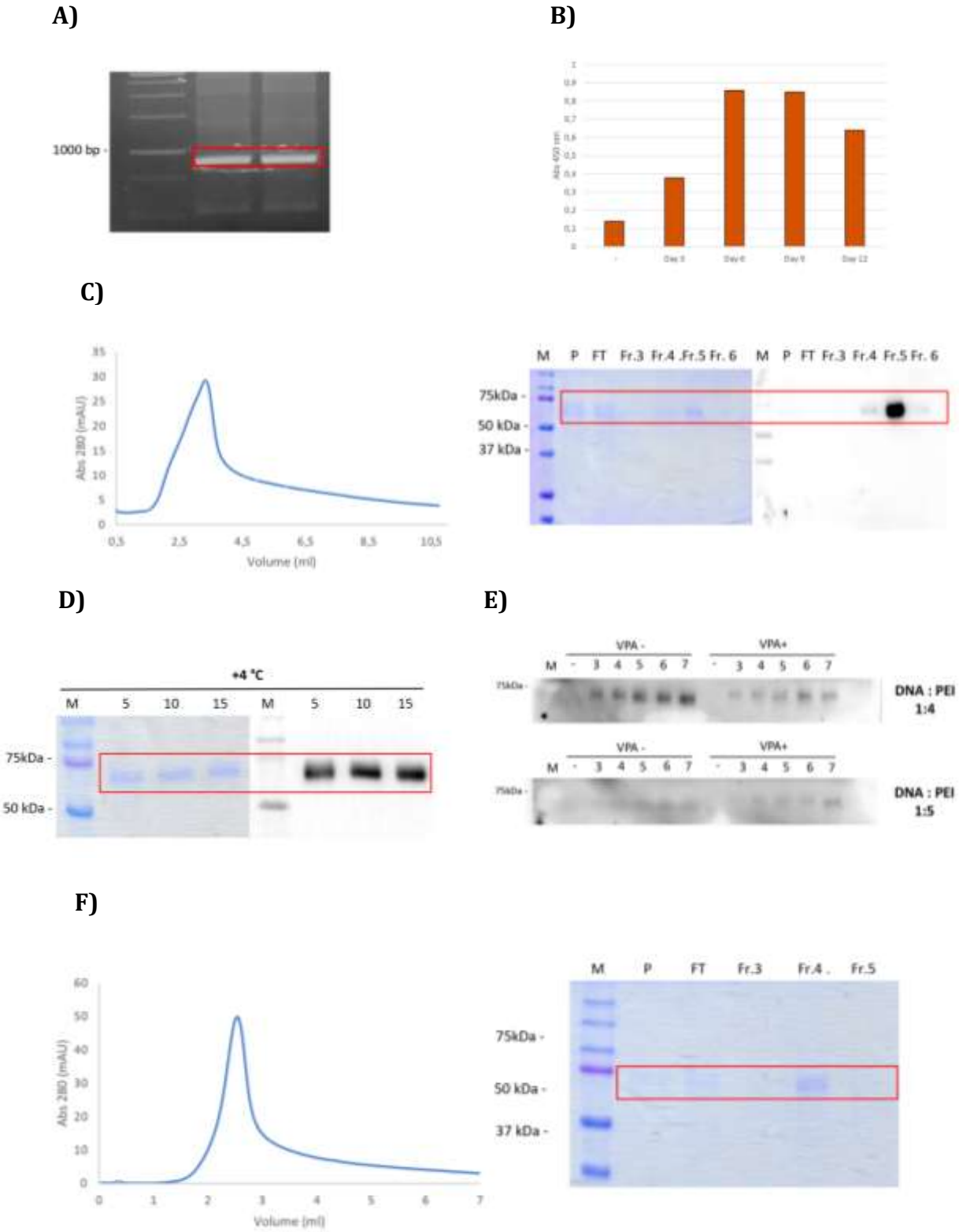

Figure 4.2 CD19EC_Fc cloning and expression panel. A) *CD19EC_hFc cloning. Insert amplification through PCR (expected length ~1000 bp).* ***B)*** *CD19EC_hFc mid-scale transfection ELISA (Time Course). Coating: Supernatant (Day 3, 6, 9, 12); detection: anti-hIgG-HRP.* ***C)*** *CD19EC_hFc large-scale purification. Chromatogram [mAb select 1 ml column (GE Healthcare), isocratic elution in 0,1 M Sodium Citrate pH 3], Coomassie and WB analysis (anti-hIgG antibody).* ***D)*** *CD19_hFc Stability Test. Pooled fractions from were stored at +4° C in neutralized 0.1 M Sodium Citrate. Samples: day 5, 10, 15. WB (anti-hIgG-HRP).* ***E)*** *CD19EC_hFc small-scale transient transfection optimization with Valproate (Time course). Samples: negative control (-), supernatants at different days of transfection.* ***F)*** *CD19_hFc_His large-scale purification (roller*

bottles). Chromatogram [mAb select 1 ml column (GE Healthcare), isocratic elution in 0,1 M Sodium Citrate pH 3], Coomassie and WB analysis (anti-hIgG antibody

Triple flasks, that provide 500 cm^2/flask, were used, as described in paragraph 3.2.2.3, as an alternative strategy for large scale expression. A total volume of 0,5 L of EXCELL medium was harvested after 10 days of transfection and purified using a protein A column (Mab select, 1 ml, GE Healthcare, Binding Buffer 0.1 M Sodium Phosphate pH 7.8) and an isocratic elution using 0.1 M Sodium Citrate pH 3 (Fig 4.3, A). A clear peak of ~ 250 mAU was obtained. Eluted fractions were immediately neutralized by adding 0,1 M Tris-HCl pH 8 and analyzed through SDS-PAGE followed by Coomassie staining (Fig. 4.3, C). The positive fraction (Fraction 3, IMAC) was purified using Gel filtration (Superose HR 12 10/30) in PBS pH 7.4, obtaining a double peak (Fig. 4.3, B). Fractions corresponding to the peak were analyzed through SDS-PAGE followed by Coomassie staining and WB (Fig. 4.3, C SEC and D). The protein resulted to be present in Fr. 3, 4, 5 and 6 after Gel Filtration. They were pooled and concentrated 4 times before protein quantification, which demonstrated again a very low concentration (20 µg/L).
A high stability of the protein was observed in the cell supernatant and was therefore maintained also in this form at + 4 °C for experiment where the purified protein was not needed.

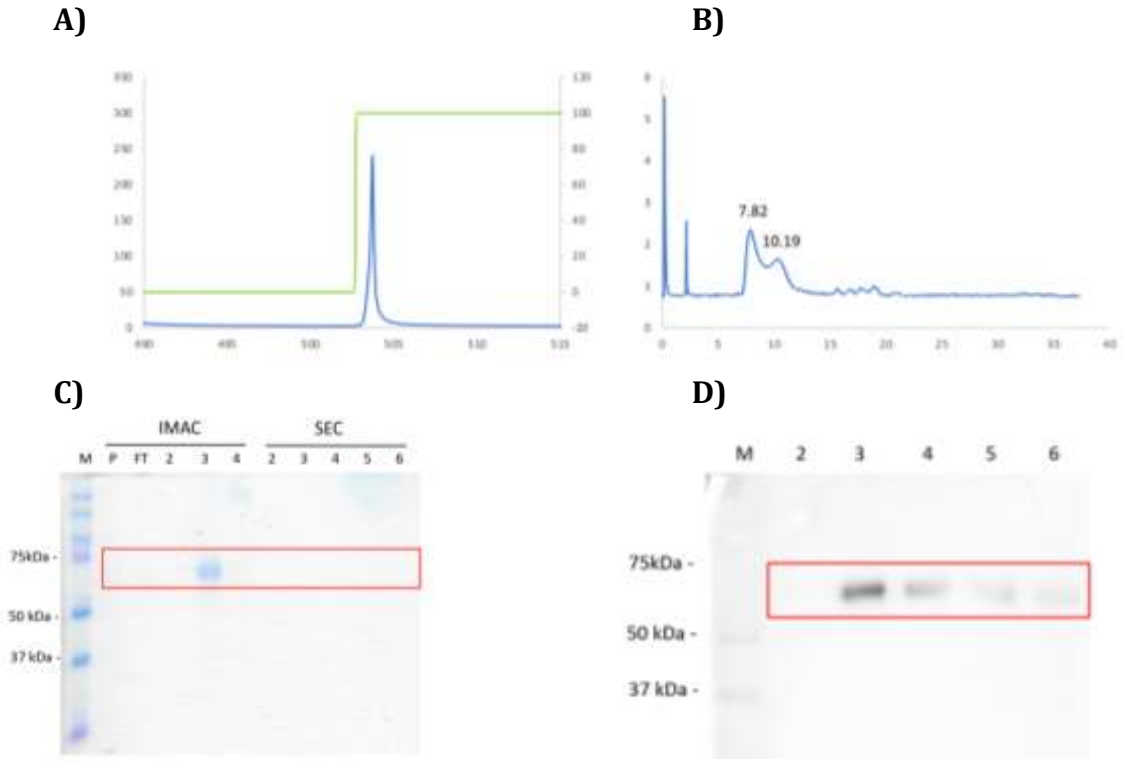

Figure 4.3 CD19EC_Fc triple flask large scale expression. A) *CD19EC_hFc large-scale (triple flask) IMAC purification. mAb select 1 ml column (GE Healthcare), isocratic elution in 0,1 M Sodium Citrate pH 3.* ***B)*** *CD19EC_hFc large-scale (triple flask) SEC purification, Superose HR 12 10/30, PBS pH 7.4.* ***C)*** *Coomassie Gel Staining, 12% Polyacrylamide. Samples loading: P = pre-loading; FT = Flow Through; IMAC Fr. 2, 3, 4; SEC Fr. 2, 3, 4, 5, 6.* ***D)*** *WB (anti-hIgG-HRP) Samples loading: P = pre-loading; FT = Flow Through; SEC Fr. 2, 3, 4, 5, 6.*

The most promising results were therefore obtained using the third construct (CD19EC_hFc) transfected in HEK293T cells in mid-scale expression experiments, with a robust protein stability showed when stored at +4 °C in the culture medium (EXCELL).

4.1.2 Recombinant CD20 expression and purification

Human CD20 transcript variant 3 (NCBI database: NM_021950.3) was imported from Origene (RC201242). Two CD20 constructs were designed and cloned, containing the extracellular loop corresponding to the Rituximab epitope binding site (UNIPROT: P11836-1) (Table 4.2). Both constructs were cloned into the pET45b(+) expression vector (paragraph 3.2.1.5) using InFusion cloning (TAKARA) as described in paragraph 3.2.1.2, and transformed into *E. coli* expression strains BL21(DE3) and Origami (DE3)- tig factor.

Small scale induction tests (25 ml) were performed for both constructs as described in paragraph 3.2.2.2. Induction in *E. coli* BL21(DE3) was achieved by adding 1 mM IPTG for 24 hrs at 25 °C, 250 rpm. Samplings of 1 ml *from induced* (+) and *non-induced* (-) cultures were performed at 0, 3, 24 h after the induction. Induction in *E. coli* Origami(DE3)-tig factor was achieved by adding 1 mM IPTG for 24 hrs at 10 °C, 250 rpm. Samplings of 1 ml *from induced* (+) and *non induced* (-) cultures were performed at 0 and 24 h after the induction start. Soluble and insoluble fractions were separated using BugBuster™ as described in paragraph 3.2.2.2 and samples were analyzed through Tricine SDS PAGE. Results are illustrated in Fig. 4.4, and show how the production of a peptide of MW compatible with the expected one was seen in Panel A and Panel C.

Table 4.2 CD20 recombinant constructs

Constructs	Borders	Expression Vector	Host	bp	aa	Expected MW (kDa)
1	141-188	pET45b(+)	*E. coli* BL21(DE3); Origami (DE3)- tig factor	162	54	6.4
2	141-184	pET45b(+)	*E. coli* BL21(DE3); Origami (DE3)- tig factor	150	50	6

A)

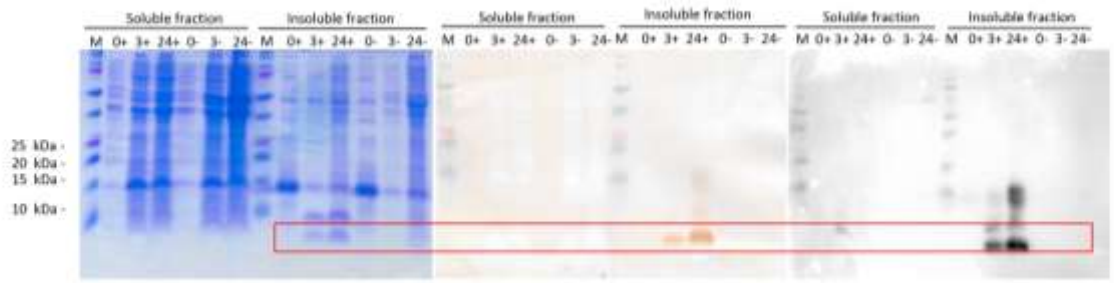

B)

C)

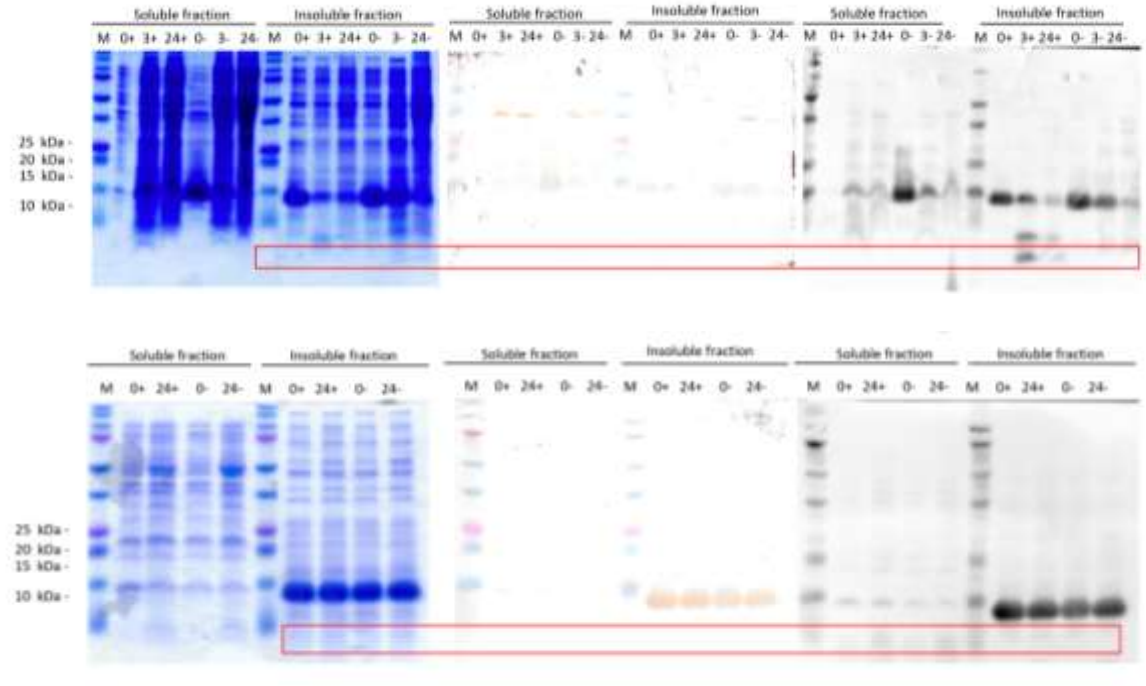

D)

***Figure 4.4 CD20 cloning and small-scale expression panel**. **A)** CD20_141_188 Small-scale expression in E. coli BL21(DE3). Coomassie, DAB, WB (anti-His antibody). Induction: 1 mM IPTG, 25 °C. Samples: + = induced, - not induced, number = hours from induction.. **B)** CD20_141_188 Small-scale expression in E. coli Origami(DE3)-tig factor. Coomassie, DAB, WB (anti-His antibody). Induction: 1 mM IPTG, 10 °C Samples: + = induced, - not induced, number = hours from induction. **C)** CD20_141_184 Small-scale expression in E. coli BL21(DE3). Coomassie, DAB, WB (anti-His antibody). Induction: 1 mM IPTG, 25 °C. Samples: + = induced, - not induced, number = hours from induction. **D)** CD20_141_184 Small-scale expression in E. coli Origami(DE3)-tig factor. Coomassie, DAB, WB (anti-His antibody). Induction: 1 mM IPTG, 10 °C Samples: + = induced, - non-induced, number = hours from induction.*

According to these results, large scale expression tests were performed using classical Inclusion Bodies (cIBs) and non classical inclusion bodies procedure (ncIBs), as described in paragraph 3.2.2.3, for both constructs into BL21(DE3). The best results were obtained with cIBS for CD20_141_188. Results are shown in Fig. 4.5. In the scale up, the renatured fraction was visible on gel, although not detectable with BCA assay.

A) **B)**

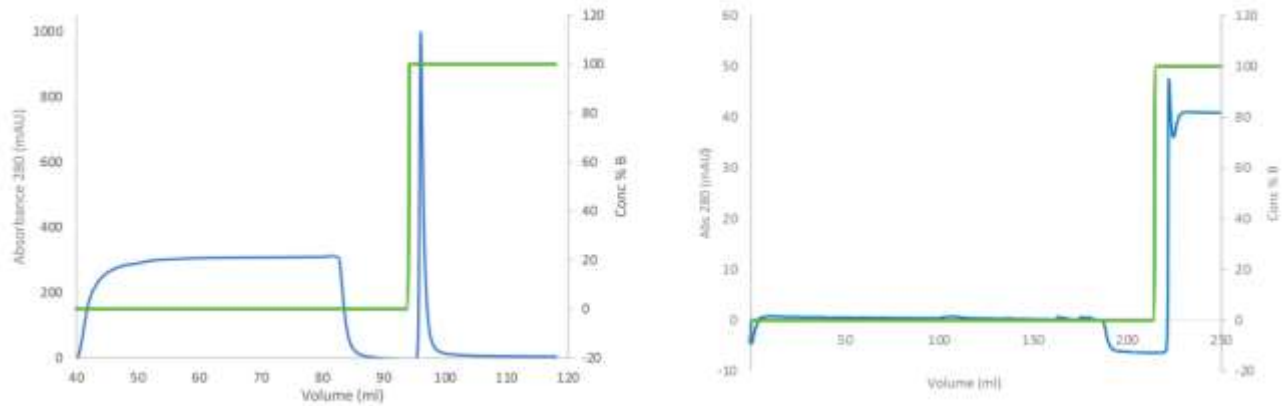

C)

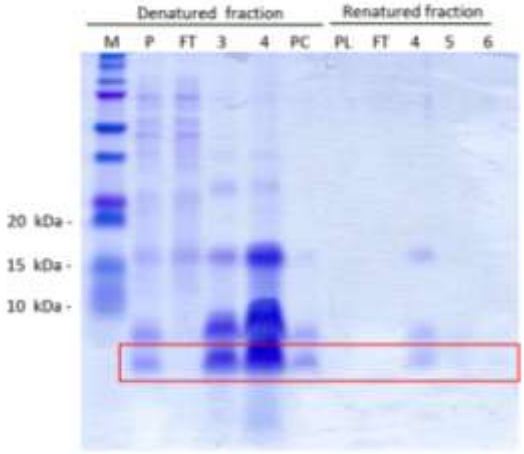

Figure 4.5 CD20 cloning and large-scale expression panel*. CD20_141_188 Classical Inclusion Bodies (1 L).* ***A)*** *Denatured fraction Affinity Chromatography (HisTrapFF 5 ml, GE Healthcare), Elution Buffer (100%) 100 mM Sodium Phosphate, 10 mM Tris-HCl, 8 M Urea, 300 mM ImOH pH 8.* ***B)*** *Refolded fraction profile in Affinity Chromatography (HisTrapFF 5 ml, GE Healthcare), Elution Buffer (100%) 50 mM Tris-HCl, 5 % v/v glycerol,500 mM ImOH.* ***C)*** *Coomassie Staining. M = marker, P = pre loading, FT = Flow Through, number = fractions, PC = post centrifugation.*

The most promising results for protein production were therefore obtained with the first construct (CD20_141_188) in *E. coli* BL21(DE3) cells using the classical inclusion bodies procedure.

4.2 Part II: Nanobody selection

4.2.1 Phage Display

For the selection of targeting nanobodies, it was decided to use the Phage Display technique, field in which our group had no previous experience.
As previously explained in detail, Phage Display is an *in vitro* selection process completely independent from any immune system, which allows the selection of different antibody formats. A human single domain antibodies (sdAbs) library ($3*10^9$ clones) for phage display (paragraph 3.2.6.1) was imported in our lab from SourceBioscience.[469] In order to set up the technique and to acquire some expertise, while working on the expression of CD19, several rounds of selection were performed against EcAII enzyme itself, given its high immunogenicity and stability. Recombinant EcAII antigen was produced in house according to established protocols.

4.2.1.1 Helper phage stock

KM13 were prepared twice as described in paragraph 3.2.6.2, obtaining 10^4 PFU/ml the first time and $2x10^{15}$ PFU/ml the second time. Aliquots of $1x10^{13}$ ph/ml were prepared and stored at -80 °C.

4.2.1.2 Library replication

The human sdAbs library was expanded as described in paragraph 3.2.6.2, obtaining 90 aliquots which were stored at – 80 °C.

4.2.1.3 Mock experiment (anti-ubiquitin scFv)

As a mock experiment, a selection round was performed using *E. coli* TG1 cells expressing an anti-ubiquitin scFv for the packaging step and ubiquitin as an antigen. These cells were provided as positive control to be used during the selection procedure.
The selection was performed using plastic absorption as antigen immobilization technique and PBS pH 7.4 as binding buffer, following the company protocol.

Among those obtained, 16 single colonies (s.c.) were analyzed through soluble ELISA in 96 well plate (96 w) as described in paragraph 3.2.6.2, resulting positive for ubiquitin antigen binding (Fig. 4.6A). Eight of these 16 s.c. clones were analyzed in WB, resulting all positive for protein production (Fig. 4.6B, four clones as an example).
Eight clones were induced for antibody expression into a larger volume (10 ml in tube vs 200 µl in 96 w plate) and analyzed through soluble ELISA (4.6C) and WB (4.6D, one clone as an example). Supernatants from all the clones resulted positive for antigen binding in ELISA and for positive for anti-ubiquitin single domain antibody expression in WB analysis (expected MW ~ 15 kDa) (Fig. 4.6).

A) Soluble ELISA – 96 w

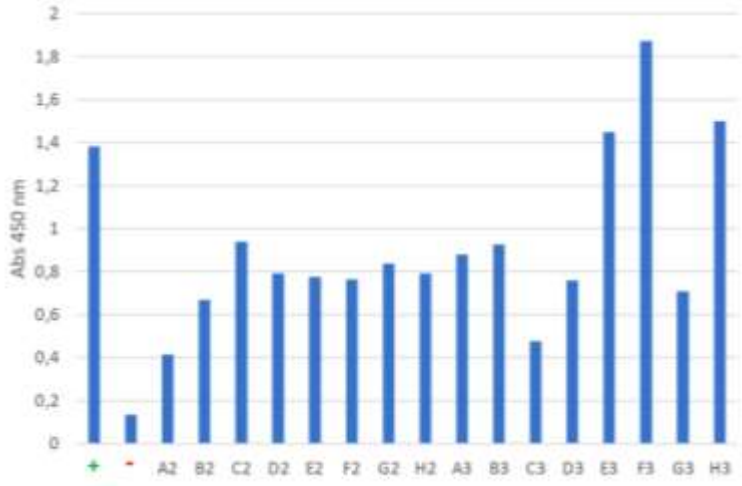

B) WB 96 w

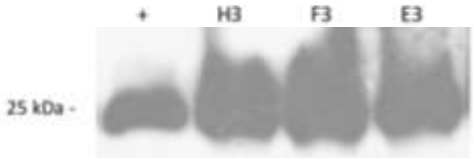

C) Soluble ELISA – 10 ml

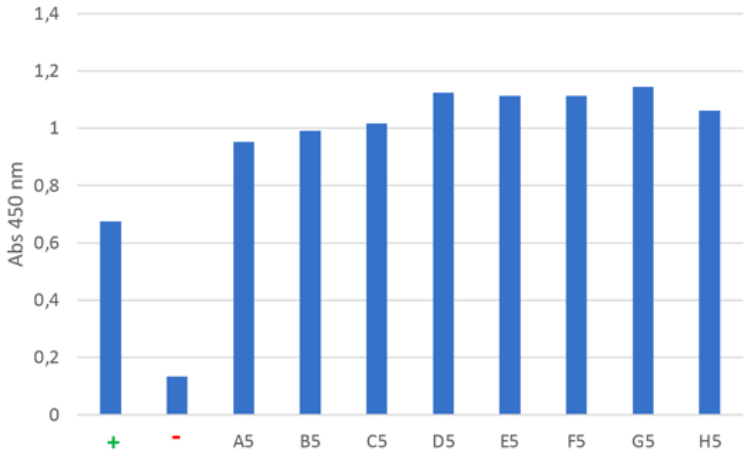

D) WB – 10 ml

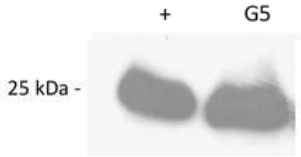

Fig. 4.6 Mock experiment (anti-ubiquitin scFv). A) *16 s.c. soluble ELISA analysis (96 w induction)* ***B)*** *Clones H3, F3, E3, F7, WB supernatants analysis (96 w induction)* ***C)*** *8 s.c. soluble ELISA analysis (10 ml induction).* ***D)*** *G5 WB supernatants analysis (10 ml induction).*

4.2.1.4 Bio panning I

A first bio panning against EcAII asparaginase, consisting in three rounds of selection, was performed as described in paragraph 3.2.6.2. The enrichment factor, which was expected to increase from 10^5-10^7 during the first two rounds up to 10^7– 10^9 during the third one, was instead stable at 10^8.

86 single colonies (s.c.) were analyzed through soluble ELISA (paragraph 3.2.6.2), all resulting negative for antigen binding. 10% of the clones were analyzed in WB in order to investigate protein expression, but they resulted all negative for protein production.
6% of the clones were induced for antibody expression into a larger volume (10 ml in tube vs 200 µl in 96 w plate) and analyzed through soluble ELISA and WB. Supernatants from all the clones resulted negative in ELISA, while 1 clone out 5 (20%) was positive for protein expression (expected MW ~ 15 kDa) (**Table 4.3**).
A PCR was performed on plasmids extracted from producer and non-producer clones, in order to check the gene presence. The gene was amplified both in producer and non-producer clones, confirming a protein expression issue (Fig. 4.7).

Table 4.3 Bio panning I

Set up		**Enrichment factor**		**Analysis of selected clones**					
		Round	**CFU/ml**	**Induction**	**ELISA**		**WB**		**Producers**
					n°	*result*	*n°*	*result*	
Antigen immobilization	Plastic Absorption	**1**	$2•10^8$						
Binding Buffer	PBS pH 7.4	**2**	$9•10^8$	**96 w**	86	×	8	×	0
Rounds	3	**3**	$9•10^8$	**10 ml**	5	×	5	✓	1

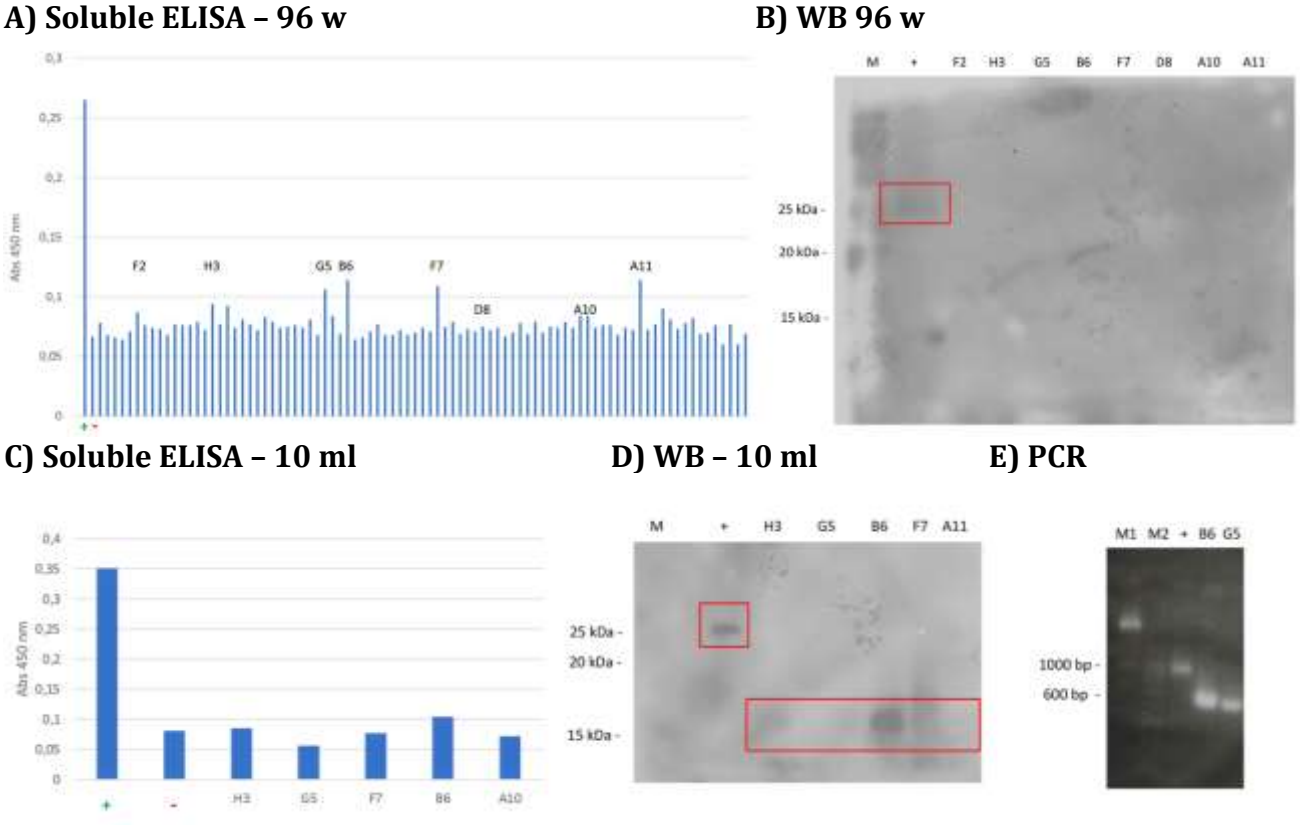

***Fig. 4.7 Bio panning I panel**. **A)** 86 s.c. soluble ELISA analysis (96 w induction) **B)** Clones F2, H3, G5, B6, F7, D8, A10, A11 WB supernatants analysis (96 w induction) **C)** H3, G5, F7, B6, A10 clones soluble ELISA analysis (10 ml induction). **D)** H3, G5, F7, B6, A10 clones WB supernatants analysis (10 ml induction). **E)** PCR amplification in order to check gene presence in a producer (B6) and a non-producer clone (G5).*

4.2.1.5 Bio panning II

A second bio panning against EcAII was performed, increasing the rounds of selection up to 5, as advised in the protocol troubleshooting, in case of binders' absence after the first selection. The

binding buffer used during the selection process was also changed from PBS pH 7.4 to TBS pH 8, as suggested in the work of Jafari et al.[470]

The enrichment factor, which was expected to increase from 10^5-10^7 during the first two rounds of selection up to 10^7– 10^9 during the third, fourth and fifth one, increased to 10^7 up to the third round, but decreased down to 10^5 during the fourth and fifth rounds (**Table 4.4**).

36 s.c. were analyzed through soluble ELISA (paragraph 3.2.6.2), all resulting negative for antigen binding (Fig. 4.8A). 15% of the clones were analyzed in WB in order to investigate protein expression, resulting all positive for protein production (Fig. 4.8B) (positive control expected MW, scFv: ~ 25 kDa; selected clones expected MW, sdAb: ~ 15 kDa).

Those clones were then induced for antibody expression into a larger volume (10 ml in tube vs 200 µl in 96 w plate) and analyzed through soluble ELISA and WB. Supernatants from all the clones resulted negative in ELISA, (Fig. 4.8C) while all clones confirmed to be positive for protein expression, even though protein bands were faint when produced in 10 ml of culture (Fig. 4.8D).

Table 4.4 Bio panning II

Set up		**Enrichment factor**		**Analysis of selected clones**					
		Round	**CFU/ml**	**Induction**	**ELISA**		**WB**		**Producers**
					n°	*result*	*n°*	*result*	
Antigen immobilization	Plastic Absorption	**1**	$4x10^4$						
		2	$1x10^7$						
		3	$3x10^7$						
Binding Buffer	TBS pH 8	**4**	$3x10^5$	**96 w**	36	×	6	✓	6
Rounds	5	**5**	$3x10^5$	**10 ml**	6	×	6	✓	6

A) Soluble ELISA – 96 w

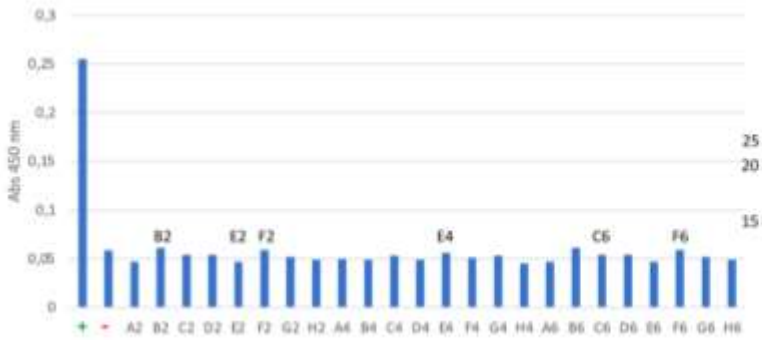

B) WB - 96 w

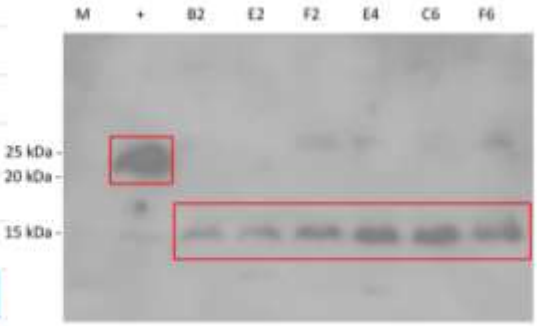

C) Soluble ELISA – 10 ml

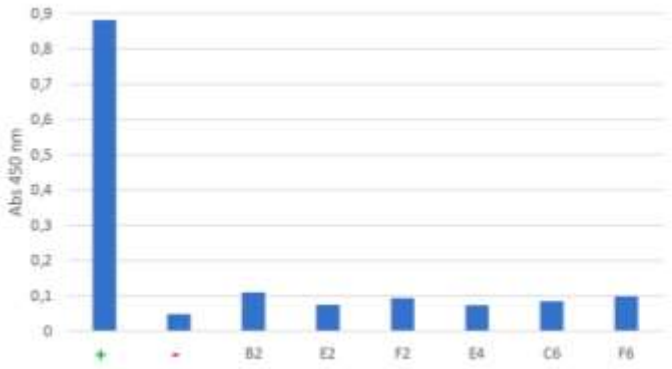

D) WB – 10 ml

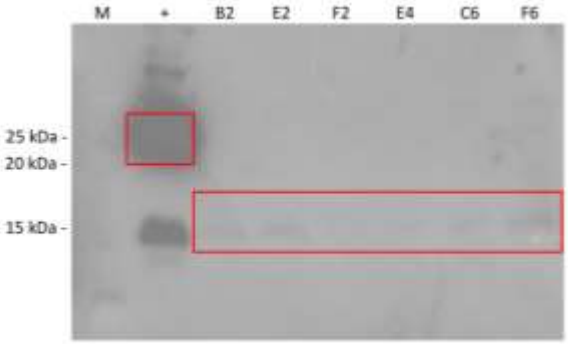

Fig. 4.8 Bio panning II panel A) *36 s.c. soluble ELISA analysis (96 w induction).* ***B)*** *Clones B2, E2, F2, E4, C6, F6 WB supernatants analysis (96 w induction)* ***C)*** *B2, E2, F2, E4, C6, F6 clones soluble ELISA analysis (10 ml induction).* ***D)*** *B2, E2, F2, E4, C6, F6 clones WB supernatants analysis (10 ml induction).*

4.2.1.6 Bio panning III

A third bio panning was performed, changing the antigen (EcAII) immobilization strategy. Instead of using direct coating immunoadsorption on plastic, a capture system based on magnetic beads was used, exploiting antigen biotinylation and streptavidin-magnetic beads, in order to increase the stringency of the selection, as suggested in Niccheri et al. [454]

The enrichment factor increased from 10^5 during the first round, to 10^7 during the second, to 10^9 during the third, as expected. (**Table 4.5**).

92 s.c. were analyzed through soluble ELISA (X), all resulting negative for antigen binding and for protein expression in WB analysis (Fig. 4.9 A, B). A Phage ELISA, in which the selected phages displaying the antibodies are tested in ELISA, was then performed, as described in paragraph 3.2.6.2, following the troubleshooting suggestions. In Phage ELISA, the 8 clones (9%) resulted positive for antigen binding in Phage ELISA (Fig 4.9 C). These clones were analyzed through Phage ELISA, soluble ELISA and WB into a larger expression volume (10 ml in tube vs 200 µl in 96 w plate) (Fig. 4.9 D, E, F, respectively). The clones confirmed to be positive in Phage ELISA, but resulted to be negative in soluble ELISA for antigen binding and in WB for protein production (Positive control expected MW, scFv: ~ 25 kDa; selected clones expected MW, sdAb: ~ 15 kDa).

Soluble ELISA, in which the nanobodies alone are expressed, and WB analysis were performed again on induced supernatants and cell lysates (Fig 4.9 G, H). They both resulted negative for antigen binding. WB analysis highlighted the presence of bands in the cell lysate of clones D3, C10 and C12 at ~65 kDa. This MW did not match the expected one (sdAb: ~ 15 kDa), but it was reasonable for a sdAb-pIII fusion protein. Since *E. coli* TG1 cells are an amber suppressor strain, sdAb-pIII fusion proteins could, in principle, be expressed, given the presence of an amber suppressor codon (TGA) between the sdAb and the pIII protein. *E. coli* HB2151 cells, a non-amber suppressor strain, were then transformed with extracted phagemids from clones D3, H4, C10, C12, in order to favor the expression of the soluble sdAb alone. Soluble ELISA and WB analysis were performed on supernatants and lysates (Fig 4.9, I, L). They both resulted negative for antigen binding and protein expression, with the exception of a band visible at the expected MW (~15 kDa) in the cell lysate of clone C12.

D3, H4, C10, C12 plasmidic DNA was sent for sequencing. Despite several efforts, the DNA sequence of the C12 clone was impossible to obtain. Several amber stop codons were present in the DNA sequence of the other three selected clones, explaining the negative results obtained in *E. coli* HB2151 cells (Fig. 4.9, M)

Table 4.5 Bio panning III

Set up		**Enrichment factor**		**Analysis of selected clones**						
		Round	**CFU/ml**	**Induction**	**Phage ELISA**		**Soluble ELISA**		**WB**	
Antigen immobilization	Antigen biotinylation	**1**	$4•10^5$		*n°*	*result*	*n°*	*result*	*n°*	*result*
Selection	Streptavidin-magnetic beads columns	**2**	$4•10^7$	**96 w**	192	✓	92	×	18	×
Rounds	3	**3**	$4•10^9$	**10 ml**	8	✓				
					Supernatants		4	×	4	✓
					Lysates		4	×	4	✓

A) Soluble ELISA – 96 w

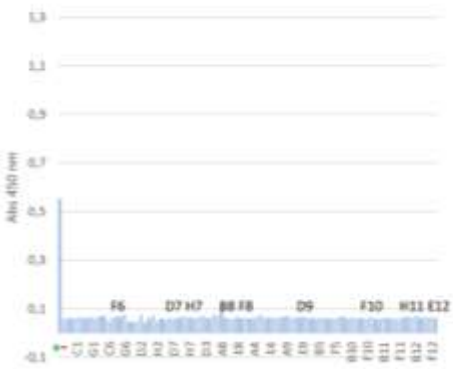

B) WB - 96 w

C) Phage ELISA – 96 w

D) Phage ELISA – 10 ml

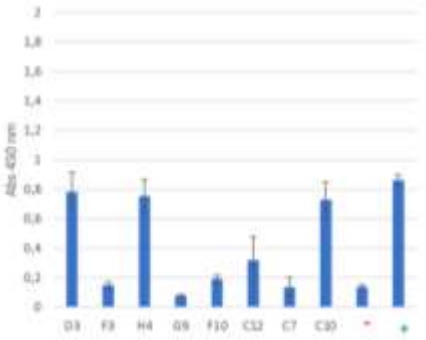

E) Soluble ELISA – 10 ml

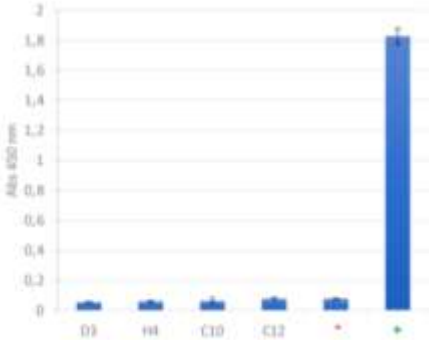

F) WB – 10 ml

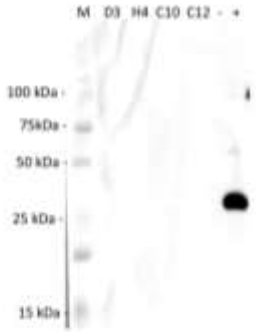

G) *E. coli* TG1 Soluble ELISA – 10 ml

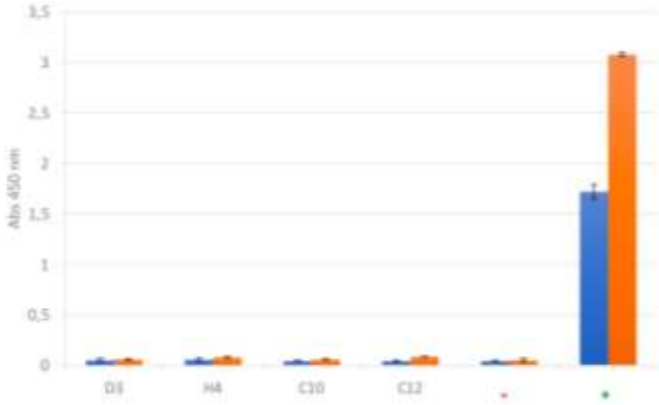

H) *E. coli* TG1 WB – 10 ml

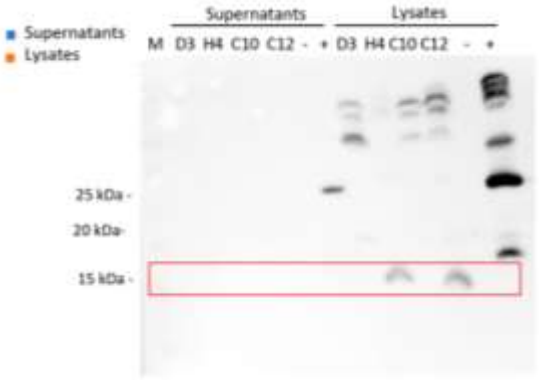

I) *E. coli* HB2151 Soluble ELISA – 10 ml

L) *E. coli* HB2151 WB – 10 ml

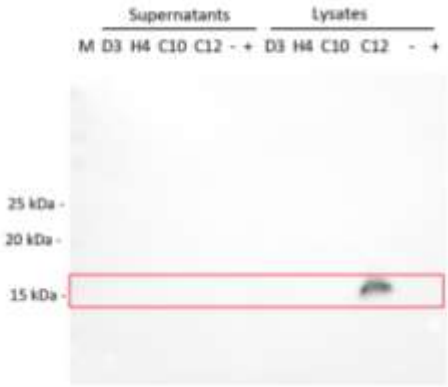

M) Protein sequence alignment

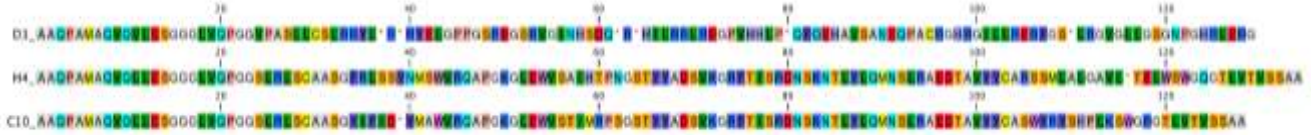

Fig. 4.9 Bio panning III panel. A) *92 s.c. soluble ELISA analysis (96 w induction).* ***B)*** *WB supernatants analysis (96 w induction).* ***C)*** *92 s.c. phage ELISA analysis (96 w induction).* ***D)*** *Phage ELISA analysis (10 ml induction).* ***E)*** *Soluble ELISA analysis (10 ml induction).* ***F)*** *D3, H4, C10, C12 supernatants: WB analysis (10 ml induction).* ***G)*** *D3, H4, C10, C12 supernatants vs lysates: soluble ELISA analysis (E. coli TG1, 10 ml induction).* ***H)*** *D3, H4, C10, C12 supernatants vs lysates: WB analysis (E. coli TG1, 10 ml induction).* ***I)*** *D3, H4, C10, C12 supernatants vs lysates: soluble ELISA analysis (E. coli HB2151, 10 ml induction).* ***L)*** *D3, H4, C10, C12 supernatants vs lysates: WB analysis (E. coli HB2151, 10 ml induction).* ***M)*** *D3, H4, C10 clones protein sequences alignment.*

During the Phage Display set up, the best results were therefore obtained using antigen-biotinylation and streptavidin-magnetic beads as antigen immobilization strategy during the selection procedure. In this way, selective binders were obtained in Phage ELISA. However, such binders were not possible to characterize due to protein expression and solubility issues.

4.2.2 Yeast Two Hybrid (IACT)

Given the difficulties in the production of a suitable amount of purified recombinant CD19 and in the setting up of the Phage Display method, a different strategy for the selection of anti-CD19 nanobodies was adopted. In particular, the Yeast Two Hybrid technique does not require to produce the purified target antigen in order to perform the selection. It is, in fact, sufficient to clone it and express it in yeasts cells as a fusion protein with the lexA binding domain. For the screening, the target antigen is expressed as a fusion protein with the lexA binding domain and is referred to as "bait", while the antibodies of the library are cloned as fusion proteins with the VP16 transcriptional activation domain, and are referred to as "preys". If the antibody-target (prey-bait) interaction occurs, the transcription of two reporter genes, *his3* and *lacZ*, is activated, allowing the yeast to grow on plates lacking Histidine (–H medium) and to develop a blue color in the presence of the X-gal synthetic substrate.

In order to perform the selection, a collaboration with Prof. Cattaneo (SNS, Pisa) was established. His research group has great expertise in IACT technology and had nanobodies libraries available for screening.
A lexA-CD19 construct (bait) was first of all cloned into the pMIC-BD1 vector (kindly provided by Prof. Cattaneo's group), using the InFusion cloning technique as described in paragraph 3.2.1.2. The construct was shipped to Pisa, where it was transformed (Fig. 4.10, A, B) into L40 *S. cerevisiae* cells as described in paragraph 3.2.7.1. L40 cells containing the CD19 bait were analyzed for lexA-CD19 expression through WB analysis (Fig. 4.10, C, D) and evaluated for the level of transactivation by growing them on plates lacking Tryptophan, Histidine and Leucine amino acids (-WHL plates, selective for interactors) (Fig. 4.10, E)
The protein (expected MW ~ 52 kDa) was successfully expressed and no transactivation was observed, showing that the bait could be suitable for the screening system.

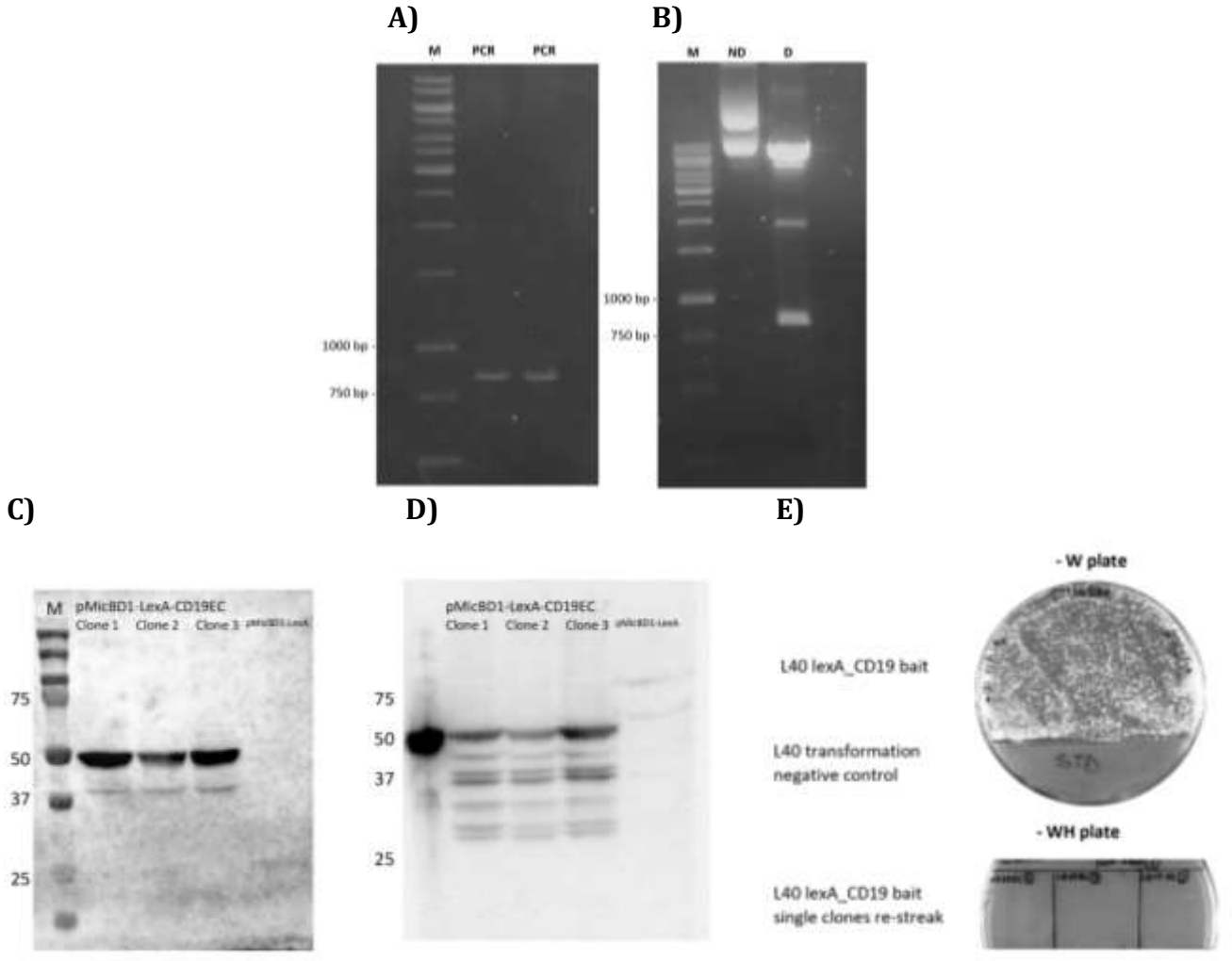

***Fig. 4.10 lexA_CD19 cloning**. **A)** PCR, insert amplification (expected length 774 bp). **B)** Control digestion. Double digestion of pMIC-BD1_lexA_CD19 construct with EcoRI and BamHI (insert expected length 774 bp). **C)** anti-lexA WB on L40 CD19 bait cell lysate. **D)** anti-HA tag WB on L40 CD19 bait cell lysate. **E)** L40 S. cerevisiae transformed with pMIC-BD1_lexA_CD19 construct plated onto -W plate (selective for transformants), 3 clones re-streaked onto -WHL plate (selective for interactors). Panel **C)**, **D)** and **E)** are a courtesy of Prof. Cattaneo.*

I spent some months in Pisa, in Prof. Cattaneo's research group as a visiting student, in order to perform the screening procedure of a VHH naïve library (10^6, lama) in L40 *S. cerevisiae* transformed with the CD19EC bait, as described in paragraph 3.2.7.1. The screening was performed using -WHL plates (lacking W, H and L amino acids - selective for positive interactors) added with 1 mM 3AT, an inhibitor of the transactivation of the *his3* gene, as selective plates. Doubling clones were allowed to grow o.n. before solid selection, as described in paragraph 3.2.7.1 (n° of duplications: 4). The results are summarized in Table 4.6. 72 candidates were isolated after the primary screening and were re-streaked on both –WHL + 1 mM 3AT plates and –WL plates (selective for positive transformants) (Fig. 4.11 A). A liquid ß-gal assay was performed as described in paragraph 3.2.7.1, in order to identify positive interactors through blue color development (Fig. 4.11B). A colony PCR followed by a DNA fingerprint was performed in order to assess how many patterns and therefore single clones were isolated (Fig. 4.11, C, D). Two general patterns were visible in the post doubling clones positive in ß-gal assay (Fig. 4.11, D. No arrows: pattern 1; arrows: pattern 2). 5 clones were sent for sequencing, resulting identical to one another. The two observed patterns were probably due to polyclonality of the isolated clones. The single

candidate obtained (VHH21A) was tested in secondary screening in order to confirm its positivity, as described in paragraph 3.2.7.1 (Fig. 4.11, E).

Table 4.6 Screening I

	Primary Screening							Secondary Screening
	Transformation efficiency	**Picked clones** (-WHL + 1 mM 3AT plates)	**Regrown clones** (-WHL plates)	**ß-gal assay** (liquid)	**Colony PCR**	**Finger-print** (*Nal* IV *Alu* I)	**DNA seq**	**n° of positive clones**
Pre-doubling	$1.87 \bullet 10^8$	6	5	/	/	/	/	/
Post-doubling	$3.2 \bullet 10^9$	66	66	66	66	2 patterns	5	1

Set up	
Positive control *(interaction)*	anti -lexA VHH
Negative control *(interaction)*	anti-pTAU VHH
Negative control *(transformation)*	Salmon testis DNA (STD)

Set up	
Bait of interest	CD19
Unrelated bait	Synuclein

A)

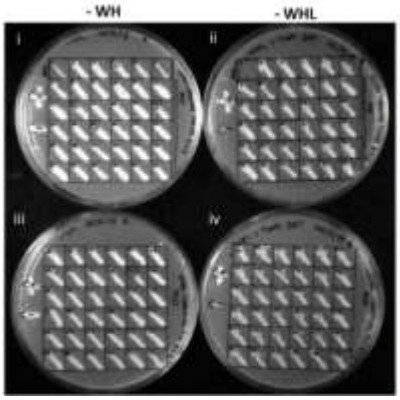

B)

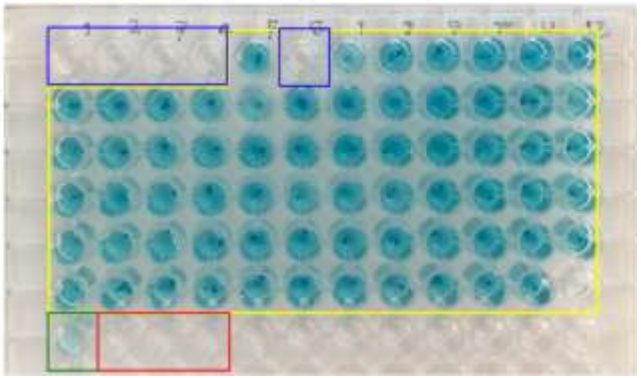

C)

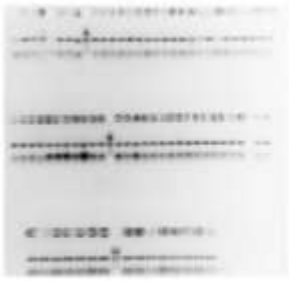

D)

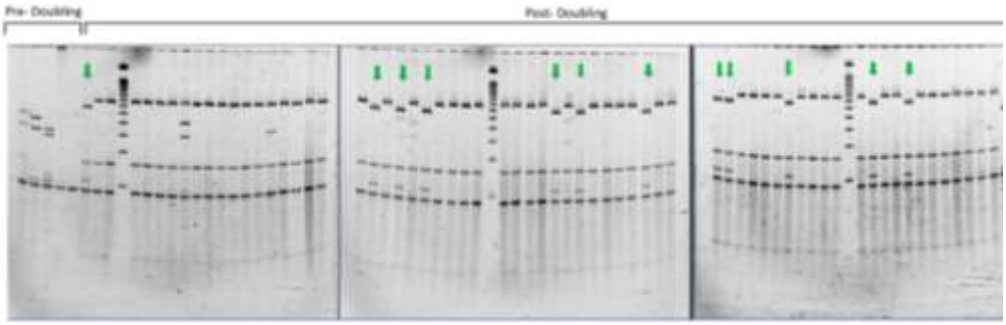

E)

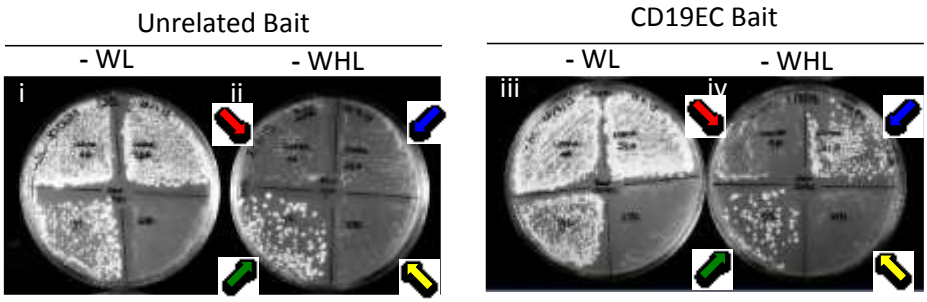

Fig. 4.11 Screening I. A) *Selected clones re-streaked onto -WL (selective for transformants) and -WHL (selective for interactors) plates.* ***B)*** *ß-gal assay (liquid). Blue: pre-doubling clones; yellow: post-doubling clones; green: positive control; red: negative control.* ***C)*** *Colony PCR.* ***D)*** *DNA fingerprint. No arrows: pattern 1; green arrows: pattern 2.* ***E)*** *Secondary screening. L40 unrelated bait transformed with VHH21A plated on -WL (selective for transformants) (i) and -WHL (selective for interactors) (ii) plates. L40 CD19 bait transformed with VHH21A plated on -WL (selective for transformants) (iii) and -WHL (selective for interactors) (iv) plates. Arrows: red: interaction negative control; green: interaction positive control; yellow: transformation negative control; blue: candidate (VHH21A)*

A second screening was performed using -WHL plates (lacking W, H and L amino acids - selective for positive interactors) without 3AT and without doubling clones. The results are summarized in Table 4.7. 394 candidates were isolated after the primary screening and were re-streaked on both –WHL + 1 mM 3AT plates and –WL plates (selective for positive transformants) (Fig. 4.12 A). A solid ß-gal assay was performed as described in paragraph 3.2.7.1, in order to identify positive interactors through blue color development (Fig. 4.12 B). A colony PCR followed by a DNA fingerprint was performed in order to assess how many patterns and therefore clones were isolated (Fig. 4.12, C, D). Several different patterns were identified (Fig. 4.12, D). 16 clones were sent for sequencing. Two clones had an identical sequence (#78=#95), while the rest were all different. 16 clones were tested in secondary screening in order to confirm their positivity, as described in paragraph 3.2.7.1, but resulted all to be negative for CD19 binding. Clone #78=#95 resulted to be positive for lexA binding instead, and therefore not suitable for our purpose (Fig. 4.12, E).

A single anti-CD19 nanobody was therefore selected through IACT technology: VHH21A.

Table 4.7. Screening II

Primary Screening								**Secondary Screening**
	Transformation efficiency	**Picked clones** (-WHL plates)	**Regrown clones** (-WHL plates)	**ß-gal assay** (liquid)	**Colony PCR**	**Finger-print** (*Nal* IV *Alu* I)	**DNA seq**	**n° of positive clones**
	$1.22 \cdot 10^8$	394	394	43	39	Several patterns	16	0

Set up	
Positive control (interaction)	anti -lexA VHH
Negative control (interaction)	anti-pTAU VHH
Negative control (transformation)	Salmon testis DNA (STD)

Set up	
Bait of interest	CD19
Unrelated bait	Synuclein

A)

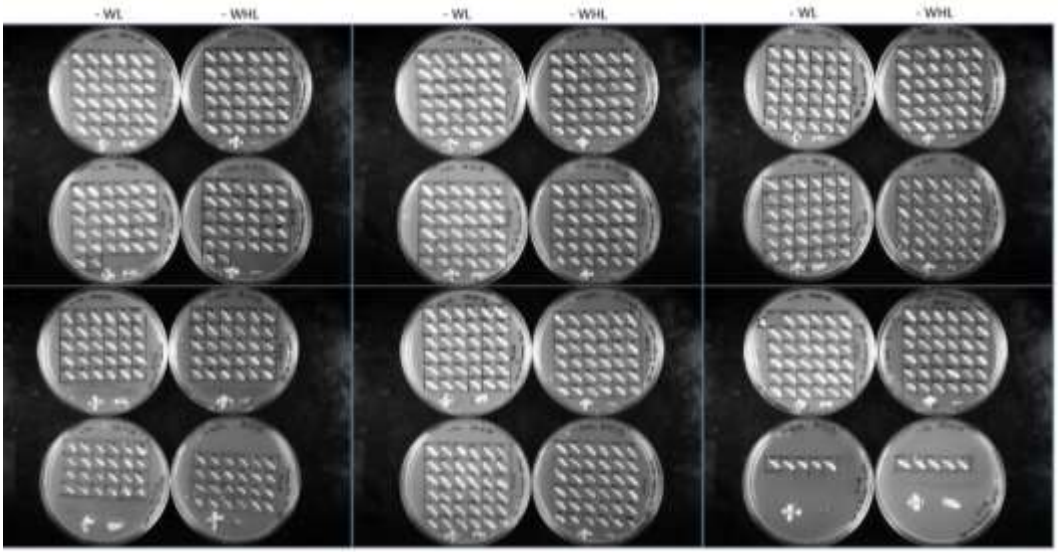

B)

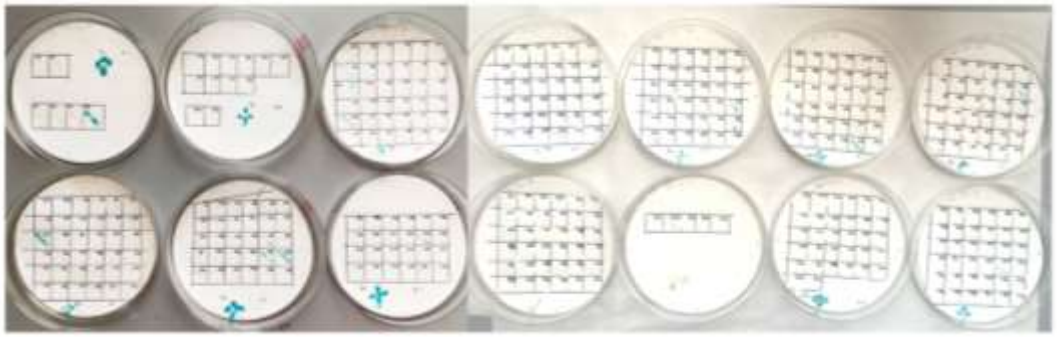

C)

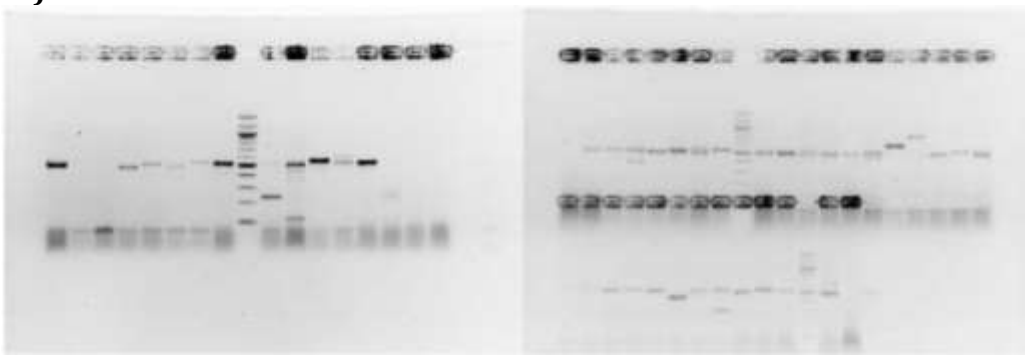

D)

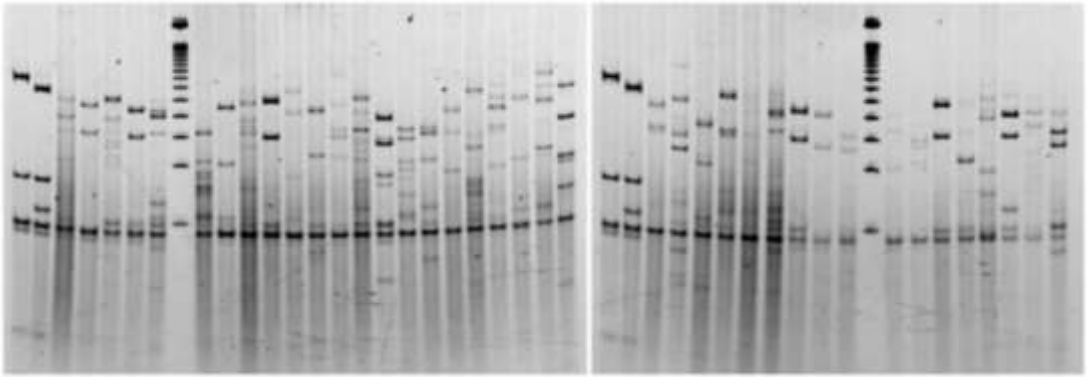

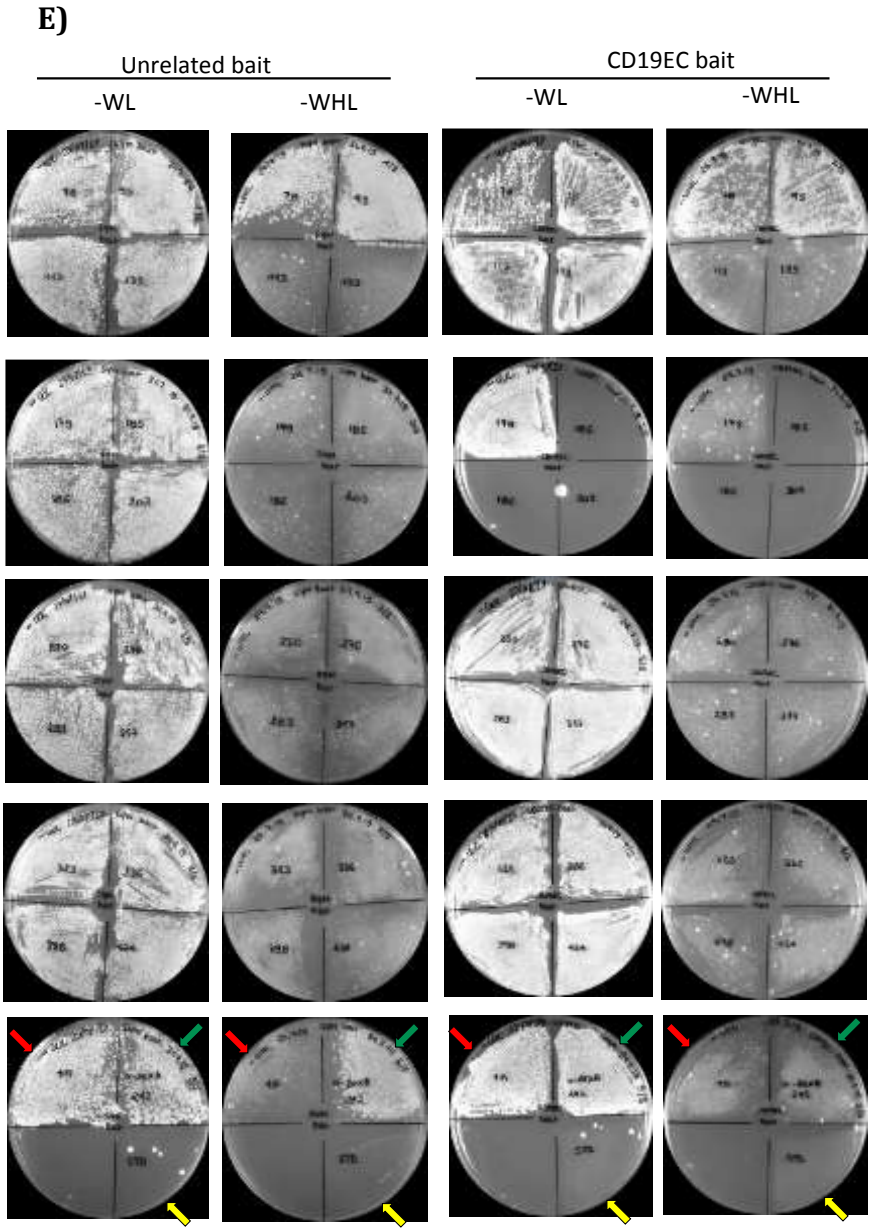

Fig. 4.12 Screening II. A) *Selected clones re-streaked onto -WL (selective for transformants) and -WHL (selective for interactors) plates.* ***B)*** *ß-gal assay (solid).* ***C)*** *Colony PCR.* ***D)*** *DNA fingerprint.* ***E)*** *Secondary screening. L40 unrelated bait transformed with the 16 candidates and then plated on -WL (selective for transformants) and -WHL (selective for interactors) (ii) plates. L40 CD19 bait transformed with the 16 candidates and then plated on -WL (selective for transformants) and -WHL (selective for interactors) plates. Arrows: red: interaction negative control; green: interaction positive control; yellow: transformation negative control; no arrows: candidate.*

4.3 Part III: Nanobodies and ADC production

4.3.1 VHH21A production

4.3.1.1 VHH21A cloning

VHH21A DNA was sequenced (Eurofins) and the recombinant construct with an 8xHis tag at the C terminus was synthetized by Twist Bioscience. The insert was excised from the donor vector pTwist Amp High Copy with *Nco* I and *Not* I and ligated into the linearized pET45b(+) expression vector (Fig. 4.13).

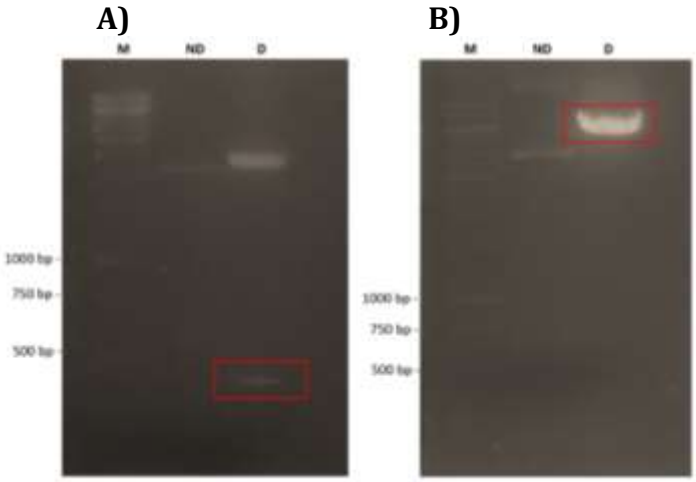

Fig. 4.13 VHH21A ligation into pET45b(+). *A) VHH21A insert excised from the donor vector* pTwist Amp High Copy *with Nco I and Not I (expected length 409 bp); B) pET45b(+) digested with Nco I and Not I (expected length 5143 bp).*

4.3.1.2 VHH21A expression in E. coli BL21(DE3) soluble fraction vs insoluble fraction

The construct obtained, pET45b(+)_VHH21A was transformed into *E. coli* BL21(DE3) cells as described in paragraph 3.2.1.4. Induction for protein expression was performed as described in paragraph 3.2.2.2. (Tab. 4.8).

The protein resulted to be highly expressed in the insoluble fraction, as showed in Fig. 4.14 (lane I). Two strategies were therefore followed in order to obtain a suitable recombinant antibody production: production of inclusion bodies with a classical and non-classical procedure and optimization of soluble expression through chaperons.

Tab. 4.8 Soluble Fraction Expression

	Strain (*E. coli*)	**Volume**	**T**	**hrs**	**Sampling (hrs)**
Induction	BL21(DE3)	1 L	25 °C	5	5

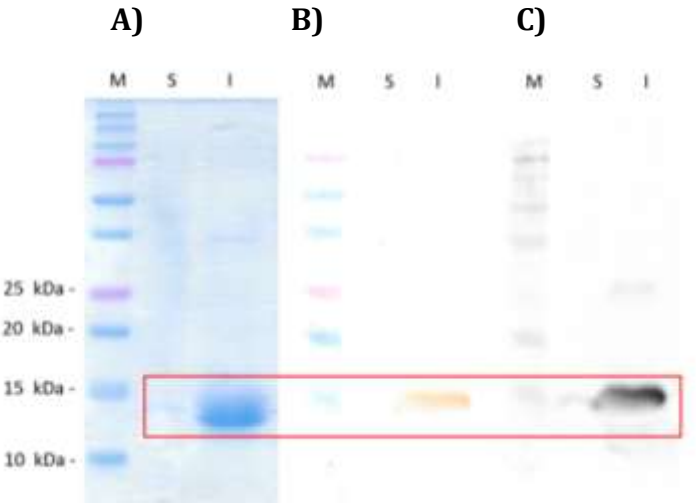

Fig. 4.14 VHH21A expression, soluble vs insoluble fraction. *SDS-PAGE analysis (15% Polyacrylamide gel) of VHH21A expression in soluble (S) and insoluble (I) fractions (expected MW: 14.4 kDa).. **A)** Coomassie staining **B)** DAB staining C) **WB** (anti-His antibody).*

4.3.1.2 VHH21A expression in E. coli BL21(DE3): Classical Inclusion Bodies (CIBs)

Induction of classical inclusion bodies was performed as described in paragraph 3.2.2.3 [197](Tab. 4.9). The first step of purification of the denatured and subsequently refolded fractions consisted in affinity chromatography (IMAC) on nickel-sepharose (HisTrap) columns (Fig. 4.15 A, B). After an SDS-PAGE of the eluted fractions followed by Coomassie staining, which confirmed the presence of refolded protein in Fr. 3 and 4, (Fig. 4.15, C), Size exclusion chromatography (SEC) was performed in order to verify the folding status of the purified, refolded protein in pooled Fr. 3 and 4 from IMAC. The chromatogram shows a peak at ~14.7 ml (expected volume) (Fig. 4.15, D). Another SDS-PAGE analysis was performed on fractions Fr. 3 and 4 eluted from affinity chromatography, o.n. stored samples, eluted fractions from SEC analysis and on the concentrated pool (5x) of the eluted fractions from SEC analysis (Fig. 4.15, E). As these results demonstrate, VHH21A inclusion bodies were successfully produced and refolded. However, during the SEC purification, the material was completely lost. A BCA test was performed in order to quantify the protein, but to no avail. Protein precipitation onto the column was hypothesized.

An indirect and sandwich ELISA were anyway performed with the material obtained, in order to test and confirm VHH21A binding capability to the CD19 antigen (Fig. 4.15, F, G). VHH21A from the concentrated pool (5x, CP) of the eluted fractions from SEC analysis was used for the ELISA, along with CD19_Fc expressed in HEK293T (supernatant, see paragraph 3.2.2.3). The ELISA schemes are reported in paragraph 3.2.5.1. Even though the signal obtained was significant in both cases ($p < 0.05$), the ELISA did not result into a clear positivity for antigen binding, suggesting that most of the binding capability was, indeed, lost upon SEC.

Table 4.9 Classical Inclusion Bodies (CIBs) production

	Strain (*E. coli*)	Volume	T	hrs	Sampling (hrs)
Induction	BL21(DE3)	1 L	25 °C	5	5

Affinity Chromatography (IMAC)

	Column	Volume	Buffer A	Buffer B (100%)	Fractions	Peak (mAU)
Denatured fraction	HisTrapFF (1 ml)	50 ml	100 mM NaH_2PO_4, 10 mM Tris-HCl, 8 M Urea, pH 8	100 mM NaH_2PO_4, 10 mM Tris-HCl, 8 M Urea, 300 mM ImOH, pH 8	2 ml	1600, (Fr. 2, 3)
Refolded fraction	HisTrap (5 ml)	320 ml	100 mM NaH_2PO_4, 10 mM Tris-HCl, 8 M Urea, pH 8	100 mM NaH_2PO_4, 10 mM Tris-HCl, 8 M Urea, 300 mM ImOH, pH 8	8 ml	60 (Fr. 3,4,5)

Size Exclusion Chromatography (SEC)

	Column	Buffer	Retention volume	Peak (mAU)	Fractions
Purification	Superdex 75 30/100	PBS pH 7.4	14.7 ml	0.6	2 ml

Yield	Not detectable
ELISA	To be confirmed

A) Denatured fraction **B)** Refolded fraction **C)**

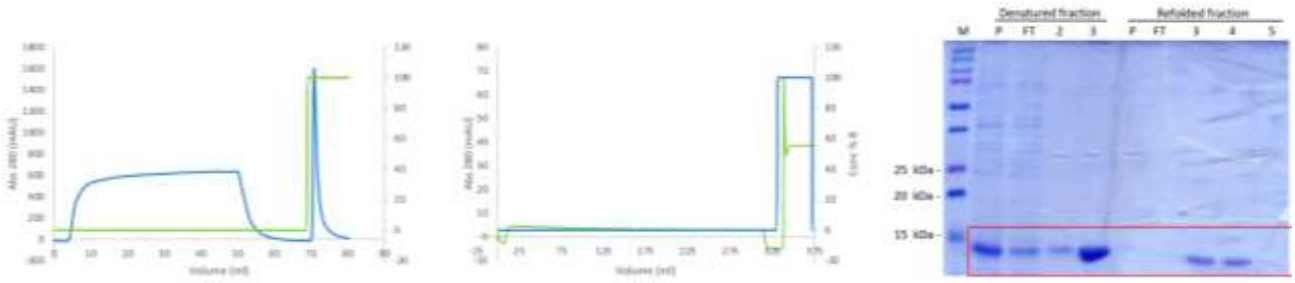

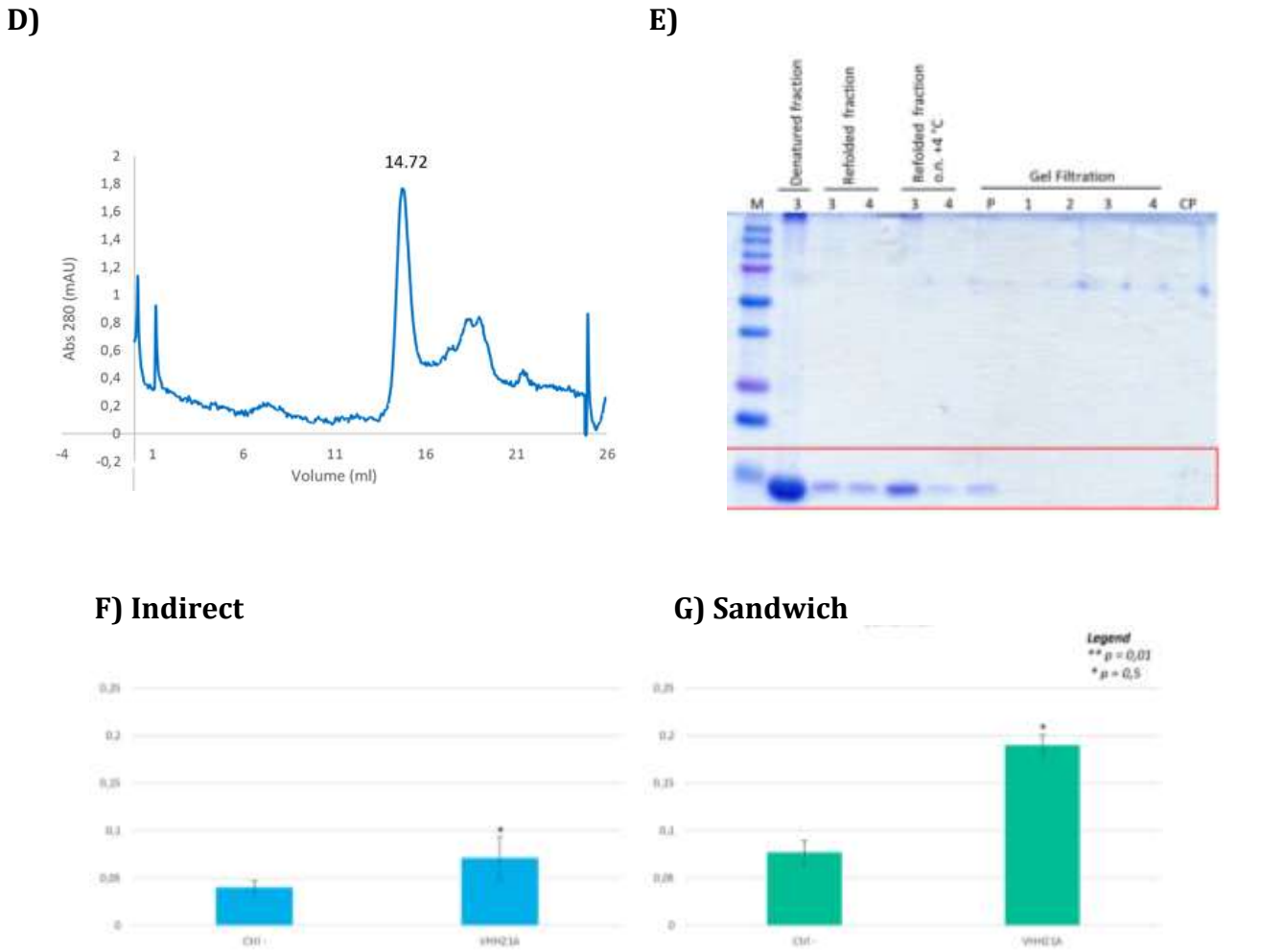

Fig. 4.15 VHH21A expression and purification, CIBs. A) *Denatured fraction purified by Affinity Chromatography (IMAC). HisTrapFF (5 ml), Elution 100% B, 2 ml fractions.* ***B)*** *Refolded protein purified by Affinity Chromatography (IMAC). HisTrapFF (5 ml), Elution 100% B, 8 ml fractions.* ***C)*** *SDS-PAGE (15% polyacrylamide) and Coomassie staining of denatured and refolded fractions.* ***D)*** *Size Exclusion Chromatography (SEC). Superdex 75 30/100 column* ***E)*** *SDS-PAGE (15% polyacrylamide) and Coomassie staining of denatured and refolded eluted fractions, o.n. storage at + 4°C and SEC eluted fractions (4 loadings of 500 µl after IMAC, plus concentrated pool CP).* ***F)*** *Indirect ELISA. Coating CD19_Fc; VHH21A pooled fraction after SEC second layer.* ***G)*** *Sandwich ELISA. Coating VHH21A: (pooled fraction after SEC). Recombinant CD19_Fc: second layer.*

4.3.1.3 VHH21A expression in E. coli BL21(DE3), non-classical Inclusion Bodies (ncIBs)

Induction of non-classic inclusion bodies was performed as described in paragraph 3.2.2.3 (Tab. 4.10). The first step of the purification consisted in affinity chromatography (IMAC) on a nickel-sepharose column (Fig. 4.16 A). A Desalting run was then performed, changing the buffer to PBS pH 7.4 (Fig. 4.16 B). An SDS-PAGE of the eluted fractions (Fig. 4.16 C) demonstrated the presence of a protein with the expected MW. However, massive protein precipitation was instantly observed after elution from the column. A BCA assay was performed, resulting in a protein concentration of 136 µg/ml (Yield 2.176 mg/L). After 1 week of storage at + 4°C, the sample was centrifuged, in order to remove protein precipitation, and quantified a second time through BCA assay, resulting in a concentration of 40 µg/ml (protein loss ~70%).

An indirect and sandwich ELISA were however performed in order to test and confirm VHH21A binding capability to the CD19 antigen (Fig. 4.16 D, E). VHH21A obtained from the concentrated pool of the fractions eluted from the Desalting column was used, along with CD19_Fc expressed in HEK293T (supernatant, see paragraph 3.2.2.3). The ELISA schemes are reported in paragraph 3.2.5.1. The ELISA confirmed a clear positivity for antigen binding ($p < 0.05$), suggesting that this could be a useful strategy for VHH21A production.

Table 4.10 Non-Classical Inclusion Bodies (nCIBs) production and purification, I

	Strain (*E. coli*)	Culture Volume	T	hrs	Sampling (hrs)
Induction	BL21(DE3)	2 L	18 °C	24	24

Affinity Chromatography (IMAC)

	Column	Volume	Buffer A	Buffer B (100%)	Fractions	Peak (mAU)
IMAC	Bio-Scale™ Mini Profinity™ (5 ml)	1,5 L	**RA Buffer** 500 mM Sodium, 50 mM Tris-HCl, pH 8,5	500 mM Sodium, 50 mM Tris-HCl, 300 mM ImOH, pH 8,5	8 ml	210, (Fr. 3,4,5)

Desalting

	Column	Sample Volume	Buffer	Fractions	Peak (mAU)
Purification	HiPrep 26/10	10 ml	PBS pH 7.4	8 ml	60 Fr. 5,6

Yield	2.176 mg/L	**ELISA**	positive

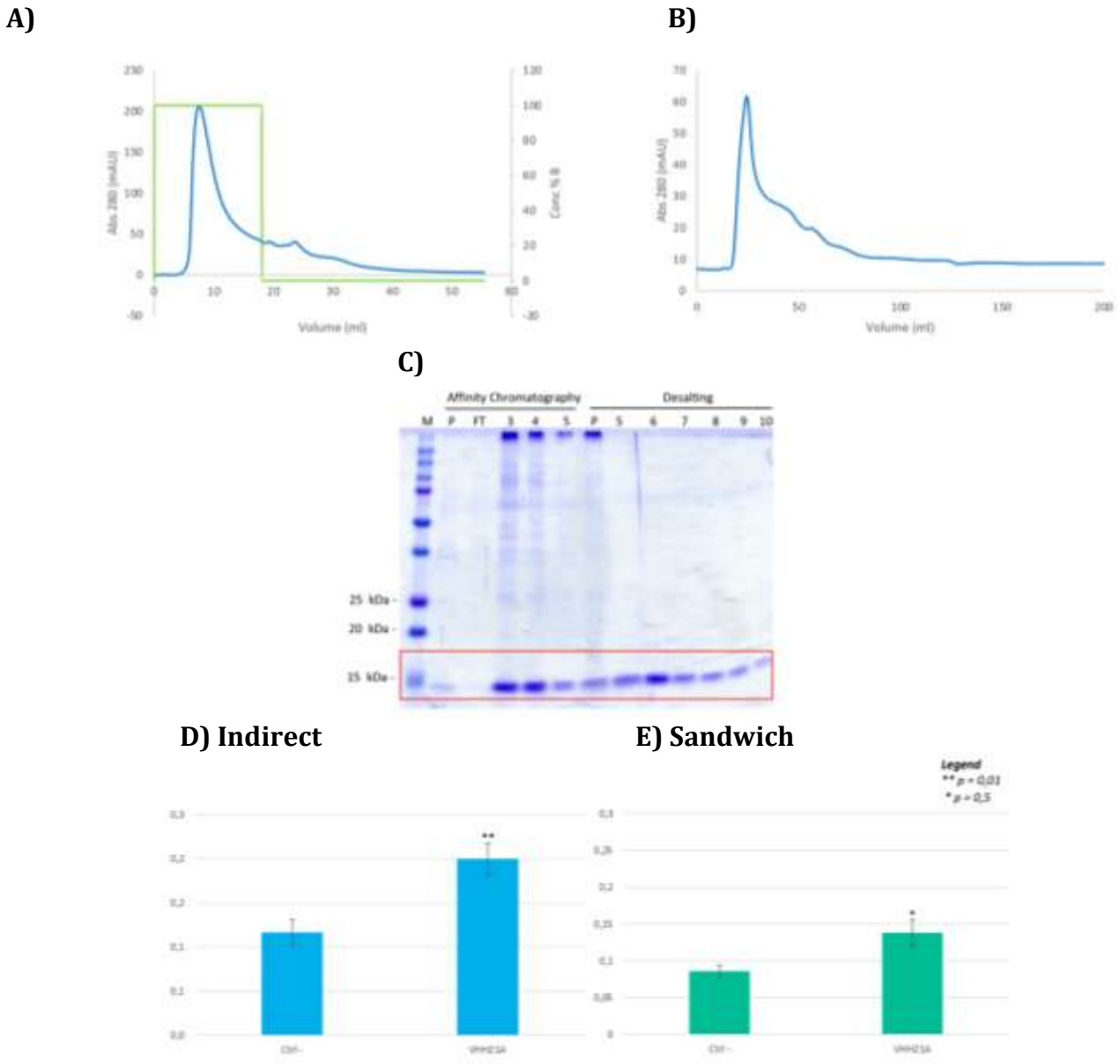

Fig. 4.16 VHH21A expression and purification, nCIBs, I. A) *Affinity Chromatography (IMAC). Bio-Scale™ Mini Profinity™ (5 ml), Elution 100% B, 8 ml fractions.* ***B)*** *Desalting, HiPrep 26/10, PBS*

pH 7,4, 8 ml fractions. ***C)*** *SDS-PAGE (15% polyacrylamide) and Coomassie staining of IMAC and Desalting eluted fractions.* ***D)*** *Indirect ELISA. Coating: CD19_Fc; VHH21A pooled fraction after Desalting: second layer.* ***E)*** *Sandwich ELISA. Coating: VHH21A (pooled fractions after Desalting). Recombinant CD19_Fc: second layer.*

Another induction of non-classical inclusion bodies was performed in conditions similar to those used above, but changing the purification conditions (Tab. 4.11).
Particularly, in the attempt to stabilize the protein and reduce its precipitation, 20 mM Arginine was added in all purification buffers, and 5% v/v glycerol was added in the PBS pH 7.4 used during the Desalting step.
The first step of the purification consisted in affinity chromatography (IMAC) on a nickel-sepharose column (Fig. 4.17 A). The following storage conditions for the eluted fractions were thus tested on a part of the sample, in order to assess the most efficient one: non-diluted protein (ND), stored both at room temperature (RT) and +4 °C; sample diluted 1:4 in elution buffer (D), stored at RT, at + 4°C either without glycerol or with 5% v/v glycerol.
A Desalting run was then performed on the remaining part of the sample, changing the elution buffer to PBS pH 7.4, 5% Glycerol (Fig. 4.17, B). Eluted fractions were pooled and concentrated to half the original volume. BCA quantification was performed on non-concentrated pooled fractions (NC, yield: 15 mg/L) and concentrated fractions (Yield: 7 mg/L). The protein loss in the concentrated pool was ~50%, and protein precipitation was again visible after a few hours in both samples.
An SDS-PAGE analysis and Coomassie staining were performed on all the available samples, showing the best result when the protein was diluted and added with glycerol (Fig. 4.17, C). An indirect and a sandwich ELISA were however executed in order to test and confirm VHH21A binding capability to the CD19 antigen (Fig. 4.17, D, E). VHH21A from the not concentrated pool of the eluted fractions from Desalting was used, along with CD19_Fc expressed in HEK293T (supernatant, see paragraph 3.2.2.3). The ELISA schemes are reported in paragraph 3.2.5.1.
The ELISA confirmed a clear positivity for antigen binding ($p < 0.05$).

Table 4.11 Non-Classical Inclusion Bodies (nCIBs) production and purification, II

	Strain (*E. coli*)	**Culture Volume**	**T**	**hrs**	**Sampling (hrs)**
Induction	BL21(DE3)	1 L	18 °C	24	24

Affinity Chromatography (IMAC)

	Column	**Sample Volume**	**Buffer A**	**Buffer B (100%)**	**Fractions**	**Peak (mAU)**
IMAC	Bio-Scale™ Mini Profinity™ (5 ml)	1,5 L	**RA Buffer** 500 mM Sodium, 50 mM Tris-HCl, 20 mM Arg pH 8,5	500 mM Sodium, 50 mM Tris-HCl, 20 mM Arg 300 mM ImOH, pH 8,5	8 ml	360, (Fr. 3,4)

Desalting

	Column	**Sample Volume**	**Buffer**	**Fractions**	**Peak (mAU)**
Purification	HiPrep 26/10	10 ml	PBS, 5% v/v Glycerol, pH 7.4	8 ml	20 Fr. 5,6

Yield	15 mg/L
ELISA	Positive

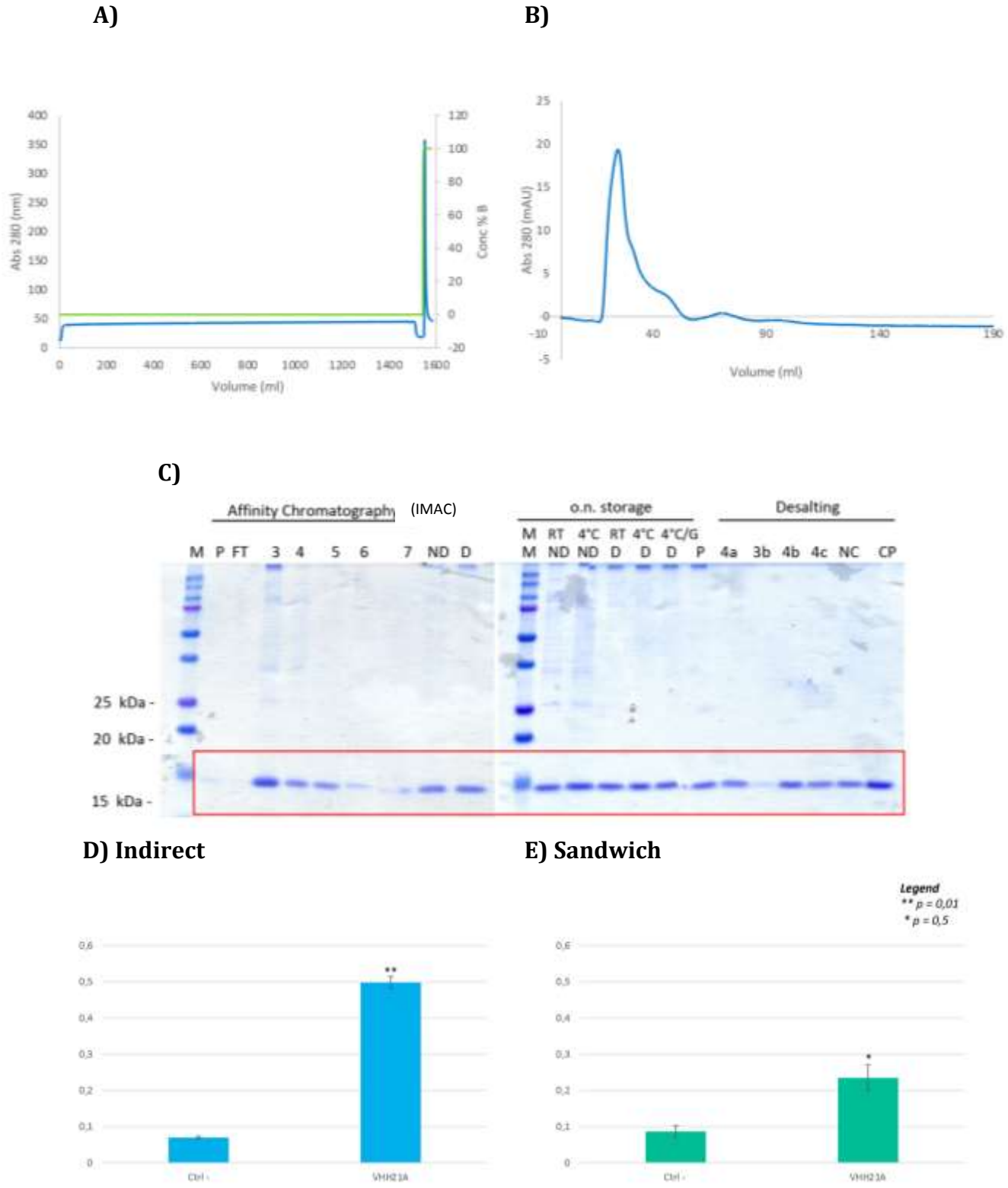

Fig. 4.17 VHH21A expression, nCIBs, II. A) *Affinity Chromatography (IMAC). Bio-Scale™ Mini Profinity™ (5 ml), Elution 100% B, 8 ml fractions.* ***B)*** *Desalting, HiPrep 26/10, PBS pH 7,4 5% v/v glycerol, 8 ml fractions.* ***C)*** *SDS-PAGE (15% polyacrylamide) and Coomassie staining: o.n. storage conditions (ND = non-diluted, D= diluted 1:4 in elution buffer, RT = room temperature, +4 °C) and Desalting eluted fractions.* ***D)*** *Indirect ELISA. CD19_Fc coating, VHH21A pooled fractions (not concentrated) after Desalting tested.* ***E)*** *Indirect ELISA. Coating: CD19_Fc; VHH21A pooled fraction after Desalting: second layer.* ***F)*** *Sandwich ELISA. Coating: VHH21A (pooled fraction not concentrated after Desalting). Recombinant CD19_Fc: second layer.*

Considering the encouraging results, another induction of non-classical inclusion bodies was performed (Tab. 4.12).
In the attempt to further stabilize the protein and reduce its precipitation, sodium chloride concentration was reduced to 200 mM in purification buffers, along with the pH, lowered from 8.5 to 7, to favor an increase of the protein net charge, according to the protein calculated isoelectric point (8.66) , which should enhance solubility and reduce precipitation.
The purification consisted in affinity chromatography (IMAC) on a nickel-Sepharose column (Fig. 4.18 A). An SDS-PAGE analysis and Coomassie Gel staining were performed on the eluted fractions, highlighting the expected bands along with some unspecific bands (Fig. 4.18 B). 5% v/v glycerol was immediately added to the eluted fractions, which were pooled and stored in two conditions: + 4 °C and -20°C. Protein precipitation was not visible.

Table 4.12 Non-Classical Inclusion Bodies (nCIBs) production and purification, III

	Strain (*E. coli*)	**Volume**	**T**	**hrs**	**Sampling (hrs)**
Induction	BL21(DE3)	1 L	18 °C	24	24

+

Affinity Chromatography (IMAC)

	Column	**Volume**	**Buffer A**	**Buffer B (100%)**	**Fractions**	**Peak (mAU)**
IMAC	Bio-Scale™ Mini Profinity™ (5 ml)	1,5 L	**RA Buffer** 200 mM Sodium, 50 mM Tris-HCl, pH 7	200 mM Sodium, 50 mM Tris-HCl, 300 mM ImOH, pH 7	2 ml	120, (Fr. 4, 5, 6, 7)

A)

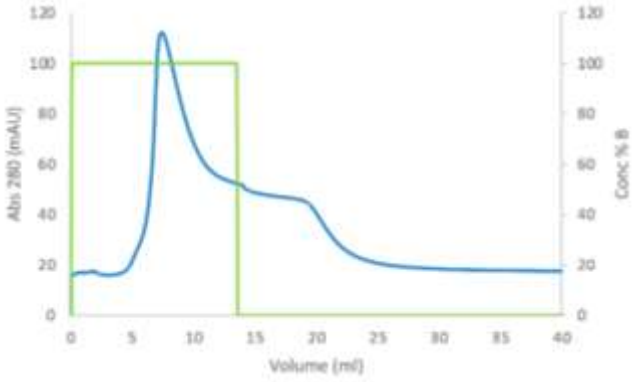

B)

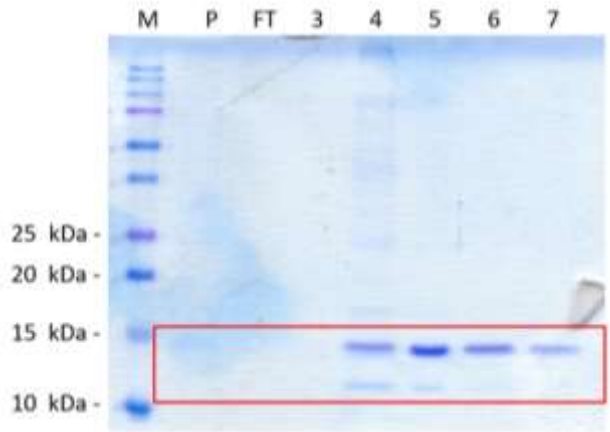

Fig. 4.18 VHH21A expression, nCIBs, II. A) *Affinity Chromatography (IMAC). Bio-Scale™ Mini Profinity™ (5 ml), Elution 100% B, 2 ml fractions.* ***B)*** *SDS-PAGE (15% polyacrylamide) and Coomassie staining of IMAC eluted fractions.*

4.3.1.3 VHH21A soluble expression in E. coli BL21(DE3): optimization with chaperons

VHH21A soluble small-scale expressions were performed as described in paragraph 3.2.2.2. (Tab. 4.13). Fig. 4.18 shows the results of the SDS-PAGE followed by Coomassie staining (left panel) and WB developed with DAB (central panel) or ECL (right panel). From these results, it can be deuced that in *E. coli* BL21(DE3) expressing *dna*K-*dna*J-*grp*E-*gro*ES-*gro*EL (Fig. 4.19 A) and *E. coli* BL21(DE3) expressing -*gro*ES-*gro*EL-tig (Fig. 4.19 B), the protein resulted to be expressed only in the insoluble fraction.
In contrast, in *E. coli* BL21(DE3) expressing the *tig factor* (Fig. 4.19 C), the protein was mostly expressed in the insoluble fraction, but also in the soluble one, with a clear band appearing at 3 h induction time and further increasing in intensity at 24 h. It was therefore possible to obtain VHH21A sdAb in soluble format, though stability issues remain.

Table 4.13 Soluble Expression Chaperon Optimization

Strain (*E. coli*)	Vector	Chaperons	Inducer	T	hrs	Sampling (hrs)
BL21(DE3)	pG-KJE8	*dna*K-*dna*J-*grp*E-*gro*ES-*gro*EL	L-arabinose Tetracycline	17 °C	24	0, 3, 24
BL21(DE3)	pG-Tf2	*gro*ES-*gro*EL-tig	Tetracycline	17 °C	24	0, 3, 24
BL21(DE3)	pTf16	*tig*	L-arabinose	17 °C	24	0, 3, 24

A) *dna*K-*dna*J-*grp*E-*gro*ES-*gro*EL

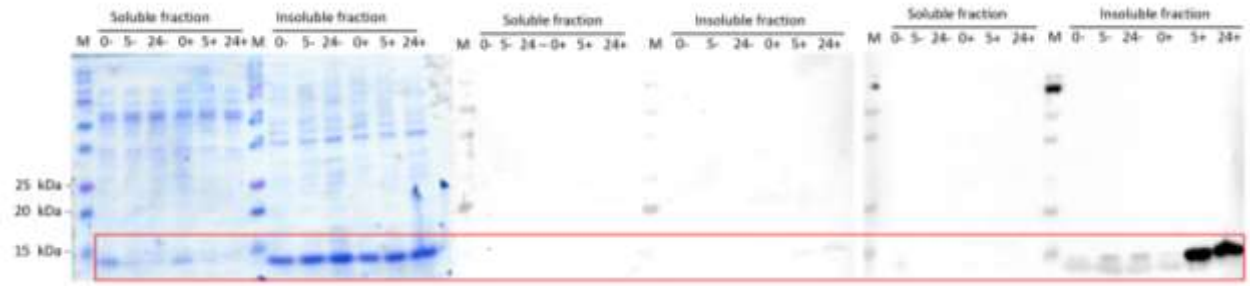

B) *gro*ES-*gro*EL-tig

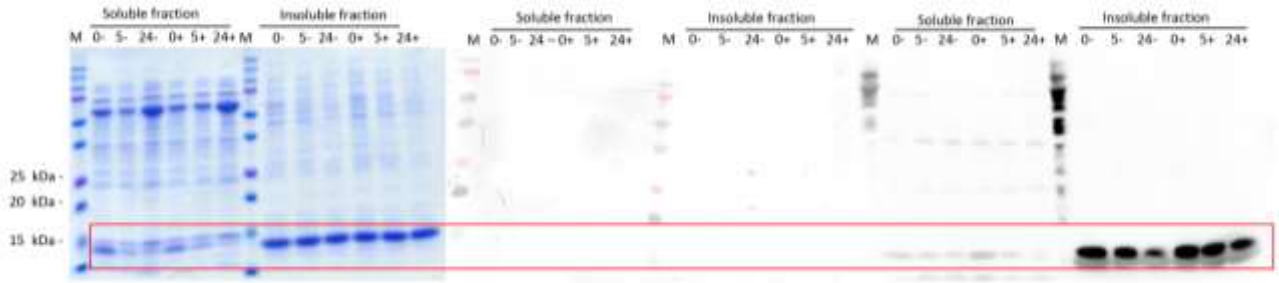

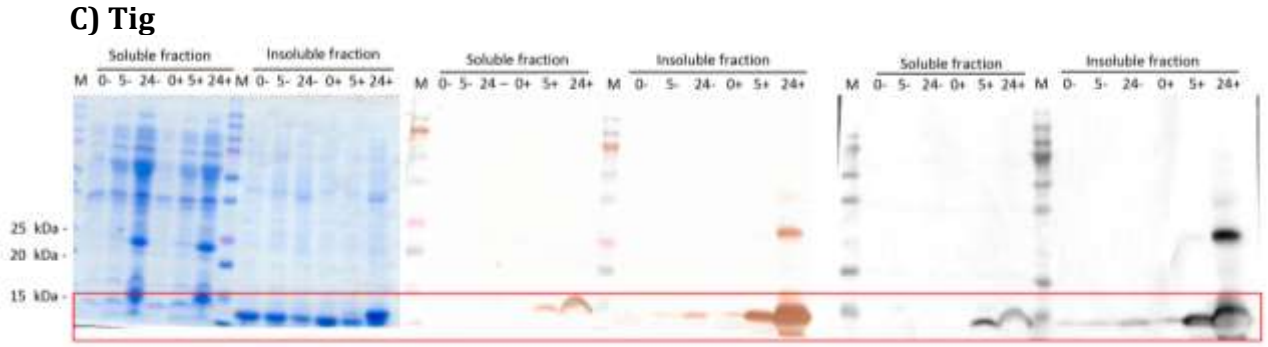

Fig. 4.19 VHH21A soluble expression, chaperon optimization. A) *Small-scale expression in E. coli BL21(DE3) expressing dnaK-dnaJ-grpE-groES-groEL. An SDS-PAGE analysis followed by Coomassie staining, DAB and ECL. WB was performed on soluble and insoluble fraction samplings at 0, 3, 24 h.* ***B)*** *Small-scale expression in E. coli BL21(DE3) expressing groES-groEL-tig. An SDS-PAGE analysis followed by Coomassie staining, DAB and ECL. WB was performed on soluble and insoluble fraction samplings at 0, 3, 24 h.* ***C)*** *Small-scale expression in E. coli BL21(DE3) expressing tig. An SDS-PAGE analysis followed by Coomassie staining, DAB and ECL. WB was performed on soluble and insoluble fraction samplings at 0, 3, 24 h (VHH21A expected MW: 14,4 kDa).*

4.3.1.4 VHH21A model

The best results for VHH21A expression were obtained using the optimized protocol for non classical inclusion bodies extraction (**Table 4.11**), and storing the purified protein at +4 °C adding 5% v/v glycerol. Nevertheless, protein instability issues were still too significant to proceed with further characterization tests.
In order to investigate if solubility issues could be due to a particular configuration of the protein surface charges, a model of the nanobody was computed using Modeller (Fig. 4.20, paragraph 3.2.4.6).[443] However, the surface charges showed in Fig. 4.20 do not highlight particular hydrophobic patterns, hence, it was impossible to design direct surface point mutations in order to favor the protein solubility and stability. It was however decided to proceed with the cloning of the TCAN3 construct, in order to study the behavior of the whole molecule.

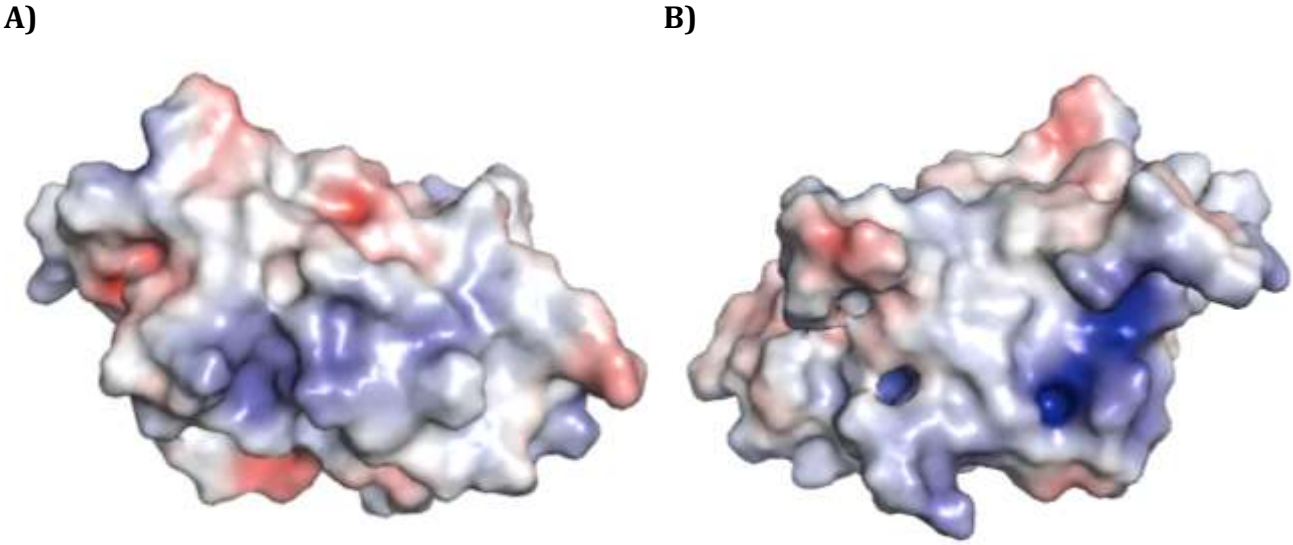

Fig. 4.20 VHH21A model. *Model obtained with Modeler; protein surface charges computed using Pymol [471] (APBS electrostatics) basing on residues hydrophobicity. Red surface: negative charges; Blue surface: positive charges.* ***A)*** *front* ***B)*** *180 ° horizontal rotation*

4.3.2 TCAN3 production

4.3.2.1 TCAN3 cloning

TCAN3 includes the catalytic single domain with ASNase activity anti-CD19 VHH21A targeting single domain, and its generation represents the 4th molecule planned to be produced.
TCAN3 DNA recombinant construct was synthetized by Twist Bioscience. The insert was double-digested with *Nco* I and *Not* I and ligated into the linearized pET45b(+) expression vector. Fig. 4.21 shows the restriction enzyme digestion. Performed to check the insert presence in the final construct. After cloning, several expression strategies were tested in *E. coli* BL21(DE3)*ΔansAansB*: IPTG induction in the soluble fraction with or without the additional expression of the pRARE vector, soluble expression optimization with chaperons and the extraction of inclusion bodies with the non-classical procedure. In the following parapraphs the main obtained results are described.

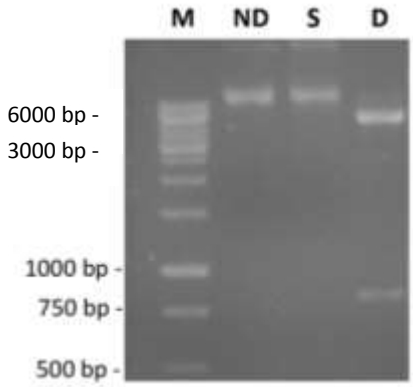

Fig. 4.21 TCAN3 ligation control Digestion. *pET45b(+)_TCAN3 construct control digestion. M: 1 KB Ladder; ND: Not Digested; S: digested with SacII (negative control); D: double digested with Nco I and Not I. TCAN3 expected length: 816 bp, pET45b(+) digested with Nco I and Not I. Expected length: 5143 bp.*

4.3.2.2 TCAN3 expression in E. coli BL21(DE3) soluble fraction vs insoluble fraction

pET45b(+)-TCAN3 was transformed into *E. coli* BL21(DE3) cells and into *E. coli* BL21(DE3) + pRARE as described in paragraph 3.2.1.4.
Induction for protein expression was performed as described in paragraph 3.2.2.2, and the main experimental details are summarized in Tab. 4.14. Fig. 4.22 reports the results obtained.
The protein resulted to be more expressed in the insoluble fraction, but some clear bands were visible in the soluble fractions of BL21(DE3) cells induced at 17 °C, up to 5 hours of induction (Fig. 4.22 C).
Two strategies were therefore followed in order to achieve suitable recombinant antibody production: large scale expression into BL21(DE3), and optimization of soluble expression through chaperons.

Table 4.14 TCAN3 Small-scale Expression

	Strain (*E. coli*)	IPTG	T	hrs	Sampling (hrs)
Induction	BL21(DE3)	0.4 mM	25 °C	24	0, 3, 5, 24
Induction	BL21(DE3) + pRARE	0.4 mM	25 °C	24	0, 3, 5, 24
Induction	BL21(DE3)	0.4 mM	17 °C	24	0, 3, 5, 24

A) **B)**

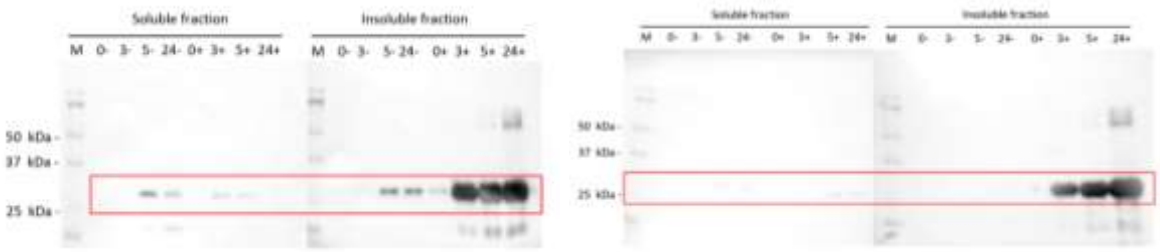

C)

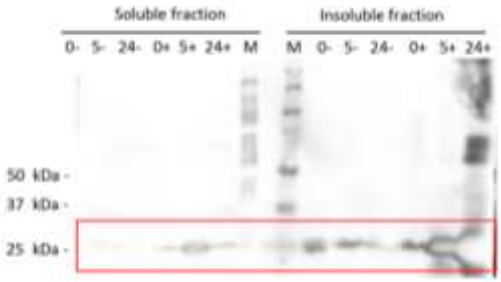

Fig. 4.22 TCAN3 expression, soluble vs insoluble fraction. A) *SDS-PAGE (12% Polyacrylamide gel) and WB analysis of TCAN3 expression in BL21(DE3), 25 °C, 0,4 mM IPTG, soluble and insoluble fraction (expected MW 30.4 kDa).* ***B)*** *SDS-PAGE (12% Polyacrylamide gel) and WB analysis of TCAN3 expression in BL21(DE3)+ pRARE, 25 °C, 0,4 mM IPTG, soluble and insoluble fraction (expected MW 30.4 kDa.* ***C)*** *SDS-PAGE (12% Polyacrylamide gel) and WB analysis of TCAN3 expression in BL21(DE3), 17 °C, 0,4 mM IPTG, soluble and insoluble fraction (expected MW 30.4 kDa).*

4.3.2.3 TCAN3 large scale expression in E. coli BL21(DE3)

TCAN3 large scale expression was performed as described in paragraph 3.2.2.3. Tab. 4.15 summarizes the experimental details.

The soluble fraction was purified using affinity chromatography (IMAC) on a nickel-Sepharose column and no peak was detected (Fig. 4.23 A). An SDS-PAGE followed by Coomassie staining and WB analysis were performed, highlighting the presence of the protein only in the pre-loading sample (Fig. 4.23 B, C).

Table 4.15 TCAN3 large scale expression in *E. coli* BL21(DE3)

	Strain (*E. coli*)	IPTG	Volume	T	hrs
Induction	BL21(DE3)	0.4 mM	1 L	18 °C	24

	Affinity Chromatography (IMAC)					
	Column	**Volume**	**Buffer A**	**Buffer B (10, 20, 50, 100%)**	**Fractions**	**Peak (mAU)**
IMAC	Bio-Scale™ Mini Profinity™ (5 ml)	50 ml	300 mM Sodium Chloride	300 mM Sodium Chloride	8 ml	No peak detected

	50 mM Sodium Phosophate 10 mM ImOH, pH 8	50 mM Sodium Phosophate 500 mM ImOH, pH 8

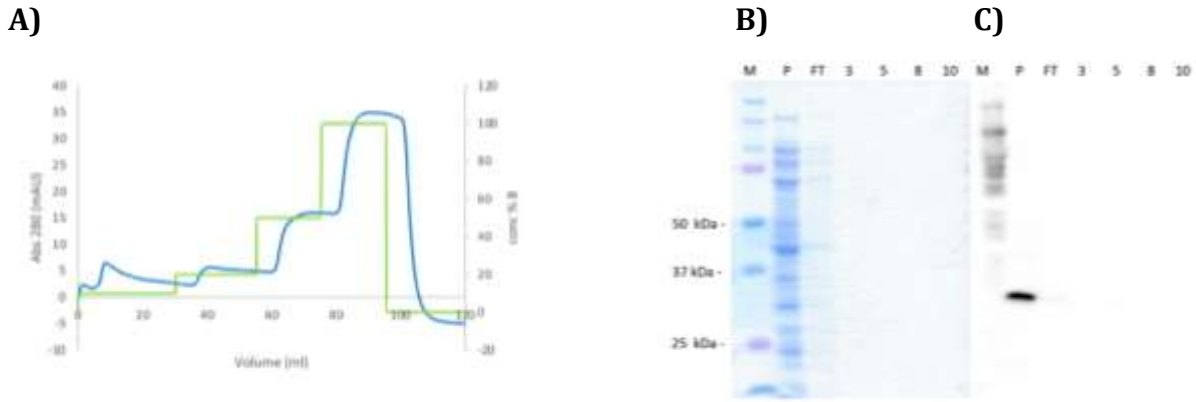

Fig. 4.23 TCAN3 large scale expression in BL21(DE3). A) *Affinity Chromatography (IMAC). Step gradient elution. SDS-PAGE and Coomassie* ***(B)*** *and WB* ***(C)*** *analysis of TCAN3 purification (expected MW 30.4 kDa). 12% Polyacrylamide gel. P = Pre-loading; FT = flow through; numbers correspond to eluted fractions.*

4.3.2.4 TCAN3 soluble expression in E. coli BL21(DE3): optimization with chaperons

TCAN3 small-scale expressions for the soluble fractions were performed as described in paragraph 3.2.2.2. (Tab. 4.16).
In *E. coli* BL21(DE3) expressing *dna*K-*dna*J-*grp*E-*gro*ES-*gro*EL and *E. coli* BL21(DE3) expressing -*gro*ES-*gro*EL-tig, the protein resulted to be expressed only in the insoluble fraction (Fig. 4.24, A, B).
In *E. coli* BL21(DE3) the expressing *tig,* the protein was mostly expressed in the insoluble fraction, but it was also present in the soluble one, appearing at 24 hrs (Fig. 4.24 C).

Table 4.16 Soluble Expression Chaperon Optimization

Strain (*E. coli*)	Vector	Chaperons	Inducer	T	hrs	Sampling (hrs)
BL21(DE3)	pG-KJE8	*dna*K-*dna*J-*grp*E-*gro*ES-*gro*EL	L-arabinose Tetracycline	17 °C	24	0, 5, 24
BL21(DE3)	pG-Tf2	*gro*ES-*gro*EL-tig	Tetracycline	17 °C	24	0, 5, 24
BL21(DE3)	pTf16	*tig*	L-arabinose	17 °C	24	0, 5, 24

A) *dna*K-*dna*J-*grp*E-*gro*ES-*gro*EL

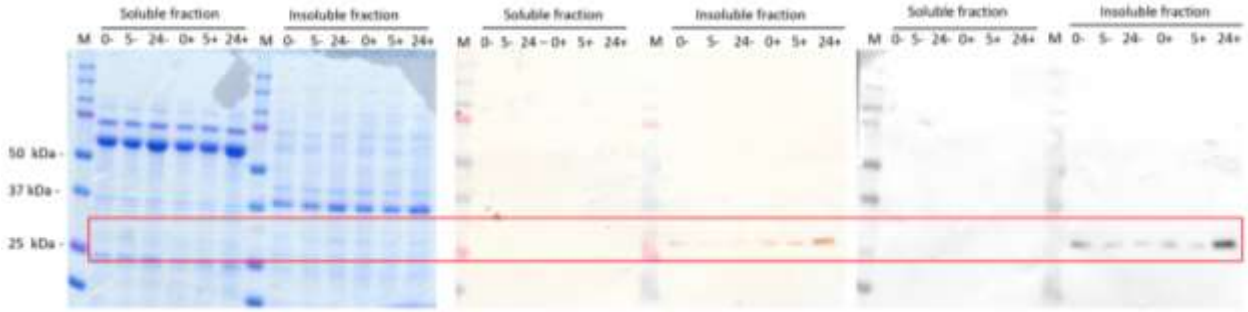

B) *gro*ES-*gro*EL-tig

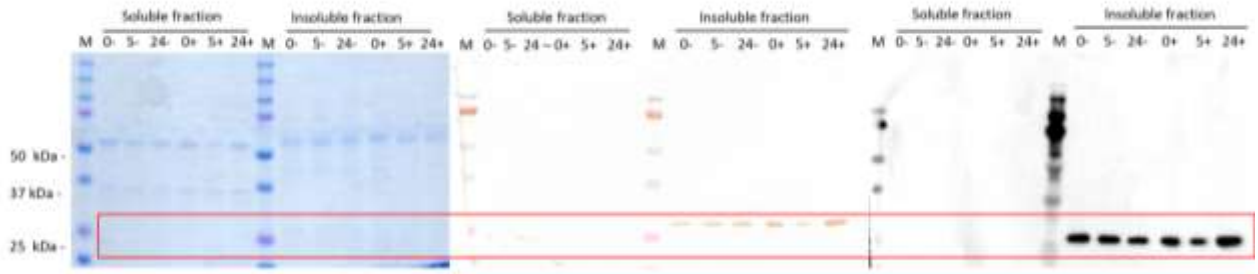

C) Tig

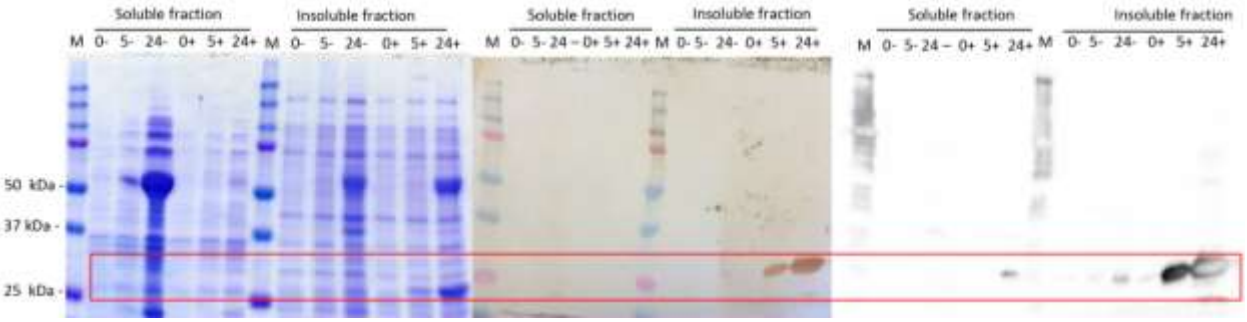

Fig. 4.24 TCAN3 soluble expression, chaperon optimization. *SDS-PAGE analysis followed by Coomassie staining, DAB and ECL. WB was performed on soluble and insoluble fraction samplings at 0, 5, 24 h. (TCAN3 expected MW: 30,4 kDa)* ***A)*** *Small-scale expression in E. coli BL21(DE3) expressing dnaK-dnaJ-grpE-groES-groEL.* ***B)*** *Small-scale expression in E. coli BL21(DE3) expressing groES-groEL-tig.* ***C)*** *Small-scale expression in E. coli BL21(DE3) expressing tig.*

4.3.2.4 TCAN3 large scale expression in E. coli BL21(DE3) + tig factor

TCAN3 expression was induced as described in paragraph 3.2.2.3 (Tab. 4.17).

The soluble fraction was purified using affinity chromatography (IMAC) on a nickel-Sepharose column and peaks were detected at 10%, 20%, and 50% Buffer B (Fig. 4.25 A). Eluted fractions were pooled and analyzed through SDS-PAGE followed by Coomassie staining (Fig. 4.25, E). Pooled fractions were purified through SEC, on two different columns (Superdex 75 30/100 and Superose HR 12 10/30) (Fig. 4.25, B, C). In both cases, no peak was detected. An indirect and sandwich ELISA were however performed in order to test TCAN3 binding capability to the CD19 antigen (Fig. 4.25, F, G). TCAN3 from the pooled eluted fractions from IMAC was used, along with CD19_Fc expressed in HEK293T (supernatant, see paragraph 3.2.2.3). The ELISA schemes are reported in paragraph 3.2.5.1.

Table 4.17 TCAN3 large scale expression in *E. coli* BL21(DE3) + Tig

	Strain (*E. coli*)	IPTG	Volume	T	hrs
Induction	BL21(DE3) + Tig	0.4 mM	1 L	17 °C	24

Affinity Chromatography (IMAC)

	Column	Volume	Buffer A	Buffer B (10, 20, 50, 100%)	Fractions	Peak (mAU)
IMAC	Bio-Scale™ Mini Profinity™ (5 ml)	50 ml	200 mM Sodium Chloride 50 mM Sodium Phosphate 10 mM ImOH, pH 8	200 mM Sodium Chloride 50 mM Sodium Phosphate 500 mM ImOH, pH 8	8 ml	~ 20 (Fr. 8-9 Fr. 12-13 Fr. 16)

Size Exclusion Chromatography (SEC)

	Column	Buffer	Retention volume	Peak (mAU)	Fractions
SEC	Superdex 75 30/100	300 mM Sodium Chloride 50 mM Sodium Phosphate pH 8	No peak detected	/	2 ml

Size Exclusion Chromatography (SEC)					
	Column	**Buffer**	**Retention volume**	**Peak (mAU)**	**Fractions**
SEC	Superose HR 12 10/30	300 mM Sodium Chloride 50 mM Sodium Phosophate pH 8	No peak detected	/	2 ml

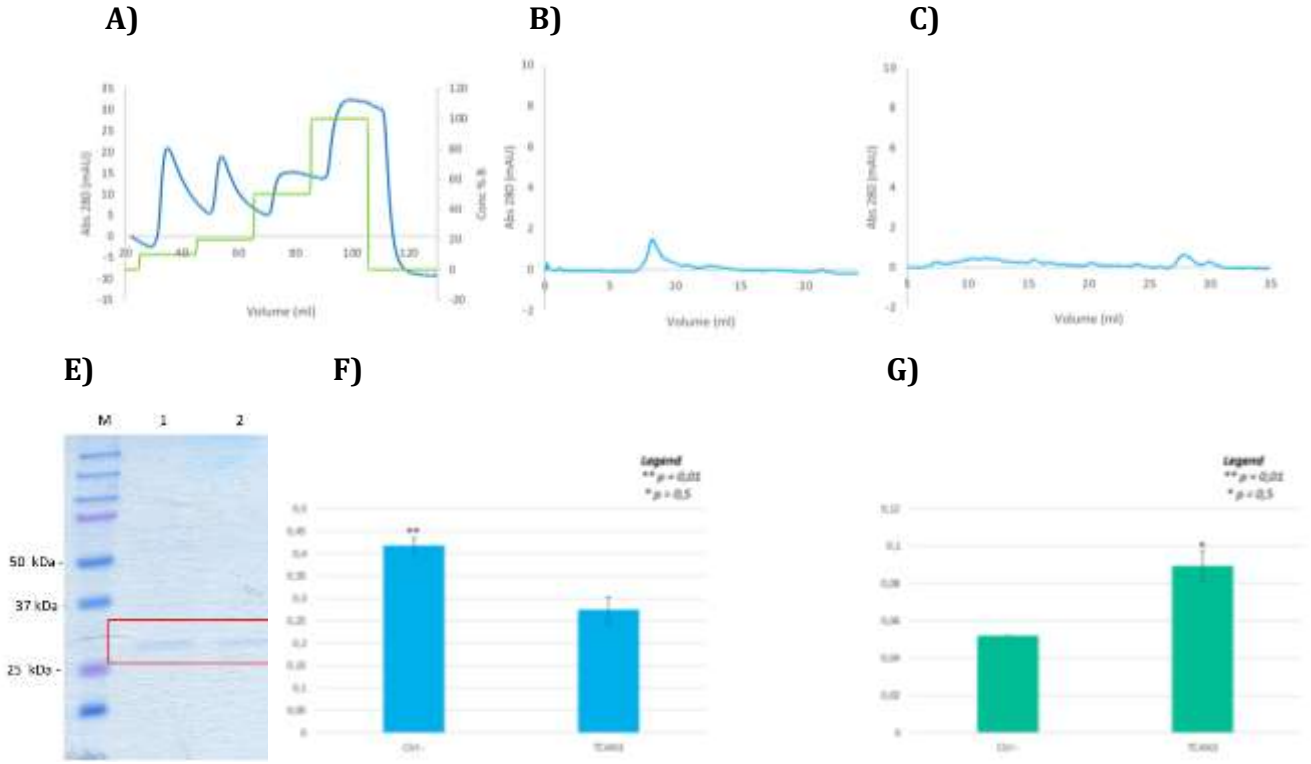

Fig. 4.25 TCAN3 large scale expression in BL21(DE3) +Tig. A) *Affinity Chromatography (IMAC). Step gradient elution (10%, 20%, 50%, 100%).* ***B)*** *SEC Chromatogram onto Superdex 75 10/300 and* ***C)*** *Superose HR 12 10/30.* ***E)*** *SDS-PAGE and Coomassie analysis of TCAN3 purification (expected MW 30.4 kDa). 12% Polyacrylamide gel. 1 = pooled fractions, 2= pooled fractions after centrifugation.* ***F)*** *Indirect ELISA. Coating: CD19_Fc. TCAN3 pooled after IMAC: second layer.* ***G)*** *Sandwich ELISA. Coating: TCAN3 (pooled fraction not concentrated after Desalting). Recombinant CD19_Fc: second layer.*

A second large scale expression was induced as described in paragraph 3.2.2.3 (Tab. 4.18), increasing the culture volume from 1 to 3 liter and processing also the insoluble fraction.
The soluble fraction was purified using affinity chromatography (IMAC) on a nickel-Sepharose column and peaks were detected at 10%, 20%, and 50% Buffer B (Fig. 4.26 A). Eluted fractions were pooled and analyzed through SDS-PAGE followed by Coomassie staining (Fig. 4.26, C). The bands were visible at the expected molecular weight in all the analyzed fractions, and particularly in the insoluble one. Pooled fractions were then purified through SEC, onto Superose HR 12 10/30 column, but no peak was detected (Fig. 4.26, B). An indirect and sandwich ELISA were performed onto the pool of IMAC eluted fractions in order to test TCAN3 binding capability to the CD19 antigen (Fig. 4.26, D, E). TCAN3 from the pooled eluted fractions from IMAC was used, along with CD19_Fc expressed in HEK293T (supernatant, see paragraph 3.2.2.3). The ELISA schemes are reported in paragraph 3.2.5.1, apart from the blocking solution for the indirect setting, where 5% MPBS 5% was used instead of 2% BSA, in order to avoid the background detected in the previous experiment coming from the anti-His antibody interaction with BSA. The results show that the TCAN3 is positive for the CD19 antigen binding ($p < 0.01$), but it is lost upon SEC purification.

Table 4.18 TCAN3 large scale expression in *E. coli* BL21(DE3) + Tig

	Strain (*E. coli*)	IPTG	Volume	T	hrs
Induction	BL21(DE3) + Tig	0.4 mM	3 L	17 °C	24

Affinity Chromatography (IMAC)

	Column	Buffer A	Buffer B (10, 20, 50, 100%)	Fractions	Peak (mAU)
IMAC	Bio-Scale™ Mini Profinity™ (5 ml)	200 mM Sodium Chloride 50 mM Sodium Phosophate 10 mM ImOH, pH 8	200 mM Sodium Chloride 50 mM Sodium Phosophate 500 mM ImOH, pH 8	8 ml	~ 20 (Fr. 8-9 Fr. 12-13 Fr. 16-17)

Size Exclusion Chromatography (SEC)

	Column	Buffer	Retention volume	Peak (mAU)	Fractions
SEC	Superose HR 12 10/30	300 mM Sodium Chloride 50 mM Sodium Phosophate pH 8	No peak detected	/	2 ml

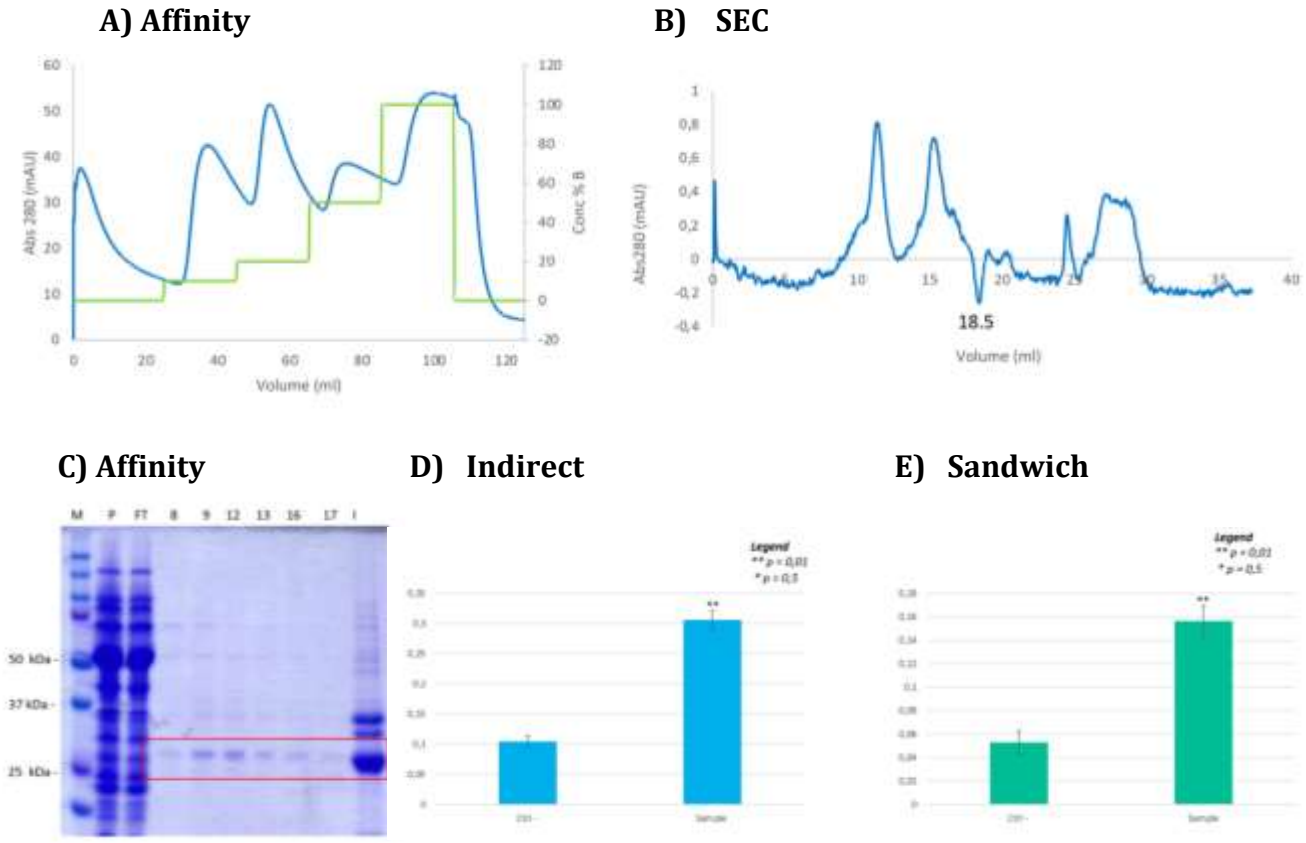

Fig. 4.26 TCAN3 large scale expression in BL21(DE3)+Tig. ***A)*** *Affinity Chromatography (IMAC). Step gradient elution (10%, 20%, 50%, 100%).* ***B)*** *SEC Chromatogram onto Superose HR 12 10/30.* ***C)*** *Coomassie analysis of TCAN3 affinity purification (expected MW 30.4 kDa). 12% Polyacrylamide gel. M= marker; P= Pre-loading; FT = Flow Through; 8,9,12,13,16,17 = eluted fractions, I = insoluble fraction.* ***D)*** *Indirect ELISA. Coating: CD19_Fc, TCAN3 pooled after IMAC: second layer.* ***E)*** *Sandwich ELISA. Coating: TCAN3 (pooled after IMAC). Recombinant CD19_Fc: second layer.*

The insoluble fraction was processed as described in paragraph 3.2.2.3 (Tab 4.19).
Extracted inclusion bodies were purified using affinity chromatography (IMAC) on a nickel-Sepharose column with 100% Buffer B (Fig. 4.27 A). No peak was detected, but eluted fractions 3

and 4 were pooled and analyzed through SDS-PAGE followed by Coomassie staining, revealing a faint band of the expected MW in Fraction 3 (Fig. 4.26, C). Pooled fractions 3 and 4 were purified through SEC, on a Superose HR 12 10/30 column with a clearly visible peak (Fig. 4.27, B, C). An indirect and sandwich ELISAs were performed onto the IMAC eluted fraction 3 in order to test TCAN3 binding capability to the CD19 antigen (Fig. 4.27, D, E). TCAN3 Fr. 3 from IMAC was used, along with CD19_Fc expressed in HEK293T (supernatant, see paragraph 3.2.2.3). The ELISA schemes are reported in paragraph 3.2.5.1, apart from the blocking solution for the indirect setting, where 5% MPBS 5% was used instead of 2% BSA. The ELISAs results were not significant ($p > 0.05$), despite showing a slight positivity.

CF19_Fc (EXCELL crude supernatant) and TCAN3 (Fr. 12,13,14 pool from SEC purification) were incubated at 37 °C for 10 minutes in a 1:1 molar ratio and then loaded onto Superose HR 12 10/30 column, in order to investigate TCAN3 complex formation and hence folding and binding capability. The elution profile confirmed the presence of both CD19_Fc and TCAN3, but separated, suggesting that the binding did not occur (Fig. 4.27, F).

Table 4.19 TCAN3 ncIBs in *E. coli* BL21(DE3) + Tig

	Strain (*E. coli*)	Volume	T	hrs	Sampling (hrs)
Induction	BL21(DE3) + Tig	3 L	17 °C	24	24

Affinity Chromatography (IMAC)

	Column	Volume	Buffer A	Buffer B (100%)	Fractions	Peak (mAU)
IMAC	Bio-Scale™ Mini Profinity™ (5 ml)	1,5 L	**RA Buffer** 300 mM Sodium, 50 mM Tris-HCl, pH 8	300 mM Sodium, 50 mM Tris-HCl, 500 mM ImOH, pH 8	8 ml	No peak (Fr. 3,4)

Size Exclusion Chromatography (SEC)

	Column	Buffer	Retention volume	Peak (mAU)	Fractions	
SEC	Superose HR 12 10/30	PBS pH 7.4	18.18	8.231	2 ml	12,13,14

A) Affinity

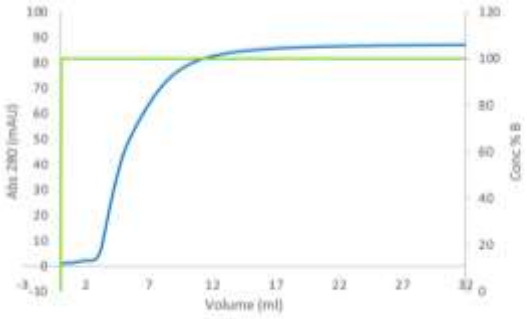

B) SEC

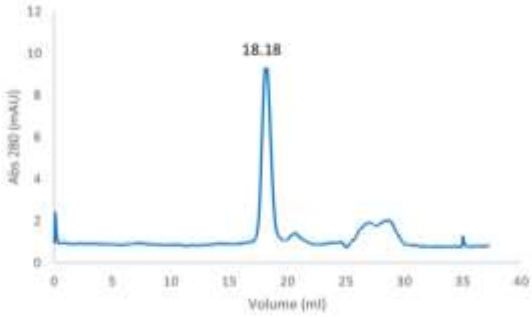

C) Affinity

D) Indirect

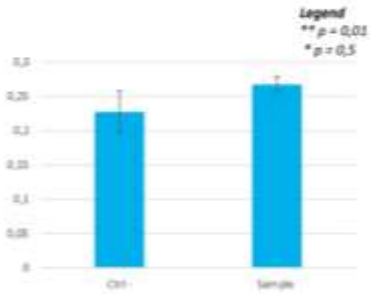

E) Sandwich

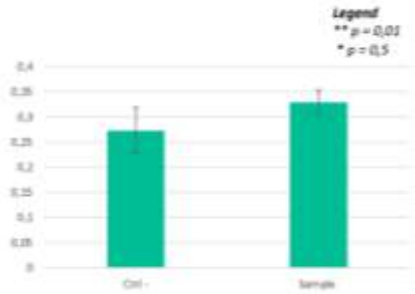

F) SEC

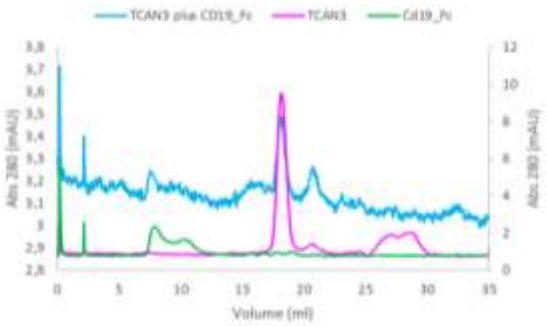

Fig. 4.27 TCAN3 ncIBs in BL21(DE3) +Tig. A) *Affinity Chromatography (IMAC).* ***B)*** *SEC Chromatogram on Superose HR 12 10/30.* ***C)*** *Coomassie analysis of TCAN3 affinity purification (expected MW 30.4 kDa). 12% Polyacrylamide gel. M= marker; P= Pre-loading; FT = Flow Through; 3, 4 = eluted fractions.* ***D)*** *Indirect ELISA. Coating: CD19_Fc, TCAN3 Fr. 3 (IMAC): second layer.* ***E)*** *Sandwich ELISA. Coating: TCAN3 (Fr. 3 IMAC). Recombinant CD19_Fc: second layer.* ***F)*** *SEC Chromatogram on Superose HR 12 10/30 of CD19_Fc added with TCAN3 (Fr. 3 IMAC) and incubated at 37 °C (10 min). Left axis: TCAN3 plus CD19_Fc absorbance; Right axis: TCAN3 alone and CD19_Fc alone absorbance.*

Considering these results, a third large scale expression was induced as described in paragraph 3.2.2.3 (Tab. 4.20), in order to confirm the positive results obtained for the soluble fraction and better investigate the negative ones obtained with the inclusion bodies.
The soluble fraction was purified using affinity chromatography (IMAC) on a nickel-Sepharose column and peaks were detected at 10%, 20%, and 50% Buffer B (Fig. 4.28 A). Eluted fractions were pooled and analyzed through SDS-PAGE followed by Coomassie staining (Fig. 4.28, C), which showed the presence of a faint band at the expected MW in fraction eluted at 10 % and 20 % of Buffer B. Pooled fractions were purified through SEC, on Superose HR 12 10/30 column with no clear detected peak at the expected volume (~18 ml) (Fig. 4.28, B). Fractions 8, 9, 10 from SEC purification were analyzed through SDS-PAGE followed by Coomassie staining, confirming that no band was visible (Fig. 4.28, D). For the indirect and sandwich ELISAs (Fig. 4.28, E, F), TCAN3 from the pooled eluted fractions from IMAC was used, along with CD19_Fc expressed in HEK293T (supernatant, see paragraph 3.2.2.3). The ELISA schemes are reported in paragraph 3.2.5.1. The results showed again a significant positive binding for the soluble fraction (indirect:$p < 0.05$; sandwich: $p < 0.01$)

Table 4.20 TCAN3 large scale expression in *E. coli* BL21(DE3) + Tig

	Strain (*E. coli*)	IPTG	Volume	T	hrs
Induction	BL21(DE3) + Tig	0.4 mM	2 L	18 °C	24

Affinity Chromatography (IMAC)

	Column	Buffer A	Buffer B (10, 20, 50, 100%)	Fractions	Peak (mAU)
IMAC	Bio-Scale™ Mini Profinity™ (5 ml)	200 mM Sodium Chloride 50 mM Sodium Phosophate 10 mM ImOH, pH 8	200 mM Sodium Chloride 50 mM Sodium Phosophate 500 mM ImOH, pH 8	8 ml	~ 20 (Fr. 8-9 Fr. 12-13 Fr. 16-17)

Size Exclusion Chromatography (SEC)

	Column	Buffer	Retention volume	Peak (mAU)	Fractions
SEC	Superose HR 12 10/30	300 mM Sodium Chloride 50 mM Sodium Phosophate pH 8	No peak detected	/	2 ml

A) Affinity

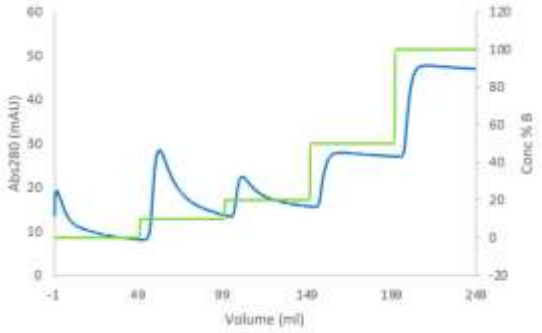

B) SEC

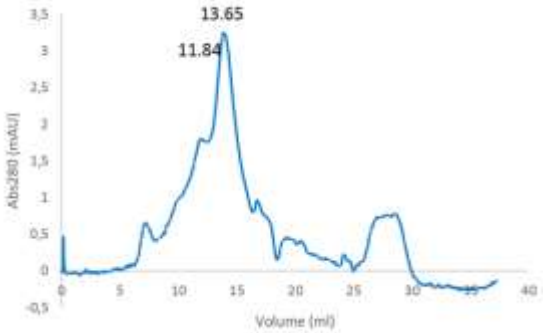

C) Affinity

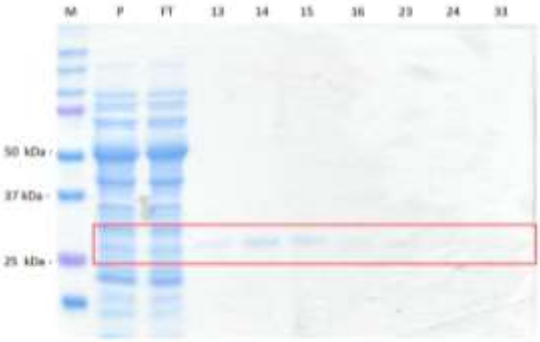

D) SEC

E) Indirect

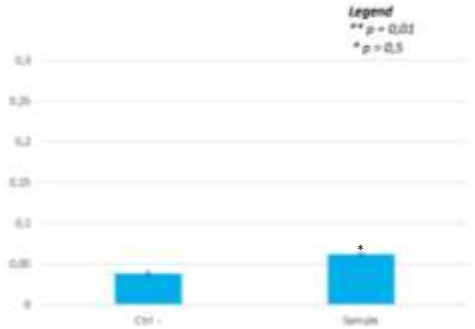

F) Sandwich

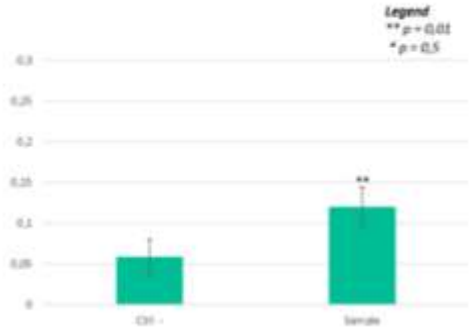

Fig. 4.28 TCAN3 large scale expression in BL21(DE3) +Tig. A) *Affinity Chromatography (IMAC). Step gradient elution (10%, 20%, 50%, 100%).* ***B)*** *SEC Chromatogram onto Superose HR 12 10/30.* ***C)*** *Coomassie analysis of TCAN3 affinity purification (expected MW 30.4 kDa). 12% Polyacrylamide gel. M= marker; P= Pre-loading; FT = Flow Through; 13, 14, 15, 16, 23, 24, 33 = eluted fractions.* ***D)*** *Coomassie analysis of TCAN3 SEC purification (expected MW 30.4 kDa). 12% Polyacrylamide gel. M= marker; P= Pre-loading; FT = Flow Through; 8, 9, 10 = eluted fractions.* ***E)*** *Indirect ELISA. Coating: CD19_Fc. TCAN3 pooled after IMAC: second layer.* ***E)*** *Sandwich ELISA. Coating: TCAN3 (pooled after IMAC). Recombinant CD19_Fc: second layer.*

The insoluble fraction was processed as described in paragraph 3.2.2.3. (Tab 4.21)

Extracted inclusion bodies were purified using affinity chromatography (IMAC) on a nickel-Sepharose column with 100% Buffer B (Fig. 4.29 A). A peak of ~55 kDa was detected, and eluted fractions 2 and 3 were analyzed through SDS-PAGE followed by Coomassie staining, revealing the protein presence in Fraction 2 (Fig. 4.29, C). Fraction 2 was further purified through SEC, on a Superose HR 12 10/30 column, with no peak visible (Fig. 4.29, B). An indirect and sandwich ELISA on the IMAC eluted fraction 3 (Fig. 4.29, D, E) showed that the protein was significantly positive for the binding of CD19 antigen only in the sandwich assay.

Table 4.21 TCAN3 ncIBs in *E. coli* BL21(DE3) + Tig

	Strain (*E. coli*)	Volume	T	hrs
Induction	BL21(DE3) + Tig	2 L	18 °C	24

Affinity Chromatography (IMAC)

	Column	Volume	Buffer A	Buffer B (100%)	Fractions	Peak (mAU)
IMAC	Bio-Scale™ Mini Profinity™ (5 ml)	1,5 L	**RA Buffer** 300 mM Sodium, 50 mM Tris-HCl, pH 8	300 mM Sodium, 50 mM Tris-HCl, 500 mM ImOH, pH 8	8 ml	55 (Fr. 2,3)

Size Exclusion Chromatography (SEC)

	Column	Buffer	Retention volume	Peak (mAU)	Fractions
SEC	Superose HR 12 10/30	PBS pH 7.4	No peak detected	/	2 ml

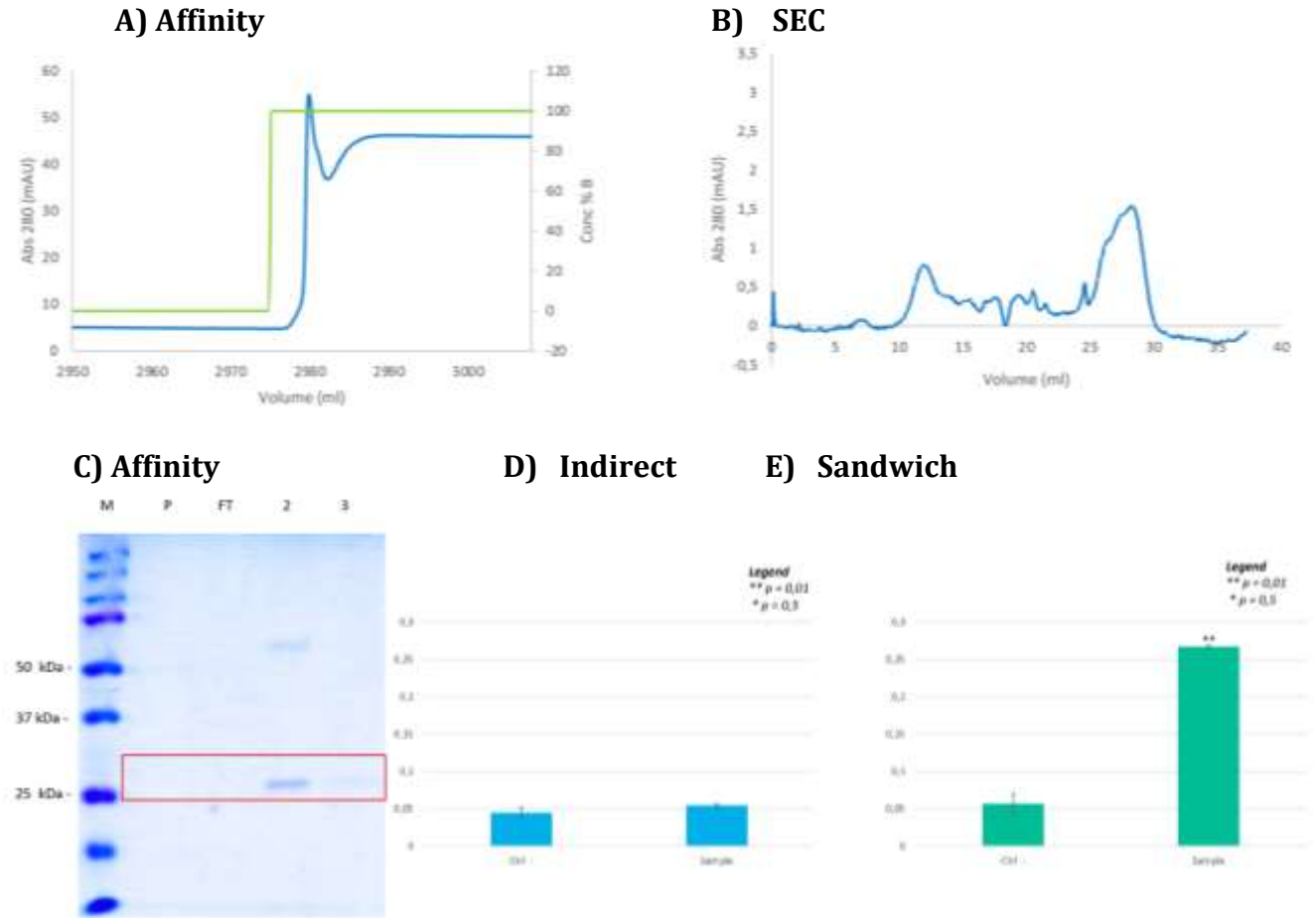

Fig. 4.29 TCAN3 ncIBs in BL21(DE3) +Tig. A) *Affinity Chromatography (IMAC) 100%).* ***B)*** *SEC Chromatogram onto Superose HR 12 10/30.* ***C)*** *Coomassie analysis of TCAN3 affinity purification (expected MW 30.4 kDa). 12% Polyacrylamide gel. M= marker; P= Pre-loading; FT = Flow Through;*

2, 3 = eluted fractions. ***D)*** *Indirect ELISA. CD19_Fc coating, TCAN3 Fr. 2 (IMAC) tested.* ***E)*** *Sandwich ELISA. TCAN3 coating (Fr. 2 IMAC). Recombinant CD19_Fc tested.*

4.4 Part IV: ADC internalization

4.4.1 Preliminary tests

4.4.1.1 Set up in adherent cells (HEK293T)

HEK293T cells were chosen as adherent positive control in order to set up the staining and the protocol for internalization experiments. In order to express CD19, HEK293T were transfected in small scale with CD19fl (full-length) imported by OriGene (Fig. 4.30) The pictures show that the anti-CD19 (HD37) antibody was able to detect the CD19 full length expressed on the transfected cell surface (Fig 4.30 ii, green), as expected, and not on negative controls (Fig. 4.30 i). An anti-LAMP-2 antibody was also tested, as internalization is expected to involve lysosomes. Also in this case, the antibody was able to detect the lysosomes, as expected (Fig. 4.30 iii). Images were acquired using confocal microscopy (STED Leica TCS SP8 WLL STEDONE Flexible Supply Unit WLL).

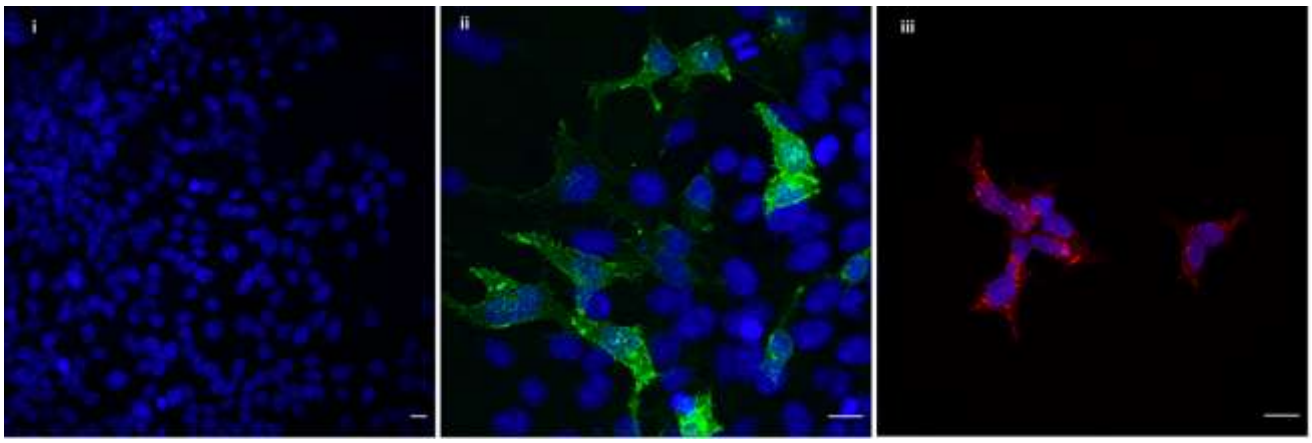

Fig. 4.30 CD19 and lysosome staining in HEK293T. *HEK293T transiently transfected with CD19 full length. Nuclei staining (blue):* Hoechst 33258. ***i) negative control*** *(non-transfected HEK293T) Primary Ab: anti CD19 (HD37) (Merck Millipore), 1:100; Secondary Ab: anti-mouse AlexaFluor488 (Invitrogen), 1:100; scale bar: 15 µm (40x magnification).* ***ii) CD19_Fc staining (green)*** *Primary Ab: anti CD19 (HD37) (Merck Millipore), 1:100; Secondary Ab: anti-mouse AlexaFluor488 (Invitrogen); scale bar: 15 µm (63x magnification).* ***iii) Lysosomes staining (red)*** *1:100anti-LAMP2 (H4B4) (Invitrogen), 1:100; Secondary Ab: 1:100 anti-mouse DyLight 594 (Invitrogen); scale bar: 15 µm (63x magnification).*

For internalization studies, HEK293T cells were transfected as described in paragraph 3.2.2.2, and then cells were incubated with commercial anti-CD19 (HD37) antibody for 10 min, 30 min, and 90 min, respectively, [465–467] before the staining, as described in paragraph 3.2.9. Fig. 4.31 suggests that CD19 is internalized after the incubation with the CD19 antibody, but this has to be confirmed with lysosome colocalization.

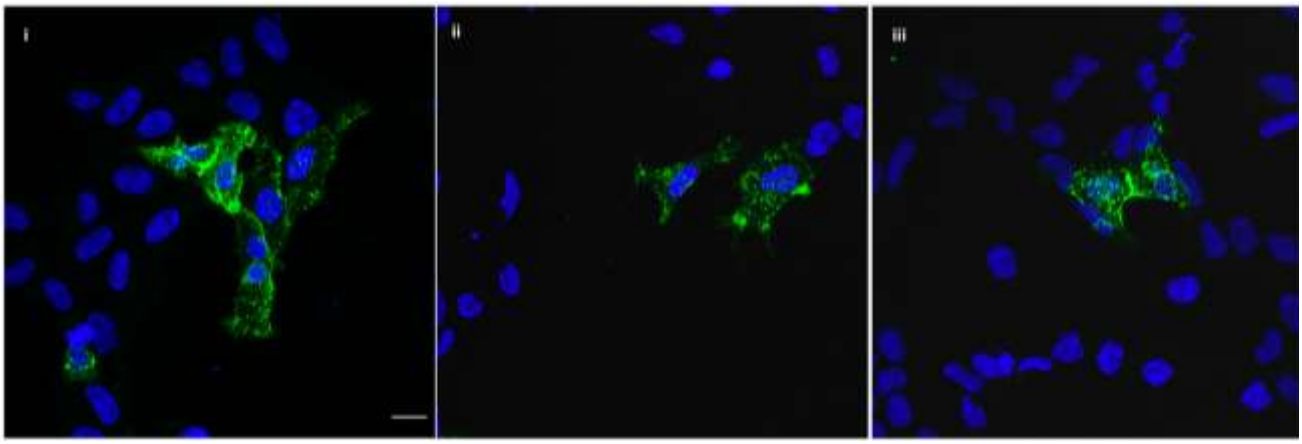

Fig. 4.31 CD19 internalization set up in HEK293T. *HEK293T transiently transfected with CD19 full length.* ***CD19 staining (green). I)*** *Incubation with anti-CD19: 10 min. Primary Ab: anti CD19 (HD37) (Merck Millipore), 1:100; Secondary Ab: anti-mouse AlexaFluor488 (Invitrogen), 1:100; scale bar: 15 µm (63x magnification).* ***ii)*** *Incubation with anti-CD19: 30 min. Primary Ab: anti-LAMP2 (H4B4) (Invitrogen), 1:100; Secondary Ab: 1:100 anti-mouse DyLight 594 (Invitrogen).* ***iii)*** *Incubation with anti-CD19: 1 h. Primary Ab: anti-LAMP2 (H4B4) (Invitrogen), 1:100; Secondary Ab: 1:100 anti-mouse DyLight 594 (Invitrogen).*

4.4.1.1 Set up in suspension cells (RAJI)

In order to study CD19 internalization, RAJI leukemic cells were used. Several optimizations set up were performed (Tab. 4.22). The best staining results were obtained performing the staining onto coverslips previously coated with poly-lysine, as showed in Fig. 4.32, where the membrane localization of CD19 is clearly visible (i). However, the results were not sufficiently satisfactory to proceed with an internalization experiment and further staining optimization has to be pursued.

Table 4.22 Leukemic cells staining set up

IF procedure	Adhesion strategy	Antibodies
Staining on coverslips	Poly-Lysine	anti-CD19, anti-LAMP2
Staining in suspension	Poly-Lysine	anti-CD19, anti-LAMP2
	Low-melting Temperature Agarose	anti-CD19, anti-LAMP2

A)

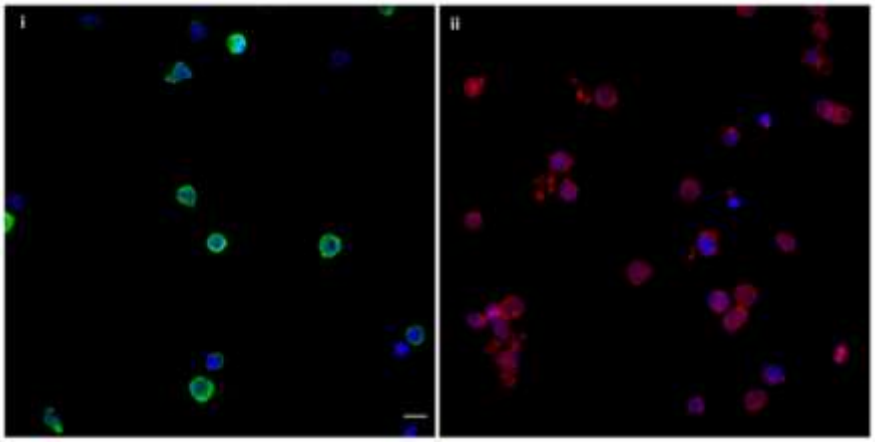

B)

C)

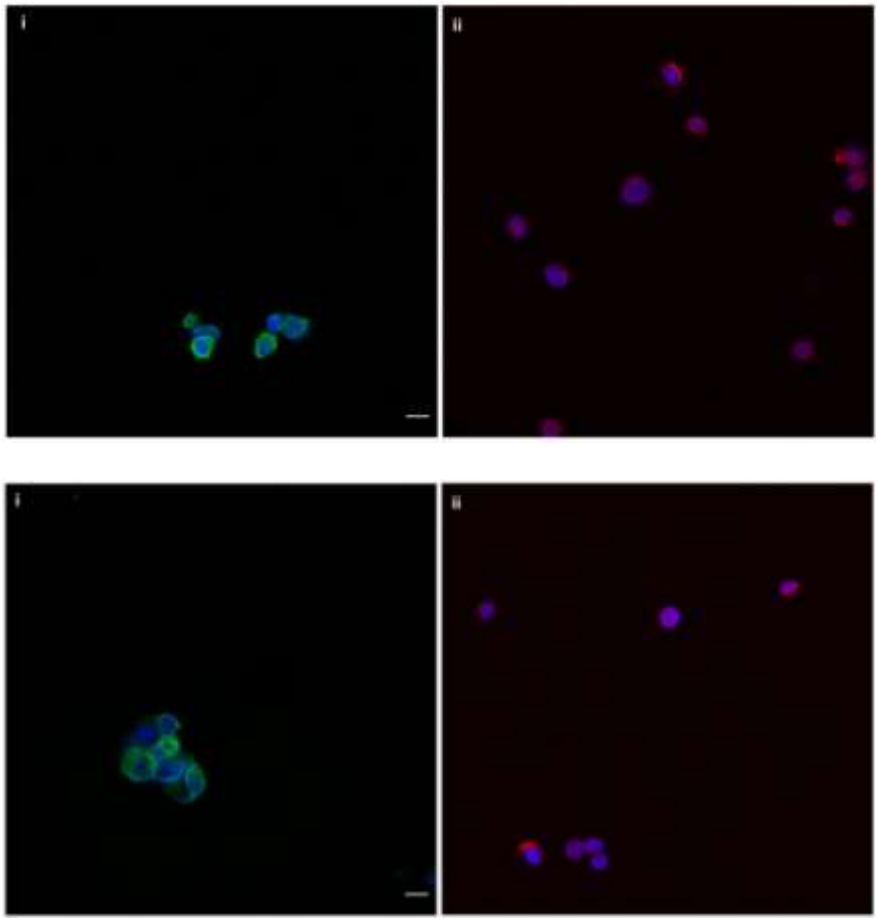

Fig. 4.32 CD19 and lysosome staining in RAJI. CD19 staining (green), Lysosomes staining (red) of RAJI cells. A) *Staining on coverslips, adhesion on poly-lysine* ***i)*** *Primary Ab: anti CD19 (HD37) (Merck Millipore), 1:100; Secondary Ab: anti-mouse AlexaFluor488 (Invitrogen);* ***ii)*** *Primary Ab: anti-LAMP2 (H4B4) (Invitrogen), 1:100; Secondary Ab: anti-mouse DyLight 594 (Invitrogen), 1:100.* ***B)*** *Staining in suspension, adhesion on poly-lysine.* ***i)*** *Primary Ab: anti CD19 (HD37) (Merck Millipore), 1:100; Secondary Ab: anti-mouse AlexaFluor488 (Invitrogen);* ***ii)*** *Primary Ab: anti-LAMP2 (H4B4) (Invitrogen), 1:100; Secondary Ab: anti-mouse DyLight 594 (Invitrogen), 1:100.* ***C)*** *Staining in suspension, adhesion with LMT Agarose.* ***i)*** *Primary Ab: anti CD19 (HD37) (Merck Millipore), 1:100; Secondary Ab: anti-mouse AlexaFluor488 (Invitrogen);* ***ii)*** *Primary Ab: anti-LAMP2 (H4B4) (Invitrogen), 1:100; Secondary Ab: anti-mouse DyLight 594 (Invitrogen), 1:100.*

4.4.1.1 Nanolive cells 3D explorer

Another strategy used to investigate CD19 internalization in leukemic cells was the set up of an experiment in RAJI cells, immobilized with poly-Lysine on ibidi 35 mm glass bottom petri, and observed with the Nanolive cells 3D explorer (paragraph 3.2.10). RAJI cells were observed in time-lapse for 20 min without stimuli. Then, anti-CD19(HD37) (Merck Millipore, 1:100) was added, and cells were observed for 90 min, in order to monitor a potential increase in endocytosis upon CD19 antigen binding.

As showed in Fig. 4.32, despite the great quality of the obtained images, cells immobilization resulted to be too weak, with high cell mobility observed in the microscope field. This prevented to draw clear conclusions regarding the potential increase of endocytosis.

A) Before stimulus with anti-CD19

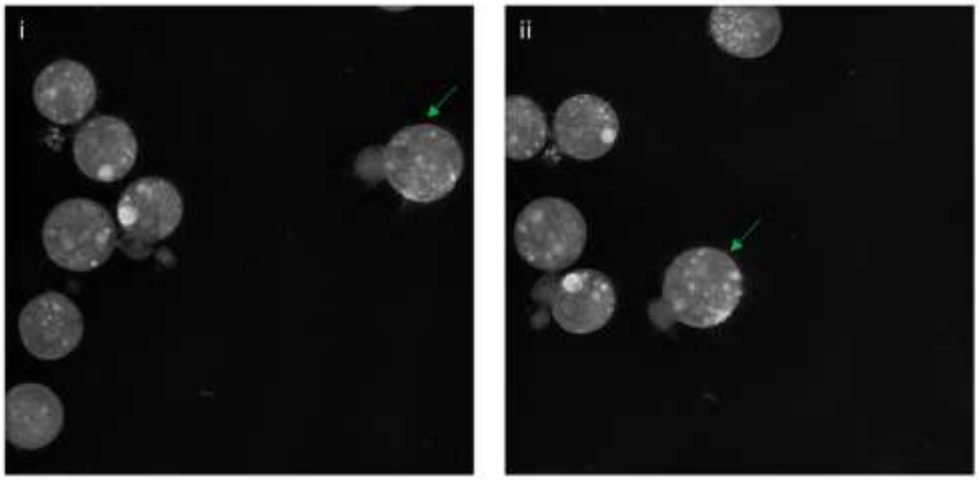

B) After stimulus with anti-CD19

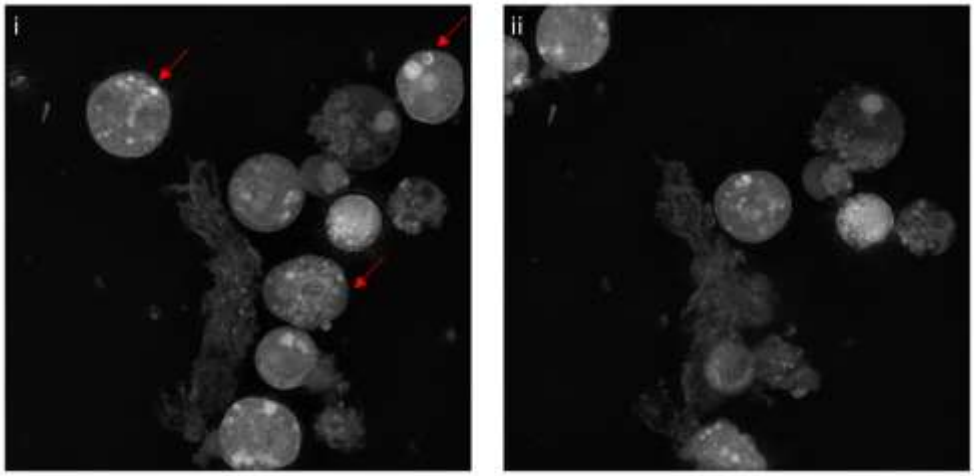

Fig. 4.32 Nanolive cells 3D explorer, RAJI cells treatment with anti-CD19. *RAJI cells treatment with anti-CD19 (HD37) (Merck Millipore, 1:100).* ***A)*** *Before the addition with anti-CD19 (stimulus).* ***i:*** *time lapse frame at 0 min;* ***ii****: time lapse frame after 20 min. Green arrows: example of cell movement from the first time-frame to the last one* ***B)*** *After stimulus.* ***i****: time lapse frame at 0 min;* ***ii****: time lapse frame after 90 min. Red arrows: cells visible only in the first time frame and lost in the second.*

5. Discussion

L-Asparaginase (**ASNase,** EC 3.5.1.1) is an amidohydrolase with prevalent asparaginolytic activity and lower glutaminolytic activity. ASNase represents a crucial component of the combined chemotherapy used for the treatment of pediatric acute lymphoblastic leukemia, having significantly increased complete remissions in patients since its introduction in 1970s.[66] Extensive clinical data support the benefits of ASNase therapy, [32,76,166] as well as the correlation between resistance to ASNase treatment and a poor prognosis.[167–170]
Currently, ASNase molecules used in the clinics derive from either *E. coli* or *E. chrysanthemi*, with the first line drug being PEG-Asparaginase (Oncaspar ®),[81] a pegylated formulation of *E. coli* ASNase, which shows longer half-life and peak of activity[79] compared to native *E. coli* and *E. chrysanthemi* molecules. ASNase therapeutic benefit comes from the depletion of asparagine from the blood stream, on which leukemic cells depends, given their absent or compromised capability to express asparagine synthetase (EC 6.3.5.4) under stress conditions.[66]
Nonetheless, several drawbacks remain in the therapeutic use of the currently available ASNase formulations, and in particular:

- high toxicity, due to its untargeted activity;
- high immunogenicity, due to its bacterial origin and large size;
- short blood serum half-life;
- poor efficacy in specific sub-classes of patients (high risk).

The aim of this thesis was to address these limitations, in order to improve EcAII efficacy, and in particular:
1) its high toxicity, by targeting the drug onto leukemic cells;
2) its high immunogenicity, by miniaturizing the drug.
Hopefully, tackling these two points could also help to increase the drug efficacy in the treatment of high-risk patients.

The adopted strategy consisted in the design of an Asparaginase-based Antibody Drug Conjugate (ADC), composed of the following units: 1) a ***targeting moiety***, represented by a nanobody with binding capability towards properly chosen target receptors (CD19 and CD20); 2) a ***catalytic moiety***, represented by a *catalytic nanobody* with asparaginolytic activity, which was previously obtained in our laboratory by transferring EcAII catalytic residues onto a llama nanobody backbone, using refined protein engineering (PATENT #E0115946).

Specifically, the main focus of my work was the selection, production, and characterization of the *targeting moiety*, with the final goal being the cloning, expression and characterization of the whole ADC molecule. As a consequence, the setting up of preliminary tests and techniques necessary to follow ADC internalization into cells was also pursued.

5.1 Recombinant CD19 production

The choice of CD19 as the main target receptor for our purpose was based on extended data available in the literature. Firstly, it is a transmembrane receptor expressed throughout the whole differentiation process of B cells and also on memory B cells, but not on differentiated plasma cells. [250,251] Secondly, CD19 is able to efficiently drive receptor-mediated endocytosis, which is considered an important feature for a receptor to be chosen as the target during an ADC design.[465–467,472,473] Moreover, successfully approved CD19-targeted therapies, such as BiTEs and CAR-Ts, confirm that CD19 works as a valuable target receptor for B-cell malignancies.[251]

In order to obtain a suitable amount of recombinant CD19 to be used for the selection of anti-CD19 antibodies through Phage Display, three recombinant CD19 constructs were tested for expression: two previously cloned in our laboratory and one cloned *de novo*.

Human CD19 is a 95 kDa transmembrane receptor and the expression constructs were designed including exons from 1 to 4,[474] in order to produce the extracellular domain of CD19 (CD19EC). Two of them were engineered in a C-terminal fusion form with the human Fc fragment in order to possibly facilitate protein stability and solubility.[475]
The CD19EC complex structure, along with the presence of crucial post-translational modifications, made mammalian cells the most suitable choice for protein expression.[476]
Expression of the CD19EC alone was impossible to obtain in mid-scale expression, probably due to protein instability, as suggested by CD19EC peculiar conformation. For these reasons, a major effort was focused on the two hFc-fusion constructs.
The His-tagged, hFc-fusion construct was expressed at mid-scale and resulted to be stable when stored at -80 °C up to 1 month. However, the obtained low protein yield was not suitable for our aims. Moreover, in order to use CD19EC for Phage Display screening, the production of Fc-free CD19EC alone was necessary. To avoid saturation of clones reactive towards the Fc domain, a hFc-fusion protein was also specifically designed without an N-terminal His tag, in order to allow the removal of the hFc fragment, when needed, by cutting it with a His-tagged TEV followed by subsequent purification of the CD19EC by IMAC.
This last construct was successfully produced in mid-scale and large-scale in both roller bottles and triple-flasks, but, again, it was impossible to obtain a suitable yield, due to protein loss upon purification. It was therefore decided to produce CD19_Fc and store it in crude EX CELL supernatant, where it proved to be folded and stable, and use it for characterization tests, such as ELISA tests, while looking for alternative selection strategies, which will not require to produce the recombinant purified target receptor for the screening procedure.

5.2 Recombinant CD20 production

Despite its inability to drive receptor-mediated endocytosis,[280,297] CD20 antigen was selected as the second target receptor, since it is considered a major target in hematological malignancies, being the B-lineage restricted antigen targeted by Rituximab, the first effective anti-cancer monoclonal antibody to be ever developed.
CD20 is a non-glycosylated membrane phosphoprotein which crosses the plasmatic membrane four times and presents two extracellular regions: a small (79-84) and a large loop (142-188). The large loop is the only one involved in known mAb interactions, presenting two residues (Ala170 and Pro 172), which are crucial for the binding to occur.[285]

Two constructs were therefore designed in order to express the CD20 large loop, which also corresponds to the Rituximab epitope.[300] Both of them were designed with a C-terminal His tag, in order to facilitate protein detection and purification.

Both constructs resulted to be expressed only in the insoluble fraction of *E. coli* BL21(DE3) in small-scale experiments, despite the several different growth conditions tested (growth temperature, concentration of inducer, and induction time). The formation of a high amount of aggregated protein, called inclusion bodies, is not unusual in *E. coli* overexpression systems.[477]
Since inclusion bodies contain relatively pure and intact recombinant proteins, several approaches that allow their recovery as biologically active folded protein exist. In particular, in this work it was decided to try to recover the insoluble protein using two procedures.
The first one is known as classical inclusion bodies (cIBs), where the accumulated protein is partially or fully unfolded, and can be therefore extracted by full denaturation operated by a denaturing agent (i.e., urea or guanidine chloride).[478] These chemical reagents lead to a decrease

of non-covalent interactions between proteins molecules, causing protein denaturation by the chaotropic effect at high concentrations. In contrast, a stabilization of the protein structure is observed when they are present at low concentrations, leading to the inhibition of protein aggregation during the refolding step, which is needed after extraction, in order to obtain a biologically active protein.
The second procedure that was used is known as non-classic inclusion bodies (ncIBs), where the expression is performed at low temperatures (17-20°C), in order to allow the aggregation of fully folded and functional protein into vesicles.[478] In this case, protein extraction does not require protein-denaturation, and is instead mediated by a high-arginine concentration buffer. The addition of arginine hydrochloride (ArgHCl) or arginine (Arg) to the refolding buffer has been reported to improve protein solubility and to inhibit protein aggregation.[479–481]

Therefore, large-scale experiments were performed for both CD20 encoding constructs using protocols for the expression and purification of classical inclusion bodies (cIBs) and non-classical inclusion bodies (ncIBs). The best results were obtained using the first construct, encoding the whole CD20 large extracellular loop from (141-188 aa), using the cIBs expression procedure, which is characterized by an induction at higher temperature (25-37°C), and by a denaturation of the protein accumulated in the inclusion bodies followed by a refolding step. This construct, in fact, resulted to be better expressed at a high temperature of induction (25°C) already in small-scale, a trend which was then confirmed in large scale. The characterization of this recombinant CD20 construct through functional tests still needs to be performed.

5.3 Nanobody selection through Phage Display

Since its introduction in 1985, which earned the Nobel price to its inventors George P. Smith and Sir Gregory P. Winter in 2017, different antibody formats have been used for the construction of phage antibody libraries, such as fragments antigen binding antibodies (Fabs), diabodies (bivalent scFv) and single chain variable fragment (scFv). In most recent times, the interest towards nanobodies, such as variable domains of heavy chains from camelid and shark antibodies (VHHs), as well as single heavy-domain human antibody fragments (VHs),[341–344] has significantly grown, and nanobody libraries have also become available for phage display screening.
The growing interest in nanobodies is due to the fact that they show great advantages both in the *production process* and in *clinical applications*. For the *production process*, according to the literature, they should to be easily expressed in bacteria and yeasts in a recombinant form,[399] and show a higher conformational stability, due to their simple monomeric structure,[400] with a simpler and less expensive overall production process when compared to the standard monoclonal antibody methods.[407] For *clinical applications*, they should show little to no immunogenicity in humans, due to the high homology of the framework regions with human ones, [411] which for the aim of the project would be a crucial point. Moreover, their small size allows them an easier penetration into intracellular spaces and tissues, [412] along with the ability to pass the blood brain barrier and therefore reach the tissues of the central nervous system, [414,415] which would also be a turning point for the efficacy of ASNase treatment in high-risk or metastatic patients.

For our purposes, it was therefore decided to use the Phage Display technique for the selection of anti-CD19 nanobodies.
A human single domain antibodies (sdAbs) library ($3*10^9$ clones) for phage display was imported from SourceBioscience.[469] Human antibodies were preferred to camelid ones to facilitate the development of clinical applications. In order to set up the technique and to acquire some expertise while working on the expression of CD19, several rounds of selection were performed against EcAII enzyme itself, given its high immunogenicity and stability.

The first biopanning, composed of three rounds of selection, resulted in the isolation of non-producers and aspecific clones, as indicated by the stable enrichment factor and the results of WB and ELISA analyses. This was probably due to a low stringency of the process, especially during the first round of selection.
The efficacy of the selection, in fact, depends on two pivotal parameters: the *stringency* and the *yield*. *Stringency* defines how much the selection of antibodies with higher affinity is favored over antibodies of lower affinity. The *yield* represents instead the amount of phages displaying high affinity antibodies after a round of biopanning. Since the yield of even the highest affinity clones rarely approaches 100% and sharply declines in successive rounds, stringency and yield need to be strictly balanced, especially during the first round of panning. In fact, at this stage, high and low affinity clones are evenly represented in the library, and a too high stringency could result in the loss of potentially high affinity clones. This happens when their yield falls below the one of aspecific isolated phages, which represents a constantly present background.
For the same reason, it is very important that each clone is represented by sufficient numbers of particles in the initial population, in order to avoid the loss of good binders.[339]
Moreover, *direct coating by immunoadsorption* on polystyrene 96-wells plates was chosen as starting strategy for antigen immobilization, due to its higher simplicity and feasibility, but it is known that it could lead to a lower stringency. However, nothing could explain the absence of sdAb production despite the gene presence, which was verified through PCR amplification.

A second biopanning was performed, trying to address stringency and protein production issues. The rounds of selection were increased up to five, as recommended in the protocol troubleshooting in case of binders absence after the selection, to increase the stringency of the process.[469] Moreover, the binding buffer, which is used in a key step of the selection process, was changed to TBS pH 8, following the successful procedure reported in the work of Jafari et al.[470] This second biopanning resulted again in the isolation of aspecific clones, as confirmed by the enrichment factor trend, which stopped increasing after the third round, and by negative ELISA results. However, the isolated clones were able to express and successfully produce the sdAb, as confirmed by WB analysis.

In order to further increase the stringency of the selection, a third biopanning was performed changing the strategy for antigen immobilization, which was performed using a *capture system based on magnetic beads* conjugated to streptavidin, preceeded by antigen biotinylation, following the successful procedure reported in Niccheri et al.[454] Antigen biotinylation was avoided up to this point since it is a challenging procedure, difficult to control, and the antigen over-biotinylation can impair phage binding by shielding antigen epitopes. Moreover, deselection steps must be incorporated into the protocol, in order to avoid the selection of antibodies binding to the beads-conjugate partner.[349] In fact, in order to remove the antibodies in the library pool which could bind to streptavidin, a preliminary selection procedure was performed against streptavidin-magnetic beads alone, before proceeding with the addition of the biotinylated antigen to the displaying phages pool during the first round of selection.
The stringency of the selection successfully increased, as confirmed by the enrichment factor trend, which raised exactly as expected. However, it was still impossible to obtain positive binders when isolated clones were tested in ELISA.
As recommended in the protocol troubleshooting, a Phage ELISA was performed, in order to detect even a small percentage of positive clones in the selected population. The reason why some clones which result to be negative in ELISA turned out to be positive in Phage ELISA, a frequently observed phenomenon, is not totally known, but is probably due to protein solubility issues in the absence of the phage fusion partners.
Eight clones resulted to be positive in Phage ELISA. To investigate solubility issues, these sdAbs were first of all investigated through WB analysis for expression in *E. coli* TG1 in cell supernatant, cell lysate and cytoplasmic insoluble fraction. The absence of protein bands in the insoluble

fraction seemed to confirm that the proteins were soluble, but the visible bands, which were expressed only in the cell lysates and not in the cell supernatants, did not match the expected molecular weight (~15 kDa). The higher MW observed (~ 65 KDa), compatible with the one of the sdAb-pIII coating protein fusion, lead to investigate protein expression issues also in *E. coli* HB2151 cells, which are a non-suppressive amber strain. In fact, given the presence of an amber stop codon in the linker of the fusion protein construct, *E. coli* HB2151 cells can only express the sdAb protein alone. In this case, the protein was not expressed in either cell supernatants, cell lysates or cytoplasmic insoluble fraction. For *E. coli* HB2151, protein expression issues were explained by the presence of several AMBER stop codons in the antibody coding sequences, while for *E. coli* TG1 cells no clear explanation could be found.

5.4 Nanobody selection through Yeast Two Hybrid (IACT)

Given the difficulties encountered in the production of a suitable amount of purified recombinant CD19 and in the effective setting up of the Phage Display on a test antigen, a different strategy for the selection of anti-CD19 nanobodies was searched. In particular, Yeast Two Hybrid IACT technology resulted to be of interest, since it does not require the production of the purified target antigen in order to perform the selection. It is, in fact, sufficient to clone the target receptor as a fusion protein with the lexA binding domain and to express it within yeasts cells. During the screening, the target antigen-lexA fusion protein is referred to as "bait", while the antibodies of the library, which are cloned as fusion proteins with VP16 transcriptional activation domain, are referred to as "preys". If the antibody-target (prey-bait) interaction occurs inside the cell, the transcription of two reporter genes, *his3* and *lacZ*, is activated, allowing the yeast to grow on a Histidine deprived medium and to develop blue color in the presence of X-gal synthetic substrate.[458]

In order to perform the selection, a collaboration with Prof. Cattaneo was established (SNS, Pisa). His research group is expert in IACT technology, and had llama nanobodies libraries available for screening.
A lexA-CD19 construct (bait) was cloned and then I spent some months in Prof. Cattaneo's research group as a visiting student, in order to perform the screening procedure of a VHH naïve llama library (10^6 clones, lama) in L40 *S. cerevisiae* carrying the CD19EC bait.
A first screening procedure was performed in the presence of 1 mM 3AT, a competitive inhibitor of the HIS3 gene product, which can be added into the selective media. In the presence of 3AT, cells are able to grow only if the level of the HIS3 gene product is sufficient to sustain the inhibitory effect of 3AT, that is to produce enough histidine to allow cell survival. Since the level of produced histidine depends on the strength of the bait-prey interaction, increasing concentrations of 3AT can be used to increase the stringency of the selection. All the isolated clones positive to both growth on interactors-selective media and in liquid ß-gal assay resulted to come from the post-doubling procedure, meaning that they were slower in expressing a sufficient level of HIS3 to sustain the inhibitory effect of 3AT, and therefore probably weaker binders. Among them, a single hit was identified (VHH21A), which was also positive when tested in secondary screening.
A second screening procedure was performed without 3AT and without doubling clones, in order to see if other hits could be isolated, but to no avail. The low number of selected hits could be due to the possibility that no anti-human CD19 nanobody was present in the initial llama nanobody pool, as well as to its relatively small size (10^6).

5.5 Anti-CD19 (VHH21A) nanobody production

In order to characterize the selected anti-CD19 llama nanobody (VHH21A), expression and purification of a suitable amount of recombinant protein was needed.

Bacterial cells were selected as expression host according to the literature,[482] in which they are recommended for the expression of camelid nanobodies. In particular, *E. coli* BL21(DE3) were chosen. The recombinant construct was designed with a C-terminal 8xHis-tag in order to facilitate protein detection and purification. The protein resulted to be highly expressed, but unstable, as demonstrated by its expression in the insoluble fraction in small scale experiments.

Three different strategies were therefore adopted in order to achieve suitable levels of recombinant sdAb production: inclusion bodies with the classical procedure (cIBs), inclusion bodies with the non-classical procedure (ncIBs) and optimization of soluble protein expression through the addition of chaperones. In fact, recombinant proteins could often benefit from the assistance of folding modulators, such as chaperone proteins, during expression in *E. coli*. [477]

The first strategy (cIBs) gave promising results, with protein expression obtained in both the denatured and refolded fraction. However, protein expression yield could not be determined, and therefore it was too low for our purposes, along with statistically non-significative results for antigen binding when the purified nanobody was tested in ELISA
Better results, after some process optimization, were obtained with the non-classical inclusion bodies (ncIBs) procedure, where significant binding was observed in ELISA, along with a maximum protein yield of 15 mg/L. However, the protein resulted to be unstable at + 4°C.
The only chaperone which favored the expression of the nanobody in the soluble fraction was the Tig factor, but large-scale experiments gave unsatisfactory results due, again, to protein instability.

In order to better explore protein solubility issues, a 3D model of VHH21A was prepared using Modeller ®.[443] Surface charges were computed to investigate if they could help in explaining such protein instability, but they resulted not to be excessively hydrophobic, preventing the model, at the moment, to help in the design of direct surface point mutations which could favor an increase of the protein solubility.
Despite the issues encountered with the sdAb solubility, the positive data regarding antigen binding were considered to be a sufficient base to proceed with the cloning of the composite TCAN3 molecule for the evaluation of the stability of the whole protein.

5.6 TCAN3 cloning and expression

As mentioned before, a strategy to reduce EcAII high immunogenicity could be to miniaturize the drug, by re-sizing it into a smaller molecule. For this purpose, in the previous years, our research group put a great effort in the rational transfer of *E. coli* type II asparaginase catalytic residues onto a camelid sdAb backbone, which is roughly ten times smaller compared to the EcAII whole molecule. A catalytic nanobody with cytotoxic asparaginolytic activity was obtained, laying the foundations for the invention of a new class of molecules, that were called Targeted Catalytic Antibodies (TCANs) (PATENT#E0115946). TCANs are molecules designed in order to target specific cancer cells through a targeting antibody moiety combined to a catalytic domain. Such molecules are therefore devised to specifically target cancer cells and at the same time show a localized cytotoxic activity onto cancer cells sensitive to metabolic deprivation. Such molecules could therefore be properly designed according to the amino-acid deprivation sensitivity of the cancer type of interest. [142] Moreover, given their targeted cytotoxic activity, they can be considered Antibody-Drug-Conjugates (ADCs).
Given the interest of our group in Acute Lymphoblastic Leukemia (ALL), and in particular in EcAII, a first molecule referred to as TCAN1 was designed. TCAN1 was composed of an N- terminal anti-CD19 scFv antibody, derived from the FMC63 antibody clone, as described in the work of Nicholson et al. [483], as targeting moiety, and of a C-terminal catalytic moiety represented by the catalytic nanobody with asparaginolytic activity described above (PATENT#E0115946). TCAN1

gave very promising results, showing a good specific catalytic activity, positive binding to recombinant CD19 in ELISA and *in vitro* onto Raji cells, as well as *in vitro* cytotoxicity on MOLT-4 cells (unpublished data). However, several issues with protein solubility hampered large scale expression production.
In the attempt to increase protein solubility, a second version of the molecule, referred to as TCAN2, was designed and cloned, switching the catalytic domain at the N-terminus and the targeting domain to the C-terminus. However, protein production resulted to be even less efficient with this second construct.
The final goal of this thesis project, as mentioned above, was therefore to design and clone a third molecule, called TCAN3, with the targeting moiety being represented by the in-house selected anti-CD19 nanobody (replacing the pre-existing scFv), and the asparaginolytic nanobody, representing the catalytic domain.

In BL21(DE3)*ΔansAansB*, small scale experiments highlighted that TCAN3 was mainly expressed in the insoluble fraction, despite a weak signal detected in the soluble fraction, while protein expression was completely absent in *E. coli* BL21(DE3)*ΔansAansB* added with the p-RARE plasmid. A large-scale experiment in optimized conditions confirmed that the protein was, however, not expressed in detectable amounts in the soluble fraction.
The same strategy used for the expression of VHH21A, that is the optimization of soluble protein expression through the addition of chaperones, was then adopted. The Tig factor confirmed to be the only chaperone able to positively impact the expression of the protein also for the TCAN3 molecule. Still, in large-scale experiments performed in the presence of the Tig factor, the yield of the protein resulted to be too low for our production aims and activity studies. However, it was sufficient to confirm the binding capability of the molecule to CD19 in direct and sandwich ELISA tests.
Aiming to reach a higher production yield, the non-classical inclusion bodies procedure was once again explored, with promising results obtained in both Gel Filtration and ELISA.

5.7 ADC internalization: preliminary tests

As a secondary goal, the setup of techniques useful to follow the drug internalization into leukemia cells was also started. In particular, it was decided to focus on the usage of confocal microscopy for colocalization studies within lysosomes.
As reported in many studies, in fact, CD19 is an antigen which is rapidly internalized upon antibody binding, and this phenomenon has already been observed in several leukemic cell lines, such as RAJI, RS4;11, REH.[465–467,472,473]
Some preliminary studies were performed on HEK293T cells, an adherent cell line unsensitive to EcAII treatment, which was therefore chosen as a positive control for the monitoring of receptor internalization via the endocytic pathway. Adherent cells were chosen in order to facilitate the technique set up, since they are more manageable for immunofluorescence manipulation. Since HEK293T cells do not express CD19, they needed to be transiently transfected with full length CD19 48 hrs before the experiments. The chosen time points for internalization monitoring were 10, 30, and 90 minutes after the incubation with the CD19 antibody.[467,472] The obtained images suggest that CD19 is internalized after the incubation with the CD19 antibody, but confirmation with lysosome colocalization still needs to be performed.
Raji cells were chosen among the leukemic cells, given the large amount of data available in the literature regarding CD19 internalization and the availability in house of both CD19 + and CD19 – (KO) Raji cells. Different strategies were tested in order to optimize Raji cell immobilization onto coverslips, and in particular the use of poly-Lysine coated coverslips and the use of Low melting temperature agarose during the mounting step. However, unsatisfactory results were obtained with both strategies.

A preliminary test was then performed onto Raji cells using label-free time-lapse microscopy (Nanolive Explorer ®), in order to investigate if an increased endocytosis uptake could be detected after antibody incubation (90 min). Such technology, which is based on the combination of holography and rotational scanning, allows a label-free time lapse observation of cell organelles and several processes in which they are involved, such as endocytosis. Despite the great quality of the obtained images, high cell mobility was observed in the microscope field, suggesting issues in cells immobilization and preventing to draw clear conclusions regarding the potential increase of endocytosis. This technique could be therefore considered for future developments, but mainly for the observations of adherent cells, such as HEK293T.

Conclusions and future perspectives

In conclusion, in this thesis, a novel anti-CD19 targeted asparaginase-based ADC was produced. Such invention was conceived by our research group after a previous, successful engineering of a sdAb with catalytic asparagynolitic activity, obtained through the rational transfer of *E. coli* type II asparaginase catalytic residues onto a camelid sdAb backbone. The idea to provide the new catalytic nanobody with a targeting domain, represented by another nanobody, led to the generation of the new concept of Targeted Catalytic Nanobodies (TCANs, PATENT# E0115946)). TCANs are molecules designed in order to target specific cancer cells through a targeting nanobody moiety combined to a catalytic domain which carries a specific catalytic activity, implanted onto a nanobody backbone. Such molecules could potentially be designed against any type of cancer which shows sensitivity to a specific amino acid deprivation.

Several steps were followed in order to design and produce the new anti-CD19 targeted asparaginase-based ADC.
Regarding **recombinant antigen production**, the CD19 antigen was cloned and expressed in recombinant form as a C- terminal fusion with the human Fc fragment, and was used for functional tests in the characterization of anti-CD19 nanobodies. The amount of produced purified recombinant CD19 produced, however, was still too low for direct screening applications.
The CD20 antigen was cloned and expressed in recombinant form. Further optimization of the purification process is needed, along with functionality studies, for example with commercially available anti-CD20 antibodies.
For **the selection of targeting nanobodies,** the Phage Display technique was set up in house, allowing to isolate positive clones in Phage ELISA. However, due to obstacles encountered in both recombinant CD19 purification and Phage Display setting, the Yeast Two Hybrid was chosen as an alternative strategy for the screening of anti-CD19 nanobodies, in collaboration with Prof. Antonino Cattaneo (SNS, Pisa). A nanobody was selected with the Yeast Two Hybrid technique, and its binding to the CD19 antigen was confirmed through ELISA tests.
For the **ADC production**, the selected anti-CD19 nanobody was used as a targeting domain for the design of a new Asparaginase-based antibody drug conjugate (TCAN3). The chosen catalytic domain of such molecule was the sdANSase nanobody previously produced in our laboratory (PATENT #E0115946). TCAN3 was expressed and purified, and its binding to CD19 antigen was confirmed through ELISA tests. In the meantime, preliminary tests for **co-localization studies** of CD19 and lysosomes were set up in adherent and leukemic cell lines.

Strategies for further characterization of the TCAN3 binding to CD19 include the use of the Biacore T200 (Ardis Srl), while enzymatic activity will be investigated through the Nessler assay, while working on further optimization of protein production. In the meantime, the set up of co-localization immunofluorescent study on leukemic cells will continue, stimulating CD19 internalization firstly with commercially available antibodies and, then, with the TCAN3 here designed and produced.

In summary, this work contributes a novel approach for the immunotherapy of cancer, focusing for the first time on the building of ADCs specifically tailored onto specific metabolic traits of a given tumor. It perfectly fits, therefore, within the growing field of personalized oncological medicine.

References

1. Campo, E. *et al.* The 2008 WHO classification of lymphoid neoplasms and beyond : evolving concepts and practical applications. **117**, 5019–5033 (2018).
2. Vardiman, J. W. *et al.* The 2008 revision of the World Health Organization (WHO) classification of myeloid neoplasms and acute leukemia : rationale and important changes. **114**, 937–952 (2018).
3. Elaine s. Jaffe, N. lee H. et al. WHO Blood And Lymphoid Organs.pdf. (2001).
4. Amriah Buang. WHO Classification 2016 - Myeloid neoplasms and acute leukemia. *Blood* **2**, 58–71 (2006).
5. Steliarova-Foucher, E. *et al.* International incidence of childhood cancer, 2001–10: a population-based registry study. *Lancet Oncol.* **18**, 719–731 (2017).
6. Tomizawa, D. & Kiyokawa, N. Acute lymphoblastic leukemia. in *Hematological Disorders in Children: Pathogenesis and Treatment* 33–60 (Springer Singapore, 2017). doi:10.1007/978-981-10-3886-0_2.
7. Hunger, S. P. & Mullighan, C. G. Redefining ALL classification: Toward detecting high-risk ALL and implementing precision medicine. *Blood* vol. 125 3977–3987 (2015).
8. Kato, M., Imamura, T., Manabe, A., … Y. H.-B. journal of & 2014, undefined. Prognostic impact of gained chromosomes in high-hyperdiploid childhood acute lymphoblastic leukaemia: a collaborative retrospective study of the Tokyo. *academia.edu*.
9. Mullighan, C. G. *et al.* Outcome of children with hypodiploid ALL treated with risk-directed therapy based on MRD levels. *Blood* vol. 126 2896–2899 (2015).
10. Russell, L. J. *et al.* A novel translocation, t(14;19)(q32;p13), involving IGHand the cytokine receptor for erythropoietin. *Leukemia* **23**, 614–617 (2009).
11. Russell, L. J. *et al.* Deregulated expression of cytokine receptor gene, CRLF2, is involved in lymphoid transformation in B-cell precursor acute lymphoblastic leukemia. *Blood* **114**, 2688–2698 (2009).
12. Aifantis, I., Raetz, E. & Buonamici, S. Molecular pathogenesis of T-cell leukaemia and lymphoma. *Nature Reviews Immunology* vol. 8 380–390 (2008).
13. Bhojwani, D. *et al.* ETV6-RUNX1-positive childhood acute lymphoblastic leukemia: Improved outcome with contemporary therapy. *Leukemia* **26**, 265–270 (2012).
14. Jeha, S. *et al.* Increased risk for CNS relapse in pre-B cell leukemia with the t(1;19)/ TCF3-PBX1. *Leukemia* **23**, 1406–1409 (2009).
15. Meyer, C. *et al.* The MLL recombinome of acute leukemias in 2013. *Leukemia* **27**, 2165–2176 (2013).
16. Koh, K. *et al.* Early use of allogeneic hematopoietic stem cell transplantation for infants with MLL gene-rearrangement-positive acute lymphoblastic leukemia. *Leukemia* **29**, 290–296 (2015).
17. Krivtsov, A. V. & Armstrong, S. A. MLL translocations, histone modifications and leukaemia stem-cell development. *Nature Reviews Cancer* vol. 7 823–833 (2007).
18. Biondi, A. *et al.* Imatinib after induction for treatment of children and adolescents with Philadelphia-chromosome-positive acute lymphoblastic leukaemia (EsPhALL): A randomised, open-label, intergroup study. *Lancet Oncol.* **13**, 936–945 (2012).
19. Schultz, K. R. *et al.* Long-term follow-up of imatinib in pediatric Philadelphia chromosome-positive acute lymphoblastic leukemia: Children's oncology group study AALL0031. *Leukemia* **28**, 1467–1471 (2014).
20. Manabe, A. *et al.* Imatinib use immediately before stem cell transplantation in children with Philadelphia chromosome-positive acute lymphoblastic leukemia: Results from Japanese Pediatric Leukemia/Lymphoma Study Group (JPLSG) Study Ph + ALL04. *Cancer Med.* **4**, 682–689 (2015).
21. Schultz, K. R. *et al.* Improved early event-free survival with imatinib in Philadelphia chromosome - Positive acute lymphoblastic leukemia: A Children's Oncology Group Study.

J. Clin. Oncol. **27**, 5175–5181 (2009).
22. Mullighan, C. G. *et al.* Genome-wide analysis of genetic alterations in acute lymphoblastic leukaemia. *Nature* vol. 446 758–764 (2007).
23. Mullighan, C. G. *et al.* CREBBP mutations in relapsed acute lymphoblastic leukaemia. *Nature* **471**, 235–241 (2011).
24. Hof, J., Groeneveld-Krentz, S. & Shalapour, S. Mutations and Deletions of the TP53 Gene Predict Nonresponse to Treatment and Poor Outcome in First Relapse of Childhood Acute Lymphoblastic Leukemia. *Artic. J. Clin. Oncol.* (2011) doi:10.1200/JCO.2011.34.8144.
25. Buitenkamp, T. D. *et al.* Acute lymphoblastic leukemia in children with Down syndrome: A retrospective analysis from the Ponte di Legno study group. *Blood* **123**, 70–77 (2014).
26. Borowitz, M. J. *et al.* Clinical significance of minimal residual disease in childhood acute lymphoblastic leukemia and its relationship to other prognostic factors: A Children's Oncology Group study. *Blood* **111**, 5477–5485 (2008).
27. Chen, X. & Wood, B. L. How do we measure MRD in ALL and how should measurements affect decisions. Re: Treatment and prognosis? *Best Pract. Res. Clin. Haematol.* **30**, 237–248 (2017).
28. Hunger, S. P. & Mullighan, C. G. Acute lymphoblastic leukemia in children. *N. Engl. J. Med.* **373**, 1541–1552 (2015).
29. Pulte, D., Gondos, A. & Brenner, H. Improvement in survival in younger patients with acute lymphoblastic leukemia from the 1980s to the early 21st century. *Blood* **113**, 1408–1411 (2009).
30. Pui, C. H. & Evans, W. E. Treatment of acute lymphoblastic leukemia. *N. Engl. J. Med.* **354**, 166–178 (2006).
31. Lanciotti, M. *et al.* Genetic polymorphism of NAD(P)H:quinone oxidoreductase is associated with an increased risk of infant acute lymphoblastic leukemia without MLL gene rearrangements. *Leukemia* **19**, 214–216 (2005).
32. Silverman, L. B. *et al.* Improved outcome for children with acute lymphoblastic leukemia: Results of Dana-Farber Consortium Protocol 91-01. *Blood* **97**, 1211–1218 (2001).
33. Bürger, B. *et al.* Diagnostic cerebrospinal fluid examination in children with acute lymphoblastic leukemia: significance of low leukocyte counts with blasts or traumatic lumbar puncture. *J. Clin. Oncol.* **21**, 184–8 (2003).
34. Pui, C. H., Robison, L. L. & Look, A. T. Acute lymphoblastic leukaemia. *The Lancet* vol. 371 1030–1043 (2008).
35. Bhatia, S. *et al.* 6MP adherence in a multiracial cohort of children with acute lymphoblastic leukemia: A Children's Oncology Group study. *Blood* **124**, 2345–2353 (2014).
36. Nguyen, K. *et al.* Factors influencing survival after relapse from acute lymphoblastic leukemia: A Children's Oncology Group study. *Leukemia* **22**, 2142–2150 (2008).
37. Aricò, M. *et al.* Clinical outcome of children with newly diagnosed Philadelphia chromosome-positive acute lymphoblastic leukemia treated between 1995 and 2005. *J. Clin. Oncol.* **28**, 4755–4761 (2010).
38. Schrappe, M. *et al.* Editorial: Educational symposium on long-term results of large prospective clinical trials for childhood acute lymphoblastic leukemia (1985-2000). *Leukemia* vol. 24 253–254 (2010).
39. Nachman, J. B. *et al.* Outcome of treatment in children with hypodiploid acute lymphoblastic leukemia. *Blood* **110**, 1112–1115 (2007).
40. Alexander, S. Clinically defining and managing high-risk pediatric patients with acute lymphoblastic leukemia. *Hematology* **2014**, 181–189 (2014).
41. Bhojwani, D., Howard, S. C. & Pui, C. H. High-risk childhood acute lymphoblastic leukemia. *Clinical lymphoma & myeloma* vol. 9 Suppl 3 S222 (2009).
42. Shaikh, F. *et al.* The risk of traumatic lumbar punctures in children with acute lymphoblastic leukaemia. *Eur. J. Cancer* **50**, 1482–1489 (2014).
43. Dutch Childhood Oncology Group *et al.* Prognostic significance of blasts in the cerebrospinal

fluid without pleiocytosis or a traumatic lumbar puncture in children with acute lymphoblastic leukemia: experience of the Dutch Childhood Oncology Group. *J. Clin. Oncol.* **24**, 2332–6 (2006).
44. Mahmoud, H. H. *et al.* Low Leukocyte Counts with Blast Cells in Cerebrospinal Fluid of Children with Newly Diagnosed Acute Lymphoblastic Leukemia. *N. Engl. J. Med.* **329**, 314–319 (1993).
45. Coustan-Smith, E. *et al.* Early T-cell precursor leukaemia: a subtype of very high-risk acute lymphoblastic leukaemia. *Lancet Oncol.* **10**, 147–156 (2009).
46. Holmfeldt, L. *et al.* The genomic landscape of hypodiploid acute lymphoblastic leukemia. *Nat. Genet.* **45**, 242–252 (2013).
47. Mullighan, C. G. *et al.* BCR-ABL1 lymphoblastic leukaemia is characterized by the deletion of Ikaros. *Nature* **453**, 110–114 (2008).
48. Pfeifer, H. *et al.* Kinase domain mutations of BCR-ABL frequently precede imatinib-based therapy and give rise to relapse in patients with de novo Philadelphia-positive acute lymphoblastic leukemia (Ph+ ALL). *Blood* **110**, 727–734 (2007).
49. Den Boer, M. L. *et al.* A subtype of childhood acute lymphoblastic leukaemia with poor treatment outcome: a genome-wide classification study. *Lancet Oncol.* **10**, 125–134 (2009).
50. Van Der Veer, A. *et al.* Independent prognostic value of BCR-ABL1-like signature and IKZF1 deletion, but not high CRLF2 expression, in children with B-cell precursor ALL. *Blood* **122**, 2622–2629 (2013).
51. Harrison, C. J. *et al.* An international study of intrachromosomal amplification of chromosome 21 (iAMP21): Cytogenetic characterization and outcome. *Leukemia* **28**, 1015–1021 (2014).
52. Moorman, A. V. *et al.* Brief report: Prognosis of children with acute lymphoblastic leukemia (ALL) and intrachromosomal amplification of chromosome 21 (iAMP21). *Blood* **109**, 2327–2330 (2007).
53. Schrappe, M. *et al.* Improved outcome in childhood acute lymphoblastic leukemia despite reduced use of anthracyclines and cranial radiotherapy: results of trial ALL-BFM 90. German-Austrian-Swiss ALL-BFM Study Group. *Blood* **95**, 3310–22 (2000).
54. Gaynon, P. S. *et al.* Children's cancer group trials in childhood acute lymphoblastic leukemia: 1983-1995. *Leukemia* **14**, 2223–2233 (2000).
55. Brüggemann, M. *et al.* Clinical significance of minimal residual disease quantification in adult patients with standard-risk acute lymphoblastic leukemia. *Blood* **107**, 1116–1123 (2006).
56. Van Dongen, J. J. M., Van Der Velden, V. H. J., Brüggemann, M. & Orfao, A. Minimal residual disease diagnostics in acute lymphoblastic leukemia: Need for sensitive, fast, and standardized technologies. *Blood* **125**, 3996–4009 (2015).
57. Borowitz, M. J. *et al.* Prognostic significance of minimal residual disease in high risk B-ALL: A report from Children's Oncology Group study AALL0232. *Blood* **126**, 964–971 (2015).
58. Bader, P. & Kreyenberg, H. The EBMT Handbook. *EBMT Handb.* 431–436 (2019) doi:10.1007/978-3-030-02278-5.
59. Bruggemann, M. *et al.* Standardized MRD quantification in European all trials: Proceedings of the second international symposium on MRD assessment in Kiel, Germany, 18-20 September 2008. *Leukemia* vol. 24 521–535 (2010).
60. van der Velden, V. H. J. *et al.* Optimization of PCR-based minimal residual disease diagnostics for childhood acute lymphoblastic leukemia in a multi-center setting. *Leukemia* **21**, 706–713 (2007).
61. Teuffel, O. *et al.* Dexamethasone versus prednisone for induction therapy in childhood acute lymphoblastic leukemia: A systematic review and meta-analysis. *Leukemia* vol. 25 1232–1238 (2011).
62. Silverman, L. B. *et al.* Long-term results of dana-farber cancer institute all consortium protocols for children with newly diagnosed acute lymphoblastic leukemia (1985-2000).

Leukemia **24**, 320–334 (2010).
63. Vora, A. *et al.* Treatment reduction for children and young adults with low-risk acute lymphoblastic leukaemia defined by minimal residual disease (UKALL 2003): A randomised controlled trial. *Lancet Oncol.* **14**, 199–209 (2013).
64. Möricke, A. *et al.* Risk-Adjusted Therapy of Acute Lymphoblastic Leukemia Can Decrease Treatment Burden and Improve Survival: Treatment Results of 2169 Unselected Pediatric and Adolescent Patients Enrolled in the Trial ALL-BFM 95. *Blood* **110**, 584–584 (2007).
65. Chan, W. K. *et al.* The glutaminase activity of L- Asparaginase is not required for anticancer activity against ASNS-negative cells. *Blood* **123**, 3596–3606 (2014).
66. Brumano, L. P. *et al.* Development of L-asparaginase biobetters: Current research status and review of the desirable quality profiles. *Frontiers in Bioengineering and Biotechnology* vol. 6 212 (2019).
67. Covini, D. *et al.* Expanding Targets for a Metabolic Therapy of Cancer: L-Asparaginase. *Recent Pat. Anticancer. Drug Discov.* **7**, 4–13 (2011).
68. Geneva. *Second Meeting of the Subcommittee of the Expert Committee on the Selection and Use of Essential Medicines*.
69. Pui, C.-H. & Evans, W. E. Treatment of Acute Lymphoblastic Leukemia. *N. Engl. J. Med.* **354**, 166–178 (2006).
70. Barba, P., Dapena, J. L., Montesinos, P. & Rives, S. Asparaginase use for the treatment of acute lymphoblastic leukemia. *Med. Clínica (English Ed.* **148**, 225–231 (2017).
71. Duval, M. *et al.* Comparison of Escherichia coli-asparaginase with Erwinia-asparaginase in the treatment of childhood lymphoid malignancies: Results of a randomized European Organisation for Research and Treatment of Cancer - Children's Leukemia Group phase 3 trial. *Blood* **99**, 2734–2739 (2002).
72. Lange, B. J. *et al.* Double-delayed intensification improves event-free survival for children with intermediate-risk acute lymphoblastic leukemia: A report from the Children's Cancer Group. *Blood* **99**, 825–833 (2002).
73. Asselin, B. & Rizzari, C. Asparaginase pharmacokinetics and implications of therapeutic drug monitoring. *Leukemia and Lymphoma* vol. 56 2273–2280 (2015).
74. Boos, J. *et al.* Monitoring of asparaginase activity and asparagine levels in children on different asparaginase preparations. *Eur. J. Cancer Part A* **32**, 1544–1550 (1996).
75. AHLKE, E. *et al.* Dose reduction of asparaginase under pharmacokinetic and pharmacodynamic control during induction therapy in children with acute lymphoblastic leukaemia. *Br. J. Haematol.* **96**, 675–681 (1997).
76. Pession, A. *et al.* Long-term results of a randomized trial on extended use of high dose L-asparaginase for standard risk childhood acute lymphoblastic leukemia. *J. Clin. Oncol.* **23**, 7161–7167 (2005).
77. Asselin, B. L. *et al.* Comparative pharmacokinetic studies of three asparaginase preparations. *J. Clin. Oncol.* **11**, 1780–1786 (1993).
78. CHMP. *ANNEX I SUMMARY OF PRODUCT CHARACTERISTICS_Native E. coli ASNASE, Spectrila*®.
79. CHMP. *ANNEX I SUMMARY OF PRODUCT CHARACTERISTICS, PEGasparaginase, Oncaspar*®.
80. *Public Assessment Report Scientific discussion Erwinase, powder for solution for injection 10,000 IU/vial (crisantaspase) C B G M E B 2/17*. (2015).
81. Li, R. J. *et al.* FDA approval summary: Calaspargase Pegol-mknl for Treatment of Acute Lymphoblastic Leukemia in Children and Young Adults. *Clin. Cancer Res.* **26**, 328–331 (2020).
82. Fda. *ERWINAZE (asparaginase Erwinia chrysanthemi) Label*. www.fda.gov/medwatch.
83. Albertsen, B. K., Jakobsen, P., Schrøder, H., Schmiegelow, K. & Carlsen, N. T. Pharmacokinetics of Erwinia asparaginase after intravenous and intramuscular administration. *Cancer Chemother. Pharmacol.* **48**, 77–82 (2001).
84. Tong, W. H. *et al.* A prospective study on drug monitoring of PEGasparaginase and Erwinia

asparaginase and asparaginase antibodies in pediatric acute lymphoblastic leukemia. *Blood* **123**, 2026–2033 (2014).
85. HO, D. H. W. *et al.* Clinical Pharmacology of Intramuscularly Administered <scp>l</scp> - Asparaginase. *J. Clin. Pharmacol.* **21**, 72–78 (1981).
86. Vieira Pinheiro, J. P. *et al.* Pharmacokinetic dose adjustment of Erwinia asparaginase in protocol II of the paediatric ALL/NHL-BFM treatment protocols. *Br. J. Haematol.* **104**, 313–320 (1999).
87. Schrey, D. *et al.* Therapeutic drug monitoring of asparaginase in the ALL-BFM 2000 protocol between 2000 and 2007. *Pediatr. Blood Cancer* **54**, n/a-n/a (2010).
88. Vrooman, L. M. *et al.* Preliminary Results Of a Pharmacokinetic Study Of Intravenous Asparaginase Erwinia Chrysanthemi Following Allergy To E Coli-Derived Asparaginase In Children, Adolescents, and Young Adults With Acute Lymphoblastic Leukemia Or Lymphoblastic Lymphoma. *Blood* **122**, 3904–3904 (2013).
89. Müller, H. Use of ?-asparaginase in childhood ALL. *Crit. Rev. Oncol. Hematol.* **28**, 97–113 (1998).
90. Panosyan, E. H. *et al.* Asparaginase Antibody and Asparaginase Activity in Children with Higher-Risk Acute Lymphoblastic Leukemia: Children's Cancer Group Study CCG-1961. *J. Pediatr. Hematol. Oncol.* **26**, 217–226 (2004).
91. Willer, A. *et al.* Anti-Escherichia coli asparaginase antibody levels determine the activity of second-line treatment with pegylated E coli asparaginase: A retrospective analysis within theALL-BFM trials. *Blood* **118**, 5774–5782 (2011).
92. Kurtzberg, J. *et al.* Polyethylene glycol-conjugated L-asparaginase versus native L-asparaginase in combination with standard agents for children with acute lymphoblastic leukemia in second bone marrow relapse: A children's Oncology Group Study (POG 8866). *J. Pediatr. Hematol. Oncol.* **33**, 610–616 (2011).
93. Vrooman, L. M. *et al.* Postinduction dexamethasone and individualized dosing of escherichia coli l-asparaginase each improve outcome of children and adolescents with newly diagnosed acute lymphoblastic leukemia: Results from a randomized study - Dana-Farber Cancer Institute ALL Consortium Protocol 00-01. *J. Clin. Oncol.* **31**, 1202–1210 (2013).
94. Albertsen, B. K. *et al.* Comparison of intramuscular therapy with Erwinia asparaginase and asparaginase Medac: pharmacokinetics, pharmacodynamics, formation of antibodies and influence on the coagulation system. *Br. J. Haematol.* **115**, 983–990 (2001).
95. HJ, L. Management and preparedness for infusion and hypersensitivity reactions. *Oncologist* **12**, 601–609 (2007).
96. Hijiya, N. & Van Der Sluis, I. M. Asparaginase-Associated toxicity in children with acute lymphoblastic leukemia. *Leuk. Lymphoma* **57**, 748–757 (2016).
97. Avramis, V. I. *et al.* A randomized comparison of native Escherichia coli asparaginase and polyethylene glycol conjugated asparaginase for treatment of children with newly diagnosed standard-risk acute lymphoblastic leukemia: A Children's Cancer Group study. *Blood* **99**, 1986–1994 (2002).
98. Wang, B. *et al.* Evaluation of immunologic crossreaction of antiasparaginase antibodies in acute lymphoblastic leukemia (ALL) and lymphoma patients. *Leukemia* **17**, 1583–1588 (2003).
99. Liu, C. *et al.* Clinical utility and implications of asparaginase antibodies in acute lymphoblastic leukemia. *Leukemia* **26**, 2303–2309 (2012).
100. Zalewska-Szewczyk, B., Gach, A., Wyka, K., Bodalski, J. & Młynarski, W. The cross-reactivity of anti-asparaginase antibodies against different l-asparaginase preparations. *Clin. Exp. Med.* **9**, 113–116 (2009).
101. Raja, R. A. *et al.* Asparaginase-associated pancreatitis in children with acute lymphoblastic leukaemia in the NOPHO ALL2008 protocol. *Br. J. Haematol.* **165**, 126–133 (2014).
102. Knoderer, H. M., Robarge, J. & Flockhart, D. A. Predicting asparaginase-associated pancreatitis. *Pediatr. Blood Cancer* **49**, 634–639 (2007).

103. Raja, R. A., Schmiegelow, K. & Frandsen, T. L. Asparaginase-associated pancreatitis in children. *Br. J. Haematol.* **159**, 18–27 (2012).
104. Kearney, S. L. *et al.* Clinical course and outcome in children with acute lymphoblastic leukemia and asparaginase-associated pancreatitis. *Pediatr. Blood Cancer* **53**, 162–167 (2009).
105. Samarasinghe, S. *et al.* Incidence and outcome of pancreatitis in children and young adults with acute lymphoblastic leukaemia treated on a contemporary protocol, UKALL 2003. *Br. J. Haematol.* **162**, 710–713 (2013).
106. Treepongkaruna, S. *et al.* Acute Pancreatitis in Children With Acute Lymphoblastic Leukemia After Chemotherapy. *J. Pediatr. Hematol. Oncol.* **31**, 812–815 (2009).
107. Stock, W. *et al.* Prevention and management of asparaginase/pegasparaginase-associated toxicities in adults and older adolescents: Recommendations of an expert panel. *Leuk. Lymphoma* **52**, 2237–2253 (2011).
108. Hernández-Espinosa, D. *et al.* L-asparaginase-induced antithrombin type I deficiency: Implications for conformational diseases. *Am. J. Pathol.* **169**, 142–153 (2006).
109. Mitchell, L. G. *et al.* Effect of disease and chemotherapy on hemostasis in children with acute lymphoid leukemia. *Am. J. Pediatr. Hematol. Oncol.* **16**, 120–126 (1994).
110. Hongo, T. *et al.* Low plasma levels of hemostatic proteins during the induction phase in children with acute lymphoblastic leukemia: A retrospective study by the JACLS. *Pediatr. Int.* **44**, 293–299 (2002).
111. Mitchell, L., Hoogendoorn, H., Giles, A. R., Vegh, P. & Andrew, M. Increased Endogenous Thrombin Generation in Children With Acute Lymphoblastic Leukemia: Risk of Thrombotic Complications in L'Asparaginase-Induced Antithrombin I11 Deficiency. *Blood* (1994).
112. Andrew, M., Brooker, L. & Mitchell, L. Acquired antithrombin III deficiency secondary to asparaginase therapy in childhood acute lymphoblastic leukaemia. *Blood Coagul. Fibrinolysis* **5**, S24-36 (1994).
113. Jaing, T.-H. *et al.* Hyperammonemic Encephalopathy After Induction Chemotherapy for Acute Lymphoblastic Leukemia. *J. Pediatr. Hematol. Oncol.* **31**, 955–956 (2009).
114. Frantzeskaki, F. *et al.* L-asparaginase fatal toxic encephalopathy during consolidation treatment in an adult with acute lymphoblastic leukemia. *Am. J. Case Rep.* **14**, 311–314 (2013).
115. Sudour, H., Schmitt, C., … A. C.-A. journal of & 2011, U. Acute metabolic encephalopathy in two patients treated with asparaginase and ondasetron. *Am. J. Hematol.* **86**, 323–325 (2011).
116. Raetz, E. A. & Salzer, W. L. Tolerability and Efficacy of L-Asparaginase Therapy in Pediatric Patients With Acute Lymphoblastic Leukemia. *J. Pediatr. Hematol. Oncol.* **32**, 554–563 (2010).
117. Howard, S. C. & Pui, C. H. Endocrine complications in pediatric patients with acute lymphoblastic leukemia. *Blood Reviews* vol. 16 225–243 (2002).
118. Carpentieri, U. & Balch, M. T. Hyperglycemia associated with the therapeutic use of l-asparaginase: Possible role of insulin receptors. *J. Pediatr.* **93**, 775–778 (1978).
119. Pui, C. H., Burghen, G. A., Bowman, W. P. & Aur, R. J. A. Risk factors for hyperglycemia in children with leukemia receiving l-asparaginase and prednisone. *J. Pediatr.* **99**, 46–50 (1981).
120. Cremer, P., Lakomek, M., Beck, W. & Prindull, G. The effect of L-asparaginase on lipid metabolism during induction chemotherapy of childhood lymphoblastic leukaemia. *Eur. J. Pediatr.* **147**, 64–67 (1988).
121. Parsons, S. K. *et al.* Asparaginase-associated lipid abnormalities in children with acute lymphoblastic leukemia. *Blood* **89**, 1886–1895 (1997).
122. Salvador, C., Meister, B., Crazzolara, R. & Kropshofer, G. Management of hypertriglyceridemia in children with acute lymphoblastic leukemia under persistent therapy with glucocorticoids and L-asparaginase during induction chemotherapy. *Pediatr.*

Blood Cancer **59**, 771–771 (2012).
123. Douer, D. Is asparaginase a critical component in the treatment of acute lymphoblastic leukemia? *Best Practice and Research: Clinical Haematology* vol. 21 647–658 (2008).
124. Boissel, N. *et al.* Should Adolescents With Acute Lymphoblastic Leukemia Be Treated as Old Children or Young Adults? Comparison of the French FRALLE93 and LALA-94 Trials. *J. Clin. Oncol.* **21**, 774–780 (2003).
125. Stock, W. *et al.* What determines the outcomes for adolescents and young adults with acute lymphoblastic leukemia treated on cooperative group protocols? A comparison of Children's Cancer Group and Cancer and Leukemia Group B studies. *Blood* **112**, 1646–1654 (2008).
126. de Bont, J. M. *et al.* Significant difference in outcome for adolescents with acute lymphoblastic leukemia treated on pediatric vs adult protocols in the Netherlands [1]. *Leukemia* vol. 18 2032–2035 (2004).
127. Hallböök, H., Gustafsson, G., Smedmyr, B., Söderhäll, S. & Heyman, M. Treatment outcome in young adults and children >10 years of age with acute lymphoblastic leukemia in Sweden. *Cancer* **107**, 1551–1561 (2006).
128. Ramanujachar, R. *et al.* Adolescents with acute lymphoblastic leukaemia: Outcome on UK national paediatric (ALL97) and adult (UKALLXII/E2993) trials. *Pediatr. Blood Cancer* **48**, 254–261 (2007).
129. Michalska, K. & Jaskolski, M. Structural aspects of l -asparaginases , their friends and relations *. **53**, 627–640 (2006).
130. Carter, P. & Wells, J. A. Dissecting the catalytic triad of a serine protease. *Nature* **332**, 564–568 (1988).
131. Swain, A. L., Jaskolski, M., Housset, D., Rao, J. K. M. & Wlodawer, A. Crystal structure of Escherichia coli L-asparaginase, an enzyme used in cancer therapy. *Proc. Natl. Acad. Sci. U. S. A.* **90**, 1474–1478 (1993).
132. Branden, C. & Tooze, J. *Introduction to Protein Structure Second Edition*. https://books.google.com/books?hl=it&lr=&id=eUYWBAAAQBAJ&oi=fnd&pg=PP1&dq=Branddn,+C.+%26+Tooze,+J.+(1991)+Introduction+to+Protein+Struc-+ture+(Garland,+New+York),+p.+51.&ots=PAa-Nw93gY&sig=z7Cr9MCKXFoZIsc0Va4u8YRF9Rs (2012).
133. Greenquist, A. C. & Wriston, J. C. Chemical evidence for identical subunits in l-asparaginase from Escherichia coli B. *Arch. Biochem. Biophys.* **152**, 280–286 (1972).
134. Aung, H. P., Bocola, M., Schleper, S. & Röhm, K. H. Dynamics of a mobile loop at the active site of Escherichia coli asparaginase. *Biochim. Biophys. Acta - Protein Struct. Mol. Enzymol.* **1481**, 349–359 (2000).
135. Dodson, G. & Wlodawer, A. Catalytic triads and their relatives. *Trends in Biochemical Sciences* vol. 23 347–352 (1998).
136. Palm, G. J. *et al.* A covalently bound catalytic intermediate in *Escherichia coli* asparaginase : Crystal structure of a Thr-89-Val mutant. *FEBS Lett.* **390**, 211–216 (1996).
137. Ortlund, E., Lacount, M. W., Lewinski, K. & Lebioda, L. Reactions of Pseudomonas 7A glutaminase-asparaginase with diazo analogues of glutamine and asparagine result in unexpected covalent inhibitions and suggests an unusual catalytic triad Thr-Tyr-Glu. *Biochemistry* **39**, 1199–1204 (2000).
138. Derst, C., Wehner, A., Specht, V. & Rohm, K.-H. States and Functions of Tyrosine Residues in Escherichia coli Asparaginase II. *Eur. J. Biochem.* **224**, 533–540 (1994).
139. Derst, C., Henseling, J. & Röhm, K.-H. Engineering the substrate specificity of Escherichia coli asparaginase II. Selective reduction of glutaminase activity by amino acid replacements at position 248 . *Protein Sci.* **9**, 2009–2017 (2000).
140. Lubkowski, J. & Wlodawer, A. Geometric considerations support the double-displacement catalytic mechanism of <scp>l</scp> -asparaginase. *Protein Sci.* **28**, 1850–1864 (2019).
141. Sanches, M., Barbosa, J. A. R. G., De Oliveira, R. T., Neto, J. A. & Polikarpov, I. Structural

comparison of Escherichia coli L-asparaginase in two monoclinic space groups. *Acta Crystallogr. - Sect. D Biol. Crystallogr.* **59**, 416–422 (2003).
142. Maggi, M. & Scotti, C. Enzymes in metabolic anticancer therapy. in *Advances in Experimental Medicine and Biology* vol. 1148 173–199 (Springer New York LLC, 2019).
143. Neuman, R. E. & Mccoy, T. A. Dual requirement of Walker carcinosarcoma 256 in vitro for asparagine and glutamine. *Science (80-.).* **124**, 124–125 (1956).
144. Loayza-Puch, F. *et al.* Tumour-specific proline vulnerability uncovered by differential ribosome codon reading. *Nature* **530**, 490–494 (2016).
145. Ubuka, T., Institute, A. M.-J. of the N. C. & 1971, undefined. Studies on the utilization of asparagine by mouse leukemia cells. *academic.oup.com*.
146. Pavlova, N. N. *et al.* As Extracellular Glutamine Levels Decline, Asparagine Becomes an Essential Amino Acid. *Cell Metab.* **27**, 428-438.e5 (2018).
147. Krall, A. S., Xu, S., Graeber, T. G., Braas, D. & Christofk, H. R. Asparagine promotes cancer cell proliferation through use as an amino acid exchange factor. *Nat. Commun.* **7**, 1–13 (2016).
148. Lomelino, C. L., Andring, J. T., McKenna, R. & Kilberg, M. S. Asparagine synthetase: Function, structure, and role in disease. *Journal of Biological Chemistry* vol. 292 19952–19958 (2017).
149. Shan, J., Lopez, M. C., Baker, H. V. & Kilberg, M. S. Expression profiling after activation of amino acid deprivation response in HepG2 human hepatoma cells. *Physiol. Genomics* **41**, 315–327 (2010).
150. Balasubramanian, M. N., Butterworth, E. A. & Kilberg, M. S. Asparagine synthetase: Regulation by cell stress and involvement in tumor biology. *American Journal of Physiology - Endocrinology and Metabolism* vol. 304 E789 (2013).
151. Garcia-Bermudez, J., Williams, R. T., Guarecuco, R. & Birsoy, K. Targeting extracellular nutrient dependencies of cancer cells. *Molecular Metabolism* vol. 33 67–82 (2020).
152. Su, N. *et al.* Correlation between asparaginase sensitivity and asparagine synthetase protein content, but not mRNA, in acute lymphoblastic leukemia cell lines. *Pediatr. Blood Cancer* **50**, 274–279 (2008).
153. Haskell, C. M. & Canellos, G. P. l-Asparaginase resistance in human leukemia-Asparagine synthetase. *Biochem. Pharmacol.* **18**, 2578–2580 (1969).
154. Scherf, U. *et al.* A gene expression database for the molecular pharmacology of cancer. *Nat. Genet.* **24**, 236–244 (2000).
155. Li, H. *et al.* The landscape of cancer cell line metabolism. *Nat. Med.* **25**, 850–860 (2019).
156. Krasotkina, J., Borisova, A. A., Gervaziev, Y. V. & Sokolov, N. N. One-step purification and kinetic properties of the recombinant l-asparaginase from Erwinia carotovora. *Biotechnol. Appl. Biochem.* **39**, 215–221 (2004).
157. Borek, D. & Jaskólski, M. Sequence analysis of enzymes with asparaginase activity. *Acta Biochim. Pol.* **48**, 893–902 (2001).
158. Souba, W. W. Glutamine and cancer. *Annals of Surgery* vol. 218 715–728 (1993).
159. Cooney, D. A., Capizzi, R. L. & Handschumacher, R. E. Evaluation of l-asparagine Metabolism in Animals and Man. *Cancer Res.* **30**, 929–935 (1970).
160. Reinert, R. B. *et al.* Role of glutamine depletion in directing tissue-specific nutrient stress responses to L-asparaginase. *J. Biol. Chem.* **281**, 31222–31233 (2006).
161. Dams, D. & Briers, Y. *Enzybiotics: Enzyme-based antibacterials as therapeutics*. *Advances in Experimental Medicine and Biology* vol. 1148 (2019).
162. Willems, L. *et al.* Inhibiting Glutamine uptake represents an attractive new strategy for treating acute myeloid leukemia. *Blood* **122**, 3521–3532 (2013).
163. OLLENSCHLÄGER, G. *et al.* Asparaginase-induced derangements of glutamine metabolism: the pathogenetic basis for some drug-related side-effects. *Eur. J. Clin. Invest.* **18**, 512–516 (1988).
164. Bunpo, P. *et al. Alanyl-Glutamine Consumption Modifies the Suppressive Effect of L-Asparaginase on Lymphocyte Populations in Mice 1,2*. *The Journal of Nutrition Nutritional Immunology J. Nutr* vol. 138 https://academic.oup.com/jn/article-

abstract/138/2/338/4665025 (2008).
165. Offman, M. N. *et al.* Rational engineering of L-asparaginase reveals importance of dual activity for cancer cell toxicity. *Blood* **117**, 1614–1621 (2011).
166. Moghrabi, A. *et al.* Results of the Dana-Farber Cancer Institute ALL Consortium Protocol 95-01 for children with acute lymphoblastic leukemia. *Blood* **109**, 896–904 (2007).
167. Kaspers, G. J. L. *et al.* In vitro cellular drug resistance and prognosis in newly diagnosed childhood acute lymphoblastic leukemia. *Blood* **90**, 2723–2729 (1997).
168. Appel, I. M. *et al.* Pharmacokinetic, pharmacodynamic and intracellular effects of PEG-asparaginase in newly diagnosed childhood acute lymphoblastic leukemia: Results from a single agent window study. *Leukemia* **22**, 1665–1679 (2008).
169. Pieters, R. *et al.* Relation of cellular drug resistance to long-term clinical outcome in childhood acute lymphoblastic leukaemia. *Lancet* **338**, 399–403 (1991).
170. Chen, S. H. *et al.* Clinical impact of in vitro cellular drug resistance on childhood acute lymphoblastic leukemia in Taiwan. *Leuk. Lymphoma* **53**, 1536–1542 (2012).
171. Chen, X. & Wood, B. L. How do we measure MRD in ALL and how should measurements affect decisions. Re: Treatment and prognosis? *Best Practice and Research: Clinical Haematology* (2017) doi:10.1016/j.beha.2017.07.002.
172. Kiriyama, Y. *et al.* Biochemical characterization of U937 cells resistant to L-asparaginase: The role of asparagine synthetase. *Leukemia* **3**, 294–297 (1989).
173. Holleman, A. *et al.* Gene-Expression Patterns in Drug-Resistant Acute Lymphoblastic Leukemia Cells and Response to Treatment. *N. Engl. J. Med.* **351**, 533–542 (2004).
174. Fine, B. M., Kaspers, G. J. L., Ho, M., Loonen, A. H. & Boxer, L. M. A genome-wide view of the in vitro response to L-asparaginase in acute lymphoblastic leukemia. *Cancer Res.* **65**, 291–299 (2005).
175. Ramakers-Van Woerden, N. L. *et al.* TEL/AML1 gene fusion is related to in vitro drug sensitivity for L- asparaginase in childhood acute lymphoblastic leukemia. *Blood* **96**, 1094–1099 (2000).
176. Stams, W. A. G. *et al.* Sensitivity to L-asparaginase is not associated with expression levels of asparagine synthetase in t(12;21)+ pediatric ALL. *Blood* **101**, 2743–2747 (2003).
177. Krejci, O. *et al.* Upregulation of asparagine synthetase fails to avert cell cycle arrest induced by L-asparaginase in TEL/AML1-positive leukemic cells. *Leukemia* **18**, 434–441 (2004).
178. Chen, Z. *et al.* Human monoclonal antibodies targeting the haemagglutinin glycoprotein can neutralize H7N9 influenza virus. *Nat. Commun.* **6**, 1–10 (2015).
179. ASLANIAN, A. M., FLETCHER, B. S. & KILBERG, M. S. Asparagine synthetase expression alone is sufficient to induce l-asparaginase resistance in MOLT-4 human leukaemia cells. *Biochem. J.* **357**, 321–328 (2001).
180. Hutson, R. G. *et al.* Amino acid control of asparagine synthetase: Relation to asparaginase resistance in human leukemia cells. *Am. J. Physiol. - Cell Physiol.* **272**, (1997).
181. Hinze, L. *et al.* Synthetic Lethality of Wnt Pathway Activation and Asparaginase in Drug-Resistant Acute Leukemias. *Cancer Cell* **35**, 664-676.e7 (2019).
182. Iwamoto, S., Mihara, K., Downing, J. R., Pui, C. H. & Campana, D. Mesenchymal cells regulate the response of acute lymphoblastic leukemia cells to asparaginase. *J. Clin. Invest.* **117**, 1049–1057 (2007).
183. Dimitriou, H., Choulaki, C., Perdikogianni, C., Stiakaki, E. & Kalmanti, M. Expression levels of ASNS in mesenchymal stromal cells in childhood acute lymphoblastic leukemia. *Int. J. Hematol.* **99**, 305–310 (2014).
184. Laranjeira, A. B. A. *et al.* IGFBP7 participates in the reciprocal interaction between acute lymphoblastic leukemia and BM stromal cells and in leukemia resistance to asparaginase. *Leukemia* **26**, 1001–1011 (2012).
185. Behan, J. W. *et al.* Adipocytes impair leukemia treatment in mice. *Cancer Res.* **69**, 7867–7874 (2009).
186. Ehsanipour, E. A. *et al.* Adipocytes cause leukemia cell resistance to l-asparaginase via

release of glutamine. *Cancer Res.* **73**, 2998–3006 (2013).
187. Holleman, A. *et al.* The expression of 70 apoptosis genes in relation to lineage, genetic subtype, cellular drug resistance, and outcome in childhood acute lymphoblastic leukemia. *Blood* **107**, 769–776 (2006).
188. Courtois, F., Schneider, C. P., Agrawal, N. J. & Trout, B. L. Rational Design of Biobetters with Enhanced Stability. *J. Pharm. Sci.* **104**, 2433–2440 (2015).
189. Sauna, Z. E. *et al.* Recent advances in (therapeutic protein) drug development. *F1000Research* vol. 6 (2017).
190. Nguyen, H. A., Su, Y. & Lavie, A. Structural Insight into Substrate Selectivity of Erwinia chrysanthemi L-Asparaginase. *Biochemistry* **55**, 1246–1253 (2016).
191. Ardalan, N., Mirzaie, S., Sepahi, A. A. & Khavari-Nejad, R. A. Novel mutant of Escherichia coli asparaginase II to reduction of the glutaminase activity in treatment of acute lymphocytic leukemia by molecular dynamics simulations and QM-MM studies. *Med. Hypotheses* **112**, 7–17 (2018).
192. Jr, R. W., Arlin, Z., Gee, T., … T. C.-C. T. & 1982, U. *Clinical evaluation of succinylated Acinetobacter glutaminase-asparaginase in adult leukemia*. *Cancer Treatment* (1982).
193. Jianhua, C., Yujun, W., Ruibo, J., Min, W. & Wutong, W. Probing the antigenicity of E. coli L-asparaginase by mutational analysis. *Mol. Biotechnol.* **33**, 57–65 (2006).
194. Mehta, R. K. *et al.* Mutations in subunit interface and B-cell Epitopes improve Antileukemic activities of Escherichia Coli asparaginase-II:Evaluation of Immunogenicity in Mice. *J. Biol. Chem.* **289**, 3555–3570 (2014).
195. Mahboobi, M. *et al.* Applying bioinformatic tools for modeling and modifying type II E. coli L-Asparginase to present a better therapeutic agent/drug for acute lymphoblastic leukemia. *Int. J. Cancer Manag.* **10**, (2017).
196. Patel, N. *et al.* A dyad of lymphoblastic lysosomal cysteine proteases degrades the antileukemic drug L-asparaginase. *J. Clin. Invest.* **119**, 1964–1973 (2009).
197. Maggi, M. *et al.* A protease-resistant Escherichia coli asparaginase with outstanding stability and enhanced anti- leukaemic activity in vitro. *Sci. Rep.* 1–16 (2017) doi:10.1038/s41598-017-15075-4.
198. Ginn, C., Khalili, H., Lever, R. & Brocchini, S. PEGylation and its impact on the design of new protein-based medicines. *Future Medicinal Chemistry* vol. 6 1829–1846 (2014).
199. Kolate, A. *et al.* PEG - A versatile conjugating ligand for drugs and drug delivery systems. *Journal of Controlled Release* vol. 192 67–81 (2014).
200. Turecek, P. L., Bossard, M. J., Schoetens, F. & Ivens, I. A. PEGylation of Biopharmaceuticals: A Review of Chemistry and Nonclinical Safety Information of Approved Drugs. *Journal of Pharmaceutical Sciences* vol. 105 460–475 (2016).
201. Dinndorf, P. A., Gootenberg, J., Cohen, M. H., Keegan, P. & Pazdur, R. FDA Drug Approval Summary: Pegaspargase (Oncaspar®) for the First-Line Treatment of Children with Acute Lymphoblastic Leukemia (ALL). *Oncologist* **12**, 991–998 (2007).
202. Ho, D. H. *et al.* Clinical pharmacology of polyethylene glycol-L-asparaginase. *Drug Metab. Dispos.* **14**, (1986).
203. Keating, M. J., Holmes, R., Lerner, S. & Ho, D. H. L-asparaginase and PEG asparaginase- past, present, and future. *Leuk. Lymphoma* **10**, 153–157 (1993).
204. Panosyan, E. H. *et al.* Deamination of Glutamine is a Prerequisite for Optimal Asparagine Deamination by Asparaginases In Vivo (CCG-1961). *Anticancer Res.* **24**, 1121–1125 (2004).
205. Zalipsky, S. Chemistry of polyethylene glycol conjugates with biologically active molecules. *Advanced Drug Delivery Reviews* vol. 16 157–182 (1995).
206. Milton Harris, J. & Chess, R. B. Effect of pegylation on pharmaceuticals. *Nature Reviews Drug Discovery* vol. 2 214–221 (2003).
207. Santos, J. H. *et al. In situ* purification of periplasmatic L-asparaginase by aqueous two phase systems with ionic liquids (ILs) as adjuvants. *J. Chem. Technol. Biotechnol.* **93**, 1871–1880 (2018).

208. Carter, M. C. & Meyerhoff, M. E. Instability of succinyl ester linkages in O2′-monosuccinyl cyclic AMP-protein conjugates at neutral pH. *J. Immunol. Methods* **81**, 245–257 (1985).
209. Blanco, E., Shen, H. & Ferrari, M. Principles of nanoparticle design for overcoming biological barriers to drug delivery. *Nature Biotechnology* vol. 33 941–951 (2015).
210. Keck, C. M. & Müller, R. H. Nanotoxicological classification system (NCS) - A guide for the risk-benefit assessment of nanoparticulate drug delivery systems. *European Journal of Pharmaceutics and Biopharmaceutics* vol. 84 445–448 (2013).
211. Dawidczyk, C. M., Russell, L. M. & Searson, P. C. Nanomedicines for cancer therapy: State-of-the-art and limitations to pre-clinical studies that hinder future developments. *Frontiers in Chemistry* vol. 2 69 (2014).
212. van den Berg, H. Asparaginase revisited. *Leuk. Lymphoma* **52**, 168–178 (2011).
213. Domenech, C. *et al.* l-asparaginase loaded red blood cells in refractory or relapsing acute lymphoblastic leukaemia in children and adults: results of the GRASPALL 2005-01 randomized trial. *Br. J. Haematol.* **153**, 58–65 (2011).
214. No, P. Graspa; INN-L-asparaginase. **44**, (2019).
215. Tabandeh, M. R. & Aminlari, M. Synthesis, physicochemical and immunological properties of oxidized inulin-l-asparaginase bioconjugate. *J. Biotechnol.* **141**, 189–195 (2009).
216. Zhang, Y. Q. *et al.* Synthesis, characterization and immunogenicity of silk fibroin-L-asparaginase bioconjugates. *J. Biotechnol.* **120**, 315–326 (2005).
217. Phelan, K. W. & Advani, A. S. Novel Therapies in Acute Lymphoblastic Leukemia. *Current Hematologic Malignancy Reports* vol. 13 289–299 (2018).
218. Herter, S. *et al.* Preclinical activity of the type II CD20 antibody GA101 (obinutuzumab) compared with rituximab and ofatumumab in vitro and in xenograft models. *Mol. Cancer Ther.* **12**, 2031–2042 (2013).
219. Hu, Y. *et al.* Investigation of the mechanism of action of alemtuzumab in a human CD52 transgenic mouse model. *Immunology* **128**, 260–270 (2009).
220. Martinelli, G. *et al.* Complete Hematologic and Molecular Response in Adult Patients With Relapsed/Refractory Philadelphia Chromosome–Positive B-Precursor Acute Lymphoblastic Leukemia Following Treatment With Blinatumomab: Results From a Phase II, Single-Arm, Multicenter Study. *J. Clin. Oncol.* **35**, 1795–1802 (2017).
221. Dai, H., Wang, Y., Lu, X. & Han, W. Chimeric antigen receptors modified T-cells for cancer therapy. *J. Natl. Cancer Inst.* **108**, (2016).
222. Frey, N. The what, when and how of CAR T cell therapy for ALL. *Best Pract. Res. Clin. Haematol.* **30**, 275–281 (2017).
223. Hantschel, O., Rix, U. & Superti-Furga, G. Target spectrum of the BCR-ABL inhibitors imatinib, nilotinib and dasatinib. *Leuk. Lymphoma* **49**, 615–619 (2008).
224. Porkka, K. *et al.* Dasatinib crosses the blood-brain barrier and is an efficient therapy for central nervous system philadelphia chromosome positive leukemia. *Blood* **112**, 1005–1012 (2008).
225. Ferrando, A. A. The role of NOTCH1 signaling in T-ALL. *Hematology / the Education Program of the American Society of Hematology. American Society of Hematology. Education Program* vol. 2009 353–361 (2009).
226. Thomas, A., Teicher, B. A. & Hassan, R. *Antibody-drug conjugates for cancer therapy*. www.thelancet.com/oncology (2016).
227. Chau, C. H., Steeg, P. S. & Figg, W. D. Antibody–drug conjugates for cancer. *Lancet* **394**, 793–804 (2019).
228. De Claro, R. A. *et al.* U.S. Food and Drug Administration approval summary: Brentuximab vedotin for the treatment of relapsed Hodgkin lymphoma or relapsed systemic anaplastic large-cell lymphoma. *Clin. Cancer Res.* **18**, 5845–5849 (2012).
229. Wynne, J., Wright, D. & Stock, W. Inotuzumab: From preclinical development to success in B-cell acute lymphoblastic leukemia. *Blood Adv.* **3**, 96–104 (2019).
230. Jen, E. Y. *et al.* Fda approval: Gemtuzumab ozogamicin for the treatment of adults with newly

diagnosed cd33-positive acute myeloid leukemia. *Clin. Cancer Res.* **24**, 3242–3246 (2018).
231. Norsworthy, K. J. *et al.* FDA Approval Summary: Mylotarg for Treatment of Patients with Relapsed or Refractory CD33-Positive Acute Myeloid Leukemia. *Oncologist* **23**, 1103–1108 (2018).
232. Damle, N. K. & Frost, P. Antibody-targeted chemotherapy with immunoconjugates of calicheamicin. *Current Opinion in Pharmacology* vol. 3 386–390 (2003).
233. Ritchie, M., Tchistiakova, L. & Scott, N. Implications of receptor-mediated endocytosis and intracellular trafficking dynamics in the development of antibody drug conjugates. *MAbs* **5**, 13–21 (2013).
234. MacMillan, K. S. & Boger, D. L. Fundamental relationships between structure, reactivity, and biological activity for the duocarmycins and CC-1065. *Journal of Medicinal Chemistry* vol. 52 5771–5780 (2009).
235. Thorson, J. *et al.* Understanding and Exploiting Natures Chemical Arsenal: The Past,Present and Future of Calicheamicin Research. *Curr. Pharm. Des.* **6**, 1841–1879 (2005).
236. Francisco, J. A. *et al.* cAC10-vcMMAE, an anti-CD30-monomethyl auristatin E conjugate with potent and selective antitumor activity. *Blood* **102**, 1458–1465 (2003).
237. Jain, N., Smith, S. W., Ghone, S. & Tomczuk, B. Current ADC Linker Chemistry. *Pharmaceutical Research* vol. 32 3526–3540 (2015).
238. McCombs, J. R. & Owen, S. C. Antibody Drug Conjugates: Design and Selection of Linker, Payload and Conjugation Chemistry. *AAPS J.* **17**, 339–351 (2015).
239. Tsuchikama, K. & An, Z. Antibody-drug conjugates: recent advances in conjugation and linker chemistries. *Protein and Cell* vol. 9 33–46 (2018).
240. Beck, A., Goetsch, L., Dumontet, C. & Corvaïa, N. Strategies and challenges for the next generation of antibody-drug conjugates. *Nature Reviews Drug Discovery* vol. 16 315–337 (2017).
241. Lu, J., Jiang, F., Lu, A. & Zhang, G. Linkers Having a Crucial Role in Antibody–Drug Conjugates. *Int. J. Mol. Sci.* **17**, 561 (2016).
242. Frigerio, M. & Kyle, A. F. The Chemical Design and Synthesis of Linkers Used in Antibody Drug Conjugates. *Curr. Top. Med. Chem.* **17**, 3393–3424 (2018).
243. Kalim, M. *et al.* Intracellular trafficking of new anticancer therapeutics: Antibody–drug conjugates. *Drug Design, Development and Therapy* vol. 11 2265–2276 (2017).
244. Galy, A., Travis, M., Cen, D. & Chen, B. Human T, B, natural killer, and dendritic cells arise from a common bone marrow progenitor cell subset. *Immunity* **3**, 459–473 (1995).
245. Medvinsky, A. & Dzierzak, E. Definitive hematopoiesis is autonomously initiated by the AGM region. *Cell* **86**, 897–906 (1996).
246. Nuñez, C. *et al.* B cells are generated throughout life in humans. *J. Immunol.* **156**, 866–72 (1996).
247. Krop, I. *et al.* Self-renewal of B-1 lymphocytes is dependent on CD19. *Eur. J. Immunol.* **26**, 238–242 (1996).
248. Harada, H. *et al. Phenotypic Difference of Normal Plasma Cells From Mature Myeloma Cells*. www.bloodjournal.org (1993).
249. Scheuermann, R. H. & Racila, E. CD19 antigen in leukemia and lymphoma diagnosis and immunotherapy. *Leuk. Lymphoma* **18**, 385–397 (1995).
250. Carter, R. H., Wang, Y. & Brooks, S. Role of CD19 signal transduction in B cell biology. *Immunol. Res.* **26**, 45–54 (2002).
251. Li, X. *et al.* CD19, from bench to bedside. *Immunology Letters* vol. 183 86–95 (2017).
252. Van Zelm, M. C. *et al. An Antibody-Deficiency Syndrome Due to Mutations in the CD19 Gene A bs tr ac t. N Engl J Med* vol. 354 www.nejm.org (2006).
253. Sato, S., Ono, N., Steeber, D. A., Pisetsky, D. S. & Tedder, T. F. CD19 regulates B lymphocyte signaling thresholds critical for the development of B-1 lineage cells and autoimmunity. *J. Immunol.* **157**, 4371–4378 (1996).
254. Tedder, T. F. & Isaacs, C. M. Isolation of cDNAs encoding the CD19 antigen of human and

mouse B lymphocytes. A new member of the immunoglobulin superfamily. *J. Immunol.* **143**, 712–7 (1989).
255. Zhou, L. J., Ord, D. C., Hughes, A. L. & Tedder, T. F. Structure and domain organization of the CD19 antigen of human, mouse, and guinea pig B lymphocytes. Conservation of the extensive cytoplasmic domain. *J. Immunol.* **147**, 1424–32 (1991).
256. Tedder, T. F. CD19: A promising B cell target for rheumatoid arthritis. *Nature Reviews Rheumatology* vol. 5 572–577 (2009).
257. Zhou, L. J., Ord, D. C., Omori, S. A. & Tedder, T. F. Structure of the genes encoding the CD19 antigen of human and mouse B lymphocytes. *Immunogenetics* **35**, 102–111 (1992).
258. Haas, K. M. & Tedder, T. F. Role of the CD19 and CD21/35 receptor complex in innate immunity, host defense and autoimmunity. in *Advances in Experimental Medicine and Biology* vol. 560 125–139 (Springer, Boston, MA, 2005).
259. Hobeika, E., Nielsen, P. J. & Medgyesi, D. Signaling mechanisms regulating B-lymphocyte activation and tolerance. *Journal of Molecular Medicine* vol. 93 143–158 (2015).
260. UniProt Consortium. UniProt: the universal protein knowledgebase. *Nucleic Acids Res.* (2018).
261. Teplyakov, A., Obmolova, G., Luo, J. & Gilliland, G. L. Crystal structure of B-cell co-receptor CD19 in complex with antibody B43 reveals an unexpected fold. *Proteins Struct. Funct. Bioinforma.* **86**, 495–500 (2018).
262. P. Bork, L. Holm & C. Sander. The Immunoglobulin Fold. *J. Mol. Biol.* **242**, 309–320 (1994).
263. Lesk, A. M. & Chothia, C. Evolution of proteins formed by β-sheets. II. The core of the immunoglobulin domains. *J. Mol. Biol.* **160**, 325–342 (1982).
264. Uckun, F. *et al.* Detailed studies on expression and function of CD19 surface determinant by using B43 monoclonal antibody and the clinical potential of anti- CD19 immunotoxins. *Blood* **71**, 13–29 (1988).
265. Rossi, G. De *et al.* Immunophenotype of acute lymphoblastic leukemia cells: The experience of the italian cooperative group (gimema). *Leuk. Lymphoma* **9**, 221–228 (1993).
266. Schwonzen, M. *et al.* Immunophenotyping of low-grade B-cell lymphoma in blood and bone marrow: poor correlation between immunophenotype and cytological/histological classification. *Br. J. Haematol.* **83**, 232–239 (1993).
267. Robbins, B., Ellison, D., Spinosa, J. & Carey, C. Diagnostic application of two-color flow cytometry in 161 cases of hairy cell leukemia. *Blood* (1993).
268. Raponi, S. *et al.* Flow cytometric study of potential target antigens (CD19, CD20, CD22, CD33) for antibody-based immunotherapy in acute lymphoblastic leukemia: Analysis of 552 cases. *Leuk. Lymphoma* **52**, 1098–1107 (2011).
269. Boye, J. & Elter, T. An overview of the current clinical use of the anti-CD20 monoclonal antibody rituximab. *Ann. Oncol.* (2003).
270. Coiffier, B. Monoclonal antibodies combined to chemotherapy for the treatment of patients with lymphoma. *Blood Rev.* **17**, 25–31 (2003).
271. Dillman, R. O. Treatment of low-grade B-cell lymphoma with the monoclonal antibody rituximab. *Semin. Oncol.* **30**, 434–447 (2003).
272. Liang, Y. & Tedder, T. F. Identification of a CD20-, Fc∈RIβ-, and HTm4-related gene family: Sixteen new MS4A family members expressed in human and mouse. *Genomics* **72**, 119–127 (2001).
273. Liang, Y., Buckley, T. R., Tu, L., Langdon, S. D. & Tedder, T. F. Structural organization of the human MS4A gene cluster on Chromosome 11q12. *Immunogenetics* **53**, 357–368 (2001).
274. Li, H. *et al.* The CD20 calcium channel is localized to microvilli and constitutively associated with membrane rafts: Antibody binding increases the affinity of the association through an epitope-dependent cross-linking-independent mechanism. *J. Biol. Chem.* **279**, 19893–19901 (2004).
275. Léveillé, C., Al-Daccak, R. & Mourad, W. CD20 is physically and functionally coupled to MHC class II and CD40 on human B cell lines. *Eur. J. Immunol.* **29**, 65–74 (1999).

276. Szöllósi, J., Horejsí, V., Bene, L., Angelisová, P. & Damjanovich, S. Supramolecular complexes of MHC class I, MHC class II, CD20, and tetraspan molecules (CD53, CD81, and CD82) at the surface of a B cell line JY. *J. Immunol.* **157**, 2939–46 (1996).
277. Petrie, R. J. & Deans, J. P. Colocalization of the B Cell Receptor and CD20 Followed by Activation-Dependent Dissociation in Distinct Lipid Rafts. *J. Immunol.* **169**, 2886–2891 (2002).
278. Li, H., Ayer, L. M., Lytton, J. & Deans, J. P. Store-operated Cation Entry Mediated by CD20 in Membrane Rafts. *J. Biol. Chem.* **278**, 42427–42434 (2003).
279. Stamenkovic, I. & Seed, B. Analysis of two cDNA clones encoding the B lymphocyte antigen CD20 (BI, Bp35), a type III integral membrane protein. *J. Exp. Med.* **167**, 1975–1980 (1988).
280. Einfeld, D. A., Brown, J. P., Valentine, M. A., Clark, E. A. & Ledbetter, J. A. Molecular cloning of the human B cell CD20 receptor predicts a hydrophobic protein with multiple transmembrane domains. *EMBO J.* **7**, 711–717 (1988).
281. Tedder, T. F. & Engel, P. CD20: a regulator of cell-cycle progression of B lymphocytes. *Immunol. Today* **15**, 450–454 (1994).
282. Polyak, M. J. & Deans, J. P. Alanine-170 and proline-172 are critical determinants for extracellular CD20 epitopes; heterogeneity in the fine specificity of CD20 monoclonal antibodies is defined by additional requirements imposed by both amino acid sequence and quaternary structure. *Blood* **99**, 3256–3262 (2002).
283. Claude Chan, H. T. *et al. CD20-induced Lymphoma Cell Death Is Independent of Both Caspases and Its Redistribution into Triton X-100 Insoluble Membrane Rafts 1*. *CANCER RESEARCH* vol. 63 (2003).
284. Deans, J. P., Robbins, S. M., Polyak, M. J. & Savage, J. A. Rapid redistribution of CD20 to a low density detergent-insoluble membrane compartment. *J. Biol. Chem.* **273**, 344–348 (1998).
285. Cragg, M. S., Walshe, C. A., Ivanov, A. O. & Glennie, M. J. The biology of CD20 and its potential as a target for mAb therapy. *Curr. Dir. Autoimmun.* **8**, 140–174 (2005).
286. Pickartz, T. *et al.* Selection of B-cell chronic lymphocytic leukemia cell variants by therapy with anti-CD20 monoclonal antibody rituximab. *Exp. Hematol.* **29**, 1410–1416 (2001).
287. Jilani, I. *et al.* Transient down-modulation of CD20 by rituximab in patients with chronic lymphocytic leukemia. *Blood* **102**, 3514–3520 (2003).
288. Kennedy, A. D. *et al.* Rituximab Infusion Promotes Rapid Complement Depletion and Acute CD20 Loss in Chronic Lymphocytic Leukemia. *J. Immunol.* **172**, 3280–3288 (2004).
289. Holder, M., Grafton, G., Macdonald, I., Finney, M. & Gordon, J. Engagement of CD20 suppresses apoptosis in germinal center B cells. *Eur. J. Immunol.* **25**, 3160–3164 (1995).
290. Clark, E. A. & Shu, G. Activation of human B cell proliferation through surface Bp35 (CD20) polypeptides or immunoglobulin receptors. *J. Immunol.* **138**, 720–5 (1987).
291. Tedder, T. F., Forsgren, A., Boyd, A. W., Nadler, L. M. & Schlossman, S. F. Antibodies reactive with the B1 molecule inhibit cell cycle progression but not activation of human B lymphocytes. *Eur. J. Immunol.* **16**, 881–887 (1986).
292. Shan, D., Ledbetter, J. A. & Press, O. W. Signaling events involved in anti-CD20-induced apoptosis of malignant human B cells. *Cancer Immunol. Immunother.* **48**, 673–683 (2000).
293. Hofmeister, J. K., Cooney, D. & Coggeshall, K. M. Clustered CD20 induced apoptosis: Src-family kinase, the proximal regulator of tyrosine phosphorylation, calcium influx, and caspase 3- dependent apoptosis. *Blood Cells, Mol. Dis.* **26**, 133–143 (2000).
294. Pedersen, I. M., Buhl, A. M., Klausen, P., Geisler, C. H. & Jurlander, J. The chimeric anti-CD20 antibody rituximab induces apoptosis in B-cell chronic lymphocytic leukemia cells through a p38 mitogen activated protein-kinase-dependent mechanism. *Blood* **99**, 1314–1319 (2002).
295. Cardarelli, P. M. *et al.* Binding to CD20 by anti-B1 antibody or F(ab')2 is sufficient for induction of apoptosis in B-cell lines. *Cancer Immunol. Immunother.* **51**, 15–24 (2002).
296. Cragg, M., Asidipour, A., O'Brien, L., Tutt, A. & Chan, H. Leukocyte Typing VII. *Oxford Univ. Press* (2002).

297. Press, O., Appelbaum, F., Ledbetter, J. & Martin, P. Monoclonal antibody 1F5 (anti-CD20) serotherapy of human B cell lymphomas. *Blood* **69**, 58491 (1987).
298. Nadler, L. M. *et al.* A unique cell surface antigen identifying lymphoid malignancies of B cell origin. *J. Clin. Invest.* **67**, 134–140 (1981).
299. Cragg, M. S. *et al.* Complement-mediated lysis by anti-CD20 mAb correlates with segregation into lipid rafts. *Blood* **101**, 1045–1052 (2003).
300. van Meerten, T. & Hagenbeek, A. CD20-Targeted therapy: The next generation of antibodies. *Semin. Hematol.* **47**, 199–210 (2010).
301. Dhingra, S. & Sachdeva, M. Obinutuzumab: A FDA approved monoclonal antibody in the treatment of untreated chronic lymphocytic leukemia. *Int. J. Appl. Basic Med. Res.* **5**, 54 (2015).
302. Kakkar, A. K. & Balakrishnan, S. Obinutuzumab for chronic lymphocytic leukemia: promise of the first treatment approved with breakthrough therapy designation. *J. Oncol. Pharm. Pract.* **21**, 358–63 (2015).
303. Schroeder, H. W. & Cavacini, L. Structure and function of immunoglobulins. *J. Allergy Clin. Immunol.* **125**, S41–S52.
304. Bournazos, S. & Ravetch, J. V. Fcγ receptor pathways during active and passive immunization. *Immunol. Rev.* **268**, 88–103 (2015).
305. Beers, S. A., Glennie, M. J. & White, A. L. Influence of immunoglobulin isotype on therapeutic antibody function. *Blood* vol. 127 1097–1101 (2016).
306. Stapleton, N. M., Einarsdóttir, H. K., Stemerding, A. M. & Vidarsson, G. The multiple facets of FcRn in immunity. *Immunol. Rev.* **268**, 253–268 (2015).
307. Chiu, M. L. & Gilliland, G. L. Engineering antibody therapeutics. *Current Opinion in Structural Biology* vol. 38 163–173 (2016).
308. Köhler, G. & Milstein, C. Continuous cultures of fused cells secreting antibody of predefined specificity. *Nature* **256**, 495–497 (1975).
309. The Antibody Society. No Title. *Approv. antibodies* **www. antib**,.
310. Ecker, D. M., Jones, S. D. & Levine, H. L. The therapeutic monoclonal antibody market. *MAbs* **7**, 9–14 (2015).
311. Lu, R. M. *et al.* Development of therapeutic antibodies for the treatment of diseases. *Journal of Biomedical Science* vol. 27 1–30 (2020).
312. Neri, D. Antibody–cytokine fusions: Versatile products for the modulation of anticancer immunity. *Cancer Immunol. Res.* **7**, 348–354 (2019).
313. Larson, S. M., Carrasquillo, J. A., Cheung, N. K. V. & Press, O. W. Radioimmunotherapy of human tumours. *Nature Reviews Cancer* vol. 15 347–360 (2015).
314. Labrijn, A. F., Janmaat, M. L., Reichert, J. M. & Parren, P. W. H. I. Bispecific antibodies: a mechanistic review of the pipeline. *Nature Reviews Drug Discovery* vol. 18 585–608 (2019).
315. Ohradanova-Repic, A. *et al.* Fab antibody fragment-functionalized liposomes for specific targeting of antigen-positive cells. *Nanomedicine Nanotechnology, Biol. Med.* **14**, 123–130 (2018).
316. June, C. H. & Sadelain, M. Chimeric Antigen Receptor Therapy. *N. Engl. J. Med.* **379**, 64–73 (2018).
317. Ducancel, F. & Muller, B. H. Molecular engineering of antibodies for therapeutic and diagnostic purposes. *mAbs* vol. 4 445–457 (2012).
318. Harding, F. A., Stickler, M. M., Razo, J. & DuBridge, R. The immunogenicity of humanized and fully human antibodies. *MAbs* **2**, 256–265 (2010).
319. Hansel, T. T., Kropshofer, H., Singer, T., Mitchell, J. A. & George, A. J. T. The safety and side effects of monoclonal antibodies. *Nature Reviews Drug Discovery* vol. 9 325–338 (2010).
320. Lonberg, N. *et al.* Antigen-specific human antibodies from mice comprising four distinct genetic modifications. *Nature* **368**, 856–9 (1994).
321. Green, L. L. *et al.* Antigen–specific human monoclonal antibodies from mice engineered with human Ig heavy and light chain YACs. *Nat. Genet.* **7**, 13–21 (1994).

322. Mendez, M. J. *et al.* Functional transplant of megabase human immunoglobulin loci recapitulates human antibody response in mice. *Nat. Genet.* **15**, 146–156 (1997).
323. Osborn, M. J. *et al.* High-Affinity IgG Antibodies Develop Naturally in Ig-Knockout Rats Carrying Germline Human IgH/Igκ/Igλ Loci Bearing the Rat C H Region . *J. Immunol.* **190**, 1481–1490 (2013).
324. Lee, E. C. *et al.* Complete humanization of the mouse immunoglobulin loci enables efficient therapeutic antibody discovery. *Nat. Biotechnol.* **32**, 356–363 (2014).
325. Murphy, A. J. *et al.* Mice with megabase humanization of their immunoglobulin genes generate antibodies as efficiently as normal mice. *Proc. Natl. Acad. Sci. U. S. A.* **111**, 5153–5158 (2014).
326. Cox, K. S. *et al.* Rapid isolation of dengue-neutralizing antibodies from single cell-sorted human antigen-specific memory B-cell cultures. *MAbs* **8**, 129–140 (2016).
327. Woda, M. *et al.* The Journal of Infectious Diseases Dynamics of Dengue Virus (DENV)-Specific B Cells in the Response to DENV Serotype 1 Infections, Using Flow Cytometry With Labeled Virions. (2016) doi:10.1093/infdis/jiw308.
328. Iizuka, A. *et al.* Identification of cytomegalovirus (CMV)pp65 antigen-specific human monoclonal antibodies using single B cell-based antibody gene cloning from melanoma patients. *Immunol. Lett.* **135**, 64–73 (2011).
329. Bailey, M. J. *et al.* Human antibodies targeting Zika virus NS1 provide protection against disease in a mouse model. *Nat. Commun.* **9**, 1–11 (2018).
330. Bushey, R. T. *et al.* A Therapeutic Antibody for Cancer, Derived from Single Human B Cells. *Cell Rep.* **15**, 1505–1513 (2016).
331. Rijal, P. *et al.* Therapeutic Monoclonal Antibodies for Ebola Virus Infection Derived from Vaccinated Humans. *Cell Rep.* **27**, 172-186.e7 (2019).
332. Awi, N. J. & Teow, S.-Y. Antibody-Mediated Therapy against HIV/AIDS: Where Are We Standing Now? (2018) doi:10.1155/2018/8724549.
333. Nakamura, G. *et al.* An in vivo human-plasmablast enrichment technique allows rapid identification of therapeutic influenza A antibodies. *Cell Host Microbe* **14**, 93–103 (2013).
334. Schofield, D. J. *et al.* Application of phage display to high throughput antibody generation and characterization. *Genome Biol.* **8**, R254 (2007).
335. Daugherty, P. S., Chen, G., Olsen, M. J., Iverson, B. L. & Georgiou, G. Antibody affinity maturation using bacterial surface display. *Protein Eng.* **11**, 825–832 (1998).
336. Feldhaus, M. J. *et al.* Flow-cytometric isolation of human antibodies from a nonimmune Saccharomyces cerevisiae surface display library. *Nat. Biotechnol.* **21**, 163–170 (2003).
337. Mottershead, D. G., Alfthan, K., Ojala, K., Takkinen, K. & Oker-Blom, C. Baculoviral display of functional scFv and synthetic IgG-binding domains. *Biochem. Biophys. Res. Commun.* **275**, 84–90 (2000).
338. McCafferty, J., Griffiths, A. D., Winter, G. & Chiswell, D. J. Phage antibodies: filamentous phage displaying antibody variable domains. *Nature* **348**, 552–554 (1990).
339. Smith, G. P. & Petrenko, V. A. Phage Display. **2665**, (1997).
340. Li, W. & Caberoy, N. B. New perspective for phage display as an efficient and versatile technology of functional proteomics. *Applied Microbiology and Biotechnology* vol. 85 909–919 (2010).
341. Dooley, H., Flajnik, M. F. & Porter, A. J. Selection and characterization of naturally occurring single-domain (IgNAR) antibody fragments from immunized sharks by phage display. *Mol. Immunol.* **40**, 25–33 (2003).
342. Sidhu, S. S. Engineering M13 for phage display. *Biomol. Eng.* **18**, 57–63 (2001).
343. Mandrup, O. A., Friis, N. A., Lykkemark, S., Just, J. & Kristensen, P. A Novel Heavy Domain Antibody Library with Functionally Optimized Complementarity Determining Regions. *PLoS One* **8**, e76834 (2013).
344. Abraham, R. *et al.* Determination of binding constants of diabodies directed against prostate-specific antigen using electrochemiluminescence-based immunoassays. *J. Mol.*

Recognit. **9**, 456–461 (1996).
345. Bazan, J., Całkosiñski, I. & Gamian, A. Phage displaya powerful technique for immunotherapy: 1. Introduction and potential of therapeutic applications. *Human Vaccines and Immunotherapeutics* vol. 8 1817–1828 (2012).
346. Rasched, I. & Oberer, E. Ff coliphages: Structural and functional relationships. *Microbiological Reviews* vol. 50 401–427 (1986).
347. O'Callaghan, R., Bradley, R. & Paranchych, W. The effect of M13 phage infection upon the F pili of E. coli. *Virology* **54**, 220–229 (1973).
348. Hobbs, Z. & Abedon, S. T. Diversity of phage infection types and associated terminology : the problem with ' Lytic or lysogenic '. 1–8 (2016) doi:10.1093/femsle/fnw047.
349. Ledsgaard, L., Kilstrup, M., Karatt-Vellatt, A., McCafferty, J. & Laustsen, A. Basics of Antibody Phage Display Technology. *Toxins (Basel).* **10**, 236 (2018).
350. van Wezenbeek, P. M. G. F., Hulsebos, T. J. M. & Schoenmakers, J. G. G. Nucleotide sequence of the chromosomal gene for human fibroblast (β1) interferon and of the flanking regions. *Gene* **14**, 137–143 (1981).
351. Clackson, T. & Lowman, H. Phage display: a practical approach. *Oxford Univ. Press* (2004).
352. Hoogenboom, H. R. *et al.* Antibody phage display technology and its applications. *Immunotechnology* **4**, 1–20 (1998).
353. Donini, C., D'Ambrosio, L., Grignani, G., Aglietta, M. & Sangiolo, D. Next generation immune-checkpoints for cancer therapy. *Journal of Thoracic Disease* vol. 10 S1581–S1601 (2018).
354. Lane, D. P. & Stephen, C. W. Epitope mapping using bacteriophage peptide libraries. *Curr. Opin. Immunol.* **5**, 268–271 (1993).
355. Lu, R. M., Chang, Y. L., Chen, M. S. & Wu, H. C. Single chain anti-c-Met antibody conjugated nanoparticles for in vivo tumor-targeted imaging and drug delivery. *Biomaterials* **32**, 3265–3274 (2011).
356. Chan, C. E. Z., Chan, A. H. Y., Lim, A. P. C. & Hanson, B. J. Comparison of the efficiency of antibody selection from semi-synthetic scFv and non-immune Fab phage display libraries against protein targets for rapid development of diagnostic immunoassays. *J. Immunol. Methods* **373**, 79–88 (2011).
357. Marks, J. D. *et al.* By-passing immunization. Human antibodies from V-gene libraries displayed on phage. *J. Mol. Biol.* **222**, 581–597 (1991).
358. Huse, W. D. *et al.* Generation of a large combinatorial library of the immunoglobulin repertoire in phage lambda. *Science (80-.).* **246**, 1275–1281 (1989).
359. Barbas, C. F., Bain, J. D., Hoekstra, D. M. & Lerner, R. A. Semisynthetic combinatorial antibody libraries: A chemical solution to the diversity problem. *Proc. Natl. Acad. Sci. U. S. A.* **89**, 4457–4461 (1992).
360. Hoogenboom, H. R. & Winter, G. By-passing immunisation. Human antibodies from synthetic repertoires of germline VH gene segments rearranged in vitro. *J. Mol. Biol.* **227**, 381–388 (1992).
361. Richard, G. *et al.* In Vivo Neutralization of α-Cobratoxin with High-Affinity Llama Single-Domain Antibodies (VHHs) and a VHH-Fc Antibody. *PLoS One* **8**, e69495 (2013).
362. Stewart, C. S., MacKenzie, C. R. & Christopher Hall, J. Isolation, characterization and pentamerization of α-cobrotoxin specific single-domain antibodies from a naïve phage display library: Preliminary findings for antivenom development. *Toxicon* **49**, 699–709 (2007).
363. Nixon, A. E., Sexton, D. J. & Ladner, R. C. Drugs derived from phage display. *MAbs* **6**, 73–85 (2014).
364. Kennedy, P. J., Oliveira, C., Granja, P. L. & Sarmento, B. Monoclonal antibodies: technologies for early discovery and engineering. *Crit. Rev. Biotechnol.* **38**, 394–408 (2018).
365. Weinblatt, M. E. *et al.* Adalimumab, a fully human anti–tumor necrosis factor α monoclonal antibody, for the treatment of rheumatoid arthritis in patients taking concomitant methotrexate: The ARMADA trial. *Arthritis Rheum.* **48**, 35–45 (2003).

366. Sanz, I., Yasothan, U. & Kirkpatrick, P. Belimumab. *Nature Reviews Drug Discovery* vol. 10 335–336 (2011).
367. A, D.-S., A, S.-T. & L., P.-A. Necitumumab for the treatment of advanced non-small-cell lung cancer. *Futur. Oncol.* **15**, 705–16 (2019).
368. De Haard, H. J. *et al.* A large non-immunized human Fab fragment phage library that permits rapid isolation and kinetic analysis of high affinity antibodies. *J. Biol. Chem.* **274**, 18218–18230 (1999).
369. Arrieta, O., Zatarain-Barrón, Z. L., Cardona, A. F., Carmona, A. & Lopez-Mejia, M. Ramucirumab in the treatment of non-small cell lung cancer. *Expert Opinion on Drug Safety* vol. 16 637–644 (2017).
370. Aprile, G. *et al.* Ramucirumab for the treatment of gastric cancers, colorectal adenocarcinomas, and other gastrointestinal malignancies. *Expert Rev. Clin. Pharmacol.* **9**, 877–885 (2016).
371. Boyerinas, B. *et al.* Antibody-dependent cellular cytotoxicity activity of a Novel Anti-PD-L1 antibody avelumab (MSB0010718C) on human tumor cells. *Cancer Immunol. Res.* **3**, 1148–1157 (2015).
372. Machado, Á. & Torres, T. Guselkumab for the Treatment of Psoriasis. *BioDrugs* vol. 32 119–128 (2018).
373. Busse, P. J. *et al.* Lanadelumab for the Prophylactic Treatment of Hereditary Angioedema with C1 Inhibitor Deficiency: A Review of Preclinical and Phase I Studies. *BioDrugs* vol. 33 33–43 (2019).
374. Elgundi, Z., Reslan, M., Cruz, E., Sifniotis, V. & Kayser, V. The state-of-play and future of antibody therapeutics. *Advanced Drug Delivery Reviews* vol. 122 2–19 (2017).
375. Chames, P., Van Regenmortel, M., Weiss, E. & Baty, D. Therapeutic antibodies: successes, limitations and hopes for the future. *Br. J. Pharmacol.* **157**, 220–233 (2009).
376. Woof, J. M. & Burton, D. R. Human antibody-Fc receptor interactions illuminated by crystal structures. *Nature Reviews Immunology* vol. 4 89–99 (2004).
377. Ward, E. S. *et al.* From sorting endosomes to exocytosis: Association of Rab4 and Rab11 GTPases with the Fc receptor, FcRn, during recycling. *Mol. Biol. Cell* **16**, 2028–2038 (2005).
378. Holliger, P. & Hudson, P. J. Engineered antibody fragments and the rise of single domains. *Nat. Biotechnol.* **23**, 1126–1136 (2005).
379. Revets, H., De Baetselier, P. & Muyldermans, S. Nanobodies as novel agents for cancer therapy. *Expert Opinion on Biological Therapy* vol. 5 111–124 (2005).
380. De Genst, E. *et al.* Chemical basis for the affinity maturation of a camel single domain antibody. *J. Biol. Chem.* **279**, 53593–53601 (2004).
381. De Genst, E. *et al.* Strong in vivo maturation compensates for structurally restricted H3 loops in antibody repertoires. *J. Biol. Chem.* **280**, 14114–14121 (2005).
382. Dooley, H. & Flajnik, M. Shark immunity bites back: affinity maturation and memory response in the nurse shark,Ginglymostoma cirratum. *Eur. J. Immunol.* **35**, 936–945 (2005).
383. Streltsov, V., letters, S. N.-I. & 2005, undefined. Do sharks have a new antibody lineage? *Immunol. Lett.* **97**, 159–160 (2005).
384. Muyldermans, S. Single domain camel antibodies: Current status. *Rev. Mol. Biotechnol.* **74**, 277–302 (2001).
385. Wolfson, W. Ablynx Makes Nanobodies from Llama Bodies. *Chemistry and Biology* vol. 13 1243–1244 (2006).
386. Khodabakhsh, F., Behdani, M., Rami, A. & Kazemi-Lomedasht, F. Single-Domain Antibodies or Nanobodies: A Class of Next-Generation Antibodies. *Int. Rev. Immunol.* **37**, 316–322 (2018).
387. Daley, L. P., Gagliardo, L. F., Duffy, M. S., Smith, M. C. & Appleton, J. A. Application of monoclonal antibodies in functional and comparative investigations of heavy-chain immunoglobulins in new world camelids. *Clin. Diagn. Lab. Immunol.* **12**, 380–386 (2005).
388. Maass, D. R., Sepulveda, J., Pernthaner, A. & Shoemaker, C. B. Alpaca (Lama pacos) as a

convenient source of recombinant camelid heavy chain antibodies (VHHs). *J. Immunol. Methods* **324**, 13–25 (2007).
389. Muyldermans, S. Nanobodies: Natural Single-Domain Antibodies. *Annu. Rev. Biochem.* **82**, 775–797 (2013).
390. Nguyen, V., Hamers, R., journal, L. W.-T. E. & 2000, undefined. Camel heavy-chain antibodies: diverse germline VHH and specific mechanisms enlarge the antigen-binding repertoire. *EMBO J* **19**, 921–930 (2000).
391. Schmitz, K. R., Bagchi, A., Roovers, R. C., Van Bergen En Henegouwen, P. M. P. & Ferguson, K. M. Structural evaluation of EGFR inhibition mechanisms for nanobodies/VHH domains. *Structure* **21**, 1214–1224 (2013).
392. Greenberg, A. S. *et al.* A new antigen receptor gene family that undergoes rearrangement and extensive somatic diversification in sharks. *Nature* **374**, 168–173 (1995).
393. Nuttall, S. D. *et al.* Selection and affinity maturation of IgNAR variable domains targeting Plasmodium falciparum AMA1. *Proteins Struct. Funct. Bioinforma.* **55**, 187–197 (2004).
394. Nuttall, S. D. *et al.* Isolation of the new antigen receptor from wobbegong sharks, and use as a scaffold for the display of protein loop libraries. *Mol. Immunol.* **38**, 313–326 (2001).
395. Zielonka, S. *et al.* Structural insights and biomedical potential of IgNAR scaffolds from sharks. *mAbs* vol. 7 15–25 (2015).
396. Barelle, C., Gill, D. S. & Charlton, K. Shark novel antigen receptors the next generation of biologic therapeutics? *Adv. Exp. Med. Biol.* **655**, 49–62 (2009).
397. Stanfield, R. L., Dooley, H., Flajnik, M. F. & Wilson, I. A. Crystal structure of a shark single-domain antibody V region in complex with lysozyme. *Science (80-.).* **305**, 1770–1773 (2004).
398. Diaz, M., Greenberg, A. S. & Flajnik, M. F. Somatic hypermutation of the new antigen receptor gene (NAR) in the nurse shark does not generate the repertoire: possible role in antigen-driven reactions in the absence of germinal centers. *Proc. Natl. Acad. Sci. U. S. A.* **95**, 14343–8 (1998).
399. Rahbarizadeh, F., Ahmadvand, D. & Sharifzadeh, Z. Nanobody; an Old Concept and New Vehicle for Immunotargeting. *Immunol. Invest.* **40**, 299–338 (2011).
400. Dumoulin, M. *et al.* Single-domain antibody fragments with high conformational stability. *Protein Sci.* **11**, 500–515 (2009).
401. Walper, S. A. *et al.* Rugged single domain antibody detection elements for bacillus anthracis spores and vegetative cells. *PLoS One* **7**, (2012).
402. Hussack, G., Hirama, T., Ding, W., MacKenzie, R. & Tanha, J. Engineered Single-Domain Antibodies with High Protease Resistance and Thermal Stability. *PLoS One* **6**, e28218 (2011).
403. Conrath, K. E., Lauwereys, M., Wyns, L. & Muyldermans, S. Camel Single-domain Antibodies as Modular Building Units in Bispecific and Bivalent Antibody Constructs. *J. Biol. Chem.* **276**, 7346–7350 (2001).
404. Zhang, J. & MacKenzie, C. R. Multivalent display of single-domain antibodies. *Methods Mol. Biol.* **911**, 445–456 (2012).
405. Zhang, J. *et al.* Pentamerization of single-domain antibodies from phage libraries: A novel strategy for the rapid generation of high-avidity antibody reagents. *J. Mol. Biol.* **335**, 49–56 (2004).
406. Cortez-Retamozo, V. *et al.* Efficient Cancer Therapy with a Nanobody-Based Conjugate. *Cancer Res.* **64**, 2853–2857 (2004).
407. Moghimi, S. M., Rahbarizadeh, F., Ahmadvand, D. & Parhamifar, L. Heavy chain only antibodies: A new paradigm in personalized HER2+ breast cancer therapy. *BioImpacts* vol. 3 1–4 (2013).
408. Kijanka, M., Dorresteijn, B., Oliveira, S. & van Bergen en Henegouwen, P. M. Nanobody-based cancer therapy of solid tumors. *Nanomedicine* **10**, 161–174 (2015).
409. Vincke, C. *et al.* Generation of Single Domain Antibody Fragments Derived from Camelids

and Generation of Manifold Constructs. in 145–176 (Humana Press, Totowa, NJ, 2012). doi:10.1007/978-1-61779-974-7_8.
410. Eyer, L., Hruska, K., Eyer, L. & Hruska, K. Single-Domain Antibody Fragments Derived from Heavy-Chain Antibodies: A Review Drug Discovery and Development for Flaviviruses View project Brassinosteroids View project Single-domain antibody fragments derived from heavy-chain antibodies: a review. *Vet. Med. (Praha).* **57**, 439–513 (2012).
411. Sarker, S. A. *et al.* Anti-rotavirus protein reduces stool output in infants with diarrhea: A randomized placebo-controlled trial. *Gastroenterology* **145**, 740-748.e8 (2013).
412. Cortez-Retamozo, V. *et al.* Efficient tumor targeting by single-domain antibody fragments of camels. *Int. J. Cancer* **98**, 456–462 (2002).
413. Paalanen, M. M. I. *et al.* The development of activating and inhibiting camelid VHH domains against human protein kinase C epsilon. *Eur. J. Pharm. Sci.* **42**, 332–339 (2011).
414. Abulrob, A., Sprong, H., en Henegouwen, P. V. B. & Stanimirovic, D. The blood-brain barrier transmigrating single domain antibody: mechanisms of transport and antigenic epitopes in human brain endothelial cells. *J. Neurochem.* **95**, 1201–1214 (2005).
415. Rutgers, K. S. *et al.* Transmigration of beta amyloid specific heavy chain antibody fragments across the in vitro blood-brain barrier. *Neuroscience* **190**, 37–42 (2011).
416. Abel, P. & Smith, D. D. Calcitonin gene-related peptide. in *xPharm: The Comprehensive Pharmacology Reference* 1–4 (Elsevier Inc., 2007). doi:10.1016/B978-008055232-3.61434-5.
417. Baral, T. N., MacKenzie, R. & Arbabi Ghahroudi, M. Single-Domain Antibodies and Their Utility. *Curr. Protoc. Immunol.* **103**, 2.17.1-2.17.57 (2013).
418. Vandenbroucke, K. *et al.* Orally administered L. lactis secreting an anti-TNF Nanobody demonstrate efficacy in chronic colitis. *Mucosal Immunol.* **3**, 49–56 (2010).
419. Sukhanova, A. *et al.* Oriented conjugates of single-domain antibodies and quantum dots: Toward a new generation of ultrasmall diagnostic nanoprobes. *Nanomedicine Nanotechnology, Biol. Med.* **8**, 516–525 (2012).
420. Van Audenhove, I. & Gettemans, J. Nanobodies as Versatile Tools to Understand, Diagnose, Visualize and Treat Cancer. *EBioMedicine* vol. 8 40–48 (2016).
421. Häsler, J., Flajnik, M. F., Williams, G., Walsh, F. S. & Rutkowski, J. L. VNAR single-domain antibodies specific for BAFF inhibit B cell development by molecular mimicry. *Mol. Immunol.* **75**, 28–37 (2016).
422. Roberts, K. G. *et al.* Targetable Kinase-Activating Lesions in Ph-like Acute Lymphoblastic Leukemia. *N. Engl. J. Med.* **371**, 1005–1015 (2014).
423. Wild, J. *et al.* Neutralization of (NK-cell-derived) B-cell activating factor by Belimumab restores sensitivity of chronic lymphoid leukemia cells to direct and Rituximab-induced NK lysis. *Leukemia* **29**, 1676–1683 (2015).
424. Fang, T. *et al.* Structurally Defined αMHC-II Nanobody-Drug Conjugates: A Therapeutic and Imaging System for B-Cell Lymphoma. *Angew. Chemie Int. Ed.* **55**, 2416–2420 (2016).
425. Allegra, A. *et al.* Cancer Investigation Nanobodies and Cancer: Current Status and New Perspectives. (2018) doi:10.1080/07357907.2018.1458858.
426. Slørdahl, T. S. *et al.* Anti-c-MET Nanobody ® - a new potential drug in multiple myeloma treatment. *Eur. J. Haematol.* **91**, 399–410 (2013).
427. Engler, C. & Marillonnet, S. Golden Gate Cloning. in *Methods in molecular biology (Clifton, N.J.)* vol. 1116 119–131 (2014).
428. Binder, A. *et al.* A Modular Plasmid Assembly Kit for Multigene Expression, Gene Silencing and Silencing Rescue in Plants. *PLoS One* **9**, e88218 (2014).
429. Clontech (Takara). In-Fusion® HD Cloning Kit User Manual. *In-Fusion Cloning* **1**, 1–15 (2012).
430. Mandel, M. & Higa, A. Calcium-dependent bacteriophage DNA infection. 1970. *Biotechnology* **24**, 198–201 (1992).
431. Visintin, M., Quondam, M. & Cattaneo, A. The intracellular antibody capture technology:

Towards the high-throughput selection of functional intracellular antibodies for target validation. *Methods* **34**, 200–214 (2004).
432. Jonasson, P., Liljeqvist, S., Nygren, P.-Å. & Ståhl, S. Genetic design for facilitated production and recovery of recombinant proteins in Escherichia coli. *Biotechnol. Appl. Biochem.* **35**, 91 (2002).
433. Nishihara, K., Kanemori, M., Kitagawa, M., Yanagi, H. & Yura, T. Chaperone coexpression plasmids: Differential and synergistic roles of DnaK-DnaJ-GrpE and GroEL-GroES in assisting folding of an allergen of Japanese cedar pollen, Cryj2, in Escherichia coli. *Appl. Environ. Microbiol.* **64**, 1694–1699 (1998).
434. Nishihara, K., Kanemori, M., Yanagi, H. & Yura, T. Overexpression of trigger factor prevents aggregation of recombinant proteins in Escherichia coli. *Appl. Environ. Microbiol.* **66**, 884–889 (2000).
435. Longo, P., Kavran, J., Kim, M., enzymology, D. L.-M. in & 2013, undefined. Transient mammalian cell transfection with polyethylenimine (PEI). *Elsevier*.
436. Backliwal Gaurav *et al.* Rational vector design and multi-pathway modulation of HEK 293E cells yield recombinant antibody titers exceeding 1 g/l by transient transfection under serum-free conditions | Nucleic Acids Research | Oxford Academic. *Nucleic Acids Res.* **36**, (2008).
437. Jevševar, S. *et al.* Production of Nonclassical Inclusion Bodies from Which Correctly Folded Protein Can Be Extracted. *Biotechnol. Prog.* **21**, 632–639 (2008).
438. Mahlawat, P., Ilangovan, U., Biswas, T., Sun, L. Z. & Hinck, A. P. Structure of the Alk1 extracellular domain and characterization of its bone morphogenetic protein (BMP) binding properties. *Biochemistry* **51**, 6328–6341 (2012).
439. Tsumoto, K. *et al.* Role of arginine in protein refolding, solubilization, and purification. *Biotechnology Progress* vol. 20 1301–1308 (2004).
440. Laemmli, U. K. Cleavage of structural proteins during the assembly of the head of bacteriophage T4. *Nature* **227**, 680–685 (1970).
441. Schägger, H. Tricine-SDS-PAGE. *Nat. Protoc.* **1**, 16–22 (2006).
442. Balcão, V. M., Mateo, C., Fernández-Lafuente, R., Malcata, F. X. & Guisán, J. M. Coimmobilization of L-asparaginase and glutamate dehydrogenase onto highly activated supports. *Enzyme Microb. Technol.* **28**, 696–704 (2001).
443. Šali, A. & Blundell, T. L. Comparative protein modelling by satisfaction of spatial restraints. *J. Mol. Biol.* **234**, 779–815 (1993).
444. Lee, C. M. Y., Iorno, N., Sierro, F. & Christ, D. Selection of human antibody fragments by phage display. *Nat. Protoc.* **2**, 3001–3008 (2007).
445. Skerra, A. & Plückthun, A. Assembly of a functional immunoglobulin Fv fragment in Escherichia coli. *Science (80-.).* **240**, 1038–1041 (1988).
446. Barbas, C. F., Kang, A. S., Lerner, R. A. & Benkovic, S. J. Assembly of combinatorial antibody libraries on phage surfaces: The gene III site. *Proc. Natl. Acad. Sci. U. S. A.* **88**, 7978–7982 (1991).
447. Hamers-Casterman, C. *et al.* Naturally occurring antibodies devoid of light chains. *Nature* **363**, 446–448 (1993).
448. Roux, K. H. *et al.* Structural analysis of the nurse shark (new) antigen receptor (NAR): Molecular convergence of NAR and unusual mammalian immunoglobulins. *Proc. Natl. Acad. Sci. U. S. A.* **95**, 11804–11809 (1998).
449. Ward, E. S., Güssow, D., Griffiths, A. D., Jones, P. T. & Winter, G. Binding activities of a repertoire of single immunoglobulin variable domains secreted from Escherichia coli. *Nature* **341**, 544–546 (1989).
450. HB, J. III. On a new substance occurring in the urine of a patient with mollities ossium. *Philos. Trans. R. Soc. London* **138**, 55–62 (1848).
451. Christ, D., Famm, K. & Winter, G. Repertoires of aggregation-resistant human antibody domains. *Protein Eng. Des. Sel.* **20**, 413–416 (2007).

452. Holt, L. J., Herring, C., Jespers, L. S., Woolven, B. P. & Tomlinson, I. M. Domain antibodies: Proteins for therapy. *Trends in Biotechnology* vol. 21 484–490 (2003).
453. Schirrmann, T., Meyer, T., Schütte, M., Frenzel, A. & Hust, M. Phage Display for the Generation of Antibodies for Proteome Research, Diagnostics and Therapy. 412–426 (2011) doi:10.3390/molecules16010412.
454. Niccheri, F. *et al.* Human recombinant domain antibodies against multiple sclerosis antigenic peptide CSF114(Glc). *J. Mol. Recognit.* **27**, 618–626 (2014).
455. Fields, S. & Song, O.-K. *A novel genetic system to detect protein-protein interactions*. *Springer* https://link.springer.com/content/pdf/10.1038/340245a0.pdf (1989).
456. Durfee, T. *et al.* The retinoblastoma protein associates with the protein phosphatase type 1 catalytic subunit. *Genes Dev.* **7**, 555–569 (1993).
457. Brückner, A., Polge, C., Lentze, N., Auerbach, D. & Schlattner, U. Yeast two-hybrid, a powerful tool for systems biology. *Int. J. Mol. Sci.* **10**, 2763–2788 (2009).
458. Visintin, M. & Cattaneo, A. Selecting Intracellular Antibodies Using the Two-Hybrid System. in *Antibody Engineering* 213–233 (Springer Berlin Heidelberg, 2001).
459. Schiestl, R. H. & Gietz, R. D. High efficiency transformation of intact yeast cells using single stranded nucleic acids as a carrier. *Curr. Genet.* **16**, 339–346 (1989).
460. Visintin, M., Tse, E., Axelson, H., Rabbitts, T. H. & Cattaneo, A. Selection of antibodies for intracellular function using a two-hybrid in vivo system. *Proc. Natl. Acad. Sci. U. S. A.* **96**, 11723–11728 (1999).
461. Serebriiskii, I. G. & Golemis, E. A. Uses of lacZ to study gene function: Evaluation of β-galactosidase assays employed in the yeast two-hybrid system. *Anal. Biochem.* **285**, 1–15 (2000).
462. Liu, J., Liu, C. & He, W. Fluorophores and Their Applications as Molecular Probes in Living Cells. *Curr. Org. Chem.* **17**, 564–579 (2013).
463. Kogata, N. & Howard, B. A. A whole-mount immunofluorescence protocol for three-dimensional imaging of the embryonic mammary primordium. *Journal of Mammary Gland Biology and Neoplasia* vol. 18 227–231 (2013).
464. Joshi, S. & Yu, D. *Immunofluorescence*. *Basic Science Methods for Clinical Researchers* (Elsevier Inc., 2017). doi:10.1016/B978-0-12-803077-6.00008-4.
465. Cherukuri, A., Cheng, P. C. & Pierce, S. K. The Role of the CD19/CD21 Complex in B Cell Processing and Presentation of Complement-Tagged Antigens. *J. Immunol.* **167**, 163–172 (2001).
466. Krishnan, V. *et al.* CD19-targeted nanodelivery of doxorubicin enhances therapeutic efficacy in B-cell acute lymphoblastic leukemia. *Mol. Pharm.* **12**, 2101–2111 (2015).
467. Du, X., Beers, R., FitzGerald, D. J. & Pastan, I. Differential cellular internalization of anti-CD19 and -CD22 immunotoxins results in different cytotoxic activity. *Cancer Res.* **68**, 6300–6305 (2008).
468. Cotte, Y. *et al.* Marker-free phase nanoscopy. *Nat. Photonics* **7**, 113–117 (2013).
469. Lee, C. M. Y., Iorno, N., Sierro, F. & Christ, D. Selection of human antibody fragments by phage display. *Nat. Protoc.* **2**, 3001 (2007).
470. Jafari, B., Hamzeh-Mivehroud, M. & Dastmalchi, S. 2018_Jafari_Identification of Novel Single-Domain Antibodies against FGF7 Using Phage Display Technology.pdf. *SLAS Discov.* (2018).
471. PyMOL Molecular Graphics System, Version 1.2r3pre, Schrödinger, L. PyMOL.
472. Yan, J., Wolff, M. J., Unternaehrer, J., Mellman, I. & Mamula, M. J. Targeting antigen to CD19 on B cells efficiently activates T cells. **17**, 869–877 (2005).
473. Ingle, G. S. *et al.* High CD21 expression inhibits internalization of anti-CD19 antibodies and cytotoxicity of an anti-CD19-drug conjugate. *Br. J. Haematol.* **140**, 46–58 (2008).
474. Oliveira, S. N. De *et al.* A CD19 / Fc fusion protein for detection of anti-CD19 chimeric antigen receptors. *J. Transl. Med.* **11**, 1 (2013).
475. Greenfield Edward A. *Antibodies, A laboratory Manual*. (2012).
476. Khan, K. H. Gene expression in Mammalian cells and its applications. *Adv. Pharm. Bull.* **3**,

257–63 (2013).
477. Baneyx, F. & Mujacic, M. Recombinant protein folding and misfolding in Escherichia coli. *Nature Biotechnology* vol. 22 1399–1407 (2004).
478. García-Fruitós, E. Insoluble proteins: Methods and protocols. *Insoluble Proteins Methods Protoc.* **1258**, 1–422 (2014).
479. Reddy K., R. C. L-Arginine increases the solubility of unfolded species of hen egg white lysozyme. *Protein Sci.* **14**, 929–935 (2005).
480. Kudou, M., Yumioka, R., Ejima, D., Arakawa, T. & Tsumoto, K. A novel protein refolding system using lauroyl-l-glutamate as a solubilizing detergent and arginine as a folding assisting agent. *Protein Expr. Purif.* **75**, 46–54 (2011).
481. Ohtake, S., Kita, Y. & Arakawa, T. Interactions of formulation excipients with proteins in solution and in the dried state. *Advanced Drug Delivery Reviews* vol. 63 1053–1073 (2011).
482. Harmsen, M. M. & De Haard, H. J. Properties, production, and applications of camelid single-domain antibody fragments. *Applied Microbiology and Biotechnology* vol. 77 13–22 (2007).
483. Nicholson, I. C. *et al.* Construction and characterisation of a functional CD19 specific single chain Fv fragment for immunotherapy of B lineage leukaemia and lymphoma. *Mol. Immunol.* **34**, 1157–1165 (1997).

Scientific production arisen from this thesis

Peer-reviewed publications

Scotti C, Maggi M, De Jonge H, **Pessino G**, Iamele L, *Anti-cancer autoantibodies: a review*, Cancers, 2021

Patents

Maggi M, **Pessino G**, Scotti C, PCT/IB2018/057259, *An antibody drug conjugate based on asparaginase*.

Abstracts at international meetings

Maggi M, **Pessino G**, Scotti C. *Asparaginases*. "The IDEA of a center - Symposium", Pavia (Italy), 6-7 February 2019.

EACR-AACR Basic and Translational Research Conference in partnership with ASPIC: "Tumor Microevironment". Poster: Maggi M, **Pessino G**, Scotti C. *Hepatocyte Growth Factor receptor cMET: a novel, targetable marker of Asparaginase resistance in leukemia.* Lisbon, 02-04 March 2020.

Acknowledgements

I would like to thank all the people who contributed to this work, being of extreme importance for the fulfillment of this project.

First of all, I have to thank my supervisor, Dr. Claudia Scotti, who let me work into her laboratory as a full member of the team and guided me through the three past years, being a great mentor and leader.
Then I want to thank all the members of the Unit of Immunology and Pathology of the Department of Molecular Medicine of the University of Pavia, who often helped me in further improve this work with precious comments, advices and expertise. Special thanks are due to Dr. Maristella Maggi, post-doc fellow in our research team, who has been a constant source of support and inspiration.
Also, I would like to thank Prof. Marjia Jäättelä from the Danish Cancer Society Research Center (DCSRC, Copenhagen), who allowed me to learn precious techniques by hosting me in her laboratory with great kindness,
Finally, I would like to thank with special gratitude Prof. Cattaneo from Scuola Normale Superiore di Pisa, along with his whole research group, and in particular Dr. Simonetta Lisi, for welcoming me into their laboratory with special care and for helping me in the selection of the anti-CD19 VHH nanobody, which turned out to be a crucial turning point for the development of this project.